

Università degli Studi della Calabria

Facoltà di Scienze Matematiche Fisiche e Naturali

Tesi di Dottorato di Ricerca in Metodologie Chimiche
Inorganiche (XXI ciclo)

AREA 03 - Scienze Chimiche, SSD-CHIM03/Chimica Generale ed Inorganica

Dioxygen Activation by Transition Metal Complexes for
some Homogeneous Catalyzed Reactions

Candidato

Sugata Chowdhury

Supervisore

Prof Nino Russo

Coordinatore

Prof. Nino Russo

A.A. 2007-2008

Dottorato di Ricerca in "Metodologie Chimiche Inorganiche"
Università della Calabria

Verbale Collegio dei docenti Dottorato di Ricerca in Metodologie Chimiche Inorganiche del 20-10-2008

Presenti: N. Russo, E. Sicilia, M. Toscano, A. Crispini, D. Pucci, T. Marino, M.C. Michelini, M. La Deda, D. Armentano

Assenti Giustificati: G. De Munno

Assenti: F. Capozzi, C. Zanchini, F. Neve

O.d.G

1. Comunicazioni
2. Valutazione finale attività dottorandi: A. Aprea, I. Lanzo, N. Marino, A. Martino, S. Chowdhury
3. Data esami finali
4. Commissioni per la valutazione finale
5. Elezione membro per il CD della Scuola di Dottorato in Scienza e Tecnologia
6. Varie ed eventuali

Alle ore 15.30 del giorno 20.10.08 il Collegio dei docenti del Dottorato di ricerca in Metodologie Chimiche Inorganiche si è riunito presso l'aula Seminari del cubo 14c del Dipartimento di Chimica come da O. d. G.

7. Valutazione finale attività dottorandi: A. Aprea, I. Lanzo, N. Marino, A. Martino, S. Chowdhury

OMISSIS

Candidato: dott. Sugata Chowdhury

Supervisore: Prof. Nino Russo

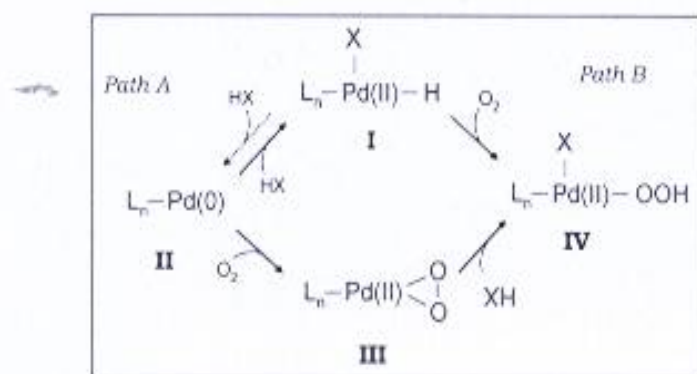
Progetto di Ricerca: Dioxygen Activation by Transition Metal Complexes for some Homogeneous Catalyzed Reactions

Il dott. Sugata Chowdhury ha iniziato nel novembre 2005 il corso di dottorato in Metodologie Chimiche Inorganiche (MCI) con un progetto di ricerca avente come oggetto lo studio dell'attivazione dell'ossigeno molecolare tramite complessi metallici in una serie di reazioni catalizzate in fase omogenea, utilizzando i metodi basati sulla teoria del funzionale densità.

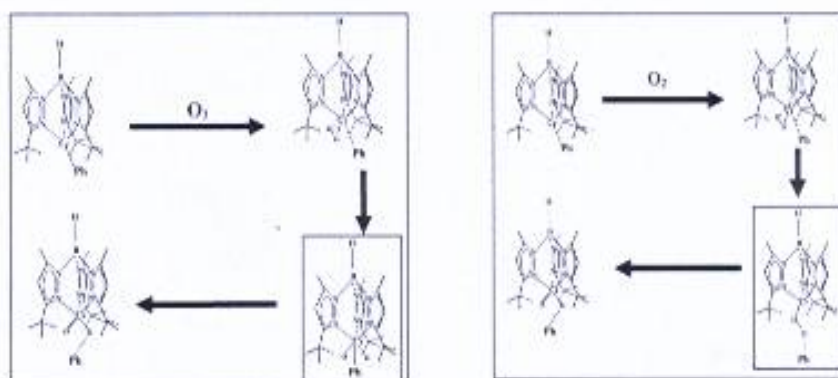
Durante i tre anni di attività il dottorando ha affrontato lo studio:

- A) dell'ossidazione del Pd⁰ e l'inserzione diretta di O₂ nel legame Pd(II)-H
- B) dell'inserzione dell'ossigeno molecolare nel legame Cromo-fenile
- C) della riduzione dell'ossigeno in catalizzatori per celle ad idrogeno.
-

A) Per l'addizione dell'ossigeno molecolare sul legame metallo-idrogeno sono stati considerati diversi complessi del palladio e diversi cammini di reazione come mostrato dallo schema seguente. Per ognuno dei cammini esaminati sono stati considerati sia gli stati di singoletto che quelli di tripletto. Il punto di incrocio tra le due superfici è stato individuato e caratterizzato.



B) L'inserzione dell'ossigeno molecolare nel legame metallo-carbonio è stata studiata in un complesso recentemente sintetizzato e caratterizzato. Sono stati considerati due cammini di reazione diversi come mostrato negli schemi seguenti. Nel primo meccanismo si considera la rottura del legame ossigeno-ossigeno mentre nel secondo si prende in esame l'inserzione dell'ossigeno senza rottura del legame O-O come suggerito sperimentalmente.



C) Lo studio riguardante questa tematica ha avuto come oggetto il meccanismo di idrogenazione e conseguente ossigenazione dei complessi $Cp^*Ir(TsDPEN-H)$ a 16 elettroni e $Cp^*Ir H (TsDPEN)$ a 18 elettroni. Anche in questo caso sono stati considerati diversi meccanismi di reazione. Infatti, per quanto riguarda l'idrogenazione è stato considerato sia il meccanismo dell'inserzione diretta di H_2 al complesso neutro che a quello protonato. I risultati mostrano che il secondo meccanismo è quello preferito da un punto di vista energetico. L'addizione di ossigeno molecolare avviene tramite la formazione di un intermedio stabile iridio-perossido. L'incrocio tra le superfici di singoletto e quelle di tripletto è stato identificato e caratterizzato. Per l'eliminazione dell'acqua sono stati studiati tre diversi meccanismi: 1. formazione di un complesso con due idrossiammine ed eliminazione di due molecole di acqua; 2. formazione degli stessi intermedi con un meccanismo concertato di eliminazione delle molecole di acqua; 3. eliminazione sequenziale di molecole di acqua da un intermedio idroperossidico. I risultati mostrano come questo ultimo sia quello favorito.

Questo lavoro è stato in parte compiuto durante il semestre trascorso dal dottorando presso il Dipartimento di Chimica Teorica del Royal Institute of Technology di Stoccolma, sotto la supervisione del Prof. Fahmi Himo.

L'esperienza del candidato in Svezia è stata proficua e formativa poiché ha permesso di approfondire diversi argomenti relativi alla chimica dei complessi dei metalli di transizione. Inoltre

ha permesso di integrare la formazione complessiva del dottorando seguendo un consistente numero di seminari tenuti da esperti del settore.

Sin dagli inizi della sua attività come dottorando, il dott. Chowdhury ha dimostrato di possedere una sufficiente preparazione di base nelle scienze chimiche e durante il triennio ha acquisito una discreta dimestichezza nel campo della Chimica Quantistica e dei vari metodi computazionali utilizzati. La sua formazione è stata completata attraverso la frequentazione di tutti i corsi organizzati dal Dottorato in MCI.

L'attività di ricerca ha prodotto tre articoli già pubblicati e due in fase di preparazione. Inoltre, l'attività svolta è stata esposta sia nei seminari semestrali che tramite poster e comunicazioni orali in congressi scientifici nazionali ed internazionali.

Lavori Pubblicati:

- 1) S. Chowdhury, I. Rivalta, N. Russo, E. Sicilia
"On the insertion mechanism of molecular oxygen into a Pd(II)-H bond. Something to add"
Chemical Physics Letters 443 (2007) 183-189
- 2) S. Chowdhury, I. Rivalta, N. Russo, E. Sicilia
"The recognition of a new pathway for the reaction of molecular oxygen with a Pd(II)-hydride to produce a Pd(II)-hydroperoxide"
Chem. Phys. Lett. 456 (2008) 41-46
- 3) S. Chowdhury, I. Rivalta, N. Russo, and E. Sicilia
"Theoretical Investigation of the Mechanism of Acid-Catalyzed Oxygenation of a Pd(II)-Hydride to Produce a Pd(II)-Hydroperoxide"
J. Chem. Theory Comput. 4 (2008), 1283-1292

Partecipazioni a congressi:

- 1) Insertion of Molecular Oxygen into Pd(II)-H Bonds to Form Pd(II)-OOH", Sugata Chowdhury, Ivan Rivalta, Nino Russo, Emilia Sicilia, delivered in 1st International Symposium on Molecular Oxygen in Catalysis, Institute of Physical Chemistry, University of Stuttgart, Germany, October, 2007
- 2) Theoretical Calculation of Palladium-Catalyzed reactions for the selective aerobic oxidation of organic molecules. Sandro Chiodo, Sugata Chowdhury, Nino Russo, Emilia Sicilia, presented in IX Scuola Nazionale per Dottorandi della Divisione di Chimica Inorganica, Università della Calabria, Arcavacata (Cosenza), Italy, Novembre, 2006.
- 3) Theoretical investigation of Palladium-Catalyzed reactions for the selective aerobic oxidation of organic molecules. (Invited participant) Sandro Chiodo, Sugata Chowdhury, Nino Russo, Emilia Sicilia, presented in 13th International Workshop on Computational Physics and Materials Science: Total Energy and Force Methods, The Abdus Salam International Centre for Theoretical Physics, Trieste, Italy, January, 2007.
- 4) Theoretical Investigation of the Mechanistic Aspect of Palladium Catalyzed Oxidation Reactions. Sugata Chowdhury, Ivan Rivalta, Nino Russo, Emilia Sicilia, presented in XXXIV Congresso dei Chimici Teorici di Espressone Latina, Università della Calabria, Italy, July, 2008.

Il lavoro di ricerca dal Dott. Chowdhury è stato portato a termine sviluppando tutti gli aspetti previsti dal progetto iniziale.

Il dottorando ha raggiunto un sufficiente grado di autonomia nel proporre soluzioni e nella razionalizzazione dei risultati del suo progetto di ricerca.

Nell'interazione con docenti, colleghi e studenti il Dott. Chowdhury ha dimostrato desiderio di apprendere e di approfondire le proprie conoscenze.

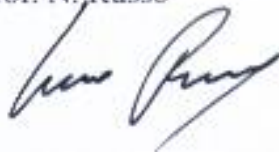
Il giudizio complessivo sulla formazione raggiunta, sull'attività di ricerca svolta nel corso del triennio, sulla personalità scientifica e l'attitudine alla ricerca della Dott. Chowdhury è, pertanto, **positivo**.

Il Collegio giudica quindi il dott. Chowdhury meritevole di aspirare al titolo di "Dottore di Ricerca in Metodologie Chimiche Inorganiche".

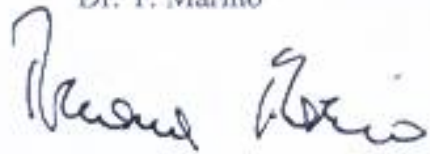
OMISSIS

Letto, approvato e sottoscritto in Rende 05-11-07

Il coordinatore
Prof. N. Russo



Il segretario
Dr. T. Marino



Acknowledgement

I would like to take this opportunity to thank my research guide, Prof. Nino Russo for his encouragement, support and guidance. He has been a source of inspiration throughout the course of my research in Dipartimento di Chimica, Universita della Calabria, not to mention the lectures he conducted for all of us which added immensely to my knowledge. He has been a friend and a well wisher.

It is perhaps not possible to express in words my gratitude towards Prof. Emilia Sicilia for her guidance and support during the past three years. My interaction with her had an enormous influence on my scientific development. Prof Sicilia has given me invaluable scientific knowledge and has encouraged me to develop independent thinking. I am very grateful to her for being a friend and well wisher.

I am grateful to the Director, University della Calabria for providing the infrastructure and facilities for my research during the course of my PhD. I would like to acknowledge the International School of Hard science "Bernadino Telesio" the source of my research funding.

I wish to thank Prof. Himo Fahmi, Department of Theoretical Chemistry, School of Biotechnology, Royal Institute of Technology, Stockholm, Sweden who have helped me in several ways and encouraged me to visit to his lab in Sweden. He always encouraged me to develop independent thinking. I am very grateful to him for being a friend and well wisher.

My thanks to Dr. Sourav Pal for all his help. I wish to thank all the people in Electronic Structure Theoretical Group, National Chemical Laboratory, Pune, India who have helped me in several ways.

In the Theoretical and Inorganic Chemistry Dept. in the Universita della Calabria I met good friends such as Domenico, Franscesca, Donatella, Ida, Orazio, Sandro and Monica. The interesting discussions about my work I had with Ivan were very helpful in my reseach. My special thanks to Harry for being such a nice friend, and for inspiring me to write my thesis in Latex, and for helping me out with the details.

Words won't suffice to thank my family, especially my parents, and my elder brother for all

the sacrifices, support, love, care and freedom they gave to me. My life partner Debanjana has been my inspiration during my research and thesis writing days. I dedicate my thesis to all of them.

Contents

1	Introduction	1
1.1	Catalysts	2
1.2	Homogeneous Catalysis	4
1.2.1	Historical Notes	5
1.2.2	Homogeneous Catalysts	6
1.3	Activation of Dioxygen	7
1.3.1	Electronic Structure of Oxygen	8
1.3.2	Dioxygen for Selective Oxidation	9
1.4	Reactions with Transition Metal Complex	10
1.4.1	Selective Oxidation	10
1.4.2	Early Transition Metals	15
1.4.3	Transfer Hydrogen Catalysts	22
2	Theoretical Background	34
2.1	Wavefunction Theory	35
2.1.1	Hartree-Fock Theory	36
2.2	Development of Density Functional Theory	36
2.2.1	Thomas-Fermi Model	37
2.2.2	The X_α Method	38
2.2.3	Density Matrix Theory	38
2.3	Density Functional Theory	39
2.3.1	The Hohenberg-Kohn theorem	40

2.3.2	Representability problems	41
2.3.3	Constrained-Search Formulation	41
2.3.4	Kohn-Sham Approach	42
2.4	The Exchange-Correlation Functional	45
2.5	B3LYP	46
2.6	Continuum Solvation Model	46
2.6.1	Basics of The Continuum Model	46
2.6.2	Cavity	48
2.6.3	Polarizable Continuum Model (PCM)	49
2.7	Spin Contamination	50
2.8	Minimum Energy Crossing Point	51
2.9	Conclusion	52
3	Selective Oxidation of Palladium-hydride Bond	57
3.1	Introduction	57
3.2	Articles	58
4	Oxygen Insertion into the Metal-Carbon Bond of the $\text{Tp}^{t\text{Bu},\text{Me}}\text{Cr}^{(\text{IV})}\text{Ph}$ Complex: Exploring the Nature of Oxygen Migration Using DFT.	87
4.1	Introduction	87
4.2	Computational Details	89
4.3	Results and Discussion	90
4.3.1	Mechanism 1: O-O Breaking	91
4.3.2	Mechanism 2: O_2 Insertion	95
4.4	Conclusion	99
5	Mechanistic Investigation of Homogeneous Catalytic Reduction of Dioxygen Using Transfer Hydrogenation Catalysts	102
5.1	Introduction	102
5.2	Computational Details	105

5.3	Results and Discussion	107
5.3.1	Addition of H_2 to Neutral System	107
5.3.2	Insertion of O_2 into the metal-hydride bond	114
5.3.3	Mechanism for elimination for H_2O	118
5.4	Conclusion	132

List of Figures

1.1	Potential energy profile for an exothermic reaction, showing the lower activation energy of the catalysed reaction.	4
1.2	Molecular orbital scheme: Electronic structure of O_2	8
1.3	Principal types of presently known metal-dioxygen geometries.	16
1.4	Examples of metal hydride.	22
1.5	Examples of the hydrido complexes.	25
4.1	Potential energy surface for the O-O breaking mechanism. Gibbs free energies changes at 298.15 K in solvent are also reported in parentheses. Excited state structures are, also, mentioned to locate the spin crossing. Energies are relative to the ground state reactants.	92
4.2	Ground-state structures of the reactant, intermediates and transition states along the O-O breaking pathway. Labels introduced to individuate geometrical parameters have to be used to read information reported in Table 4.1.	93
4.3	Potential energy surface for the migratory insertion of coordinated molecular oxygen pathway. Gibbs free energies changes at 298.15 K in solvent are also reported in parentheses. Excited states structures are, also, mentioned to locate the spin crossing. Energies are relative to the ground state reactants.	95
4.4	Ground-state structures of the reactant, intermediates and transition states along the migratory insertion of coordinated molecular oxygen pathway. Labels introduced to individuate geometrical parameters have to be used to read information reported in Table 4.2.	96

5.1	Potential Energy Surface (PES) for H_2 insertion into $Cp^*Ir(TsDPEN - H)$. The values in parentheses are reported to the solvent phase. Energies are in kilocalories and relative to the ground-state reactants.	107
5.2	Ground-state structures of the reactant, intermediates and transition states for addition of H_2 into $Cp^*Ir(TsDPEN - H)$. Labels introduced to individuate geometrical parameters have to be used to read information reported in Table 5.1	108
5.3	PES for H_2 addition into $Cp^*Ir(TsDPEN)^+$. The values in parentheses are reported to the solvent phase. Energies are in kilocalories and relative to the ground-state reactants.	110
5.4	Ground-state structures of the reactant, intermediates and transition states for addition of H_2 into $Cp^*Ir(TsDPEN)^+$. Labels introduced to individuate geometrical parameters have to be used to read information reported in Table 5.2.	111
5.5	Comparison for addition of H_2 into $Cp^*Ir(TsDPEN - H)$ (dashed line) and $Cp^*Ir(TsDPEN)^+$ (solid line) systems. The values in parentheses are reported to the solvent phase. Energies are in kilocalories and relative to the ground-state reactants.	113
5.6	PES for O_2 insertion into $Cp^*IrH(TsDPEN)$ to form $Cp^*IrOOH(TsDPEN)$. The values in parentheses are reported to the solvent phase. Energies are in kilocalories and relative to the ground-state reactants.	114
5.7	Ground-state structures of the reactant, intermediates and transition states for insertion of O_2 into $Cp^*IrH(TsDPEN)$ to form $Cp^*IrOOH(TsDPEN)$ along the singlet-path. Labels introduced to individuate geometrical parameters have to be used to read information reported in Table 5.3	115
5.8	Ground-state structures of the reactant, intermediates and transition states for insertion of O_2 into $Cp^*IrH(TsDPEN)$ to form $Cp^*IrOOH(TsDPEN)$ along the triplet-path. Labels introduced to individuate geometrical parameters have to be used to read information reported in Table 5.4.	117

5.9	PES for formation of two $Cp^*IrOH(TsDPEN)$. The values in parentheses are reported to the solvent phase. Each $Cp^*IrOH(TsDPEN)$ will separately eliminate one H_2O molecule to form a $Cp^*Ir(TsDPEN - H)$. Energies are in kilocalories and relative to the ground-state reactants.	119
5.10	Ground-state structures of the reactant, intermediates and transition states in order to form two $Cp^*IrOH(TsDPEN)$. Labels introduced to individuate geometrical parameters have to be used to read information reported in Table 5.5.	120
5.11	PES for formation of two $Cp^*IrOH(TsDPEN)$. The values in parentheses are reported to the solvent phase. Two $Cp^*IrOH(TsDPEN)$ molecules will react subsequently and eliminate two H_2O molecules to form two $Cp^*Ir(TsDPEN - H)$. Energies are in kilocalories and relative to the ground-state reactants. . .	122
5.12	Ground-state structures of the reactant, intermediates and transition states for simultaneous elimination of $2H_2O$ from $Cp^*IrOOH(TsDPEN)$ according to the Scheme 5.3(B). Labels introduced to individuate geometrical parameters have to be used to read information reported in Table 5.6.	123
5.13	PES for the stepwise elimination of H_2O molecule to form $Cp^*Ir(TsDPEN - H)$. The values in parentheses are reported to the solvent phases. Energies are in kilocalories and relative to the ground-state reactants.	125
5.14	Ground-state structures of the reactant, intermediates and transition states for stepwise elimination of H_2O from $Cp^*IrOOH(TsDPEN)$. Labels introduced to individuate geometrical parameters have to be used to read information reported in Table 5.7.	126
5.15	PES for the elimination of H_2O molecule from $Cp^*IrOH(TsDPEN)$ in order to form $Cp^*Ir(TsDPEN - H)$. The values in parentheses are reported to the solvent phase. Energies are in kilocalories and relative to the ground-state reactants.	128
5.16	Ground-state structures of the reactant, intermediates and transition states for elimination of H_2O from $Cp^*IrOH(TsDPEN)$. Labels introduced to individuate geometrical parameters have to be used to read information reported in Table 5.8.	129

5.17 Energetics comparison for H_2O elimination. The values in parentheses are reported to the solvent phase. Energies are in kilocalories and relative to the ground-state reactants.	131
--	-----

List of Tables

4.1	Selected geometrical parameter of Ground-State Reactants, Intermediates and transition States computed along the O-O breaking pathway. Available experimental geometrical parameters of $\text{Tp}^{t\text{Bu},\text{Me}}\text{Cr}^{\text{IV}}(\text{O})\text{OPh}$ are also reported in parantheses. Bond length are in \AA and angles are in degree.	94
4.2	Selected geometrical parameter of Ground-State Reactants, Intermediates and transition States computed along the migratory insertion of coordinated molecular oxygen pathway. Available experimental geometrical parameters of $\text{Tp}^{t\text{Bu},\text{Me}}\text{Cr}^{\text{IV}}(\text{O})\text{OPh}$ are also reported in parantheses. Bond length are in \AA and angles are in degree.	98
5.1	Selected geometrical parameters of Ground-State Reactants, Intermediates and transition States computed for addition of H_2 into $\text{Cp}^*\text{Ir}(\text{TsDPEN} - \text{H})$. . .	109
5.2	Selected geometrical parameters of Ground-State Reactants, Intermediates and transition States computed for addition of H_2 into $\text{Cp}^*\text{Ir}(\text{TsDPEN})^+$	112
5.3	Selected geometrical parameters of Ground-State Reactants, Intermediates, MECP and Transition States computed for insertion of O_2 into $\text{Cp}^*\text{IrH}(\text{TsDPEN})$ to form $\text{Cp}^*\text{IrOOH}(\text{TsDPEN})$ along the Singlet-Path. .	116
5.4	Selected geometrical parameters of Ground-State Reactants, Intermediates and Transition States computed for insertion of O_2 into $\text{Cp}^*\text{IrH}(\text{TsDPEN})$ to form $\text{Cp}^*\text{IrOOH}(\text{TsDPEN})$ along Triplet-Path.	118
5.5	Selected geometrical parameters of Ground-State Reactants, Intermediates and Transition States computed in order to form two $\text{Cp}^*\text{IrOH}(\text{TsDPEN})$ according to Scheme 5.3(A).	121

5.6	Selected geometrical parameters of Ground-State Reactants, Intermediates and Transition States computed in order to elimination of two H ₂ O from <i>Cp*IrOOH(TsDPEN)</i> according to Scheme 5.3(B).	124
5.7	Selected geometrical parameters of Ground-State Reactants, Intermediates and Transition States computed for elimination of H ₂ O from <i>Cp*IrOOH(TsDPEN)</i> according to Scheme 5.3(C).	127
5.8	Selected geometrical parameters of Ground-State Reactants, Intermediates and Transition States computed for elimination of H ₂ O from <i>Cp*IrOH(TsDPEN)</i>	130

Preface

The ability to selectively oxidize organic molecules directly using oxygen gas is one of the “Holy Grails” in catalytic chemistry. This is due to the huge energy savings possible if organic molecules can be converted directly and efficiently into other reactive molecules and intermediates used throughout the chemical industry. As a consequence, considerable efforts are being made to replace traditional methods by catalytic processes that use molecular oxygen as oxidant, that is clean and cheap, environmentally friendly and gives no hazardous by-products

Transition metal-catalyzed oxidation reactions with molecular oxygen in biological, industrial, and laboratory processes involve a plethora of intermediates of various lifetimes, reactivities, and roles. As a result, theoretical and experimental investigation of the oxygen activation chemistry is a vibrant and extremely active field of research, aiming to remove the obstacle represented by the inadequate understanding of the mechanistic details of the involved processes.

The aim of this work is to study a few examples of the chemistry of dioxygen activation by transition metal complexes and show how application of computational chemistry methods can be used to solve real problems for which the theoretical chemist can significantly contribute to find an answer.

The organization of the dissertation work will be as follows:

Chapter 1:

In chapter 1, we have introduced the history and the general concepts of catalysis with a particular focus on the homogeneous catalysis. In the same chapter we have discussed the electronic structure of molecular oxygen and the problem of the intrinsic reactivity and selectivity challenges posed by the chemistry of dioxygen for its use in selective oxidation reaction. Some examples of reactions between dioxygen and different transition metal complexes have been discussed.

Chapter 2:

The development of catalytic processes needs a better theoretical understanding, which has to be confirmed by the experimental evidence. The quantum chemical calculations can result very helpful in the exploration of the mechanistic details of catalytic reactions once an adequate computational protocol is used. In chapter 2, we have presented the basic density functional theory (DFT) and the Continuum Solvation Model. Also we have discussed the approach used to correct the effects of spin-contamination of unrestricted-DFT and the algorithm used to intercept minimum energy crossing points (MECP).

Chapter 3:

Pd-catalyzed oxidations in homogeneous phase have emerged as a particularly promising reaction type for selective and efficient aerobic oxidation of organic substrates by dioxygen. But an inadequate understanding of reaction mechanism has hampered the development of new and more efficient catalytic strategies. Our idea is to study O₂ activation by the different kinds of Pd-complexes in homogenous phase.

In Chapter 3, we have elucidated the insertion mechanism of O₂ into a Pd(II)-hydride bond in order to form a (η^1 -hydroperoxo)palladium(II) complex using density functional theory (DFT) [Article I]. Also, we have presented a mechanistic study of the reaction of O₂ with trans-(IMes)₂Pd(H)OAc, which yields trans-(IMes)₂Pd(OOH)OAc. For our work, we have considered two different pathways: (1) direct insertion of O₂ and (2) reductive elimination of the carboxylic acid group followed by oxygenation of Pd⁰. In this case we have considered three different carboxylic acids (acetic, benzoic, p-nitrobenzoic) [Article II and III]. All the results and the computational details about these studies are collected in the attached articles.

Chapter 4:

The insertion of oxygen into metal-carbon bonds is an important step of metal mediated catalytic reactions for the oxidation of organic substrates by air. Despite the importance of this transformation very few studies aiming to unravel the mechanistic details are available in the literature. In this work we have carried out a mechanistic study of the reaction O₂ with the divalent chromium phenyl complex, Tp^{tBu,Me}Cr(IV)Ph, using DFT. For our work, we have considered two different pathways: (1) O-O bond breaking and (2) migratory insertion of dioxygen into the metal-phenyl bond. The outcomes of this study are reported in Chapter 4.

Chapter 5:

The hydrogenation of dioxygen by conventional homogeneous catalysts is challenging. Many complexes that are reactive toward H₂ are rapidly and irreversibly oxidized upon treatment

with O₂ This is the second topic we have studied in chapter 4. We have investigated a relatively new generation of transfer hydrogenation catalysts (Cp*IrH(TsDPEN)) for their use as unconventional metal hydrides for oxygen reduction. The recent experimental studies supported that this kind of transfer hydrogenation catalysts could be effective for both the oxidation as well as for the reduction reaction.

The results presented in this chapter concern the hydrogenation process of the amido complex (Cp*Ir(TsDPEN-H)) followed by the reduction of dioxygen by Cp*IrH(TsDPEN) using DFT. All the results and the computational details about this study are reported in Chapter 5.

Chapter 1

Introduction

The selective oxidation of hydrocarbons by homogeneous, heterogeneous and enzymatic catalysis is of fundamental and industrial interest, because the use of hydrocarbons as feed-stock, both in nature and in laboratory synthesis, typically requires an oxidation step. A transition metal compound in turn mediates the oxidation step. Therefore, the progress with regards to the preparation of valuable product will be facilitated by a better mechanistic understanding of the oxidation process. The chlorine and transition metal oxides are used for this kind of selective oxidation, but there are problems due to environmentally hazardous by-products. On the other hand, the oxygen is a plentiful, inexpensive and highly reactive reagent. It, if properly controlled, can effect a variety of useful synthetic transformations. Reactions of hydrocarbons with oxygen are among the least energy-intensive functionalization reactions. Thus, the liquid phase oxidation of organic substrates using metal complexes as catalysts has become a profitable means of obtaining industrially important chemicals. Stimulated by success in the catalytic activation of other small molecules, an intensive effort has been made during past decades to activate molecular oxygen by transition metal complexes.

The ultimate goal of this work is to understand the interaction of dioxygen with transition metal complexes and to discuss the reactivity of coordinated oxygen. However the investigation of individual reaction steps contributes to the fundamental understanding of transition metal chemistry and should be valuable for the design of catalytic oxidation process and gives a general view of the catalytic strategies of selective aerobic oxidation.

1.1 Catalysts

In the study of a chemical reaction, two considerations are important. First of all it is important that: will the reaction proceed and if so how far? All the reaction must stop short of absolute completion: at what particular equilibrium positions will the system come to rest? All these questions can be answered by chemical thermodynamics. Secondly, how fast does the reaction go? How quickly will the reaction attain the equilibrium? The answers to these and related questions are the province of chemical kinetics. To design the chemical process both considerations matter. A system with large equilibrium constant has no value if the reaction rate is slow. The thermodynamics of the system will determine the maximum attainable yield of the products under the specific conditions. If the reaction is fast but the equilibrium constant is small, then a viable process can't result. In almost every case, economic factors require both favorable yields and rates.

The changes in Gibb's free energy G , enthalpy H , and entropy S depend only upon initial and final states of the system and not upon the reaction path. On the other hand, the chemical kinetics parameters, (activation energy E , order of reaction and rates coefficient k) depend sensitively on a reaction path. It is necessary to consider the reaction pathway, which is faster and reduces the activation energy. The introduction of a catalysed pathway changes not only the values of these parameters, but also their significance. With the development of theories of reaction rates it became clear that catalysts in general lower the activation energy of a reaction. A catalyst breaks down the normal forces which inhibit the reactions between molecules.

The concept of catalyst was introduced in the early of 19th century, it was noticed that a number of chemical reactions were effected by trace amounts of substances that were not consumed in the reaction. A *catalyst*, is a substance that enhances the rate at which a chemical system approaches equilibrium, it is not consumed. *Catalysis* is the phenomenon of a catalyst in action. The word catalyst comes from two Greek words, the prefix *cata-* meaning down, and the verb *lysin*, meaning to split or break. The concept of catalyst was first introduced by Berzelius [2]. He defined this concept as the ability of substances to awaken affinities, which are asleep at a particular temperature, by their mere presence and not by their own affinity. As a tool for reactions catalysis had been exploited much earlier. It has been applied for thousands of years in processes such as fermentation. The production of sulphuric acid is an interesting example. Russian chemist Gottlieb Sigismund Constantin Kirchhoff (1764-1833) studied the

behavior of starch in boiling water [3]. Under most circumstances, Kirchoff found, no change occurred when starch was simply boiled in water. But adding just a few drops of concentrated sulfuric acid to the boiling water had a profound effect on the starch. In very little time, the starch broke down to form the simple sugar known as glucose. When Kirchoff found that the sulfuric acid remained unchanged at the completion of the experiment, he concluded that it had simply played a helping role in the conversion of starch to sugar [3].

At the end of the 18th century and beginning of 19th many scientists studied the influence of metals and oxides on the decomposition of several substances. Humphry Devy discovered that the oxidation of coal gas is catalyzed by platinum and palladium was also active, whereas copper, silver and gold did not show any catalytic activity [4]. Regarding surfaces, Faraday proposed that the reactants have to adsorb simultaneously, but he did not explain the catalytic action. Also Berzelius did not give the explanation, but he nicely generalized many results in a simple way. Subsequently, Ostwald gave the definition that: *A catalyst is a substance that increases the rate of a chemical reaction, without being consumed or produced by the reaction or does not influence the thermodynamic equilibrium of reactants and products.* [5].

The catalyst only has a kinetic effect. It accelerates a reaction that is thermodynamically possible. It increases the reaction rates, because it generates new reaction routes (different transition states), which have lower activation energies. This can be observed in the energy profile diagram (Figure 1.1). From Figure 1.1 it is clear that, the net free energy of a reaction is the same whether a catalyst is used or not. The chemical nature of catalysts is as diverse as catalysts themselves. Proton acids are probably the most widely used catalysts. Zeolites and alumina are also used as catalysts. Transition metal complexes are used to catalyse the hydrogenation and oxidation.

Catalysis reactions are usually categorized as either homogeneous or heterogeneous reactions. A heterogeneous catalysis reaction is one in which the catalyst is in a different phase from the substances on which it acts. In a catalytic converter, for example, the catalyst is a solid, usually a precious metal such as platinum or rhodium. The substances on which the catalyst acts, however, are gases, such as nitrogen(II) oxide and other gaseous products of combustion. A homogeneous catalysis reaction is one in which both the catalyst and the substances on which it works are all in the same phase (solid, liquid, or gas). The reaction studied by Kirchoff is an example of a homogeneous catalysis. Both the sulfuric acid and the starch were in the same phase a water solution during the reaction [3].

Some of the most interesting and important catalysts are those that occur in living systems:

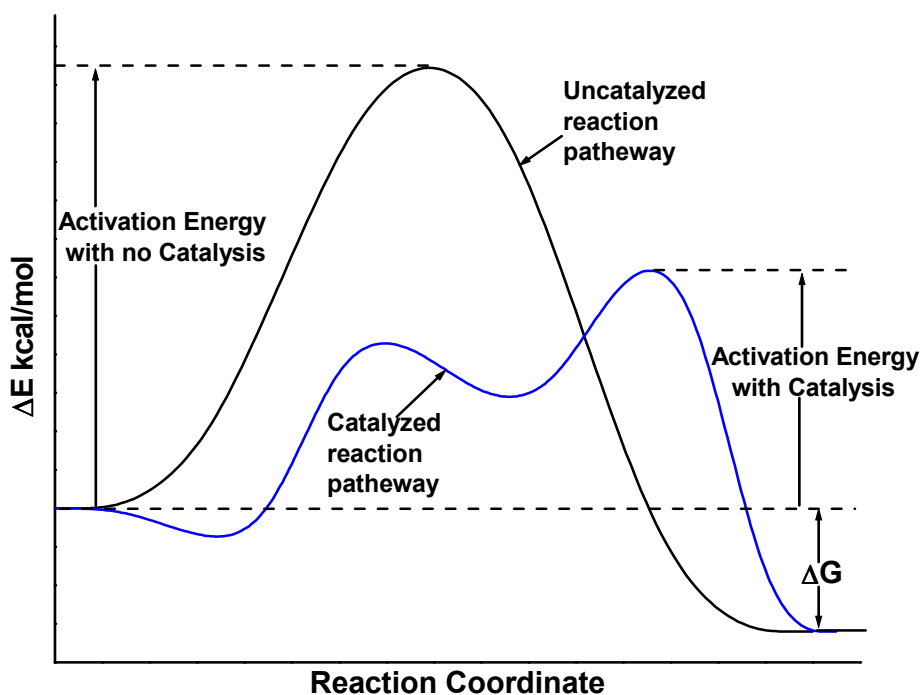


Figure 1.1: Potential energy profile for an exothermic reaction, showing the lower activation energy of the catalysed reaction.

the enzymes. All of the reactions that take place within living bodies occur naturally, whether or not a catalyst is present. But they take place so slowly on their own that they are of no value to the survival of an organism. For example, if you place a sugar cube in a glass of water, it eventually breaks down into simpler molecules with the release of energy. But that process might take years. A person who ate a sugar cube and had to wait that long for the energy to be released in the body would die. Fortunately, our bodies contain catalysts (enzymes) that speed up such reactions. They make it possible for the energy stored in sugar molecules to be released in a matter of minutes.

1.2 Homogeneous Catalysis

Homogeneous catalysis is among the most important areas of contemporary chemistry and chemical technology. Homogeneous catalysis received attention after the discovery of “oxosynthesis” by Otto Rolen in 1938 [6]. Historically, heterogeneous catalysis is more popular than homogeneous catalysis. However, homogeneous catalysis has many advantages compared

to heterogeneous catalysis:

- The activity and selectivity is high.
- No diffusion problem.
- Mild reaction conditions.
- The probability of catalyst poisoning is low.
- The electronic and steric properties of the catalysts can be varied.

The challenge of homogeneous catalysis is solving the problem of separating the reactants, the catalyst, and the reaction products (which are all in the same phase). Homogeneous catalysis occurs in solution and involves soluble transition metal complexes. A tremendous amount of research work and application effort were done for the development of homogeneous catalysis.

1.2.1 Historical Notes

The metallo-enzymes are the oldest catalysts in homogeneous catalysis, as examples, iron porphyrin active for oxidation, nickel complexes in hydrogenase enzymes for hydrogen activation, etc [7]. The making of sulfuric acid via “lead chamber process” (1750) is a very old catalytic process, in this process the nitrogen oxidise oxides sulfur dioxide to the trioxides and nitrogen oxides is reoxidised by air to nitrogen dioxide [7]. Again NO_2 reoxidised by air. Here, NO/NO_2 , are the catalysts and since they all reside in the gas-phase, this should be called homogeneous catalysis[7]. In the nineteen twenties mercury sulfate was used for the conversion of acetylene to acetaldehyde [7]. This was the first industrially applied catalyst working in solution [7]. It can be said that, this process is the predecessor of the Wacker chemistry, where oxygen was used for conversion of ethylene to acetaldehyde in water in the presence of a tetrachloropalladate catalyst [8, 9].

The oligomerization of ethene was another major process in the fifties, but in the homogeneous catalyzed processes remained low in the sixties. From the seventies usage of homogeneous catalysis has been increasing with the success of rhodium catalyzed carbonylation of methanol (Monsanto) [10], rhodium catalysed hydroformylation (Wilkinson’s) [11], asymmetric hydrogenation to L-DOPA (Monsanto) [12], and ring-opening polymerization of cyclohexene using tungsten metathesis catalysts (Huels) [7].

Before the nineties most of the homogeneous processes were developed for bulk chemical products. From the beginning of nineties the development of fine chemical products took off and a large academic effort had been set up for the development of homogeneous catalysis.

1.2.2 Homogeneous Catalysts

It was mentioned earlier that, the homogeneous catalysis has lots of advantages compared to the heterogeneous catalysis. Homogeneous catalysis is becoming increasingly respectable, showing in the real worlds of the chemical and petroleum industries. The goals of green chemistry are a synonym to environmentally benign chemicals and processes, including sustainable development. These goals are afforded by homogeneous catalysis and most of the contribution to “Green Chemistry” comes from the homogeneous catalysis.

The catalysts used in homogeneous catalysis are basically acid-base catalysts. The classical and transition metal catalysts are containing one metal atom surrounded by a number of attached atoms or groups which are commonly referred to as ligands [13]. Modern homogeneous catalysis comprises more than the development of catalysts and catalyst-ligand systems. Their interplay governs decisively the activity, productivity, and selectivity of the catalytic system. The proper choice of tailor-made and fine tuned ligands may change considerably the behavior of the catalytic system. Depending on the nature of the ligands and on the desired product distribution, nearly all grades of combinations of activity \rightleftharpoons productivity \rightleftharpoons selectivity may be chosen [14]. The construction of combinations of central atoms and ligands depends on thermodynamic considerations and is the foundation of mechanistic studies.

Transition metal complexes deserve the special attention for their versatility. Now the question is why the transition metal complexes, as examples, the metal complexes with ligands such as phosphines, hydrides or amines are catalyzing reactions and accelerate the breaking and forming of chemical bonds without being consumed in the process. There are several reasons [15]. First of all, the reactivity of any molecule with the functional group depends on the coordination with the metal center and there is a possibility that it could be changed dramatically [14]. Secondly, there is a possibility to enhance the probability of a reaction if two molecules coordinate to the same metal center [14, 15]. Thirdly, highly reactive species can be stabilized and react further in a controlled and productive way [14, 15]. Lastly, the presence of a ligand can control the selectivity transformation [14, 15].

On the other hand, there are some drawbacks. All these kinds of catalysts are very sensitive. Some times these kinds of catalysts make the reaction pathways much more difficult to understand. It is established that most catalytic reactions can be described using a finite number of elementary steps and can be explained with the help of kinetic and structural information. Development work in the area of transition metal catalyzed reactions is a manifold and comprises support of running processes and improvement of their feedstock base, as well as the search for new applications. There are lots of challenges in the development of homogeneous catalysis. The selective oxidation chemistry remains one of the foremost challenges in the chemical industry. Over the past decade numerous schemes have been reported regarding selective oxidation, but their scope was limited. The recent development of “Chemical oxidase” methods represents an attractive alternative strategy for the development of selective aerobic oxidation methods. In the following sections will shed light upon the electronic structure of dioxygen, problem regarding the reaction with dioxygen and dioxygen reactions with transition metal complexes.

1.3 Activation of Dioxygen

It was mentioned earlier that, for economic and environmental reasons, the oxidation processes of bulk chemical industries predominantly involve the usage of molecular oxygen as the primary oxidant. Their success depends largely on the use of metal catalysts to promote both the rate of reaction and the selectivity to partial oxidation products. It was also mentioned that, the traditional methods of many fine chemical oxidations involve stoichiometric quantities of toxic inorganic reagents. These reactions generate large amounts of inorganic salt-containing effluent along with the target products. A clean synthetic technology should proceed by minimizing the cost of waste disposal [16]. An ideal catalyst for dioxygen (O_2) oxidations would be selective, useful for tackling a variety of substrates and chemical structures, reasonably fast, and stable [17]. Thus, the current goal of the research and industry is the development of effective metal catalysts that can activate the molecular oxygen at ambient conditions. Several books and review articles have appeared, which are wholly or partly devoted to the metal-catalyzed aerobic oxidations [18-22]. In the following we will discuss the chemistry of electronic states of oxygen, and the problems in selective oxidation.

1.3.1 Electronic Structure of Oxygen

The molecule of oxygen in its ground state has two unpaired electrons. The chemistry of molecular oxygen is dominated by the fact that it is a biradical. In Fig 1.2, it's explained the energy level diagram of O_2 due to interaction of s and p orbitals. From Fig 1.2 it is clear that the two lowest lying orbitals result due to the interaction of the 2s orbitals and

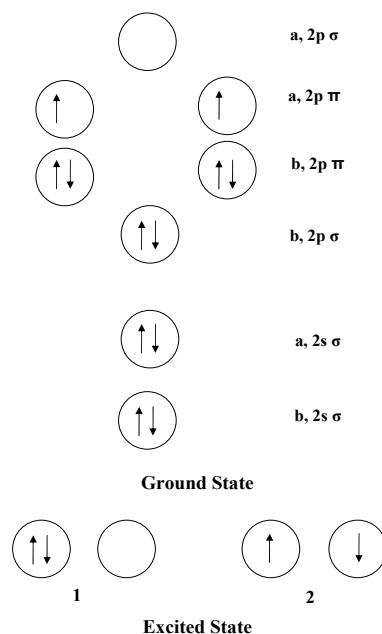


Figure 1.2: Molecular orbital scheme: Electronic structure of O_2 .

the $2p\sigma(b)$ and $2p\sigma(a)$ orbitals arise due to the interaction of the two p orbitals directed along the internuclear axis [23]. The four remaining orbitals arise from overlap of the two p orbitals, directed perpendicular to the internuclear axis. Those orbitals are called π orbitals. In molecular oxygen each oxygen atom contributes 6 valence electrons and the double degenerate $2p\pi(a)$ orbitals are only half-filled. They lead to higher energies due to the greater electron-electron repulsion and they correspond to the excited states of the molecular oxygen. It is depicted in Fig 1.2 that the number of bonding electrons are more than number of antibonding electrons. The electronic configurations of $2p\pi(a)$ in excited states are also depicted in Fig 1.2. and the spins are opposed for each and thus the arrangements (1) and (2) represent singlet states. The total orbital angular momentum quantum number is 2 for configuration (1) and for configuration (2) it is zero. Usually $^1\Delta$ and $^1\Sigma$ are the notations for configurations (1) and (2), respectively. The $^1\Delta$ state lies 23.4 kcal above the ground state ($^3\Sigma$ is the notation for

ground state), and the $^1\Sigma$ lies 37.5 kcal above it (1) [23]. The spin state change takes place from $^1\Sigma$ or $^1\Delta$ level to the $^3\Sigma$ (ground state) in some reactions. The life time of the excited molecules in solution or in gas phase at ordinary pressure depends on the collisions [23]. In such collisions there is then the possibility that the active species will undergo reaction.

1.3.2 Dioxygen for Selective Oxidation

It was mentioned that molecular oxygen possess triplet ground state and is diradical in nature, whereas almost everything else possesses a singlet ground state. Due to the difference in the ground state electronic structure and low activation barriers the chemical reactivity is spin forbidden. There are some problems regarding the dioxygen activation. For the diradical nature of dioxygen, once it is activated, then it is tough to control its reaction with organic substrates. This uncontrollable reaction leads to formation of highly reactive and nonselective intermediates and radical-chain processes [24]. Such oxidations are thermodynamically unstable and exothermic in nature, which leads to decreases in selectivity. On the other hand dioxygen is the most abundant, inexpensive, energy-efficient and environmentally compatible oxidant. For all these reason the dioxygen activation is a challenge. The design of homogeneous catalysts for both activation and selective use of O_2 is an extraordinarily tough task. Dioxygen has four oxidizing electron equivalents and in some reactions molecular oxygen partially reduces to peroxides or other reduced species that are more active and selective than molecular oxygen [25, 26]. Many extremely useful homogeneous systems catalyse the selective reactions of reduced oxygen compounds [27]. Sometimes electrons are coming from the target substrate for the reductive activation of O_2 , such an example is the epoxidation of alkenes by O_2 alone, catalysed by a ruthenium-porphyrin [28]. In this reaction, due to the presence of porphyrin ligand, a key intermediate $RuOORu$ is forming, which subsequently forms $Ru(IV)=O$ and $O=Ru(VI)=O$, but not $RuORu$. These kind of metal-oxygen-metal species are usually structuraly and kinetically dead-end species in homogeneous catalysed oxidations. Ruthenium and other metal-oxo ($M=O$) species can participate in nonradical and highly selective reactions [24]. The rates and selectivity of $M=O$ can be changed by changing the ligand on the metal center.

Ideally a catalyst must be stable, but in reality, most of the catalysts, from enzymes to synthetic metal complexes are subject to degradation during reactions including the heterogeneous metal oxide surfaces [24]. Most of the homogeneous oxidation catalysts are vulnerable due to

the presence of organic ligands that are thermodynamically unstable under operating conditions. The instability problems of soluble oxidation catalysts have been solved by using particular derivatives of polyoxometalates [29, 30, 31, 32], where the derivatives are defect structures containing several oxygen atoms with some metal ions [32]. Neumann and Dahan have used a sterically hindered Ru-containing polyoxometalate, $([WZnRu_2(OH)(H_2O)](ZnW_9O_{34})_2)^{11-}$ [33], which is preventing the formation of dead-end metal-oxygen-metal species, but this polyoxometalate devoids of organic structure [24].

Now the question is how to achieve broader applicability, faster reaction rates and compatibility with a range of reaction conditions. In the following section we describe the recent advances in selective aerobic oxidation using transition metal complexes as a catalysts to encounter all these problems.

1.4 Reactions with Transition Metal Complex

The reactions between transition metal complex and oxygen are very interesting. One transition metal ion can differ from another quite dramatically in chemistry so that the reaction of each transition metal ion reducing agent with oxygen has some distinctive and unusual feature. Now the questions concern how the dioxygen reacts with transition metal complexes or what factors determine the particular reaction path that the system chooses. Any reaction of the type to be considered here begins with the interaction of an organometallic compound with O_2 . This may lead to the formation of a dioxygen complex. In this section we will discuss the available results. Several books and review articles have appeared, which are wholly or partly devoted to the transition metal catalyzed aerobic oxidations. In this section we will discuss the selective oxidation of the metal-hydride bond and also the dioxygen reaction with the early transition metals and hydrogen transfer catalysts.

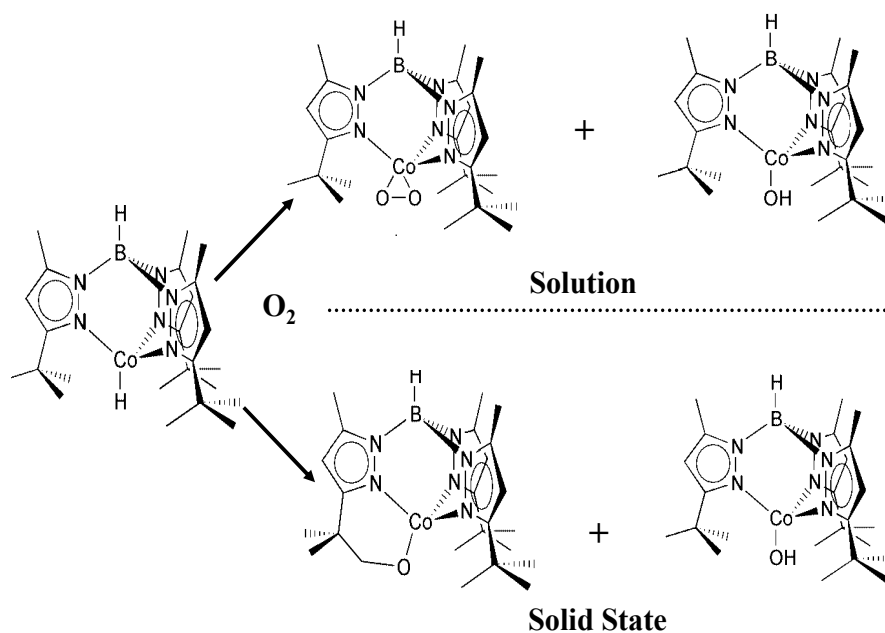
1.4.1 Selective Oxidation

The selective catalytic oxidation using inexpensive and environmentally friendly oxidants is of immense interest to the chemical community and of great potential benefit to the world economy and ecology. There are lots of examples regarding the oxidative addition of alkenes C-H

bonds to transition metal species for the fictionalization of the metal alkyl hydride products [34, 35, 36]. On the other hand, a clean and cheap oxidant such as air (oxygen) is required for the development of a commercially viable oxidation process [37, 38]. However, it is not clear how the transition metal complexes activate the molecular oxygen, due to this problem the effective utilization of this reagent in selective oxidation reactions has been limited. Recently few papers have reported about the selective oxidation of the metal-hydride bond using molecular oxygen. In this section we will discuss about the recent developments in this area. Earlier, it was mentioned that, oxygen constitutes the quintessential terminal oxidant, because the reagent is available at virtually no cost and produces no environmentally hazardous by-products. There are some challenges regarding the activation of molecular oxygen. The challenges are over oxidation of the starting material ('combustion') or spin constraints in these typically spin-forbidden processes. In recent years, some efforts are going on to solve these problems.

A limited number of reports have described the selective oxidation of the metal-hydride bond using O_2 . There are some early examples, regarding, the insertion of O_2 into transition metal-hydrides to form a hydroperoxo complexes for a small number of organometallic and coordination compounds of Co(III), Rh(III), Ir(III), and Pt(II) [39-45]. Mechanisms of metal deprotonation are followed by oxygen binding and protonation [42, 44], whereas radical chain pathways involve hydrogen radical abstraction from the metal hydride [43, 45]. Recently, Goldberg and coworkers have reported that, a Pt(IV) dialkyl hydride complex reacts cleanly with dioxygen to produce a dialkyl Pt(IV) hydroperoxide species [46]. This is the first report about the reaction between a transition metal alkyl hydride and dioxygen. A solution of Pt(IV) complex $Tp^{Me_2}PtMe_2H$ (1, Tp^{Me_2} = hydridotris(3,5-dimethylpyrazolyl)borate) in C_6D_6 exposed to dioxygen at ambient temperature and it will produce the hydroperoxo Pt(IV) species, $Tp^{Me_2}PtMe_2(OOH)$. The experimental result supported that, this reaction occurs by a radical chain mechanism.

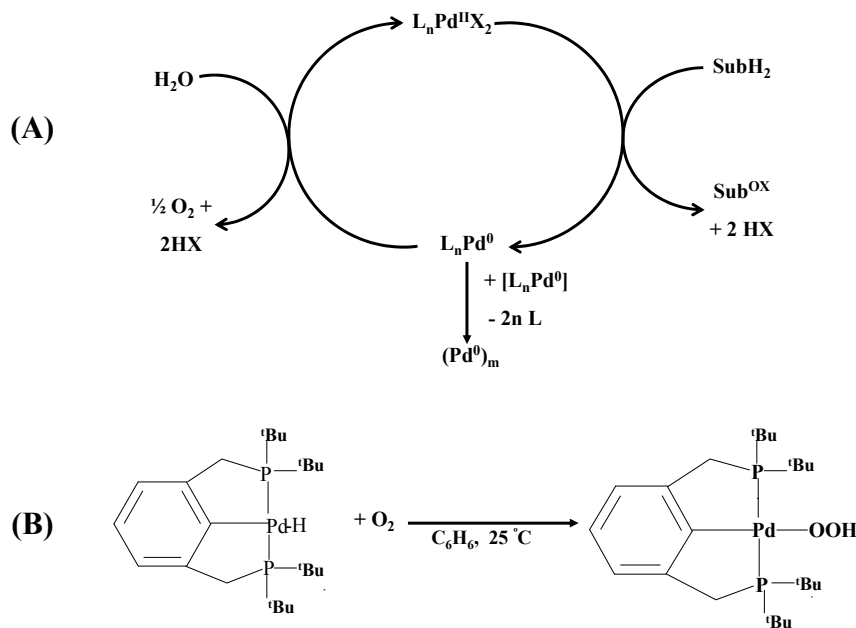
In another example, Theopold and coworkers also described the reaction between $Tp^{t-Bu,Me}Co-H$ and O_2 at room temperature [47]. The authors reported that, exposure of a C_6D_6 solution of $Tp^{t-Bu,Me}Co-H$ to an excess of O_2 gas at room temperature caused a rapid reaction that yielded only the known complexes $Tp^{t-Bu,Me}Co(O_2)$ and $Tp^{t-Bu,Me}Co-OH$ in approximately equal amounts (Scheme 1.1). The experimental observation supported that the formation of a reactive hydroperoxide intermediate. The authors proposed that, the hydroperoxide intermediate is formed due to a migratory insertion of bound O_2 into the



Scheme 1.1: Reaction of $Tp^{t-Bu,Me}$ Co-H with O_2 proceeds via cobalt(II) hydroperoxide intermediate.

metal-hydrogen bond. The experimental observation ruled out any radical chain mechanism.

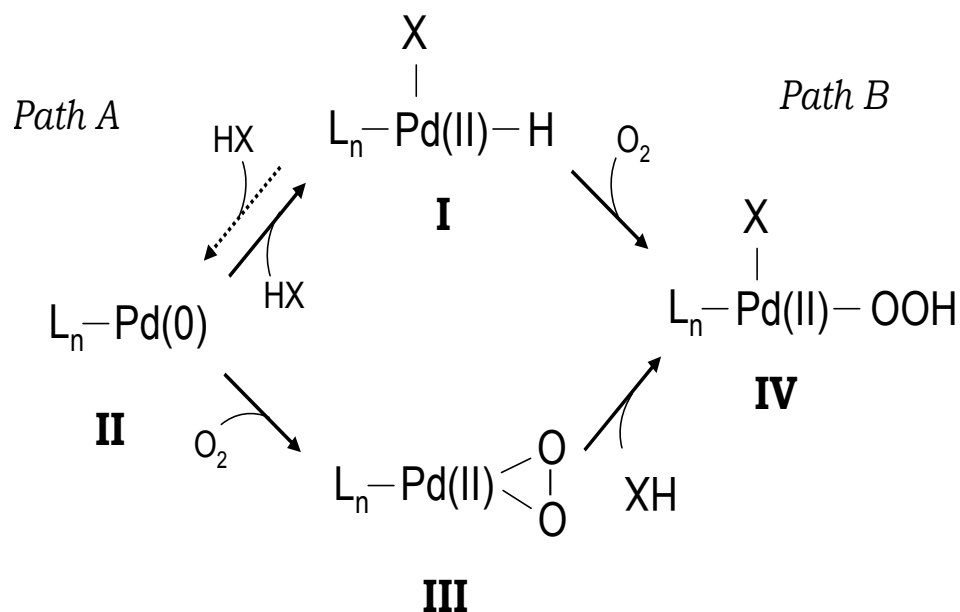
Recent progress about the palladium catalysts for selective aerobic oxidation has emphasized the importance of developing a thorough comprehension of reactions between palladium complexes and molecular oxygen [48, 49, 50]. Still there are several questions unresolved, such as how to insert the molecular oxygen into metal-hydride bond or the interaction of molecular oxygen with metal(0) complexes. Stahl and co-workers have proposed that the reaction pathway for oxygen activation in palladium-catalyzed oxidations, is the reaction of palladium(0) with oxygen to form (η^2 -peroxo)palladium species, with experimental support, even if the reaction between Pd(0) and triplet oxygen is spin forbidden (Scheme 1.2(A)) [49, 50, 51, 52]. Also, there are some other reports about the insertion of molecular oxygen into the metal-hydride bond [46, 47, 52, 53, 54, 57, 58]. Goldberg and co-workers have reported the first direct observation of the insertion of molecular oxygen into a palladium(II) hydride bond, to form an (η^1 -hydroperoxo)palladium(II) complex (Scheme 1.2(B)) [58]. The reaction was unaffected by radical inhibitors and light. It has a second-order reaction rate that is, first-order in palladium and first-order in oxygen, and was documented that the Pd-H bond cleavage is the



Scheme 1.2: (A) Simplified catalytic cycle for palladium-catalyzed aerobic oxidation reaction. (B) Insertion of O_2 into metal-hydride bond.

rate-determining step [58]. There are few papers, which have demonstrated density functional theory investigation about the insertion mechanism [57, 59], but still now, there are questions remain to be answered.

There are two proposed pathways to explain how dioxygen activation in palladium-catalyzed oxidation proceeds (Scheme 1.3). In Scheme 1.3, oxygenation is considered as **Path A** and direct insertion of O_2 is considered as **Path B**. One of the first fundamental studies of a model Pd^0 complex based on catalyst was reported earlier by Bianchi *et al* at Enichem [60]. In recent years several studies have demonstrated fundamental insights into the reactions between molecular oxygen and Pd^0 complexes bearing catalytically relevant ligands [49, 61, 62]. It should be mentioned that, ligands can stabilize Pd^0 to prevent catalyst decomposition and promote efficient oxygenation of Pd^0 [48]. Landis, Stahl and coworkers have demonstrated a combined experimental and theoretical investigation about Pd(0) oxygenation for the same kind of system [62]. According to the theoretical investigation, the authors concluded that, this is an exothermic process and there is a spin-crossing between triplet and singlet surfaces due to the spin-orbit coupling [62]. The NHC-Pd⁰ complex $(IMes)_2Pd^0$, reacts with molecular

Scheme 1.3: Reaction of $[Pd(IMes)_2]$ complexes with O_2 .

oxygen (Scheme 1.2(A)) very rapidly in solution at very low temp ($-78^\circ C$) as well as in the solid state [49]. Also Yamashita and coworkers reported about the solid-state reaction with dioxygen for the related Pd^0 complex, $(ITmt)_2Pd^0$ [63]. Landis, Stahl, and coworkers performed a computational study in order to probe electronic structural issues in the Pd^0 oxygenation reaction [64]. The authors concluded that triplet dioxygen initially approaches the palladium center with an end-on trajectory and charge is transferred from Pd^0 to O_2 resulting in the formation of a triplet biradical η^1 -superoxopalladium(I) species (Scheme 1.2 (A)) [57, 64]. The energy difference between singlet and triplet surfaces is very small (3 kcal/mol), because dioxygen is coordinating with the metal center and this reduces the electronic exchange interaction between the unpaired spins [61]. Due to the small distance between palladium-oxygen, triplet-singlet spin crossover occurs in order to enable the formation of the second Pd-O bond. Landis and collaborators have concluded that, intersystem crossing will have little influence on the rate of the overall reaction [62]. From the above discussion it can be suggested that direct addition of O_2 to a Pd^0 center can be extremely facile.

Both pathways were considered viable by Stahl and coworkers in their investigation of the conversion of a new class of N-Heterocyclic carbenes (NHCs) coordinated palladium(II)-hydride

complex into corresponding palladium(II)-hydroperoxides complex (Scheme 1.3) [52]. In that study, they have examined the three different carboxylic acids (acetic, benzoic, p-nitrobenzoic) in order to understand the ability of the carboxylic acids to catalyze the oxygenation of Pd^{II}-hydride [52]. The experimental observation indicated that, the oxygenation process of the p-nitrobenzoic acid is faster than the other two possibilities and that carboxylic acids can enhance the stability of the catalyst [52]. Popp and Stahl have theoretically investigated the four possible alternative pathways for insertion of dioxygen into the Pd-H bond [65], but still many questions remain to be answered.

However till today, neither the lighter congener of Pd and Pt, *i.e.*, nickel hydride derivatives nor Fe-based compounds have been examined. Recently, Schlange and Schwarz have examined the thermal reactions of molecular oxygen with structurally rather simple transition metal hydride cations $[M(H)(OH)]^+$ (M = Ni, Fe, Co) in the gas phase [66]. In this report the authors stated that the insertion of molecular oxygen in a metal-hydride bond and dissociation of the resulting metal hydroperoxide intermediate(s) are facile gas-phase processes for the late transition metal cation complexes $[M(H)(OH)]^+$, with M = Fe, Co, Ni. On the other hand, for the diatomic $[MH]^+$ species, with M = Fe, Co, Ni, Pd, and Pt, the analogous reactions are rather inefficient. However, the reactivity can be recovered by the addition of an inert H_2O ligand to a metal(II) hydride, as in $[M(H)(H_2O)]^+$ (M = Fe, Co, Ni) [66].

Considering all examples mentioned above, still now many questions concerning the mechanistic details of the Pd-catalyzed oxidation reactions are open. In the framework of an extended project the aim of this work is to explain the mechanistic details of the selective oxidation of organic molecules by molecular oxygen in the presence of a metal catalyst. Here in this thesis we have presented a detailed DFT investigation of the direct insertion mechanism of molecular oxygen into the metal-hydride bond of different kinds of Pd-complexes. Taking into account the kinetic measurements and rate determining steps, we have considered both pathways demonstrated by Stah and coworkers [13] in order to explain some of the unsolved problems regarding the mechanism of the oxygenation process of the Pd-hydride complex.

1.4.2 Early Transition Metals

The long-standing question is how does dioxygen bind and activates at metal centers in early transition metals systems? There are several reports of dioxygen-metal complexes that have

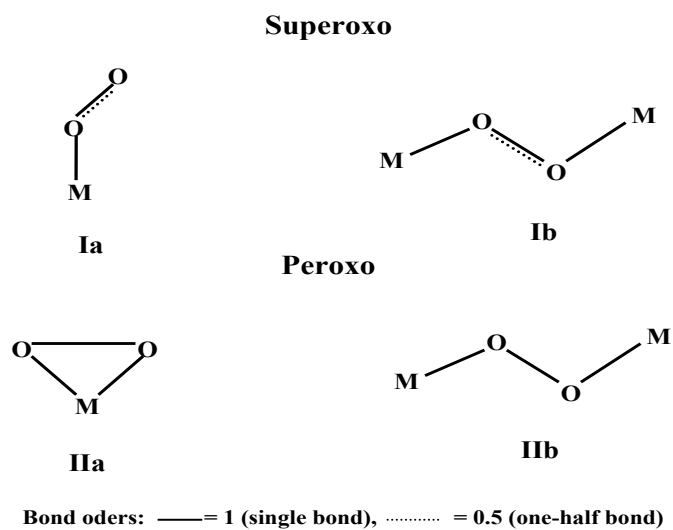
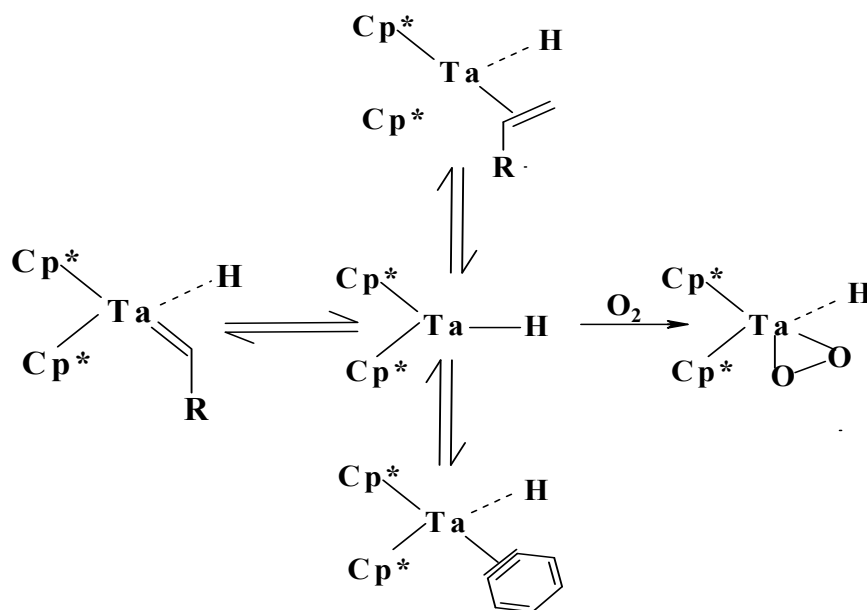


Figure 1.3: Principal types of presently known metal-dioxygen geometries.

appeared in the recent years. Nearly all currently known O_2 -metal compounds can conveniently be divided into two types according to the characteristics of the dioxygen ligand: superoxo (I) and peroxy (II) complexes (Fig 1.3). The coordinated O_2 shows, or at least strongly tends to show, a *constant state* in either class of compounds [67]. All these two class complexes can be categorized in according to whether the dioxygen ligand is coordinated to one or two metal atoms. The principal M-O bonding properties of the four subclasses, relevant to this interpretative summary, are evident from Fig 1.3. In the next few paragraphs we will discuss the reaction with early transition metal systems.

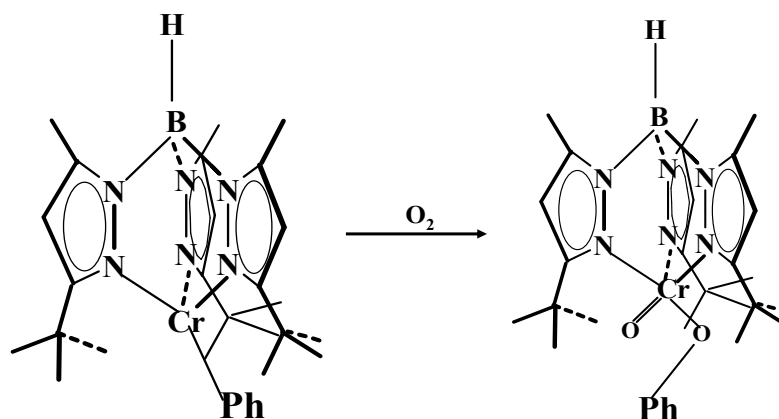
In the above discussion it was mentioned the kind of compounds that will form after the reaction of the transition metal with O_2 . All these compounds are more or less stable dioxygen complexes. These metals are electropositive and oxophilic in nature, due to that all their complexes will resist the transfer of oxygen atoms to carbon, up to and including release of oxygenated products. Asselt *et al* reported about this kind of transformation of stable peroxy alkyl complexes of the type $Cp_2^*Ta(\eta^2 - O_2)R$ (R= Me, Et, Pr, Bn, Ph) (Scheme 1.4) [68]. In this reaction O_2 presumably oxidatively adds to the 16-electron fragments Cp_2^*TaR , which are in rapid equilibrium with the 18-electron olefin hydrides or alkylidene hydrides [69]. According to the X-ray diffraction observation the O-O bond distance is 1.48\AA and the stretching frequency is $\nu_{O-O} = 863\text{cm}^{-1}$, which are consistent with peroxy ligand (O_2^{2-}), where tantalum



Scheme 1.4: Formation of a tantalum peroxy complex

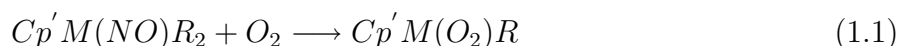
is in the highest possible formal oxidation state (+V) [69]. In the presence of triethylamine $Cp_2^*Ta(\eta^2-O_2)Me$ is a very stable complex, which confirms that the presence of a base will increase stability. The reaction of chromium complexes with molecular oxygen is more interesting, an example is the reaction of the divalent chromium phenyl complex $Tp^{tBu,Me}CrPh$ ($Tp^{tBu,Me}$ = hydrotris(3-tert-butyl-5-methylpyrazolyl)borate) with O_2 [3]. The end product of this reaction results from the insertion of O_2 into the Cr-C bond [3]. The experimental observation indicated that, the product is chromium(III) superoxide complex (Scheme 1.5) [3, 71]. This chromium(III) superoxide complex has been assigned an unusual “side-on” (η_2) coordination [71], while most of the superoxo complexes have been assigned a “bent, end-on” coordination mode [72]. There are other examples of superoxide complexes which are structurally characterized, including $Tp^{tBu,Me}Cr(\eta^2-O_2)Cl$ and $Tp^{tBu,Me}Cr(pz')(\eta^2-O_2)$ [71, 69]. In all cases the metals are not in the highest oxidation state. From the above discussion it is clear that, the organometallic derivatives of early transition metals can and will form the dioxygen complexes and the stability of these complexes varies widely. This is because binding of O_2 depends on some degree of electron transfer.

There are many examples, where organometallic compounds containing oxygen as ligand after the reaction with O_2 [73, 74, 75]. Legzdins *et. al.* have described the formation of oxo alkyls

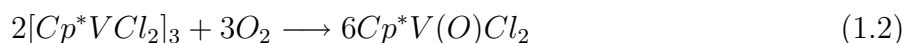


Scheme 1.5: Formation of a chromium phenyl superoxo intermediate and a stable analog thereof.

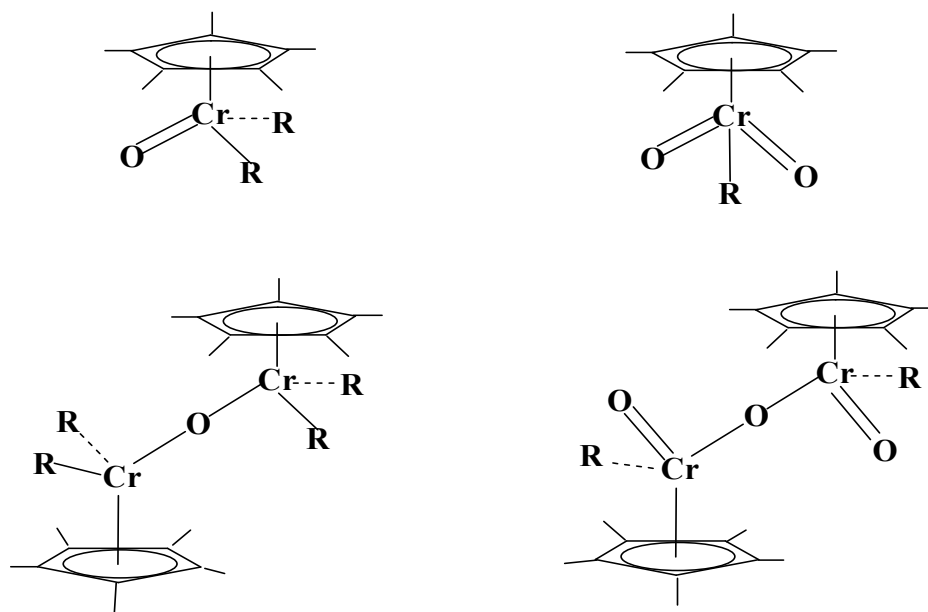
of tungsten and molybdenum in moderate yields according to Eqn. 1.1 [74, 75].



where, $Cp' = Cp$ or Cp^* , $M = Mo$ or W , $R = Me, Np, Bn, CH_2SiMe_3, CH_2CMe_2Ph$. Paramagnetic chromium alkyls in the +II and +III oxidation states have been reacted with O_2 . For example, treatment of $Cp^*Cr(py)Me_2$ [76] or $[Cp^*Cr(\mu - Me)]_2$ [77] yielded a set of oxo alkyls ranging in oxidation state from +IV to +VI (Scheme 1.6). All these alkyl complexes are very rich in electrons, and they react very fast with O_2 . Bottomley [78] and Doherty [79] reported independently about the unusual reaction of metal(III) halides with O_2 (Eqn. 1,2).



In all these reactions, the activation of dioxygen by these organometallic compounds generates high valent metal oxo compounds. All these metal oxo complexes may undergo oxygen atom transfer reaction with organic substrates, which are useful as catalysts for aerobic oxidations. The reactions between O_2 and the early metal alkyls in high oxidation states are quite interesting. From the early examples, the oxygenation of alkylzirconium(IV) complexes of the

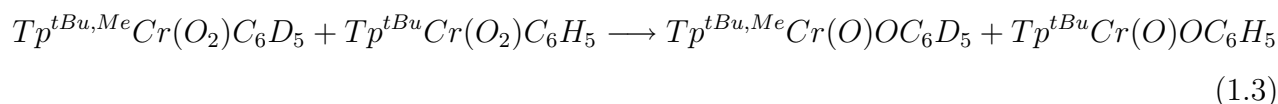


Scheme 1.6: Various chromium oxo alkyls

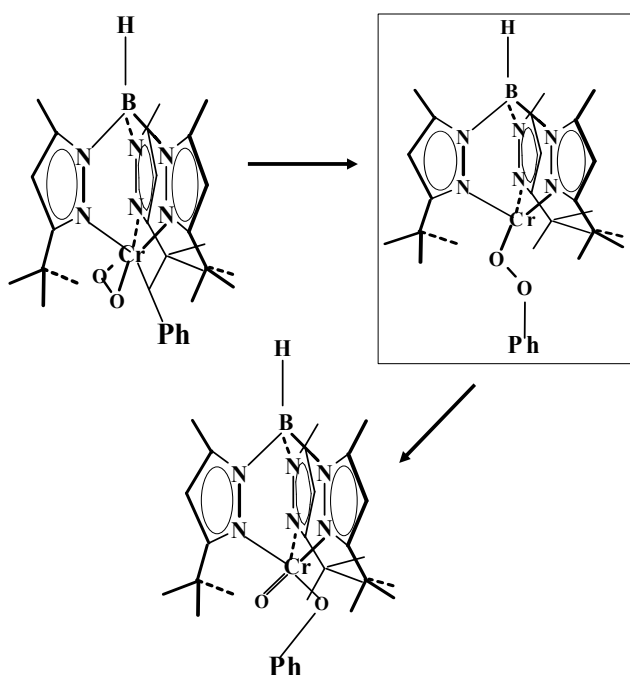
type $Cp_2Zr(R)Cl$, is one yielding the corresponding alkoxides $Cp_2Zr(OR)Cl$, which can be hydrolyzed to the alcohols [80] and Cp_2ZrR_2 is another example of similar autoxidations [81]. Lubben and Wolczanski have investigated the reactions of a series of alkoxy alkyls of group 4 ($M = Ti, Zr, Hf$) with O_2 [82]. Crossover experiments demonstrated scrambling of the methyl groups between metal atoms during the oxygenation, and various other observations indicated the occurrence of a radical chain process [83, 84]. Despite the radical character of the autoxidations, they may exhibit some selectivity [85]. There are two modes of reactivity of early transition metal alkyls with O_2 . When the metal is not in its highest oxidation state, then the molecular oxygen complex of variable stability may form and the metal-carbon bond may or may not involve its subsequent reaction. On the other hand, d^0 -alkyls will react with O_2 through a radical chain mechanism that invariably leads to formation of alkoxide complexes. As mentioned above the initial reaction between the early transition metal and molecular oxygen may produce a variety of complexes, like superoxo (O_2^-), peroxy (O_2^{2-}), oxo (O^{2-}) ligands. Further transformations, such as insertion reactions or oxygen atom transfer could be possible due to the presence of these functional groups in the complexes. We will further discuss about such a possibility.

There are very few examples about the migratory insertion of a coordinated O_2 . Earlier it

was mentioned that, $Cp_2^*Ta(\eta_2 - O_2)Me$ is a very stable compound in the presence of triethylamine. This complex will transform to $Cp_2^*Ta(O)OMe$ in solution in the absence of any base. This is an example of a reaction where migratory insertion of a coordinated O_2 into a metal alkyl bond takes place. Chromium complex is another probable candidate for an O_2 insertion (Eqn. 1.3).



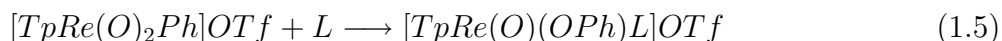
As it was mentioned above, the initial reaction of chromium complexes with O_2 may produce a superoxo (O_2) complex. Furthermore, there is a possibility of transformation such as insertion reactions or oxygen atom transfer. The final product of the above reaction is $Tp^{tBu,Me}Cr(O)OPh$ [3]. It means that, $Tp^{tBu,Me}Cr(O_2)Ph$ has been transformed into the paramagnetic oxo alkoxide $Tp^{tBu,Me}Cr(O)OPh$ (Scheme 1.6) [3]. This reaction proceeds at below room temperature. Now the question is: how is the reaction proceeding? There are two



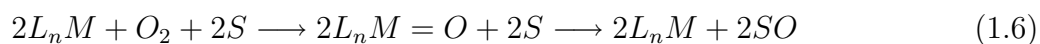
Scheme 1.7: Intermediate O_2 insertion into chromium phenyl bond yield oxo alkoxide.

possibilities: (1) homolytic reaction and (2) the transformation would be oxidative addition of O_2 to chromium, yielding $Tp^{tBu,Me}Cr(O)_2Ph$, followed by an insertion of an oxo ligand. The authors also examined a radical chain process with the help of a crossover experiment [3]. The

experimental observation did not establish the radical chain process. This example indicates the feasibility of the insertion of coordinated O_2 into early transition metal alkyls. It can be concluded that the strong stabilization of the higher oxidation states of this oxophilic metal by oxygen π -donors and the degree of charge transfer depend on the nature of the ligands [71].



where, (L = Py, Me_2SO). The insertion of a metal bound oxo group into a metal-carbon is an important step for the oxygenation of organic molecules (Eqn. 1.4) [69]. The number of examples regarding the early transition metals is limited. Brown and Mayer have reported about the thermal insertion of an oxo group into a rhenium phenyl bond (Eqn. 1.5) [86]. This transformation is happening due to the high electrophilicity of the oxo ligands in the cationic Re(VII) precursor. On the other hand, this kind of transformation is not happening for early transition metals, due to the large kinetic barrier.



Intermolecular oxygen atom transfer from a metal complex to an organic substrate is an important reaction step in oxidation catalysis (Eqn. 1.6) [69]. The high electrophilicity of the complex and the weak metal-oxo bonds are facilitating the transfer of metal bound oxo ligands. The presence of the electron-withdrawing ligands will enhance the intermolecular transfer of the oxygen atom. Also the high oxidation state of the first-row transition metals facilitates the intermolecular transfer of the oxygen atom. Chromium complexes are an example for the intermolecular oxygen atom transfer. Chromium complexes are very useful for a stoichiometric and catalytic oxidants [87]. Leelasubcharoen *et. al.* have reported in detail about the reaction of cyclopentadienyl chromium(III) chlorides with O_2 to form the corresponding Cr(V) oxo derivatives $Cp'Cr(O)Cl_2$ ($Cp' = Cp^*$, Cp, Cp^{TMS}) [69].

One of the interesting features of these reactions is that, the reactants and products have different spin states, which indicates that these oxygen atom transfer reactions are an example of “two state reactivity” [16, 89, 68, 91]. Due to the two state reactivity, there is crossing in the potential energy surface (PES). The crossing between the energy surfaces is called “minimum energy crossing point” (MECP). In the next chapter we will discuss about MECP. Furthermore, there is obviously a tradeoff between the rate of the reaction of the reduced form of the catalyst with O_2 and the reactivity of the oxidized form with organic substrates. However,

appropriate ligand design may solve all of these problems.

Considering the potential utility of catalytic oxidations, and the need for a better understanding of the fundamental reaction steps involved, in this work we have explained the reaction mechanism of the divalent chromium phenyl complex $\text{Tp}^{t\text{Bu},\text{Me}}\text{Cr-Ph}$ ($\text{Tp}^{t\text{Bu},\text{Me}}$ = hydrotris(3-tert-butyl-5-methylpyrazolyl)borate) with O_2 [3], with the help of density functional theory. However, the results can contribute to the fundamental knowledge of organometallic chemistry, and they would be valuable for the design of catalytic oxidations.

1.4.3 Transfer Hydrogen Catalysts

Environmental concerns in chemistry have increased the demand for more selective chemical processes with a minimum amount of waste (“Green Chemistry”). Catalytic hydrogen transfer reactions are environmental friendly methodologies for the reduction of ketones or imines and oxidation of alcohols or amines in which a substrate-selective catalyst transfers hydrogen

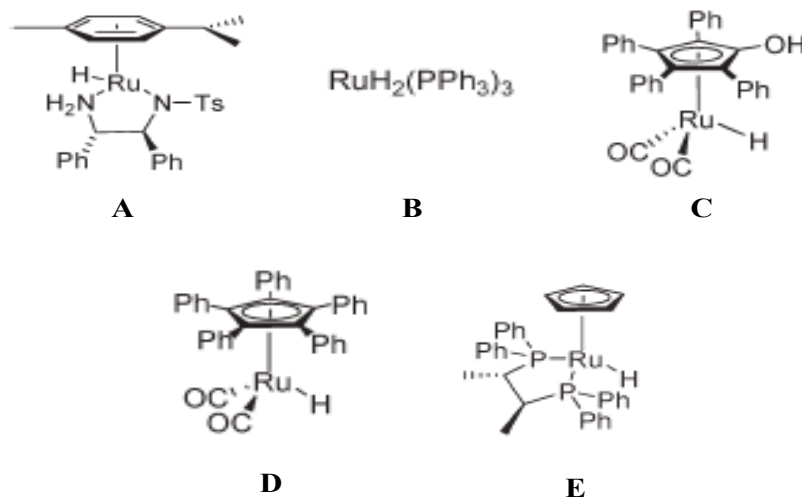


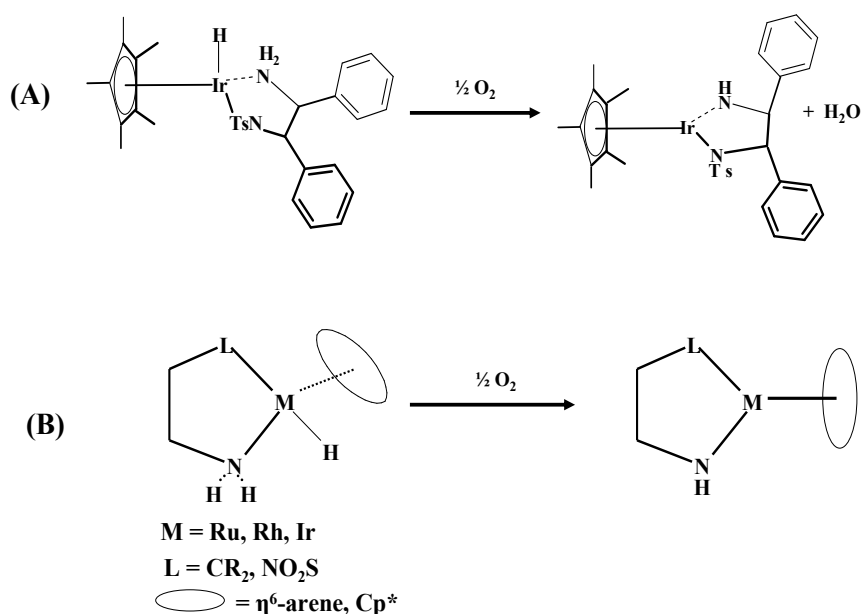
Figure 1.4: Examples of metal hydride.

between the substrate and a hydrogen donor or acceptor, respectively [92, 93, 94]. There are two main pathways that have been proposed for hydrogen transfer: (1) direct hydrogen transfer and (2) a hydridic route is involved for transition metals (Fig 4). The latter can be

further divided into dihydridic or monohydridic routes. On the other hand, the monohydridic route can operate through different pathways depending on both catalysts and substrates.

Usually the transition metal catalysts follow a hydridic route. In the 1960s, Henbest *et. al.* have reported about a transition metal-catalyzed hydrogen transfer with moderate rates and turnovers [95, 96]. This is an early example of transition metal-catalyzed hydrogen transfer. Also, Sasson and Blum have found that $RuCl_2(PPh_3)_3$ can be used at high temperature with moderate turnover frequency [97, 98, 99]. The role of a base on the $RuCl_2(PPh_3)_3$ -catalyzed transfer hydrogenation was reported in 1991 [100, 101]. All these reactions proceed under very mild conditions with low loading of the catalyst. There are lots of examples about the mechanistic details of the hydrogen transfer using a hydridic route, which is involved for transition metals [102].

Earlier it was mentioned that the catalytic hydrogen transfer reaction offers a great oppor-

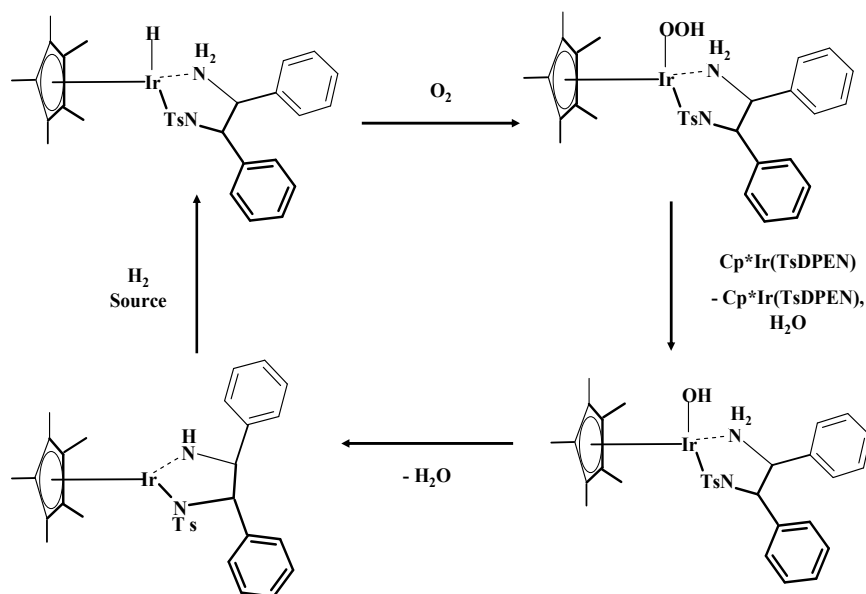


Scheme 1.8: Hydrogen transfer with bifunctional molecular catalysis.

tunity to explore an attractive molecular transformation due to the low cost and operational simplicity [102, 103, 104]. The significant feature for these catalysts is that one of the sites of the ligand acts as a basic center. This basic center is suggested to interact with the alcohol or amine through a hydrogen bond and thereby it facilitates the hydride transfer. If we consider the catalyst **A** of Fig 1.4 then the proposed mechanism for the catalyst is involved in a con-

certed hydrogen transfer without prior coordination of the substrate to the metal, on the other hand there are some examples of metal ligand bifunctional catalysts that operate in a stepwise manner or *via* an ionic mechanism. Noyori *et al.* have reported about the ruthenium(1*S*,2*S*)-*N*-(*p*-toluenesulfonyl)-1,2-diphenylethylenediamine [(*S,S*)-TsDPEN] complex as a highly effective and enantioselective catalyst in the asymmetric transfer hydrogenation of carbonyl and imino groups [105, 6]. The dehydrogenative oxidation reaction with the related amine/amide catalysts has not been investigated as much, mainly because of the lack of appropriate hydrogen acceptors, except for the ketones, the kinetic resolution of racemic alcohols [105, 107], intramolecular redox isomerization [108], and other oxidative transformations [109, 110]. Also, there are few examples about the chiral bifunctional Ru, Rh, and Ir hydride complexes, which can be useful for the asymmetric transfer hydrogenation of ketones [103,104,111-114]. All these catalysts have intrinsic reversible nature, both forward and reverse reactions can be utilized as the reduction of ketones and oxidation of alcohols, respectively. Using this reversible nature of the catalysts, recently few papers have reported that, molecular oxygen readily reacts with some of these amine-hydrido complexes leading to the amide complex (Scheme 1.8(A) and 1.8(B)) [5, 116].

The first observation of reduction of dioxygen using the transfer hydrogenation catalysis in



Scheme 1.9: Proposed catalytic cycle for hydrogenation of O_2 by $Cp^*IrH(TsDPEN)$

homogeneous solution has been documented by Rauchfuss and Co-worker (Scheme 1.8(A)) [5]. It is a relatively new generation of transfer hydrogenation catalysts for use as unconventional metal hydrides for oxygen reduction. This is an example of the oxidative reactivity of iridium-based transfer hydrogenation catalysis in a non-aqueous solution. In acetonitrile/dichloromethane the 18e amino-hydride $Cp^*IrH(TsDPEN)$ (1H(H)) reacts with molecular oxygen to give $Cp^*Ir(TsDPEN - H)$ (1) and 1 equiv of water (Scheme 1.8(A)), where the conversion is signaled by a color change. The authors have reported that, the reaction is unaffected by radical traps, supporting that a hemolytic pathway is not involved. The experimental observation supported that, there is present an intermediate iridium-hydroperoxo complex (1H(OOH)). The reaction in a solid state of 1H(H) is very slow in presence of air. The authors have also proposed a reaction mechanism for this reaction (Scheme 1.9).

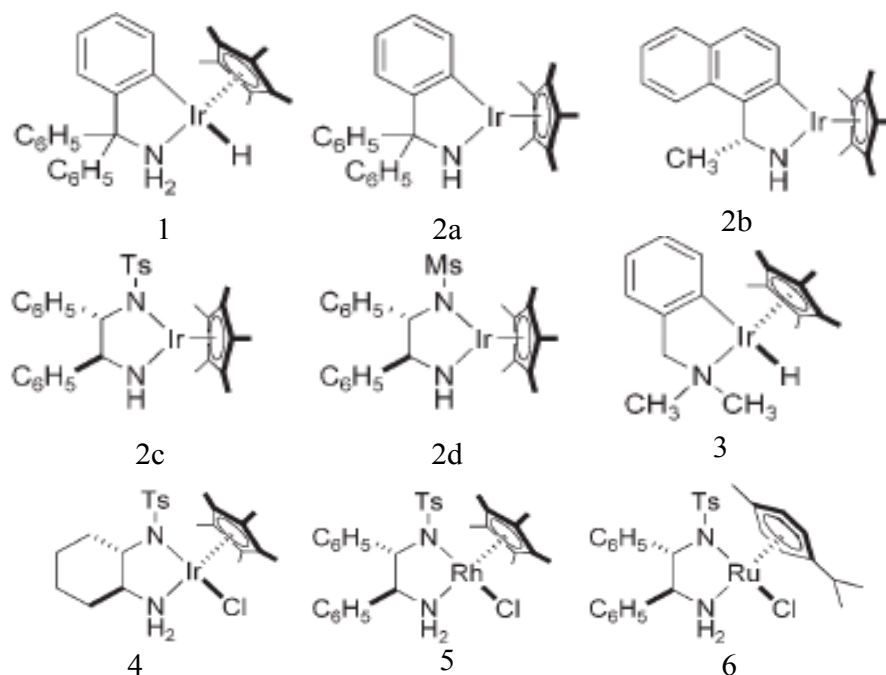


Figure 1.5: Examples of the hydrido complexes.

Recently, Ikariya and co-workers have reported about, the chiral bifunctional Ir, Rh, and Ru catalysts, where O_2 serves as a hydrogen acceptor at a room temperature (Scheme 1.8.(B)) [116]. The authors have examined different kinds of amine complex reactions with O_2 (Fig. 1.5). The experimental observation supported that, the hydrido complex 3 (Fig 1.5) bearing an N,N-dimethylamino group did not catalyze the oxidation under otherwise identical conditions, indicating that the metal/NH units possibly participate in the activation of O_2 , to

facilitate transformation to the amido complex [116]. This kind of aerobic oxidation of alcohols is more appealing when applied to the kinetic resolution of racemic secondary alcohols with chiral amido catalysts [116].

From the above discussion it is clear that facile hydrogen transfer from the amine-hydrido complex to the oxygen molecule, generating the corresponding amide complex and O_2 is a promising hydrogen acceptor. Theoretical studies on such kind of reactions are very limited and the reaction mechanisms are not clear. In this work, our goal is to investigate the mechanism of reaction with the support of the proposed pathway in the experimental paper and experimental observations. This could further enhance the understanding and provide helpful information for chemists for future exploration of such kind of reactions.

Bibliography

- [1] K. Weissermelv and H.-J. Arpe, *Industrial Organic Chemistry*, 3rd ed., VCH, New York, **1997**.
- [2] J. J. Berzelius, *J. Ann. Chim. Phys.* **1836**, 61, 146.
- [3] M.W. Roberts, *Catal. Lett.* **2000**, 67, 1.
- [4] R.A. Santen, P.W.N.M. van Leeuwen, B.A. Averill and J.A. Moulijn, *Catalysis: An Integrated Approach.*, 2nd Ed. Elsevier, **1999**.
- [5] W. Ostwald, *Z. Phys. Chem.* **1894**, 15, 705.
- [6] B. Cornils and W.A. Herrmann, *Applied Homogeneous Catalysis With Organometallic Compounds* VCH: Weinheim, **1996**.
- [7] Piet W.N.M. Leeuwen, *Homogeneous Catalysis: Understanding the Art*, Springer, **2004**.
- [8] G.W. Parshall, *Homogeneous Catalysis*, Wiley New York, **1980**.
- [9] G.W. Parshall, *J. Mol. Catal.* **1978**, 4, 243.
- [10] F. E. Paulik, A. Hershman, W. R. Knox and J. F. Roth, Monsanto Company, US Pat. **1973**.
- [11] G. Yagupsky, C.K. Brown and G. Wilkinson, *J. Chem. Soc. (A)*. **1970**, 1392.
- [12] B.D. Vineyard, W.S. Knowles, M.J. Sabacky, G.L. Bachman and D.J. Weinkauff, *J. Am. Chem.Soc.* **1970**, 99, 5946.
- [13] C. A. Tolman and J. P. Jesson, *Science* **1973**, 181, 501.
- [14] B. Cornils and W.A. Herrmann, *Journal of Catalysis.* **2003**, 216, 23.

- [15] L.D. Hegedus, *Transition Metal in the Synthesis of Complex Organic Molecules*, University Science Books, Mill Valley, **1994**.
- [16] D.E. de Vos, B.F. Sels and P.A. Jacobs, *Adv. Catal.* **2001**, 46, 1.
- [17] C. L. Hill and I. A. Weinstock, *Nature* **1997**, 388, 332.
- [18] D.H.R. Barton, A. E. Martell and D.T. Sawyer, *The Activation of Dioxygen and Homogeneous Catalytic Oxidation*; Plenum: New York, **1993**.
- [19] R.A. Sheldon and R.A. van Santen, *Catalytic Oxidation: Principles and Applications*, World Scientific: Singapore, **1995**.
- [20] *Catalytic Activation of Dioxygen by Metal Complexes*, Ed., Kluwer Academic Publishers: Dordrecht, The Netherlands, **1992**.
- [21] A.E. Shilov and G.B. Shulpin, *Activation and Catalytic Reactions of Saturated Hydrocarbons in the Presence of Metal Complexes*, Kluwer Academic Publishers: Dordrecht, The Netherlands, **2000**.
- [22] R. A. Sheldon, I. W. C. E. Arends and A. Dijksman, *Catal. Today.* **2000**, 57, 157.
- [23] H. Taube, *J. Gen. Physiol.* **1965**, 49, 29.
- [24] C.L. Hill and I. A. Weinstock, *Nature* **1997**, 388, 332.
- [25] R. A. Sheldon, *J. Mol. Catal. A: Chem. (spec. iss.)* **1997**, 117, 1489.
- [26] D. H. R. Barton, A. E. Martell and D. T Sawyer,(eds) *The Activation of Dioxygen and Homogeneous Catalytic Oxidation*, Plenum, New York, **1993**.
- [27] P. O. Norrby, H. C. Kolb and K. B. Sharpless, *J. Am. Chem. Soc.* **1994**, 116, 8470.
- [28] J. T. Groves and R. Quinn, *J. Am. Chem. Soc.* **1985**, 107, 5790.
- [29] M.T. Pope and A. Miller, *Angew. Chem. Int. Edn Engl.* **1991**, 30, 34.
- [30] D. E. Katsoulis and M. T. Pope, *J. Am. Chem. Soc.* **1984**, 106, 2737.
- [31] C. L. Hill and C. M. Prosser-McCartha, *Coord. Chem. Rev.* **1995**, 143, 407.
- [32] C. L. Hill and R. B. Brown, *J. Am. Chem. Soc.* **1986**, 108, 536.

- [33] R. Neumann and M. Dahan, *Nature* **1997**, 388, 353.
- [34] C. L. Hill, *ActiVation and Functionalization of Alkanes*, Ed. Wiley: New York, **1989**.
- [35] B. A. Arndtsen, R. G. Bergman, T. A. Mobley and T. A. Peterson, *Acc. Chem. Res.* **1995**, 28, 154.
- [36] A. E. Shilov and G. B. Shul'pin, *Chem. Rev.* **1997**, 97, 2879.
- [37] J. Ebner and D. Riley, *In ActiVe Oxygen in Chemistry*, C. s.Foote, J. S. Valentine, A. Greenberg and J. F. Liebman, Eds.; Blackie Academic Professional: London, **1995**, 205.
- [38] A. Sen, *Acc. Chem. Res.* **1998**, 31, 550.
- [39] J. H. Bayston, R. H. Beale, N. K. King and M. E. Winfield, *Aust. J. Chem.* **1963**, 16, 954.
- [40] H. L. Roberts and W. R. Symes, *J. Chem. Soc. (A)* **1968**, 1450.
- [41] L. E. Johnston and J. A. Page, *Can. J. Chem.* **1969**, 47, 4241.
- [42] R. D. Gillard, B. T. Heaton and D. H. Vaughan, *J. Chem. Soc. (A)*, **1970**, 3126.
- [43] J. F. Endicott, C. L. Wong, T. Inoue and P. Natarajan, *Inorg. Chem.* **1979**, 18, 450.
- [44] M. T. Atlay, M. Preece, G. Strukul and B. R. James, *Can. J. Chem.* **1983**, 61, 1332.
- [45] T. T. Wenzel, *In Dioxygen ActiVation and Homogeneous Catalytic Oxidation*, Simandi, L. I., Ed.; Elsevier Science Publishing Co. Inc.: New York, **1991**, 545.
- [46] D. D. Wick and K. I. Goldberg, *J. Am. Chem. Soc.* **1999**, 121, 11900.
- [47] S. Thyagarajan, C. D. Incarvito, A. L. Rheingold and K. H. Theopold, *Chem. Comm.* **2001**, 2198.
- [48] S. S. Stahl, *Angew. Chem., Int. Ed.* **2004** 43, 3400.
- [49] M. M. Konnick, I. A. Guzei and S.S. Stahl, *J. Am. Chem. Soc.* **2004**, 126, 10212.
- [50] S. S. Stahl, J. L. Thorman, R. C. Nelson and M. A. Kozee, *J. Am. Chem. Soc.* **2001**, 123, 7188.
- [51] W. R. Theil, *Angew. Chem.* **1999**, 111, 3349; W. R. Theil, *Angew. Chem. Int. Ed.* **1999**, 38, 3157,.

- [52] M. M. Konnick, B A. Gandhi, I. A. Guzei and S.S. Stahl, *Angew. Chem. Int. Ed.* **2006**, 45, 2904.
- [53] T. Hosokawa and S. Murahashi, *Acc. Chem. Res.* **1990**, 23, 49.
- [54] T. Hosokawa, T. Nakahira, M. Takano, and S. Murahashi, *J. Mol. Catal.* **1992**, 74, 489.
- [55] D. D. Wick and K. I. Goldberg, *J. Am. Chem. Soc.* **1999**, 121, 11900.
- [56] S. Thyagarajan, C. D. Incarvito, A. L. Rheingold and K. H. Theopold, *Chem. Commun.* **2001**, 2198.
- [57] J. M. Keith, R. J. Nielsen, J. Oxgaard and W. A. Goddard, III. *J. Am. Chem. Soc.* **2005**, 127, 13172.
- [58] M. C. Denney, N. A. Smythe, K. L. Cetto, R. A. Kemp and K. I. Goldberg, *J. Am. Chem. Soc.* **2006**, 128, 2508.
- [59] J. M. Keith, R. P Muller, R. A. Kemp, K. I. Goldberg, W. A. Goddard, III. and J. Oxgaard, *Inorg. Chem.* **2006**, 45, 9631.
- [60] D. Bianchi, R. Bortolo, R. D'Aloisio and M. Ricci, *Angew Chem Int Ed* **1999**, 38, 706.
- [61] B. V. Popp and S.S. Stahl, *Top Organomet Chem*, **22**, 149, (2007) and reference cited therein.
- [62] B. V. Popp, J.E. Wendlandt, C. R. Landis, and S.S. Stahl, *Angew. Chem. Int. Ed.* **2007**, 46, 601.
- [63] M. Yamashita, K. Goto and T. Kawashima, *J. Am. Chem. Soc.* **2005**, 127, 7294.
- [64] C. R. Landis, C. M. Morales and S. S. Stahl, *J. Am. Chem. Soc.* **2004**, 126, 16302.
- [65] B. V. Popp and S.S. Stahl, *J. Am. Chem. Soc.* **2007**, 129, 4410.
- [66] M. Schlangen and H. Schwarz, *Helv. Chim. Acta.* **2008**, 91, 379.
- [67] L. Vaska, *Acc. Chem. Res.* **1976**, 9, 175.
- [68] A. Van Asselt, M.S. Trimmer, L. M. Henling and J. E. Bercaw, *J. Am. Chem. Soc.* **1988**, 110, 8254.
- [69] K. H. Theopold, *Top Organomet Chem.* **2007**, 22, 17.

- [70] A. Hess, M. R. Hrzt, L. M. Liable-Sands, D. C. Lindner, A. L. Rheingold and K. H. Theopold, *Angew. Chem. Int. Ed.* **1999**, 38, 166.
- [71] C. J. Cramer, W. B. Tolman, K. H. Theopold and A. R. Rheingold, *Proc. Natl. Acad. Sci. USA* **2006**, 100, 3635.
- [72] M. H. Dickmann and M. T. Pope, *Chem. Rev.* **1994**, 94, 569.
- [73] F. Bottomle, and L. Sutin, *Adv. Organomet. Chem.* **1988**, 28, 339.
- [74] P. Legzdins, E. C. Phillips and L. Sanchez, *Organometallics* **1989**, 8, 940.
- [75] P. Legzdins P, E. C. Phillips, S. J. Rettig, L. Sanchez, J. Trotter and V. C. Yee, *Organometallics* **1988**, 7, 1877.
- [76] S. K.Noh, R. A. Heintz, B.s. Haggerty, A. L. Rheingold and K. H. Theopold, *J. Am. Chem. Soc.* **1992**, 114, 1892.
- [77] R. A. Heintz, R. L. Ostrander, A. L. Rheingold and K. H. Theopold, *J. Am. Chem. Soc.* **1994**, 116, 11387.
- [78] C. D. Abernethy, F. Bottomley, A. Decken, and R. C. Thompson, *Organometallics* **1997**, 16, 1865.
- [79] A. Aistars, C. Newton, T. Ruebenstahl and M. M. Doherty, *Organometallics* **1997**, 16, 1994.
- [80] T. P. Blackburn, J. A. Labinger and J. Schwartz, *Tetrahedron. Lett.* **1975**, 16, 3041.
- [81] P. B. Brindley and M. J. Scotton, *J. Chem. Soc. Perkin. Trans.* **1981**, 2, 419.
- [82] T. V. Lubben and P. T. Wolczanski, *J. Am. Chem. Soc.* **1987**, 109, 424.
- [83] A. G. Davies, and B. P. Roberts, *Free Radicals (Reactive Intermediates in Organic Chemistry)*, J. K. Kochi (ed) vol I. Wiley, New York, **1973**, 547.
- [84] P. L. Bailey, R. A. Coxall, C. M. Dick, S. Fabre, L. C. Henderson, C. Herber, S. T. Liddle, D. Lorono-Gonzalez, A. Parkin and S. Parsons, *Chem. Eur. J.* **2003**, 9, 4820.
- [85] S. J. Kim, D. W. Choi, Y. J. Lee, B. H. Chae, J. J. Ko and S. O. Kang, *Organometallics* **2004**, 23, 559.

- [86] S. N. Brown and J. M. Mayer, *J. Am. Chem. Soc.* **1996**, 118, 12119.
- [87] J. Muzart, *Chem. Rev.* **1992**, 92, 113.
- [88] D. Schroder, S. Shaik and H. Schwarz, *Acc. Chem. Res.* **2000**, 33, 139.
- [89] D. A. Plattner, *Angew. Chem. Int. Ed.* **1999**, 38, 82.
- [90] J. N. Harvey, R. Poli and K. M. Smith, *Coord. Chem. Rev.* **2003**, 238, 347.
- [91] C. Li, W. Wu, D. Kumar and S. Shaik, *J. Am. Chem. Soc.* **2006**, 128, 394.
- [92] S. Gladiali and E. Alberico, *Transition Metals for Organic Synthesis*, ed. M. Beller and C. Bolm, Wiley-VCH, Weinheim, **2004**, 2, 145.
- [93] S. E. Clapham, A. Hadzovic and R. H. Morris, *Coord. Chem. Rev.* **2004**, 248, 2201.
- [94] J. E. Backvall, *J. Organomet. Chem.* **2002**, 652, 105.
- [95] J. Trocha-Grimshaw and H. B. Henbest, *Chem. Commun. (London)* **1967**, 544.
- [96] H. B. Henbest, *Proc. Chem. Soc.* **1964**, 361.
- [97] Y. Sasson and J. Blum, *Tetrahedron Lett.* **1971**, 2167.
- [98] Y. Sasson and J. Blum, *J. Org. Chem.* **1975**, 40, 1887.
- [99] P. Maitlis, *J. Organomet. Chem.*, **289**, 385, (1985).
- [100] R. L. Chowdhury and J.-E. Backvall, *J. Chem. Soc., Chem. Commun.* **1991**, 1063.
- [101] A. Aranyos, G. Csajnyik, K. J. Szabo and J. E. Backvall, *Chem. Commun.* **1999**, 351.
- [102] J. S. M. Samec, J. -E. Backvall, P. G. Andersson, and P. Brandtb, *Chem. Soc. Rev.* **2006**, 35, 237 and references therein.
- [103] R. Noyori and S. Hashiguchi, *Acc. Chem. Res.* **1997**, 30, 97.
- [104] R. Noyori, M. Yamakawa, S. Hashiguchi, *J. Org. Chem.* **2001**, 66, 7931.
- [105] S. Hashiguchi, A. Fujii, J. Takehara, T. Ikariya and R. Noyori, *J. Am. Chem. Soc.* **1995**, 117, 7562.
- [106] K.-J. Haack, S. Hashiguchi, A. Fujii, T. Ikariya and R. Noyori, *Angew. Chem., Int. Ed. Engl.* **1997**, 36, 285.

- [107] Y.-Y. Li, X.-Q. Zhang, Z.-R. Dong, W.-Y. Shen, G. Chen, J.-X. Gao, *Org. Lett.* **2006**, 8, 5565.
- [108] M. Ito, S. Kitahara and T. Ikariya, *J. Am. Chem. Soc.* **2005**, 127, 6172.
- [109] T. Suzuki, K. Morita, M. Tsuchida and K. Hiroi, *Org. Lett.* **2002**, 4, 2361.
- [110] M. Ito, A. Osaku, A. Shiibashi and T. Ikariya, *Org. Lett.* **2007**, 9, 1821.
- [111] T. Ikariya and A. J. Blacker, *Acc. Chem. Res.* **2007**, 40, 1300.
- [112] T. Ikariya, K. Murata and R. Noyori, *Org. Biomol. Chem.* **2006**, 4, 393.
- [113] K. Murata, T. Ikariya and R. Noyori, *J. Org. Chem.* **1999**, 64, 2186.
- [114] K. Mashima, T. Abe and K. Tani, *Chem. Lett.* **1998**, 27, 1199.
- [115] Z. M. Heiden and T. B. Rauchfuss, *J. Am. Chem. Soc.* **2007**, 129, 14303.
- [116] S. Arita, T. Koike, Y. Kayaki and T. Ikariya, *Angew. Chem. Int. Ed.* **2008**, 47, 2447.

Chapter 2

Theoretical Background

In first chapter it was mentioned that, recent developments in homogeneous transition metal catalysis point toward new opportunities for selective aerobic oxidation chemistry. Theoretical calculations could assist to understand the mechanisms of reactions and could enhance the further understanding and provide helpful information for chemists for further exploration of such kind of reactions. First principles computations for these type of reactions have emerged only recently.

A decisive step towards a generally applicable first-principles treatment was made in the early sixties with the introduction of Density Functional Theory (DFT) by Hohenberg and Kohn. As in Thomas-Fermi theory the basic dynamical quantity is the single-particle density, yet whereas Thomas-Fermi theory is for a locally homogeneous gas of fermions, DFT is for an inhomogeneous gas. DFT differs from Hartree-Fock theory in that DFT uses densities rather than the wave functions and in its inclusion of both exchange and dynamical correlations. As formulated, Hartree-Fock treats exchange exactly but leaves out correlations (except for those arising from the exchange). On the other hand, DFT, includes both effects but, neither exactly. In some sense these two theories compliment each other, the DFT equations contain more approximations and produce less information (densities rather than wave functions). However, DFT contains more physical effects and is applied to systems with hundreds of particles, systems that would be too complicated for Hartree-Fock theory. The basic formalism, underlying the results presented in this thesis, is the DFT of electronic structure. In order to obtain a self-contained presentation, and to define terminology and notations, the important features of this theory are summarized.

2.1 Wavefunction Theory

Obtaining the solution of the energy eigenvalue problem has been the primary goal of quantum mechanics. For an isolated N-electron atomic or molecular system in Born-Oppenheimer non-relativistic approximation, this is given by,

$$\hat{H}\Psi = E\Psi \quad (2.1)$$

Where, E is the electronic energy, $\Psi = \Psi(x_1, x_2, \dots, x_n)$ is the wavefunction which describes the state of the N-electron quantum mechanical system and is a function of the space spin coordinates, \mathbf{x}_i , of all the electrons of the system, and \hat{H} is the Hamiltonian operator. The Hamiltonian operator can be written as,

$$\hat{H} = - \sum_{i=1}^N \frac{1}{2} \nabla_i^2 + \sum_{i=1}^N \nu(r_i) + \sum_{i<j}^N \frac{1}{r_{ij}} \quad (2.2)$$

The symbols have their meaning. The first term is the kinetic energy (KE) \hat{T} operator, where the last term is, \hat{V}_{ee} , the electron-electron repulsion energy operator, and the middle term is the nuclear-electron interaction operator \hat{V}_{ne} , where the external potential due to the nuclei can be written as,

$$\nu(r_i) = - \sum_{\alpha} \frac{Z_{\alpha}}{r_{i\alpha}} \quad (2.3)$$

and so Eq.2.1 can be written as

$$\hat{H} = \hat{T} + \hat{V}_{ee} + \hat{V}_{ne} \quad (2.4)$$

The total energy is obtained after adding the nuclear-nuclear repulsion energy, V_{nn} to the electronic energy, E after solving the Schrödinger equation. The term V_{nn} is a constant for a fixed arrangement of the nuclei and could be added before or after the calculation. The expectation value of the Hamiltonian operator \hat{H} is given by,

$$E[\Psi] = \frac{\langle \Psi | \hat{H} | \Psi \rangle}{\langle \Psi | \Psi \rangle} \quad (2.5)$$

From each measurement we will get one of the eigenvalues of H, we have

$$E[\Psi] \geq E_0 \quad (2.6)$$

Usually the energy is computed using the guess wavefunction in an upper bound to the true ground state energy E_0 . There are different *ab initio* rigorous theories namely the coupled-cluster (CC), Moller-Plesset (MP) perturbation theory, configuration interaction (CI) theory etc, which attempt to solve the Schrödinger equation.

2.1.1 Hartree-Fock Theory

Hartree-Fock (HF) theory [1, 2] is based on a single-particle equation. It is the starting point for understanding the other theories. We describe here the HF theory in detail. The electronic Hamiltonian in the HF framework is,

$$\hat{H} = \hat{T} + \hat{V}_{ne} + \hat{J} - \hat{K} \quad (2.7)$$

Here, the KE is written in terms of a non-interacting operator to simplify the equations, on the other hand the electrostatic Coulomb interaction, \hat{J} , is contained in average manner. The last term, \hat{K} , is the exchange energy term which takes into account the interaction between electrons with parallel spin. The correlation energy contribution for the interaction between the electrons of opposite spin is missing in the HF theory. The energy E is a functional of a single determinant constructed using an orthonormal set of single-electron spin orbital functions. The HF matrix eigenvalue equation for stationary value of the energy functional is solved by Lagrange undetermined multipliers. In this process the spin-orbitals are varied under the constraint that the spin-orbitals form an orthonormal set.

$$\int \Psi_i \Psi_j = \delta_{ij} \quad (2.8)$$

The Euler-Lagrange equation for a stationary value of the energy can be written as,

$$\partial E = \partial \langle \Psi | \hat{H} | \Psi \rangle - E \partial \langle \Psi | \Psi \rangle \quad (2.9)$$

This will give a Slater determinant corresponding to the best set of spin-orbitals and consequently the minimum energy or the ground state energy of the system. An elaborate discussion of the HF theory could be found in the chapter 3 of the book by Szabo and Ostlund [3]. The alternative to using the 3Ndimensional wavefunction is to use methods based on the electron density, which is a measurable quantity.

2.2 Development of Density Functional Theory

The first attempts to use the electron density rather than the wave function for obtaining information about atomic and molecular systems are almost as old as quantum mechanics itself and date back to the early work of Thomas in 1927 and Fermi in 1928. Thomas and Fermi proposed the idea about using the 3-dimensional electron density as a basic variable for

studying a N-electron quantum-chemical system. The basic idea of the model is the statistical approximation in order to explain the electronic distribution in an atom. This model is known as Thomas-Fermi (TF) model [4, 5, 6].

2.2.1 Thomas-Fermi Model

In this model electrons are considered as independent particles, forming a uniform electron gas. The nuclear-electron and electron-electron contributions are treated in a completely classical way [7]. The electron-electron repulsion energy arises solely due to electrostatic interactions and the KE of this noninteracting system depends on electron density, $\rho(r)$. The TF energy functional can be written as,

$$E_{TF}[\rho(r)] = \frac{3}{10}(3\pi^2)^{\frac{2}{3}} \int \rho^{\frac{5}{3}}(r)dr - Z \int \frac{\rho(r)}{r}dr + \frac{1}{2} \int \int \frac{\rho(r_1)\rho(r_2)}{|r_1 - r_2|} dr_1 dr_2 \quad (2.10)$$

The first term of the above equation is the KE, whereas the second term is the nuclear-electron attractive potential (external potential energy) and the last term is the electron-electron repulsive potential (classical Coulomb energy). The Thomas-Fermi model employs the variational principle. It is assumed that the ground state of the system is connected to the electron density for which the energy according to equation (2.10) is minimized under the constraint of :

$$\int \rho(r)dr = N \quad (2.11)$$

where N is the number of electrons. Using the TF method we can get a very crude description of the electron density and the electrostatic potential. In the past the TF model has been used for calculations of atoms and molecules [10, 9, 10]. The early work have been reviewed by Gambos and March [11, 12, 13]. Lieb and coworkers have done lots of work on TF method [14, 38, 16, 17], from there it can be realized that the TF scheme is exact in the limit of infinite nuclear charge.

There is a number of deficiencies in the TF method, some severe ones include the infinite charge density at the nucleus. This method is unable to explain the binding of atoms to give molecules or solids. Also, the charge density does not decay exponentially away from the nucleus of the atom. The model has shortcomings in the case of the shell structure of the atom. The TF model has other few defects. All these defects have to led to the modification of the model. One subsequent modification done by Dirac [18], is known as the Thomas-Fermi-Dirac (TFD) model. This model includes the kinetic and classical Coulomb contributions as well

as the quantum mechanical exchange effects. The exchange term is called, K_D , which can be written as

$$K_D[\rho] = \frac{3}{4} \left(\frac{3}{\pi}\right)^{\frac{1}{3}} \int \rho^{\frac{4}{3}}(r) dr \quad (2.12)$$

Von Weizsacker did some modification by adding a gradient term to the KE term of the TF model. This model was called Thomas-Fermi-Weizsacker (TFW) model [19]. The TF model came to be known as a first approximation to the exact description of the ground state of any system in terms of density. In the density functional description all properties of a system can be expressed in terms of the electron density, ρ , i.e. number of electrons per unit volume. The electron density can be written in terms of the wave function, *i.e.*,

$$\rho(r_1) = N \int \int |\psi(x_1, x_2, \dots, x_N)|^2 ds_1 ds_2 dx_N \quad (2.13)$$

where, $\rho(r_1)$, is a simple non-negative function of the three variable, x, y, and z, integrating to the total number of electrons, N.

2.2.2 The X_α Method

With the combination of the HF model and the TFD model, Slater proposed a new method which is called the X_α or Hartree-Fock-Slater (HFS) [20]. Slater's idea was to assume that the exchange hole is spherically symmetric and centered around the reference electron at r_1 . Slater used a numerical prefactor, α , as a semiempirical parameter for the TFD exchange potential and employed the KE part of the HF model. Typical values of α are between $\frac{2}{3}$ and 1. He kept the KE as in HF and applied the statistical approximation to the exchange part of the potential. Simultaneously it corrects for the deficiency of the TFD model and simplifies the HF model drastically. In the review articles Slater, Johnson and Connolly, have described the techniques for solving the X_α equations, choosing α values; similar discussion is found in the book by Slater [21, 22, 23, 24]. Slater has compared the TFD and X_α methods in detail [25] and an article by Gasper [26] justifies the $\alpha = 1$ value. The X_α method may be regarded as a density functional scheme which neglects of the correlation and approximates to the exchange energy.

2.2.3 Density Matrix Theory

In general, the many body wave function $\psi(q_1, \dots, q_{3N}, t)$ is far too large to calculate for a macroscopic system. So, in many body physics we are using the ground state electron density,

which contains all the information about the system and can determine all the properties. If we get the first-order derivative of the density then we will get more information about the system. The first order reduced density matrix can be written as,

$$\gamma_1(x'_1, X_1) = N \int \psi^*(x_1, x_2, \dots, x_N) \psi(x_1, x_2, \dots, x_N) dx_2 dx_3 \dots dx_N \quad (2.14)$$

This is the one particle density matrix, γ_1 is the diagonal elements of the matrix. From the trace of the matrix we will get the number of the electrons of the system, whereas the second-order density matrix, γ_2 , normalizes to the number of electron pairs and it is a two-particle density matrix. The basic Hamiltonian has only one-electron and two-electron operators. With the help of these two density matrices we will be able to construct the energy expression where all the terms and the energy itself is a functional of the density matrix. The γ_1 can be obtained from γ_2 , it can be written as,

$$\gamma_1(x'_1, x_1) = \frac{2}{N-1} \int \gamma_2(x'_1 x_2, x_1, x_2) dx_2 \quad (2.15)$$

On the one-particle and two particle Hilbert space, γ_1 and γ_2 are the co-ordinate space representation of the operators $\hat{\gamma}_1$ and $\hat{\gamma}_2$ respectively. Eq. 2.15 is required to obtain the energy expression and it can be integrated over spin to get the expression in terms of the spinless density matrices [27, 28, 29]. There have been lots of research done by Löwdin(1955) [30], Gilbert (1975) [31], Berrondo and Goscinski (1975) [32], Donnelly and Parr (1978) [33], Donnelly (1979) [34], Coleman (1963, 1981) [35, 36]. These functionals have the advantages and disadvantages. The advantages are (i) the kinetic energy is represented more directly, (ii) exchange (and hence self energy) effects can be treated exactly, and (iii) nonlocal single-particle potentials are also included. The disadvantages are (i) no explicit functionals for the correlation energy in terms of the one-particle density matrix are available and that (ii) the resulting variational equations are expected to be more difficult to handle. On the other hand the trial γ_1 must correspond to some antisymmetric wavefunctions and this occurs in the N-representability problem for the second-order density matrix.

2.3 Density Functional Theory

Although density functional theory has its conceptual roots in the Thomas-Fermi model, it was not put on a firm theoretical footing until the Hohenberg-Kohn theorems (HK) in 1964 [37]. While the original version of the Hohenberg-Kohn theorems relied on a number of

restrictions such as the assumption of non degenerate ground states, the rigorous foundation of density functional theory has since been extended to cover practically all situations of interest, as for instance degenerate ground states, spin polarized systems, thermodynamic systems, relativistic systems, multicomponent systems etc. A number of rigorous bounds has been established, and the mathematical structure of the functionals has been exposed and tied to the framework of functional analysis [38]. In this work the subject will be covered from a chemist's point of view without addressing its rigorous mathematical foundation.

2.3.1 The Hohenberg-Kohn theorem

The two basic theorems of the density functional formalism were derived by Hohenberg-Kohn [37].

Theorem 1 :- Ground state (GS) properties of a system of electrons and ions in a local external field, $\nu(r)$ can be expressed as functionals of the electron density, $\rho(r)$, *i.e.* they are determined by a knowledge of the density alone. The total energy, E , is an example.

Now we can write the energy E_ν which is explicitly dependent on ν .

$$E_\nu[\rho] = T[\rho] + V_{ne}[\rho] + V_{ee}[\rho] \quad (2.16)$$

$$= \int \rho(r)\nu(r)dr + F_{HK}[\rho] \quad (2.17)$$

The last term of Eq. 2.16, V_{ee} is containing the classical repulsion term and a non-classical term. The exchange-correlation energy is the major part of the non-classical term. Where the classical term $J[\rho]$ can be written as,

$$J[\rho] = \frac{1}{2} \int \int \frac{1}{r_{12}} \rho(r_1)\rho(r_2)dr_1dr_2 \quad (2.18)$$

The last term of Eq.2.17, F_{HK} can be written as,

$$F_{HK} = T[\rho] + V_{ee}[\rho] \quad (2.19)$$

From the last equation it is clear that, F_{HK} is independent of the external potential $\nu(r)$ and it is a universal HK functional of $\rho(r)$. The exact ground state energy could be determined by the exact form of $F_{HK}[\rho]$, but the exact form of the universal HK functional is not known.

Theorem 2 :- The total energy functionals $E_\nu[\rho]$ satisfies the variational principle, *i.e.* it is always greater than or equal to the ground state energy and the density for which the equality holds is the ground state electron density.

Being able to express the ground state energy as a functional of the density alone allows for much simpler electronic structure calculations than those where the many body wavefunction is treated as the basic variable. From the above discussion it is clear that, $F_{HK}[\rho]$ is crucial for the determination of the exact ground state energy. Since the exact form of $F_{HK}[\rho]$ is unknown, a lot of research has been done in order to find the best approximation for obtaining the ground state energy of a system.

2.3.2 Representability problems

There are some theoretical problems associated with the external potential $\nu(r)$ which appear as a restriction for the densities to be eligible in the variational problem. This restriction is known as the v-representability problem. If the ground state electron density has the v-representability then we can say that, the electron density can give all the electronic properties of the system. The electron density may or may not be v-representable. If the electron density is associated with the antisymmetric ground state wave function of a Hamiltonian of the form in Eq. 2.2, then it can be considered as v-representable. V-representable densities can be expressed from the second HK theorem,

$$E_\nu[\rho_0] = E_0 \leq E_\nu[\tilde{\rho}] \quad (2.20)$$

where, $E_\nu[\rho_0]$ is the ground state energy of the Hamiltonian with $\nu(r)$ as the external potential and ρ_0 is the ground state electron density. Levy and Lieb have been shown that many electron densities are non-v-representable [39, 40]. This problem can be solved if any reasonable density can be obtained from the antisymmetric wave function without connection to an external wavefunction. Such kind of densities are called N-representable. This N-representability is a much weaker condition for formulating the DFT in a different manner. In particular Gilbert and Harriman could be referred for more details about the N-representability [31, 40].

2.3.3 Constrained-Search Formulation

It is very important that the variational principle is connected to the Hohenberg-Kohn theorem. A new problem is posing due the N-representability of the electron density. In other words, it is necessary to find out the antisymmetric N-electron wave function, which will give the lowest expectation value of the Hamiltonian (i.e. the ground state energy). From the above discussion it is clear that, the ground state electron density ρ_0 can be obtained from the

ground state wave function ψ_0 , but it is not trivial to find out the ground state wave function from the ground state electron density. It is possible to find out ρ_0 from an infinite number of antisymmetric wavefunctions, may be the choosen one will not correspond to any ground state wave function. Levy's constrained search formulation can be used to understand the problem [41, 42, 43]. Since we know that, the external potential is a simple functional of the density, it can be expressed as,

$$E_\nu[\rho] = F_{HK}[\rho] + \int \nu(r)\rho(r)dr \geq E_\nu[\rho_0] \quad (2.21)$$

From the above it can be written that, among all the wavefunctions giving the ground state density ρ_0 , only the ground state wavefunction, ψ_0 will give the lowest expectation value i.e. the energy. Then,

$$\langle \psi_{\rho_0} | \hat{T} + \hat{V}_{ee} | \psi_{\rho_0} \rangle \geq \langle \psi_0 | \hat{T} + \hat{V}_{ee} | \psi_0 \rangle = F_{HK}[\rho_0] \quad (2.22)$$

So, the universal functional of the v-representability density can be written as,

$$F_{HK}[\rho_0] = \text{Min} \langle \psi | \hat{T} + \hat{V}_{ee} | \psi \rangle \dots \text{for } \psi \rightarrow \rho_0 \quad (2.23)$$

So, Levy's method proves the first HK theorem, as well as it also helps to find out the limitation of that, the density should correspond to a non-degenerate ground state. Thus the only constrain is on the normalization of the wavefunction. With the help of Levy's method it is easy to find out the ground state wavefunction. If we are able to find out the ρ_0 from an antisymmetric wavefunction (ground state wave function), we need not bother about v-representability of the electron density. This method gives us the freedom for explicitly searching for a v-representable density, with the help of N-representability. It requires nothing more than the non-negativity, proper normalization, and continuity of the trial electron density.

2.3.4 Kohn-Sham Approach

One year after of the Hohenberg-Kohn therorem, in 1965, Kohn-Sham proposed an indirect approach to KE functional, $T[\rho]$ [44]. In place of $F_{HK}[\rho]$ we will refer to the energy functional as $F[\rho]$. It's known that, ground state density minimizes the total energy functional $E[\rho]$ and thus staisfies the Euler Lagrange equation,

$$\left[\frac{\partial E[\rho]}{\partial \rho} \right] = \mu = \nu(r) + \frac{\partial F[\rho]}{\partial \rho(r)} \quad (2.24)$$

Where μ is the constant through all space for the ground state of a system. μ is the Lagrange multiplier associated with the constrained of Eq. 2.11 is called the chemical potential and also it is a measures of the escaping tendency of the electronic cloud.

If we consider the natural spin orbitals, ϕ_i and their occupation numbers, n_i , then the KE and electron density can be written as,

$$T[\rho] = -\frac{1}{2} \sum_{i=1}^N n_i \langle \phi_i | \nabla^2 | \phi_i \rangle \quad (2.25)$$

$$\rho(r) = \sum_{i=1}^N n_i \sum_s |\phi_i(r, s)|^2 \quad (2.26)$$

where, ϕ_i and n_i are the eigenfunction and eigenvalue of the first order reduced density matrix (γ_1 of Eq. 2.14) respectively. According to the Pauli's principle it can be written as $0 \leq n_i \leq 1$. If we consider an interacting N-electron system then possibly there will be an infinite number of expressions for the energy functional and electron density. Kohn-Sham proposed to put $n_i = 1$ for N orbitals and $n_i = 0$ for the rest of them which simplifies the expression for KE functional and the electron density to,

$$T_s[\rho] = -\frac{1}{2} \sum_i^N \langle \phi_i | \nabla^2 | \phi_i \rangle \quad (2.27)$$

$$\rho(r) = \sum_i \sum_s |\phi_i(r, s)|^2 \quad (2.28)$$

where, $T_s[\rho]$ and $\rho(r)$ correspond to non-interacting and interacting systems respectively. $T_s[\rho]$ is the major part of the exact KE. The above expressions for the $T_s[\rho]$ and $\rho(r)$ fit exactly with the determinantal form of the wavefunction for a non-interacting system of the N-electrons. It will be possible to set up a non-interacting reference system, with a Hamiltonian,

$$\hat{H}_s = -\frac{1}{2} \sum_i^N (\nabla_i^2) + \sum_1^2 \nu_s(r_i) \quad (2.29)$$

where, $\nu_s(r_i)$ does not contain the electron-electron repulsion term and the ground state electron density is $\rho(r)$ where needs to exist a non-interacting ground state. It can be called as an effective local potential. Now $T_s[\rho]$ can be defined for any density obtained from an antisymmetric wavefunction, but it is not the exact KE, $T[\rho]$. The $F[\rho]$ can be separated into the following components as,

$$F[\rho] = T_s[\rho] + J[\rho] + E_{xc}[\rho] \quad (2.30)$$

where the $T[\rho]$ is the exact KE and $E_{xc}[\rho]$ is the exchange-correlation energy which contains the non-classical part of the electron-electron repulsion energy and the remaining smaller part of the KE, $T[\rho] - T_s[\rho]$. Now the KS potential is defined as,

$$\nu_{eff} = \nu(r) + \frac{\partial J(\rho)}{\partial \rho(r)} + \frac{\partial E_{xc}[\rho]}{\partial \rho(r)} \quad (2.31)$$

$$= \nu(r) + \int \frac{\rho(r')}{|r - r'|} dr' + \nu_{xc}(r) \quad (2.32)$$

Where the exchange-correlation potential, ν_{xc} can be written as

$$\nu_{xc} = \frac{\partial E_{xc}[\rho]}{\partial \rho(r)} \quad (2.33)$$

Now the Euler equation can be written as,

$$\mu = \nu_{eff}(r) + \frac{\partial T_s[\rho]}{\partial \rho(r)} \quad (2.34)$$

where the $\rho(r)$ also satisfies the Euler equation. Its known that, the ground state wave function can be represented by a Slater determinant. From a given $\nu_{eff}(r)$ by solving the N single-particle equations of the form,

$$\left[-\frac{1}{2}\nabla^2 + \nu_{eff}(r)\right]\phi_i = \varepsilon_i\phi_i \quad (2.35)$$

We determine the one-electron solutions ϕ_i . The Eq. 2.35 needs to be solved self-consistently, because ν_{eff} depends on $\rho(r)$.

The KS equations can be constituted by Eq. 2.32, 2.33, and 2.35 along with the Eq. 2.28. An introduction of a basis is required for molecules in terms of molecular orbitals ϕ_i 's which can be written as linear combination of atomic orbitals (LCAO) in terms of contracted Gaussian, χ 's centered on atoms,

$$\phi_i(r) = \sum_{\mu}^N C_{\mu\nu}\chi_{\mu}(r) \quad (2.36)$$

Now the electron density can be written as,

$$\rho(r) = \sum_{\mu}^N \sum_{\nu}^N P_{\mu\nu}\chi_{\mu}(r)\chi_{\nu}^*(r) \quad (2.37)$$

where $P_{\mu\nu}$ is the density matrix. The one-particle KS-DFT equations in Eq.2.35 now can be transformed to the Kohn-Sham (KS) matrix equation. It can be written as,

$$HC = SCE \quad (2.38)$$

where H is called the KS operator matrix in the AO basis, C is the coefficient matrix, S and E are the overlap and energy matrices respectively.

To obtain the total energy, Eq. 2.30 for $F[\rho]$ has to be substituted in that for $E[\rho]$ below,

$$E[\rho] = \int \nu(r)\rho(r)dr + F[\rho] \quad (2.39)$$

Some review articles on DFT are informative and make an interesting reading [45, 46, 47].

2.4 The Exchange-Correlation Functional

As mentioned earlier that the exchange-correlation functional constituted by the non-classical part of the electron-electron repulsion term and a small part of the kinetic energy. The exchange-correlation term in the energy expression determines the accuracy of the DFT calculation. Its exact form is unknown and a number of approximations are available and this makes an interesting topic of research by itself.

One approach to calculate the exchange-correlation energy is based on assuming that the density only varies slowly and locally and it can be treated as a homogeneous electron gas [44]. This is known as the Local Density Approximation (LDA) [48]. This is the simplest approximation, proposed by Kohn and Sham [44], which can be computed exactly by the exchange energy of a uniform electron gas [44]. One popular correlation functional is the Vosko-Wilk-Nusair (VWN) functional [49]. The exchange-correlation energy functional for the LDA can be written as,

$$E_{xc}^{LDA}[\rho] = \int \rho(r)(\epsilon_x(\rho) + \epsilon_c(\rho))dr \quad (2.40)$$

where ϵ_x , the exchange part, is given by the Dirac exchange [18]. The correlation term ϵ_c , is given by VWN correlation functional. There is also the spin density analog of the LDA called the Local Spin-Density Approximation (LSDA). However, while the assumed homogeneous electron distribution works well for certain systems, it is not useful for most molecules, where the electron distribution is far from uniform .

A major improvement to LSDA was the introduction of the Generalized Gradient Approximation (GGA), which considers not only the density in a given point, but also its derivative [50]. The GGA can be written as,

$$E_{xc}^{GGA} = \int f(\rho(r), \nabla\rho(r))dr \quad (2.41)$$

Becke has also introduced a gradient-corrected functional for the exchange energy referred to as B88 [8], which contains one semi-empirical parameter. This parameter was fitted to the Hartree-Fock functional of six noble gas atoms (helium through radon) [8]. Another popular gradient-corrected correlation functional has been developed by Lee, Yang and Parr, which is referred as LYP [52]. The combination of B88 and LYP results in the widely used BLYP functional [7] which constructed from the Colle-Salvetti correlation energy [53] belongs to the category of semi-empirical functionals . Becke argued that a further Hartree-Fock exchange is also included in the functional [54]. This leads to the so-called hybrid functionals One popular hybrid functional is B3LYP, which has been employed for the work in this thesis.

2.5 B3LYP

The correlation and exchange functionals introduced by VWN [49], B88 [8], and LYP [52] are incorporated in B3LYP. Also, 20% exact HF exchange is included:

$$E_{xc}^{B3LYP} = (1 - a)E_{xc}^{LSDA} + aE_{xc}^{HF} + bE_{xc}^{B88} + cE_c^{LYP} + (1 - c)E_c^{VWN} \quad (2.42)$$

where $a = 0.20$, $b = 0.72$ and $c = 0.81$ are the same as in B3PW91 [7, 54]. Their values are optimized for B3PW91 through a linear least-square fit to 116 experimentally determined energies (56 atomization energies, 42 ionization potentials, 8 proton affinities and first-row total atomic energies) [54].

Of all modern functionals B3LYP, has proven to be the most popular to date. To establish the accuracy of B3LYP performance various tests have been done with respect to geometry and energies. For the B3LYP functional an unsigned error with respect to the G2 data base of only slightly above 2 kcal/mol was determined.

2.6 Continuum Solvation Model

In basic quantum mechanics, the emphasis is not placed on the continuity of the electronic distribution but on the discreteness of the molecular assembly. The concepts of continuum distribution functions to particles of different physical types, including electrons and nuclei as well are used in continuum model. A continuum model can be defined as a model in which a number of the degrees of freedom of the constituent particles (a large number) are described in a continuous way [11]. In this section we will discuss about the continuum solvation model.

2.6.1 Basics of The Continuum Model

Let us consider an infinite assembly of molecules (solvent) with a solute system \mathbf{M} in a given temperature and pressure. The effective fixed-nuclei Hamiltonian \hat{H}_M of this system is dependent on the the coordinates of N_{el} electrons $\mathbf{q} = \mathbf{q}_1, \dots, \mathbf{q}_{N_{el}}$ and parametrically, on the coordinates of N_{nuc} nuclei, $\mathbf{Q} = \mathbf{Q}_1, \dots, \mathbf{Q}_{N_{nuc}}$ [11]. Now, the Hamiltonian can be written as,

$$\hat{H}_M(\mathbf{q}; \mathbf{Q}) = \hat{H}_M^{(0)}(\mathbf{q}; \mathbf{Q}) + \hat{V}_{int} \quad (2.43)$$

where, $\hat{H}_M^{(0)}$ is the electronic Hamiltonian in vacuum according to the Born-Oppenheimer approximation, and \hat{V} is the interaction potential. The related Schrödinger equation can be expressed as,

$$\hat{H}_M(\mathbf{q}; \mathbf{Q})\Psi^{(f)}(\mathbf{q}; \mathbf{Q}) = \mathbf{E}^{(f)}(\mathbf{Q})\Psi^{(f)}(\mathbf{q}; \mathbf{Q}) \quad (2.44)$$

where, $E^{(f)}$ is the eigenvalue, which contains all relevant information about the solvent effects on the solute \mathbf{M} . To calculate the solvent effect on solute we can consider the molecular charge distribution ϱ_M in place of $\Psi^{(f)}$. Now, ϱ_M can be written as,

$$\varrho_M(\mathbf{r}; \mathbf{Q}) = \varrho_{nuc}(\mathbf{r}; \mathbf{Q}) + \varrho_{el}(\mathbf{r}; \mathbf{Q}) \quad (2.45)$$

where, ϱ_{nuc} is the discrete nuclear charge distribution

$$\varrho_{nuc}(\mathbf{r}; \mathbf{Q}) = \sum_{\alpha} \mathbf{Z}_{\alpha} \delta(\mathbf{r} - \mathbf{Q}_{\alpha}) \quad (2.46)$$

and ϱ_{el} is the electron density function,

$$\varrho_{el}(\mathbf{r}; \mathbf{Q}) = - \int |\Psi_{(f)}(\mathbf{q}; \mathbf{Q})|^2 d\mathbf{q}_2 \dots d\mathbf{q}_{N_{el}} \quad (2.47)$$

Here all the symbols have the usual meaning. On the other hand, \hat{V}_{int} is contains a thermally averaged distribution function of the solvent molecules, g_S [11], so that we may write,

$$\hat{V}_{int} = \hat{V}_{int}(\mathbf{q}; \mathbf{Q}; g_S) \quad (2.48)$$

The above expression of \hat{V}_{int} can be reduced to its classical electrostatic component \hat{V}_{σ} and g_S can be described as a linear isotropic continuum, characterized by the static dielectric constant ϵ of the bulk solvent, which depends on the temperature T [11]. \hat{V}_{int} can be written as,

$$\hat{V}_{int} = \hat{V}_{\sigma}(\mathbf{q}; \mathbf{Q}, \sigma_M, \epsilon) = \sum_{\alpha} \mathbf{Z}_{\alpha} \Phi_{\sigma}(\mathbf{Q}_{\alpha}) + \sum_i \Phi_{\sigma} \mathbf{q}_i \quad (2.49)$$

where, $\Phi_{\sigma}(\mathbf{r})$ is the value of the electrostatic field generated by the polarized dielectric at the position \mathbf{r} . The solute-solvent interaction contribution to the total energy $E_{(f)}$, can be expressed by the integral,

$$W_{MS} = \int_{allspace} \Psi^{(f)*} \hat{V}_{\sigma} \Psi^{(f)} d\mathbf{q}_1 \dots d\mathbf{q}_{N_{el}} = \int_{allspace} \varrho_M(\mathbf{r}) \Phi_{\sigma}(\mathbf{r}) dr_3 \quad (2.50)$$

where \hat{V}_{σ} is a mono-electronic operator, which depends on the total charge distribution ϱ_M , on the assumed geometry of M , and on the value of the dielectric constant, ϵ .

2.6.2 Cavity

There are a couple of approaches to describe Φ_σ and the electrostatic interaction energy between ϱ_M and Φ_σ . The approaches are: (1) multipole expansion, (2) apparent surface charge, (3) image charge, (4) finite differences, and (5) finite elements [11]. In all these methods one thing is common: an empty cavity in the dielectric medium, in which the solute M resides.

The shape and size of the cavity are critical factors to find out the solvent effect. An ideal solute cavity should reproduce the shape of the solute M, which includes the whole charge distribution ϱ_M and with the exclusion of empty spaces which can be filled by the solvent continuous distribution. The solvation effects will be reduced if the cavity is large, whereas serious errors may arise in the evaluation of the interaction energy for the portions of ϱ_M (atoms or bonds) near the boundaries, due to the small cavity. A wrong shape of the cavity will introduce distortions in the description of the reaction field and of the related solvent effects. The cavity shapes actually employed are the following ones: (1) regular shapes (sphere, ellipsoid, cylinder); or (2) molecular shapes, which include (a) unions of overlapping spheres centered on the nuclei of the solute, (b) unions of overlapping spheres centered on some chemical groups of the solute, (c) unions of overlapping spheres, some of which are not centered on the nuclei, located so as to fill all the space not accessible to the solvent, and (d) unions of overlapping spheres and cylinders, connected with portions of concave solids, to fill the space not accessible to the solvent [11].

Not only the shape of the cavity is important for the solvent-solute interactions, but also cavity volume and surface area are also important [56, 57]. Also, dispersion, repulsion, and cavitation are playing a role in the continuum model. All these additional terms require cavities of different size, and the excluded volume is related to the sum of the solute and solvent radii. Miertiis, Scrocco, and Tomasi suggested a definition for the cavity radii in there the original version of the polarizable continuum model (PCM) [58]. According to their proposed definition, the cavity is described in terms of spheres with radii R_α proportional to the van der Waals radii:

$$R_\alpha = f R_\alpha^{vdW} \quad (2.51)$$

where, the factor f must be slightly larger than 1. Bondi has given the most popular set of reference atomic radii, which is obtained from crystallographic data [59]. There is a lot of work about the f factor [60, 61, 62]. A complete discussion about this topic is beyond the

scope of this thesis.

2.6.3 Polarizable Continuum Model (PCM)

In the last section we have discussed how the cavity of the solute is influencing the solvent-solute interaction. In this work we have used the PCM model. In this section we will discuss the Polarizable Continuum Model (PCM).

According to classical electrostatics, the reaction potential Φ_σ can be described, everywhere in the space, in terms of an apparent charge distribution σ spread on the surface of the cavity. A σ -charge distribution appears at each surface of discontinuity between different regions of the dielectric medium and can be expressed in terms of the difference of the respective polarization vectors \vec{P}_i and \vec{P}_j , so the charge distribution can be expressed as,

$$\sigma_{ij} = -(\vec{P}_j - \vec{P}_i) \cdot \vec{n}_{ij} \quad (2.52)$$

where \vec{n}_{ij} is the unit vector at the boundary surface pointing from medium i to medium j, whereas the polarization vector can be written as,

$$\vec{P}_i = -\frac{\epsilon_i - 1}{4\pi} \cdot \vec{\nabla} \Phi(\vec{r}) \quad (2.53)$$

Here the regions are two, inside the cavity and outside the cavity. Inside the cavity, $\epsilon_i = 1$ and $\vec{P}_i = 0$, on the other hand outside the cavity, $\epsilon_j = \epsilon$ and $\vec{P}_j = \vec{P}$. Now, the Eqn. 2.52 can be written as,

$$\sigma = -\vec{P} \cdot \vec{n} = \frac{\epsilon - 1}{4\pi} \vec{\nabla} \Phi_{out}(\vec{r}) \cdot \vec{n} = \frac{\epsilon - 1}{4\pi\epsilon} \vec{\nabla} \Phi_{in}(\vec{r}) \cdot \vec{n} \quad (2.54)$$

The potential Φ , is composed of two contributions, $\Phi = \Phi_M + \Phi_\sigma$ and the Eqn 2.54 can be expressed as,

$$\sigma = \frac{\epsilon - 1}{4\pi\epsilon} \frac{\partial(\Phi_{M,in} - \Phi_{\sigma,in})}{\partial \vec{n}} \quad (2.55)$$

with

$$\Phi_\sigma(\vec{r}) = \int_{\Sigma} \frac{\sigma(\vec{s})}{|\vec{r} - \vec{s}|} d^2s \quad (2.56)$$

where, Σ is the cavity surface, the vector s defines a point on Σ and \vec{n} indicates the unit vector perpendicular to the cavity surface and pointing outward [12]. After its first formulation, the PCM, has been modified many times both in its theoretical aspects and in its numerical implementation [64, 65]. We have used this method for this work.

2.7 Spin Contamination

The one-electron Hartree-Fock (HF) and Kohn-Sham (KS) wave functions may exist in two forms: restricted and unrestricted with respect to the spin wave function. The application of unrestricted calculations is absolutely necessary for systems with open-shell configurations. Many transition metal complexes are open-shell systems. The unrestricted Hartree-Fock (UHF) and Kohn-Sham (UKS) calculations have, however, a serious deficiency. As a rule, UHF or UKS wave functions for biradicals, polyradicals, and a number of small molecules are heavily contaminated by higher spin components. This makes the calculation of the electronic energy with a given total spin quite unreliable [25]. The degree of spin contamination is often assessed by computing the expectation value of the \hat{S}^2 operator:

$$\langle \hat{S}^2 \rangle = S(S + 1) \quad (2.57)$$

where S has the usual meaning. As an example the expectation value of $\langle \hat{S}^2 \rangle = 0.75$ for doublet, whereas for triplet it should be 2.00. This is a typical method for assessing the spin contamination in *ab initio* methods, with the help of $\langle \hat{S}^2 \rangle$ it is possible to calculate the degree of spin contamination in DFT.

Ovchinnikov and Labanowski proposed a new method for correcting unrestricted HF or KS energies to exclude contributions from the higher spin components [25]. They have considered that, the unrestricted calculation of the singlet state is contaminated only by a triplet [25]. In this case the the unrestricted wave function of a singlet state, $\Psi_{unr,S}$ is the sum of a triplet and a singlet component. It can be written as,

$$\Psi_{unr,S} = a\Psi_S + b\Psi_T \quad (2.58)$$

and

$$a^2 + b^2 = 1 \quad (2.59)$$

where Ψ_S is the wave function for a pure singlet and Ψ_T for a pure triplet, whereas a and b are the contamination parameters for singlet and triplet, respectively. The triplet contamination parameter b^2 can be expressed easily as an \hat{S}^2 matrix element,

$$b^2 = \frac{1}{2} \langle \Psi_{unr,S} | \hat{S}^2 | \Psi_{unr,S} \rangle \quad (2.60)$$

Now using the Equ. 2.44, the energy in the unrestricted mode can be written as,

$$E_{unr,S} = \langle \Psi_{unr,S} | \hat{H} | \Psi_{unr,S} \rangle = a^2 \langle \Psi_S | \hat{H} | \Psi_S \rangle + b^2 \langle \Psi_T | \hat{H} | \Psi_T \rangle \quad (2.61)$$

where \hat{H} has the usual meaning and Ψ_S and Ψ_T are the lowest-energy wave functions corresponding to the pure singlet and triplet states, respectively. If the energy of the triplet state can be written exactly as,

$$E_T = \langle \Psi_T | \hat{H} | \Psi_T \rangle \quad (2.62)$$

then, the energy of the singlet state E_S can be obtained from Equ. 2.47 and 2.48,

$$E_S = \langle \Psi_S | \hat{H} | \Psi_S \rangle = \frac{E_{unr,S} - b^2 E_T}{1 - b^2} \quad (2.63)$$

From the above discussion it is clear that, for a given geometry the pure singlet state energy could be calculated in three steps: (I) unrestricted calculations of the triplet energy at a given geometry, (II) unrestricted calculations of the singlet energy at a given geometry using triplet orbitals [and the charge-density and exchange-correlation potential in the case of DFT calculations] to seed the SCF procedure, and (III) calculating the uncontaminated energy of the singlet by removing the triplet contamination b^2 according to Equ. 2.49. In our work we have used this method for the energy correction of the singlet state.

2.8 Minimum Energy Crossing Point

Many molecular systems have diversity about their isomeric structures. Usually, all the local minima for those molecular systems lie on the same potential energy surface (PES). On the other hand, there are many reactions of transition metal organometallic compounds whose spin state changes oftenly, due to the changes in spin state those molecular systems have different isomers that lie on different PESs. The most common example of this in organometallic chemistry is when the reaction started in triplet state, but the end product is in singlet state. All these interconversions are a non-adiabatic process [67]. This kind of interconversion leads to the crossing between two energy surfaces, which is called the minimum energy crossing point (MECP). Harvey *et. al.* reported about a new method of finding the MECP [68].

Usually, the MECP is strongly dependent on the relative energy of the two PESs. There are few methods for locating the MECP [67, 70, 71]. All these methods are used for locating the MECP between two noninteracting PESs, e.g. corresponding to states of different spin, of different spatial symmetry, or of different number of electrons [69, 70, 71, 72]. These methods that require analytical energy gradient, with computational resources, place restrictions on the level of electronic structure theory that can be applied. Recently, Harvey *et. al.* proposed a new hybrid method to locate the MECP [68]. This method is a combination of methods

proposed by Bearpark *et. al.* [70] and Morokuma and coworkers [71, 72].

Usually, to locate MECP, the energies E_i on the two PESs and corresponding energy gradients ($\partial E_i/\partial q$) with respect to the nuclear coordinates q are combined to yield two effective gradients, \mathbf{f} and \mathbf{g} . According to all previous methods for locating MECPs, using gradients and energies are calculated at the same level, which is the main difference with respect to new hybrid method. In hybride method \mathbf{f} and \mathbf{g} can be written as,

$$\mathbf{f} = (E_1^{high} - E_2^{high}) \left[\left(\frac{\partial E_1^{low}}{\partial q} \right) - \left(\frac{\partial E_2^{low}}{\partial q} \right) \right] \quad (2.64)$$

$$\mathbf{g} = \left(\frac{\partial E_1}{\partial q} \right) - \frac{x_1}{|x_1|} \left[\left(\frac{\partial E_1}{\partial q} \right) \cdot \frac{x_1}{|x_1|} \right] \quad (2.65)$$

In Equ. 2.50, the superscripts (*high*) and (*low*) refer to the level at which the corresponding number or vector is calculated [68]. The overall shape of the two PESs could be reproduced correctly by using the low-level gradients, even if their relative energies are not. Thus, the difference gradient x_1 should have the correct orientation, as should the gradient \mathbf{g} . Following the approximate gradients \mathbf{f} and \mathbf{g} will lead to a point where they are equal to zero. In this method the geometry optimization is done in *low-level* on one of the surfaces, under the constraint that the difference of the *high-level* energies is zero [68]. It can be said that, in many ways this method is equivalent to that using calculated high-level single point energies at stationary points optimized at a lower level. Using this method, in this study we have calculated MECPs between singlet and triplet surfaces.

2.9 Conclusion

In the preceding paragraphs of DFT has been presented briefly and the B3LYP the most popular and most widely used functional. The good performance of the B3LYP has demonstrated in many chemical applications such difficult areas as open-shell transition-metal chemistry. B3LYP can be an inexpensive and useful aid for assessing the reaction mechanism of transition metal compounds. While these are general conclusions, it is important to evaluate the results for each case individually and to analyze if known experimental properties are reproduced correctly.

Bibliography

- [1] D. R. Hartree. *Proc. Cambridge Philos. Soc.* **1928**, 24, 89.
- [2] V. Fock, *Z. Phys.* **1930**, 61, 126.
- [3] A. Szabo and N. S. Ostlund, *Modern Quantum Chemistry: Introduction to Advanced Electronic Structure Theory*, 1st Rev. ed., McGraw-Hill, Inc., New York, **1989**.
- [4] L. H. Thomas, *Proc. Cambridge Philos. Soc.* **1927**, 23, 542.
- [5] E. Fermi, *Z. Phys.*, **1928** 48, 73 .
- [6] N. H. March, *Self-Consistent Fields in Atoms*, Oxford: Pergamon, **1975**.
- [7] W. Koch and M.C. Holthausen *A Chemists Guide to Density Functional Theory*, 2nd Edition. Wiley-VCH Verlag GmbH. **2001**.
- [8] J. A. Alonso and L. A. Girifalco, *J. Phys. Chem. Solids.* **1977**, 38, 869.
- [9] B. Jacob, E. K. U. Gross and R. M. Dreizler, *J. Phys. B.* **1978**, 11, 22.
- [10] E. K. U. Gross and R. M. Dreizler, *Phys. Rev. A.* **1979**, 20, 1798.
- [11] P. Gombs, *Die Statistische Theorie des Atomes and ihre Anwendungen*, Springer, Berlin, **1949**.
- [12] N. H. March, *Adv. Phys.* **1957**, 6, 1.
- [13] N. H. March, *Theor. Chem: A Specialists Periodic Report* **1981**, 4, 92.
- [14] E. H. Lieb and B. Simon, *Phys. Rev. Lett.* **1973**, 31, 681.
- [15] E. H. Lieb, *Rev. Mod. Phys.* **1976**, 48, 553.
- [16] E. H. Lieb, *Rev. Mod. Phys.* **1981**, 53, 603.

- [17] E. H. Lieb and W. Thirring, *In Studies in Mathematical Physics*, ed. by E. H. Lieb, B. Simon and A. S. Wightman, Princeton University, Princeton, New Jersey, **1976**, 269.
- [18] P. A. M. Dirac, *Proc. Cambridge Philos. Soc.* **1930**, 26, 376.
- [19] C. F. von Weizsacker, *Z. Phys.*, **1935** 96, 431.
- [20] J. C. Slater, *Phys. Rev.* **1951**, 82, 538.
- [21] J. C. Slater, *In Adv. Quantum Chem.*, Ed. P. O. Lowdin, 6, Academic, New York, **1972**, 1.
- [22] K. H. Johnson, *Adv. Quantum Chem.* **1973**, 7, 143.
- [23] J. W. D. Connolly, *In Semiempirical Methods of Electronic Structure Calculations, Part A: Techniques*, Ed. G. A. Segal, VI, Chapter 4, Plenum, New York, **1977**.
- [24] J. C. Slater, *The Self-Consistent Field for Molecules and Solids: Quantum Theory of Molecules and Solids*, 4, McGraw-Hill, New York, **1974**.
- [25] J. C. Slater, *Int. J. Quantum Chem. Symp.* **1975**, 9, 7.
- [26] R. Gasper, *Acta Physica Hungaria* **1954**, 3, 263.
- [27] P. -O. Lowdin, *Phys. Rev.* **1955**, 97, 1474.
- [28] R. McWeeny, *Rev. Mod. Phys.* **1960**, 32, 335.
- [29] E. R. Davidson, *Reduced Density Matrices in Quantum Chemistry*, Academic Press, New York, **1976**.
- [30] P. -O. Lowdin, *Phys. Rev.* **1955**, 97, 1490.
- [31] T. L. Gilbert, *Phys. Rev. B.* **1975**, 12, 2111.
- [32] M. Berrondo and O. Goscinski, *Int. J. Quantum Chem. Symp.* **1975**, 9, 67.
- [33] R. A. Donnelly and R. G. Parr, *J. Chem. Phys.* **1978**, 69, 4431.
- [34] R. A. Donnelly, *J. Chem. Phys.* **1979**, 71, 2874.
- [35] J. Coleman, *Rev. Mod. Phys.* **1963**, 35, 668.

- [36] J. Coleman, *In The Force Concept in Chemistry*, Ed. B. M. Deb, Van Nostrand, Reinhold, **1981**, 418.
- [37] P. Hohenberg and W. Kohn, *Phys. Rev.* **1964**, 136, B864.
- [38] E.H. Lieb, *Density Functional Methods in Physics NATO ASI Series B123* Ed. R. M.Dreizler and J. da Providencia, Plenum, New York, **1985**.
- [39] M. Levy, *Phys. Rev. A* **1982**, 26, 1200.
- [40] E. H. Lieb, *In Physics as Natural Philosophy, Essays in Honor of Laszlo Tisza on his 75th Birthday.*, M. Fesgbach and A. Shimony, Eds., (MIT Press, Cambridge), **1982**, 111.
- [41] R. G. Parr and W. Yang, *Density Functional Theory of Atoms and Molecules*, Oxford University Press: Oxford, **1989**.
- [42] J. E. Harriman, *Phys. Rev. A.* **1980**, 24, 680.
- [43] M. Levy, *Proc. Natl. Acad. Sci. USA.* **1979**, 76, 6062.
- [44] W. Kohn and L. J. Sham, *Phys. Rev.* **1965**, 140, A1133.
- [45] A. K. Rajagopal, *Adv. Chem. Phys.* **1980** 41, 59.
- [46] A. S. Bamzai and B. M. Deb, *Rev. Mod. Phys.* **1981**, 53, 95; **1981**, 53, 593(E).
- [47] R. G. Parr, *Annu. Rev. Phys. Chem.* **1983**, 34, 631.
- [48] J. P. Dahl and J. Avery, Eds., *Local Density Approximations in Quantum Chemistry and Solid State Physics*, Plenum, New York, **1984** and references therein.
- [49] S.H. Vosko, L. Wilk and M. Nusair, *Can. J. Phys.* **1980**, 58, 1200.
- [50] J.P. Perdew and Y. Wang. *Phys. Rev. B.*, **1986**, 33, 8800.
- [51] A.D. Becke, *Phys. Rev. A.* **1988**, 38, 3098.
- [52] C. Lee, W. Yang and R. G. Parr, *Phys. Rev.* **1988**, B37, 785.
- [53] R. Colle and D. Salvetti, *Theor. Chim. Acta.* **1975**, 37, 329.
- [54] A. D. Becke, *J. Chem. Phys.* **1993**, 98, 1372.
- [55] J. Tomasi, B. Mennucci and R. Cammi, *Chem. Rev.* **2005**, 105, 2999.

- [56] A. Y. Meyer, *Chem. SOCR.e v.* **1986**, 15, 446.
- [57] P. G. Mezey, *InReuzews in Computational Chemistry; Lipkowitz, K. B., Boyd, D. B.,* Eds.; VCH: New York, **1990**, 265.
- [58] S. Miertug, E. Scrocco, and L. Tomasi, *Chem. Phys.* **1981**, 55, 117.
- [59] A. Bondi, *J. Phys. Chem.* **1964** 68, 441.
- [60] S. Miertug, J. Bartog and M. Trebaticka, *J. Mol. Liq.* **1987** 33, 139.
- [61] M. A. Aguilar, M. A. Martin, S. Tolosa and F. J. Olivares del Valle, *J. Mol. Struct. (Theochem.)* **1988**, 166, 313.
- [62] F. J. Olivares del Valle, M. A. Aguilar, and J. C. Contador, *Chem. Phys.* **1993** 170, 161.
- [63] J. Tomasi and M. Persico, *Chem. Rev.* **1994**, 94, 2027.
- [64] R. Cammi and J. Tomasi, *J. Comput. Chem.* **1995**, 16, 1449.
- [65] E. Cancès, B. Mennucci and J. Tomasi, *J. Chem. Phys.* 107, 3032, (1997).
- [66] A.A. Ovchinnikov and J. K. Labanowski, *Phys. Rev. A* **1996**, 53, 3946.
- [67] D. R. Yarkony, *J. Phys. Chem.* **1996**, 100, 18612.
- [68] J. N. Harvey, M. Aschi, H. Schwarz and W. Koch, *Theor. Chem. Acc.* **1998**, 99, 95.
- [69] D. R. Yarkony, *J. Phys. Chem.* **1993**, 97, 4407.
- [70] M. J. Bearpark, M. A. Robb, and H. B. Schlegel, *Chem. Phys. Lett.* **1994**, 223, 269.
- [71] N. Koga, and K. Morokuma, *Chem. Phys. Lett.* **1985**, 119, 371.
- [72] Q. Cui and K. Morokuma, *Chem. Phys. Lett.* **1997**, 272, 319.
- [73] J. Hrusak, D. der. Schro and Iwata, *J. Chem. Phys.* **1997**, 106, 7541.

Chapter 3

Selective Oxidation of Palladium-hydride Bond

3.1 Introduction

Oxidation chemistry of transition metal complexes is very interesting. Oxidation reactions are very important for both manipulation of functional group and introduction of heteroatoms in target synthesis. Recently, development of selective oxidation reactions using molecular oxygen has created great interest. There are some aspects to be considered for the development of the oxidation reaction, such as, selection of the stoichiometric oxidant where versatility, expense, and environmental impact need to be addressed. Significant progress in Pd-catalyzed oxidations has emerged, as a particularly promising reaction type owing to their ability to directly couple O_2 reduction [1, 2, 3, 4, 5]. In chapter 1, it was already mentioned that in Pd-catalyzed oxidation chemistry the catalysis can be separated into two distinct ways (Scheme 1.3, Chapter 1). It was also mentioned that the reaction of triplet-state O_2 with a Pd center is formally a spin-forbidden process [6, 7, 8, 9]. Now the question is: how does O_2 readily react with Pd? In this regard, several groups have demonstrated O_2 activation by different kind of Pd-complexes.

Recently, Keith *et. al.* explained the reaction mechanism of O_2 activation by Pd(sparteine)(Cl)(H) system in order to get a corresponding hydroperoxide complex [10]. The first experimental observation of insertion of O_2 into Pd^{II} -hydride bond to form an (η^1 -hydroperoxo)palladium(II) complex have been reported by Denney *et. al.* [11]. The experimental observation confirmed that a radical chain mechanism is not involved and also it

is unaffected by light. Also, Keith *et. al.* have explained the reaction mechanism about the insertion of O_2 into Pd^{II} -hydride bond to form an (η^1 -hydroperoxo)palladium(II) complex [12], but some questions are still open.

Stahl and coworkers examined the feasibility of the both pathways for the trans- $(NHC)_2Pd(H)OAc$ system [13]. In this study the authors have examined the three different carboxylic acids (acetic, benzoic, p-nitrobenzoic) in order to understand the ability of the carboxylic acids to catalyze the oxygenation of the Pd^{II} -hydride. Same group also reported about the theoretical investigation of the same systems [14]. In that Stahl and coworkers have examined both pathways: (1) a direct insertion pathway and (2) a slow reductive elimination followed by fast oxygenation, but the kinetic barriers are very similar for the both apthways [14].

From the above discussion it can be say that, experimental and theoretical evidence support the viability of both mechanisms, but further work will be required to elucidate the details of these pathways in which ligand and additives will most likely have a profound influence. Many questions concerning the mechanistic details of the Pd-catalyzed oxidation reactions are still open. In the framework of an extended project the aim of this work is to illuminate the mechanistic details. In the next section we will present the results of our works.

3.2 Articles

In this section we would like to present the results of our work. In the first two articles we will present results regarding direct insertion of molecular oxygen into Palladium-hydride bond [11, 13]. In next two articles we will present the results regarding the preferable mechanism between the two pathways and the effect of carboxylic acids [13].

Article I

On the insertion mechanism of molecular oxygen into a Pd(II)H bond. Something to add.



On the insertion mechanism of molecular oxygen into a Pd(II)–H bond. Something to add

Sugata Chowdhury, Ivan Rivalta, Nino Russo *, Emilia Sicilia

Dipartimento di Chimica and Centro di Calcolo ad Alte Prestazioni per Elaborazioni Parallele e Distribuite-Centro d'Eccellenza MURST, Università della Calabria, I-87030 Arcavacata di Rende, Italy

Received 27 April 2007; in final form 12 June 2007
Available online 21 June 2007

Abstract

Density functional theory (DFT) in its hybrid B3LYP formulation was applied to the investigation of the mechanistic details of the insertion of molecular oxygen into the palladium(II) hydride bond of the (PCP)Pd–H complex (PCP = 1,3-(CH₂P^tBu₂)₂C₆H₃[−]) to form the corresponding Pd(II) hydroperoxide. The calculations reveal that minima and transition state through which formation of the final product takes place are different along the singlet and triplet pathways. A triplet–singlet crossing occurs before the formation of a stable singlet intermediate from which the reaction straightforwardly proceeds to yield the singlet hydroperoxo complex. Differences and improvements with respect to analogous theoretical investigations are highlighted.

© 2007 Elsevier B.V. All rights reserved.

1. Introduction

The oxidative functionalization of organic molecules utilizing molecular oxygen as a reagent remains one of the major challenges for research in catalysis [1]. The ready availability of O₂ and the absence of environmentally harmful by-products are among the attractive features of such processes. However, uncatalyzed chemical reactions between molecular oxygen and organic substrates generally result in complete combustion of the starting materials and, consequently, widespread use of oxygen will require the development of catalytic strategies to produce useful and selectively oxidized products. The recent use of homogeneous catalytic systems involving palladium complexes points toward new opportunities for selective and efficient aerobic oxidation chemistry [1–8]. Fundamental studies of the role of transition metals in catalytic oxidation must naturally include investigations of the reaction pathways of organometallic molecules with O₂. One pathway involves

the direct insertion of oxygen into a palladium(II)-hydride bond to form a palladium hydroperoxide species [9–11]. The second mechanistic possibility is the formation of a Pd(0) species through the reductive elimination of HX from the Pd(II)–hydride complex followed by the oxygenation of Pd(0) to form a η^2 -peroxido Pd(II) species. Upon protonation of the peroxopalladium(II) intermediate the same palladium hydroperoxide species is formed [12–14]. The latter mechanism has substantial experimental support even if the reaction between Pd(0) and triplet oxygen is spin forbidden [12–14]. Stahl and coworkers performed a DFT theoretical study for a model ethylenediamine-coordinated palladium(0) complex that showed as the exothermic formation of the singlet Pd(II)-peroxo species requires spin crossing between triplet and singlet surfaces mediated by spin–orbit coupling [15].

The first direct observation of insertion of molecular oxygen into a Pd(II)–hydride bond to form a hydroperoxopalladium complex was reported by Goldberg and coworkers for a Pd complex that, due to the nature of the ligand, cannot undergo reductive elimination [16]. Benzene solutions of (^tBuPCP)PdH (^tBuPCP = 1,3-(CH₂P^tBu₂)₂C₆H₃[−]) exposed to O₂ were observed to cleanly react

* Corresponding author. Fax: +39 0984 492044.
E-mail address: nrusso@unical.it (N. Russo).

to yield (^tBuPCP)PdOOH, which is relatively stable at ambient temperature as a solid and was structurally characterized. The main information coming from the experimental findings can be summarized as follows. The reaction is unaffected by radical inhibitors and light, supporting that a radical mechanism is not involved. A second-order reaction rate, that is first-order in palladium and first-order in oxygen, was documented as well as the involvement of the Pd–H bond cleavage in the rate-determining step. A DFT theoretical investigation, carried out by Goddard and coworkers, of the involved mechanism has very recently appeared in literature that demonstrates how an insertion mechanism is possible and plausible [17]. In the same work is discussed the difference with respect to a previous study of Goddard and collaborators that underlined the subordination of the O₂ insertion process to the presence of a H-bond acceptor *cis* to the hydride [18].

Both pathways, that is direct insertion of O₂ into a Pd(II)–H bond and oxygenation of Pd(0), were considered viable by Stahl and coworkers in their investigation of the conversion of a new class of NHC-coordinated Pd(II)–hydride complexes (NHC = N-heterocyclic carbene) into the corresponding Pd(II)–hydroperoxides upon exposure to O₂ [19], as experimental data could support both mechanisms. A combined experimental and theoretical investigation of the Pd(0) oxygenation step for the same system has been published by Stahl and coworkers [20]. Very recently, four possible alternative pathways have been computationally examined in detail by Popp and Stahl to probe the reaction mechanism of the formal insertion of molecular oxygen into the Pd–H bond of *trans*-(NHC)₂Pd(H)OAc [21].

The computational study of Goddard et al. [17] on that system supports a low-energy mechanism of a hydrogen atom abstraction. Namely, hydrogen atom is abstracted from the Pd center by molecular oxygen to form a HOO fragment that weakly interacts with the Pd(I) center. Rotation of HO₂ moiety enables formation of a Pd–O bond to give the final Pd(II)–hydroperoxo product. A minimum energy crossing point (MECP) between triplet and singlet surfaces was located at the exit channel of the reaction, whereas the rearrangement mechanism of the HOO fragment to give the hydroperoxide product was not individuated.

The main conclusion of the computational study of Popp and Stahl on the oxygenation of the *trans*-(NHC)₂Pd(H)OAc [21] is that, among the four possible alternative studied pathways, those involving hydrogen atom abstraction and HX reductive elimination are both conceivable and exhibit barriers very similar in energy. Also in this last case the proposed steps of the hydrogen abstraction mechanism are: formation of a HOO moiety as a consequence of the hydrogen atom abstraction by molecular oxygen and formation of the final hydroperoxo product through rearrangement of the HO₂ fragment. In analogy with Goddard's analysis [17] the MECP between

singlet and triplet PES's was located at the exit channel of the reaction but no one of the surmised mechanisms for the rearrangement of the HO₂ fragment was confirmed.

Here we present the results of a detailed DFT investigation of the direct insertion mechanism of molecular oxygen into the Pd–H bond of (^tBuPCP)PdH complex. The results are relevant since, with respect to the previous theoretical investigations [17,21], new stationary points were localized along the optimized singlet PES and the transition state that enables the rearrangement of the HOO fragment to yield the hydroperoxo complex was individuated and characterized. Therefore, a new description of the mechanism corresponding to the hydrogen atom abstraction is outlined.

2. Computational details

Geometry optimizations as well as frequency calculations for all the reactants, intermediates, products and transition states were performed at the density functional level of theory, employing the Becke's three-parameter hybrid functional [22] combined with the Lee, Yang and Parr (LYP) [23] correlation functional, denoted as B3LYP as implemented by GAUSSIAN03/DFT code [24]. The same computational approach was used for the theoretical investigations of Goddard et al. [17] and Popp and Stahl [21]. For Pd the relativistic compact Stuttgart/Dresden effective core potential [25] was used in conjunction with its split valence basis set. The standard 6-311G* basis sets of Pople and coworkers were employed for the rest of the atoms. For each optimized stationary point vibrational analysis was performed to determine its character (minimum or saddle point) and zero-point vibrational energy (ZPVE) corrections were included in all relative energies (ΔE). For transition states it was carefully checked that the vibrational mode associated to the imaginary frequency corresponds to the correct movement of involved atoms. Furthermore, the intrinsic reaction coordinate (IRC) method [26,27] was used to assess that the localized TS's correctly connect to the corresponding minima along the imaginary mode of vibration.

To speed up calculations the ^tBu groups in ^tBuPCP ligand of the studied complex were substituted with methyl ones as testing calculations clearly showed that no significant structural change is introduced. For this reason, from now on we will indicate as PCP the model ligand 1,3-(CH₂PMe₂)₂C₆H₃[−].

Both triplet and singlet reaction paths were examined and for all the localized stationary points $\langle S^2 \rangle$ values were checked to assess whether spin contamination can influence the quality of the results. For triplet state structures $\langle S^2 \rangle$ values are very close to 2.0 for all the considered stationary points. On the contrary, unrestricted calculations for singlet structures revealed in some cases triplet spin contamination corresponding to $\langle S^2 \rangle$ values close to 1.0. For example, the unrestricted calculation of the singlet energy of O₂ gave a ¹Δ_g state too much stable due to the contam-

ination of the singlet wave function with the triplet state and a corresponding excitation energy of 10.5 kcal/mol, being the experimental value 22.5 kcal/mol. Adopting the method proposed by Ovchinnikov and Labanowski [28] for correcting the mixed spin energies and removing the foreign spin components, the singlet state corrected energy and a triplet–singlet energy gap of 20.7 kcal/mol were obtained, in very good agreement with the experimental value. The same correction scheme was applied to the energy of some other points, discussed in the next paragraphs, localized along the singlet pathway that revealed to be highly contaminated with the triplet. To locate the minimum energy crossing point (MECP) between the triplet surface of reactants and the singlet one of the products the methodology introduced by Harvey and coworkers was used [29]. Solvent effects were included through the polarisable continuum solvation model, PCM, initially devised by Tomasi and coworkers [30], performing single point calculations in benzene on fully optimized geometry of each stationary point along the reaction path. The cavity in which the solute is placed, defined in terms of interlocking spheres centered on solute atoms, was built up using the Gepol procedure [31,32] and the Pauling atomic radii. Non-electrostatic dispersion and repulsion [33] and cavitation free [34] contributions were also included into the solvation free energy calculation.

For the sake of comparison with previous theoretical results [17,21], single-point calculations for singlet multi-

plicity were carried out on fully optimized geometries of stationary points localized along the triplet pathway.

3. Results

The B3LYP calculated PES's for the reaction of O₂ with the (PCP)PdH complex are reported in Fig. 1, where relative energies are calculated with respect to the triplet ground state reactants asymptote. To assess whether the inclusion of thermal corrections could influence the shape of the reaction profiles, also enthalpy variations were calculated and reported.

In the same way, relative free energies in benzene solvent were calculated and reported in the same Figure for the ground state structures. No significant change, except a general stabilization of the stationary points, is introduced when solvent effects are taken into account. Geometrical structures of stationary points localized along singlet and triplet PES's are shown in Fig. 2 and the most significant geometrical parameters are collected in Table 1 along with experimental values available for the structure of the final hydroperoxide product [35].

According to previous theoretical investigations [21], the energy of the singlet stationary points obtained performing single point calculations on the fully optimized triplet structures are also reported in Fig. 1.

The first step of the reaction along the triplet pathway involves the formation of a weakly bound van der Waals

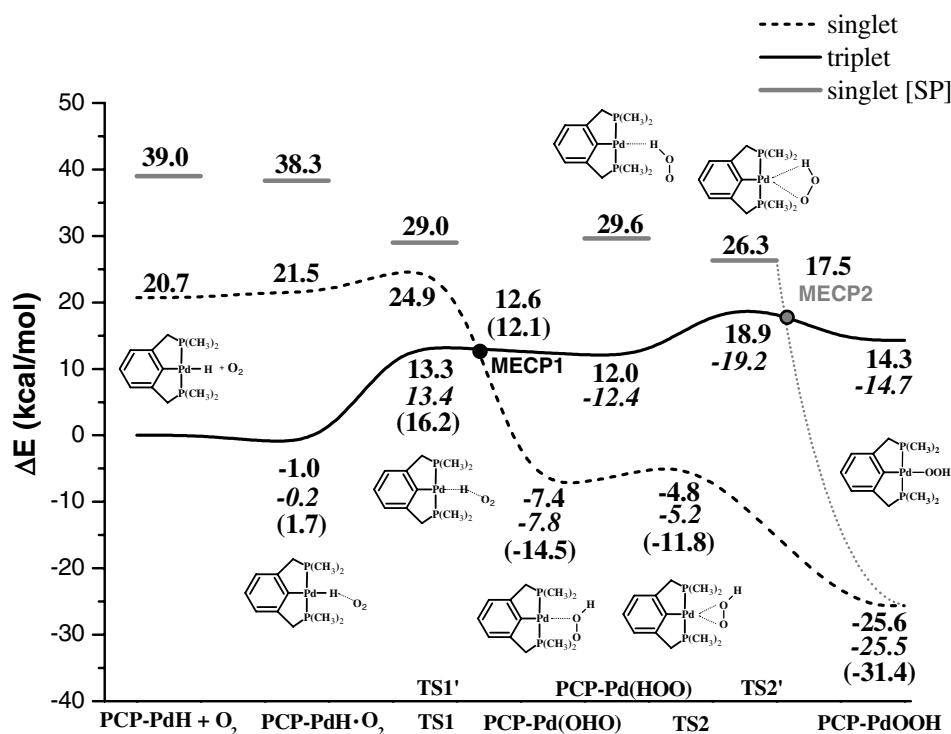


Fig. 1. Calculated potential energy surfaces for the reaction of singlet and triplet states of O₂ with (PCP)Pd(II)–H for conversion to (PCP)Pd(II)–OOH. Gibbs free energies changes at 298.15 K in benzene are also reported in parentheses for ground state structures along with enthalpy variations (in *italic*) and singlet single-point energies calculated on fully optimized structures of triplet stationary points. Energies are in kcal/mol and relative to the ground state reactants.

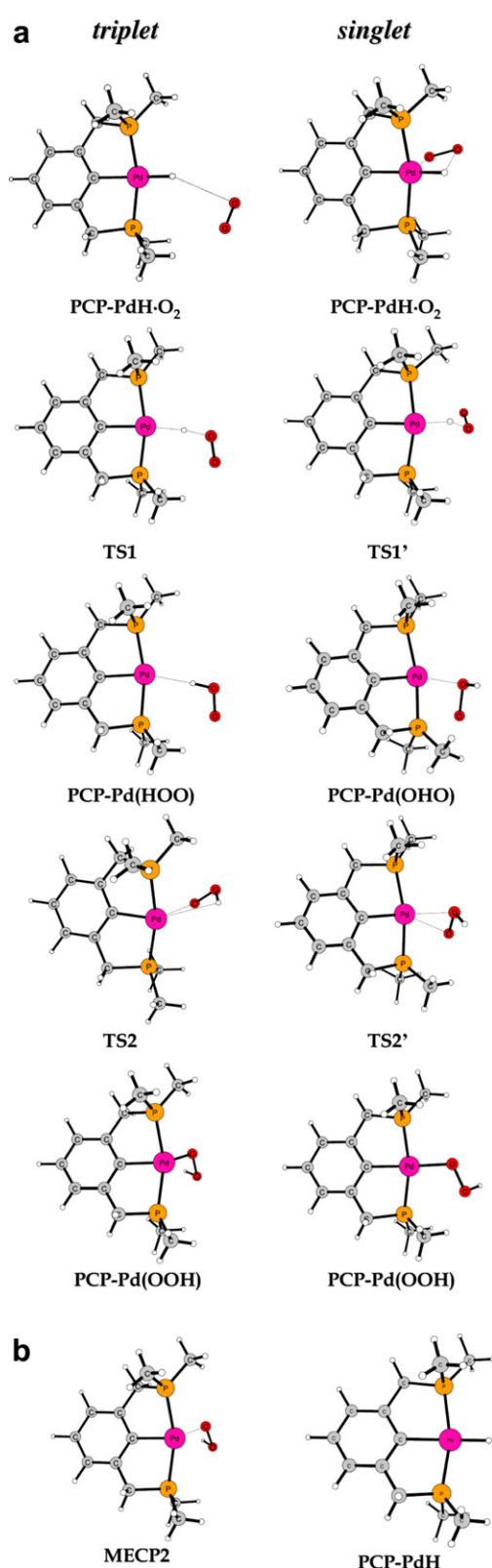


Fig. 2. (a) Calculated structures of singlet and triplet minima and transition states localized along the paths for the insertion of molecular oxygen into the Pd–H bond. In part (b) are reported also the structures of the initial (PCP)Pd–H complex and of the MECP2 crossing point.

complex that is only slightly exothermic in gas-phase (about 1 kcal/mol). Both oxygen atoms of the O₂ molecule

are about 4.6 Å far from the Pd center. The fully optimized structure of the corresponding complex in a singlet state is significantly higher in energy (about 22 kcal/mol higher in energy than the reactants asymptote). O₂ molecule is oriented parallel to the Pd–H bond and the closest oxygen atom is at about 2.3 Å from the Pd center. Since the unrestricted calculations on this adduct showed a significant amount of triplet contamination the method mentioned above [28] was applied to correct the calculated too low energy. The energy of the singlet stationary point obtained performing a single point calculation on the optimized triplet structure, according to the theoretical study reported in Ref. [21], is even higher ($\Delta E = 38.3$ kcal/mol).

The next step of the reaction along the triplet surface involves the abstraction of the hydrogen atom from the palladium center by O₂ that takes place overcoming an energy barrier of 14.3 kcal/mol for the formation of the TS1 transition state. In going from the first adduct (PCP–PdH·O₂) to TS1 the Pd–H bond distance stretches from 1.639 to 1.811 Å and at the same time the O–O bond length increases from 1.204 to 1.278 Å. The O–H distance is 1.297 Å indicating that the bond between oxygen and hydrogen is forming. The imaginary frequency for TS1 transition state is calculated to be $1401i$ cm⁻¹ and clearly corresponds to the movement of the hydrogen atom detaching from Pd and bonding to O atom. As a result a peroxy HOO radical is formed coordinated to the T-shaped Pd(I) complex through a weak interaction between hydrogen and Pd atoms. Indeed, the formation of this reaction intermediate, PCP–Pd(HOO), which lies 12 kcal/mol above the ground state reactants, is exothermic by only 1.3 kcal/mol. Along the singlet surface, instead, as molecular oxygen approaches the Pd center, at a distance of 1.817 Å between the closest oxygen and hydrogen a transition state, TS1', was localized and characterized. The normal mode associated to the imaginary frequency, calculated to be $177i$ cm⁻¹, corresponds to an in and out of plane movement of the hydrogen atom that consequently comes close to the oxygen atom forming a new O–H bond. To form the singlet TS1' transition state structure, which lies 24.9 kcal/mol above the separate reactants, is necessary to overcome a low energy barrier of 3.4 kcal/mol. Also for this stationary point the energy was corrected for spin contamination. From TS1' the reaction proceeds to yield a very stable singlet intermediate, indicated as PCP–Pd(OHO), in which hydrogen is now bonded (H–O = 0.964 Å) to the oxygen atom directly coordinated to Pd (Pd–O = 2.2 Å). Until now the existence of this intermediate, stabilized by 7.4 kcal/mol in gas-phase (14.5 kcal/mol in solvent) with respect to the reactants asymptote, was not evidenced by theoretical investigations. IRC calculations confirmed that the TS1' transition state is connected to both PCP–PdH·O₂ reactant and PCP–Pd(OHO) product. The analysis of the structures along the reaction coordinate from the transition state to the PCP–Pd(OHO) intermediate shows as the hydrogen atom approaches the proximal oxygen lengthening the O–O bond, whereas the

distal oxygen atom goes away from Pd and rotates down. Owing the stability of the singlet PCP–Pd(OHO) species that is more stable by about 19 kcal/mol than the corresponding triplet PCP–Pd(HOO) intermediate, in this region of the PES the system must undergo a spin inversion that takes place after passage of the TS1 transition state. Such a kind of spin crossover is not considered a rate-limiting factor as it involves species that are formed with excess energy and even electronically excited states become accessible. Following the procedure outlined before, the MECP between the triplet and singlet surface was localized. Fig. 3 shows the geometrical structure of the crossing point structure and its relative energy calculated in gas-phase and in solvent is reported in Fig. 1.

As it is evident from both geometry and energy of this point, the crossing occurs in the vicinity of the triplet transition state with the MECP1 structure that lies only 0.7 kcal/mol lower in energy. The main difference between the geometry of TS1 and MECP1 is the position of the hydrogen atom that is halfway between Pd and oxygen in the former case and bonded yet to oxygen in the latter.

It is worthwhile to underline that all the attempts to individuate a singlet intermediate with a structure analogous to that of the triplet PCP–Pd(HOO) complex were

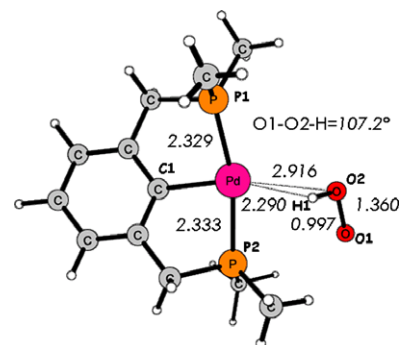


Fig. 3. MECP structure (MECP1) for spin conversion from triplet to singlet multiplicity. Selected bond lengths are in angstrom and angles in degrees. Labels employed to individuate O, P, C and H atoms have to be used to read geometrical parameters reported in Table 1.

Table 1

Selected bond lengths (Å) and angles (°) for minima, transition states and MCP2 crossing point localized along the singlet and triplet paths leading to (PCP)Pd(II)–OOH formation by insertion of molecular oxygen into the Pd–H bond of the (PCP)Pd(II)–H complex

Singlet							
Parameter	L–PdH	L–PdH · O2	TS1'	L–Pd(HOO)	TS2	L–Pd(OOH)	LPd(OOH) (exp.) ^a
Pd–C1	2.111	2.113	2.09	2.011	2.013	2.054	2.022
Pd–H1	1.64	1.643	1.671	–	–	–	–
Pd–O1	–	2.349	3.115	2.805	2.479	2.06	2.074
Pd–O2	–	3.101	2.68	2.2	2.305	–	–
O1–O2	–	1.253	1.259	1.489	1.509	1.477	1.470
O2–H1	–	3.15	1.816	0.964	0.964	0.965	1.10
Pd–P1	2.294	2.318	2.308	2.323	2.277	2.315	–
Pd–P2	2.294	2.311	2.305	2.362	2.333	2.304	–
Pd–O1–O2	–	115.5	58.5	51.1	65.4	110.6	108.5
O1–O2–H1	–	73.4	121.8	102.5	102.6	100.2	99.0
P1–Pd–P2	163.91	164.2	164.4	169.1	167.5	165.6	167.7
P2–Pd–C1	81.9	82.5	82.5	82.8	83.8	83.1	84.3
C1–Pd–O1	–	–	–	133.8	147.6	177.6	175.3
Pd–O1–O2–H1	–	–	–	119.0	117.0	134.5	–
Triplet							
	L–PdH · O2	TS1	L–Pd(OHO)	TS2'	MECP2	L–Pd(OOH)	
Pd–C1	2.113	2.114	2.113	2.115	2.147	2.137	
Pd–H1	1.639	1.811	2.29	–	–	–	
Pd–O1	–	–	–	2.867	2.167	2.166	
Pd–O2	–	–	–	–	–	–	
O1–O2	1.204	1.278	1.319	1.342	1.401	1.408	
O2–H1	3.411	1.297	1.015	0.979	0.97	0.969	
Pd–P1	2.297	2.306	2.329	2.344	2.422	2.416	
Pd–P2	2.294	2.319	2.332	2.342	2.425	2.419	
Pd–O1–O2	–	–	–	96.5	116.8	115.8	
O1–O2–H1	–	110.9	107.1	104.9	103.5	103.2	
P1–Pd–P2	163.5	165.1	165.6	164.9	162.2	162.0	
P2–Pd–C1	81.8	82.3	82.7	82.5	81.4	81.5	
C1–Pd–O1	–	–	–	–	114.3	116.8	
Pd–O1–O2–H1	–	1.0	2.1	43.8	103.6	105.2	

L = PCP. The available experimental geometrical parameters for the hydroperoxide complex are also reported.

^a Ref. [35].

unsuccessful in spite of the numerous strategies used to find it out.

The final step of the reaction that leads to formation of the final hydroperoxo palladium(II) complex takes place along the singlet pathway through the detachment of the proximal oxygen from Pd and formation of a new bond with the distal oxygen. Triplet hydroperoxide product formation involves, instead, rearrangement of the HOO fragment in such a way that the terminal oxygen and hydrogen atoms move in opposite directions towards and away from the Pd center, respectively. Both the corresponding transition states that is necessary to surmount were localized and confirmed by IRC analysis. The singlet TS2 structure lies 4.8 kcal/mol (11.8 kcal/mol when solvent effects are included) below the reactants dissociation limit and is characterized by an imaginary frequency of $230i\text{ cm}^{-1}$. Along the triplet PES the TS2' structure is destabilized respect to reactants by 18.9 kcal/mol and the corresponding imaginary frequency is calculated to be $214i\text{ cm}^{-1}$.

Formation of the hydroperoxide product in its singlet multiplicity is calculated to be highly exothermic in gas phase (25.6 kcal/mol) and in benzene solvent (31.4 kcal/mol). On the contrary, the overall conversion process of the palladium hydride to the Pd–OOH species along the spin conserving triplet surface is endothermic by 14.3 kcal/mol. Comparison between theoretical and experimental [34] geometries of the final singlet Pd(II) hydroperoxide species is very satisfactory (see Table 1).

Finally, it worthwhile to underline that the calculated single-point energies of the singlet stationary points (see Fig. 1) are always higher than the corresponding triplet optimized structures. Analogously to previous theoretical works, the MECP between optimized triplet and single-point singlet surfaces was located and the energy and structure of MECP2 are shown in Figs. 1 and 2, respectively. Localization and discussion of the characteristics of this crossing point were of obvious importance in previous works as MCP2 appears to allow the triplet–singlet surfaces hopping and even to play the role of the unidentified transition state for the rearrangement of the HOO fragment to form the final product. In the present study, instead, MECP2 is can be considered a 'fictitious' crossing point between a really viable triplet pathway and a singlet surface built up using energies coming from singlet single-point calculations.

4. Conclusions

A detailed DFT study of the mechanism for the conversion of the Pd(II)–hydride complex (PCP)PdH to the corresponding Pd(II)–hydroperoxide (PCP)PdOOH in presence of molecular oxygen was undertaken. The reaction under investigation is the first experimentally studied example of what is assumed to be a direct insertion of O_2 into a Pd(II)–H bond. The results show that along the triplet pathway the reaction evolves through the abstraction of the hydrogen atom by O_2 and formation of a HOO fragment

weakly bonded to the Pd(I) center. After the rearrangement of the HOO moiety, through the corresponding transition state, the final hydroperoxo product is formed. The reaction mechanism along the optimized singlet PES involves as a result of the hydrogen atom abstraction the formation of a very stable intermediate, PCP–Pd(OHO), in which hydrogen atom is bonded to the oxygen coordinated to the Pd center. Due to the stabilization of this intermediate, the crossing between triplet and singlet multiplicities occurs in this region of the PES's. The crossing point optimized structure and energy appear to be very close to those of the preceding transition state. From the stabilized PCP–Pd(OHO) intermediate exothermic formation of the final product takes place, overcoming the low barrier associated to the transition state for the contemporary breaking of the bond with proximal oxygen and bond forming with distal oxygen atom. The description of the triplet PES reported here parallels that of a recently reported theoretical investigation on the same system, carried out at the same level of theory. On the contrary, the mechanism proposed to occur along the singlet PES is completely new as well as is new the outline of the overall reaction mechanism. Moreover, the precise pathway for the rearrangement of the HOO moiety along the triplet PES was individuated, even if, in light of the new results the role it plays is of minor importance. The reported results are of particular interest as they contribute to shed light on the elementary steps of the mechanism, not yet established, of this kind of palladium-catalyzed oxidation reactions.

Acknowledgement

Financial support from the Università degli Studi della Calabria is gratefully acknowledged.

References

- [1] S.S. Stahl, *Science* 309 (2005) 1824.
- [2] S.S. Stahl, *Angew. Chem. Int. Ed.* 43 (2004) 3400.
- [3] M.S. Sigman, M.J. Schultz, *Org. Biomol. Chem.* 2 (2004) 2551.
- [4] B.M. Stoltz, *Chem. Lett.* 33 (2004) 362.
- [5] T. Nishimura, S. Uemura, *Synlett* (2004) 201.
- [6] R.A. Sheldon, I.W.C.E. Arends, G.-J. ten Brink, A. Dijkman, *Acc. Chem. Res.* 35 (2002) 774.
- [7] M. Toyota, M. Ihara, *Synlett* (2002) 1211.
- [8] K.M. Gligorich, M.S. Sigman, *Angew. Chem. Int. Ed.* 45 (2006) 6612.
- [9] T. Nishimura, T. Onoue, K. Ohe, S. Uemura, *J. Org. Chem.* 64 (1999) 6750.
- [10] T. Hosokawa, S.-I. Murahashi, *Acc. Chem. Res.* 23 (1990) 49.
- [11] J. Muzart, J.P. Pete, *J. Mol. Catal.* 15 (1982) 373.
- [12] M.M. Konnick, I.A. Guzei, S.S. Stahl, *J. Am. Chem. Soc.* 126 (2004) 10212.
- [13] S.S. Stahl, J.L. Thorman, R.C. Nelson, M.A. Kozee, *J. Am. Chem. Soc.* 123 (2001) 7188.
- [14] W.R. Thiel, *Angew. Chem.* 111 (1999) 3349; W.R. Thiel, *Angew. Chem. Int. Ed.* 38 (1999) 3157.
- [15] C.R. Landis, C.M. Morales, S.S. Stahl, *J. Am. Chem. Soc.* 126 (2004) 16302.
- [16] M.C. Denney, N.A. Smythe, K.L. Cetto, R.A. Kemp, K.I. Goldberg, *J. Am. Chem. Soc.* 128 (2006) 2508.

- [17] J.M. Keith, R.P. Muller, R.A. Kemp, K.I. Goldberg, W.A. Goddard III, J. Oxgaard, *Inorg. Chem.* 45 (2006) 9631.
- [18] J.M. Keith, R.J. Nielsen, J. Oxgaard, W.A. Goddard III, *J. Am. Chem. Soc.* 127 (2005) 13172.
- [19] M.M. Konnick, B.A. Gandhi, I.A. Guzei, S.S. Stahl, *Angew. Chem. Int. Ed.* 45 (2006) 2904.
- [20] B.V. Popp, J.E. Wendlandt, C.R. Landis, S.S. Stahl, *Angew. Chem. Int. Ed.* 46 (2007) 601.
- [21] B.V. Popp, S.S. Stahl, *J. Am. Chem. Soc.* 129 (2007) 4410.
- [22] A.D. Becke, *J. Chem. Phys.* 98 (1993) 5648.
- [23] P.J. Stephens, F.J. Devlin, C.F. Chabalowski, M.J. Frisch, *J. Phys. Chem.* 98 (1994) 11623.
- [24] M.J. Frisch et al., GAUSSIAN 03, Revision A.1, Gaussian, Inc., Pittsburgh, PA, 2003.
- [25] D. Andrae, U. Häußermann, M. Dolg, H. Stoll, H. Preuß, *Theor. Chim. Acta* 77 (1990) 123.
- [26] K. Fukui, *J. Phys. Chem.* 74 (1970) 4161.
- [27] C. Gonzalez, H.B. Schlegel, *J. Chem. Phys.* 90 (1989) 2154.
- [28] A.A. Ovchinnicov, J.K. Labanowski, *Phys. Rev. A* 53 (1996) 3946.
- [29] J.N. Harvey, M. Aschi, H. Schwarz, W. Koch, *Theor. Chem. Acc.* 99 (1998) 95.
- [30] S. Miertus, E. Scrocco, J. Tomasi, *Chem. Phys.* 55 (1981) 117.
- [31] S. Miertus, J. Tomasi, *Chem. Phys.* 65 (1982) 239.
- [32] J.L. Pascual-Ahuir, E. Silla, J. Tomasi, R. Bonaccorsi, *J. Comput. Chem.* 8 (1987) 778.
- [33] R.A. Pierotti, *Chem. Rev.* 76 (1976) 717.
- [34] J. Caillet, P. Clavarie, *Acta Crystallogr., Sect. B* 34 (1978) 3266.
- [35] L.R. Farrugia, *J. Appl. Crystallogr.* 30 (1997) 565.

Article II

The recognition of a new pathway for the reaction of molecular oxygen with a Pd(II)-hydride to produce a Pd(II)-hydroperoxide.



The recognition of a new pathway for the reaction of molecular oxygen with a Pd(II)-hydride to produce a Pd(II)-hydroperoxide

Sugata Chowdhury, Ivan Rivalta, Nino Russo*, Emilia Sicilia

Dipartimento di Chimica and Centro di Calcolo ad Alte Prestazioni per Elaborazioni Parallele e Distribuite-Centro d'Eccellenza MURST, Università della Calabria, I-87030 Arcavacata di Rende, Italy

ARTICLE INFO

Article history:

Received 24 January 2008

In final form 5 March 2008

Available online 10 March 2008

ABSTRACT

Significant recent developments in homogeneous palladium catalysis for selective aerobic oxidation have emphasized the importance of developing a thorough comprehension of reactions of palladium complexes with O₂. Density functional theory (DFT) calculations, employing the B3LYP exchange–correlation functional, have been performed to probe the mechanism for the insertion reaction of molecular oxygen into the palladium(II) hydride bond of the *trans*-[PdH(O₂Ac)(IMes)₂] complex to form the corresponding Pd(II)-hydroperoxide. A crossing between triplet and singlet surfaces occurs before the formation of a stable singlet intermediate from which the reaction straightforwardly proceeds to yield the singlet hydroperoxo complex. Results appear to be different with respect to previous analogous theoretical investigations providing a new minimum energy pathway.

© 2008 Elsevier B.V. All rights reserved.

1. Introduction

The use of homogeneous systems involving Pd(II) complexes as efficient oxidation catalysts continue to emerge as a versatile tool for the selective aerobic oxidation of organic molecules [1]. Two are the major mechanistic proposals to explain how the oxygen activation in palladium-catalyzed oxidations proceeds: (a) reaction of palladium(0) with oxygen to form a η²-peroxo palladium species and (b) direct insertion of oxygen into the Pd–H bond of a Pd(II)-hydride complex to form a Pd(II)-hydroperoxo product. The former mechanism has substantial experimental support [1d,2] although the reaction between Pd(0) and triplet oxygen is spin forbidden [3].

Only recently two examples of reactions of Pd(II)-hydrides with molecular oxygen to produce the corresponding Pd-hydroperoxides have been reported in the literature [4,5]. Goldberg and co-workers reported that molecular oxygen reacts with the (^tBuPCP)PdH (^tBuPCP = 1,3-(CH₂P^tBu)₂C₆H₃)[−] complex to yield (^tBuPCP)PdOOH [4]. DFT theoretical investigations on this system carried out by Goddard and co-workers [6] and by us [7] have demonstrated how an insertion mechanism is possible and plausible and supported the hypothesis that the hydrogen atom abstraction is the key step of the reaction.

Stahl and co-workers [5] have reported the preparation of the *N*-heterocyclic-carbene (NHC)-coordinated Pd(II)-hydride *trans*-[PdH(O₂Ac)(IMes)₂] (IMes = Mesityl) complex, along with that of its benzoate derivatives, and their oxygenation reaction to yield

the corresponding hydroperoxides. Because the experimental findings could support both direct insertion of O₂ into the Pd(II)–H bond and oxygenation of Pd(0), both pathways have been considered viable by the authors. Four possible alternative pathways have been computationally examined in detail by Popp and Stahl to probe the reaction mechanism of the formal insertion of molecular oxygen into the Pd–H bond of *trans*-[PdH(OAc)(IMes)₂] [8]. The proposed steps of the hydrogen abstraction mechanism, in analogy with the work of Goddard and co-workers [6], are: formation of a HOO moiety as a consequence of the hydrogen atom abstraction by molecular oxygen and formation of the final hydroperoxo product through rearrangement of the HO₂ fragment. An intersystem crossing from triplet to singlet surface has been found to take place at the exit channel of the reaction but no one of the surmised mechanisms for the rearrangement of the HO₂ fragment has been confirmed.

Here we present the outcome of a detailed density functional theory (DFT) investigation of the direct insertion mechanism of molecular oxygen into the Pd–H bond of *trans*-[(AcO)(IMes)₂PdH]. The results of our computations, carried out at the same level of theory of previous investigations [3,6,8] are relevant because stationary points with geometrical structures undisclosed until now have been intercepted along the singlet PES and the structure of the transition state that enables the rearrangement of the HOO fragment to yield the hydroperoxo complex has been individuated and characterized. Therefore, this study clearly shows that full optimization of stationary points for both singlet and triplet multiplicities are mandatory to individuate the right minimum energy pathway for reactions involving molecular oxygen. Since many questions concerning the mechanistic details of the Pd-catalyzed

* Corresponding author. Fax: +39 0984 494 044.

E-mail address: nrusso@unical.it (N. Russo).

oxidation reactions are still open [1a], the individuation of the true pathway for the interaction between molecular oxygen and Pd(II)–H complexes is of fundamental importance.

2. Computational details

Geometry optimizations as well as frequency calculations for all the reactants, intermediates, products and transition states have been performed at the Density Functional level by using the B3LYP exchange–correlation functional [9,10] as implemented in GAUSSIAN 03 code [11]. For Pd the relativistic compact Stuttgart/Dresden effective core potential [12] has been used in conjunction with its split valence basis set. The standard 6-311G* basis sets of Pople and co-workers were employed for the rest of the atoms. For each optimized stationary point vibrational analysis has been performed to determine its character (minimum or saddle point) and zero-point vibrational energy (ZPVE) corrections have been included in all relative energies (ΔE). For transition states it has been carefully checked that the vibrational mode associated to the imaginary frequency corresponds to the correct movement of involved atoms. Furthermore, the intrinsic reaction coordinate (IRC) method [13,14] has been used to assess that the localized TSs correctly connect to the corresponding minima along the imaginary mode of vibration.

To save computer time we have replaced the bulky 2,4,6-trimethylphenyl substituents on the IMes ligands with methyl groups to obtain a palladium hydride complex that, although less sterically hindered, can give analogous results [8]. Therefore, as the starting point for the study we have chosen the (AcO)(1,3-di(methyl)imidazoline-2-ylidene)₂PdH species, abbreviated for the sake of clarity as (AcO)(IME)₂PdH and that from now on will be indicated as **I**(1), and both singlet and triplet reaction paths have been examined due to the addition of triplet molecular oxygen. $\langle S^2 \rangle$ values have been checked to assess whether spin contamination can influence the quality of the results. The method proposed by Ovchinnikov and Labanowski [15] has been adopted for correcting the mixed spin energies and removing the foreign spin components. For triplet state structures $\langle S^2 \rangle$ values are very close to 2.0 for all the considered stationary points. On the contrary, unrestricted calculations for singlet structures revealed in some cases triplet spin contamination corresponding to $\langle S^2 \rangle$ values close to 1.0. Unrestricted calculations of the singlet energy of O₂ gave a ¹Δ_g state too much stable due to the contamination of the singlet wave function with the triplet state and a corresponding excitation energy of 10.5 kcal/mol, being the experimental value 22.5 kcal/mol. Correction of the mixed spin energy of the singlet state has given a triplet–singlet energy gap of 20.7 kcal/mol in very good agreement with the experimental value. The same correction scheme has been applied, as it will be underlined later on, to the energy of some other singlet stationary points that revealed to be highly contaminated with the triplet.

Implicit solvent effects have been calculated through the polarisable continuum solvation model [16], PCM, performing single-point calculations on fully optimized gas-phase geometries of stationary points, since preliminary calculations clearly have shown that geometry relaxation effects are not significant. The solvation Gibbs free energies have been evaluated using the well-known thermodynamic cycle [17], where the reaction Gibbs free energy in solution, ΔG_{sol} , is calculated for each process as the sum of two contributions: a gas-phase reaction free energy, ΔG_{gas} , and a solvation reaction free energy term calculated with the continuum approach, ΔG_{sol} .

$$\Delta G_{\text{sol}} = \Delta G_{\text{gas}} + \Delta G_{\text{sol}}$$

The gas-phase reaction free energy is the sum of two parts: electronic plus nuclear repulsion energy (ΔE_{ele}) and thermal contribu-

tion including zero-point energy ($\Delta G_{\text{gas}}^{\text{T}} = \Delta H + T\Delta S$). The last term, $T\Delta S$, that is the thermal correction, is evaluated using the calculated quantum mechanical vibrational frequencies.

Minimum energy crossing points (MECP) computation between the triplet surface of reactants and the singlet one of the products has been carried out using the methodology introduced by Harvey [18]. For the sake of comparison with previous theoretical results [6,8] single-point calculations for singlet multiplicity have been carried out on fully optimized geometries of triplet stationary points.

3. Results

The B3LYP calculated singlet and triplet PESs for the reaction of O₂ with the *trans*-[(AcO)(IME)₂PdH] complex are reported in Fig. 1, where relative energies are calculated with respect to the triplet ground state reactants asymptote (**I**(1) + ³O₂). Relative free energies in benzene solvent are reported in the same Figure along with the relative energy of the singlet stationary points obtained performing single-point calculations on the fully optimized triplet structures. Geometrical structures of singlet and triplet minima and transition states are shown in Figs. 2 and 3, respectively.

Along the triplet pathway the interaction of oxygen with the *trans*-[(AcO)(IME)₂PdH] complex leads to the formation of a weakly bound van der Waals complex, **II**(3), whose formation is endothermic in solvent and only slightly exothermic in gas-phase. Both oxygen atoms of the O₂ molecule are about 4.5 Å far from the Pd center. The fully optimized structure, **II**(1), of the corresponding complex in a singlet state, is by about 29 kcal/mol higher in energy in benzene solvent. O₂ molecule is oriented parallel to the Pd–H bond and the closest oxygen atom is at about 2.3 Å from the Pd center. The energy reported for this adduct has been properly corrected since it showed a significant amount of triplet contamination.

The gas-phase energy of the singlet stationary point obtained performing a single-point calculation on the optimized triplet structure, according to the theoretical study reported in Ref. [8], is higher by about 39 kcal/mol.

Along the triplet surface the reaction evolves through the abstraction of the hydrogen atom from the palladium center by O₂. This step takes place overcoming a free energy barrier of 18.9 kcal/mol for the formation of the **TSI**(3) transition state. In

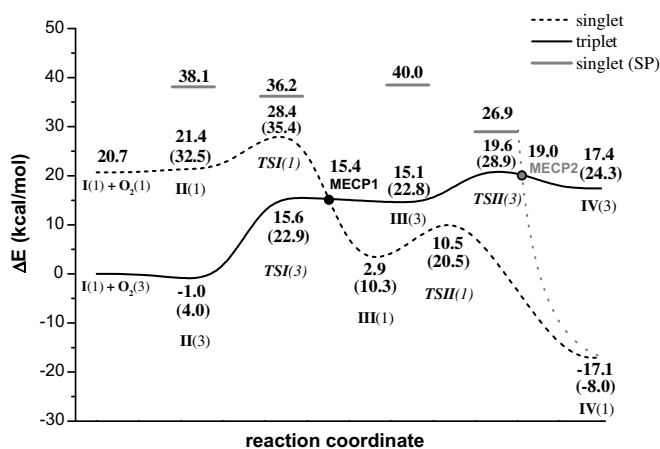


Fig. 1. Calculated potential energy surfaces for the reaction of singlet and triplet states of O₂ with (Ac)(IME)₂Pd(II)–H to yield (Ac)(IME)₂Pd(II)–OOH. Gibbs free energies changes at 298.15 K in benzene are also reported in parentheses along with singlet single-point energies calculated on fully optimized structures of triplet stationary points. Energies are in kcal/mol and relative to the ground-state reactants.

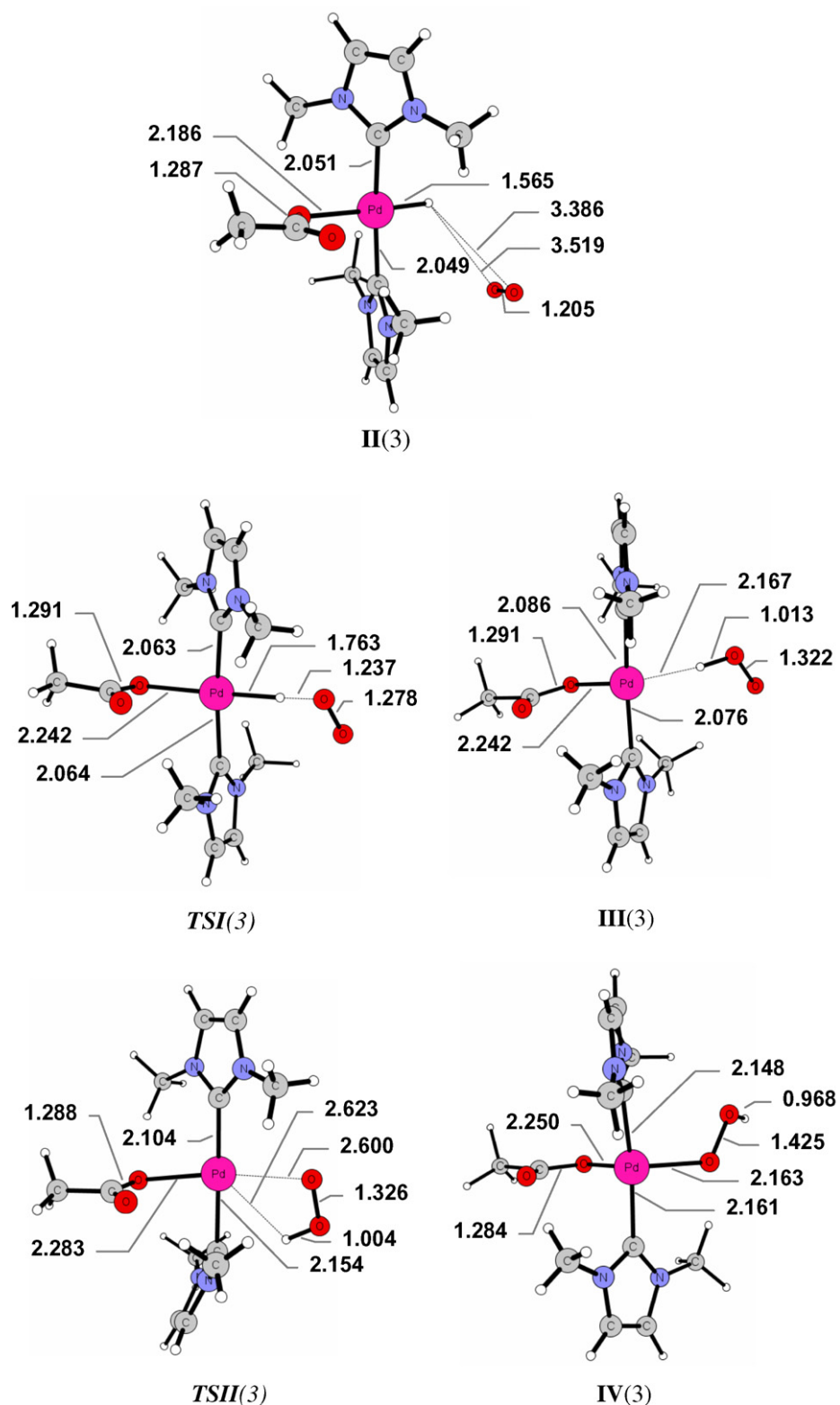


Fig. 2. Geometrical structures of singlet minima and transition states. Bonds are in Å and angles in degrees. The available experimental geometrical parameters for the benzoate analogue of the hydride complex are also reported in parentheses.

going from the first adduct to **TSI(3)** the Pd–H bond distance stretches from 1.565 to 1.763 Å and at the same time the O–O bond length increases from 1.205 to 1.278 Å. The O–H distance is 1.237 Å indicating that the bond between oxygen and hydrogen is forming. The imaginary frequency for **TSI(3)** is calculated to be $1516i \text{ cm}^{-1}$

and corresponds to the shift of the hydrogen from Pd to O atom. As a result, an intermediate **III(3)** is formed in which a peroxy HOO radical is coordinated to the T-shaped Pd(I) complex through a weak interaction between hydrogen and Pd atoms. Indeed, this reaction intermediate lies 22.8 kcal/mol above the ground state

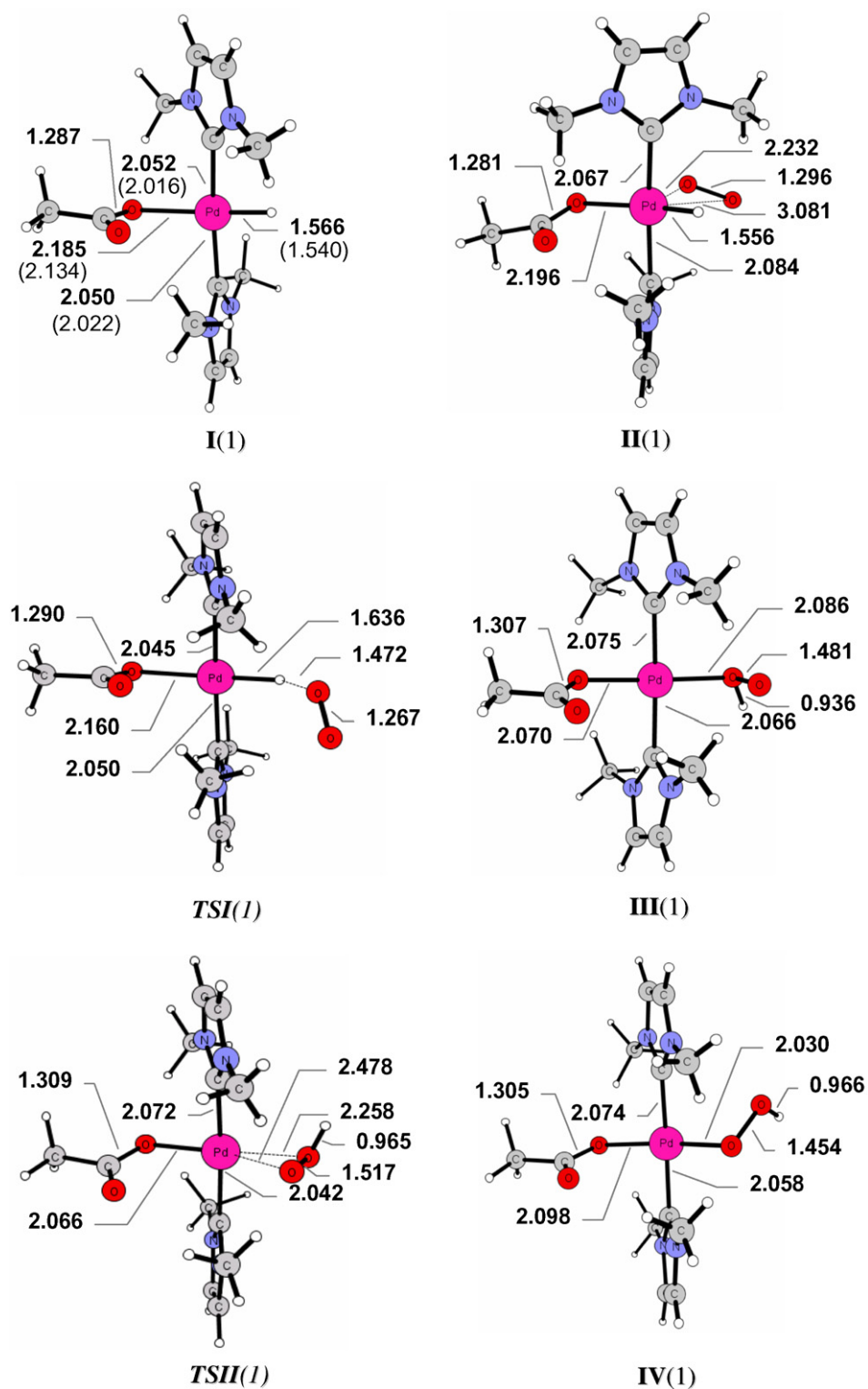


Fig. 3. Geometrical structures of triplet minima and transition states. Bonds are in Å and angles in degrees.

reactants in solvent and is as stable as the **TSI(3)** transition state. Along the singlet surface, instead, once molecular oxygen approaches the Pd center, at a distance of 1.472 Å between the closest oxygen and hydrogen, a transition state, **TSI(1)**, has been intercepted and characterized. The normal mode associated to the imaginary frequency, calculated to be $224i \text{ cm}^{-1}$, corresponds the movement of the hydrogen atom that comes close the oxygen atom forming a new O–H bond. Also for this singlet **TSI(1)** transi-

tion state, which lies 35.4 kcal/mol above the separate reactants (28.4 kcal/mol in gas-phase), the absolute energy has been corrected for spin contamination. From **TSI(1)** the reaction proceeds to yield a singlet intermediate, **III(1)**, whose formation is endothermic by 2.9 kcal/mol in gas-phase (endothermic by 10.3 kcal/mol in solvent). The main feature of this intermediate is that the hydrogen atom is bonded (H–O = 0.963 Å) to the proximal oxygen. Until now the existence of this kind of intermediates has not been evidenced

by theoretical investigations [6,8]. IRC calculations confirmed that the **TSI**(1) transition state is connected to both reactant **II**(1) and product **III**(1). The analysis of the structures along the reaction coordinate from the transition state to the **III**(1) intermediate shows that the hydrogen atom approaches the proximal oxygen lengthening the O–O bond, whereas the distal oxygen atom rotates upwards.

Owing to the stability of the singlet **III**(1) intermediate, in this region of the PES the system must undergo a spin inversion that takes place after passage of the **TSI**(3) transition state. In the framework of the Two-State Reactivity paradigm such a kind of spin crossover is not considered a rate-limiting factor as it involves species that are formed with excess energy and even electronically excited states become accessible [19]. The computed structure of the minimum energy crossing point, **MECP1**, between the triplet and singlet surfaces, is shown in Fig. 4 and its relative energy calculated in gas-phase is reported in Fig. 1.

The crossing occurs in the vicinity of the triplet transition state and the **MECP1** structure lies very close in energy to the preceding transition state.

It is worthwhile to underline that all the attempts to individuate a singlet intermediate with a structure analogous to that of the triplet complex were unsuccessful in spite of the numerous strategies used to find it out.

The final step of the reaction that leads to formation of the final hydroperoxo palladium (II) complex, takes place along the singlet pathway through the detachment of the proximal oxygen from Pd and formation of a new bond with the distal oxygen. Triplet hydroperoxide product formation involves, instead, rearrangement of the HOO fragment in such a way that terminal oxygen and hydrogen atoms move in opposite directions towards to and away from the Pd center, respectively. Both the corresponding transition states that is necessary to surmount have been intercepted and confirmed by IRC analysis.

The singlet **TSII**(1) structure lies 10.5 kcal/mol, 20.5 kcal/mol when solvent effects are included, above the reactants dissociation limit and is characterized by an imaginary frequency of $339i \text{ cm}^{-1}$. Along the triplet PES the **TSII**(3) structure is destabilized respect to reactants by 19.6 kcal/mol in gas-phase and by 28.9 kcal/mol in benzene and the corresponding imaginary frequency is calculated to be $102i \text{ cm}^{-1}$.

Formation of the hydroperoxide product in its singlet multiplicity, **IV**(1), is calculated to be exothermic in gas-phase (17.1 kcal/

mol) and in benzene solvent (8.0 kcal/mol). On the contrary, the overall conversion process of the palladium hydride to the Pd–OOH species, **IV**(3), along the spin conserving triplet surface is endothermic by 17.4 kcal/mol in gas-phase and 24.3 kcal/mol in solvent.

Finally, it is worthwhile to underline that the calculated single-point energies of the singlet stationary points (see Fig. 1) are always higher than the corresponding triplet optimized structures. This means that if the singlet PES is obtained by performing only single-point calculations on triplet optimized geometries the right minimum energy pathway cannot be singled out and, consequently, the thermodynamics and kinetics of the reaction cannot be correctly determined.

Analogously to previous theoretical works [6,8], the MECP structure for the crossing from the optimized triplet to the single-point singlet surfaces in this region of the PESs (**MECP2** in Figs. 1 and 4) has been computed. Computation of the structure and discussion of the characteristics of this crossing point were of obvious importance in previous theoretical papers [6,8] as **MECP2** appears to allow the triplet–singlet surfaces hopping and even to play the role of the unidentified transition state for the rearrangement of the HOO fragment in order to form the final product. In the present study, instead, **MECP2** can be considered a ‘fictitious’ crossing point between a really viable triplet pathway and a singlet surface built up using energies coming from singlet single-point calculations on fully optimized triplet structures. It is worth to underline that also the individuation of the region where the spin crossing occurs and of the MECP structure relies on the proper computation of the involved PESs.

4. Conclusions

A detailed DFT study of the mechanism for the conversion of the Pd(II)-hydride complex, $(\text{AcO})(\text{IMes})_2\text{PdH}$ to the corresponding Pd(II)-hydroperoxide in presence of molecular oxygen has been undertaken. The results show that along the triplet pathway the reaction evolves through the abstraction of the hydrogen atom by O_2 and formation of a HOO fragment weakly bonded to the Pd(I) center. After the rearrangement of the HOO moiety, through the corresponding transition state, the final hydroperoxo product is formed. The reaction mechanism along the optimized singlet PES involves as a result of the hydrogen atom abstraction the formation of a stable intermediate, in which hydrogen atom is bonded to the proximal

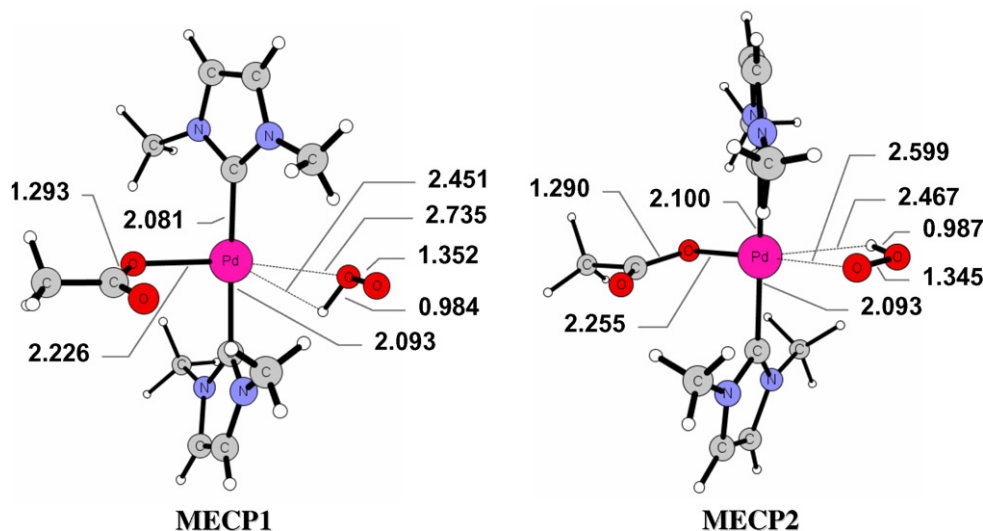


Fig. 4. **MECP1** and **MECP2** structures for spin conversion from triplet to singlet multiplicity. Bond lengths are in angstrom and angles in degrees.

oxygen. Due to the stabilization of this intermediate, the crossing between triplet and singlet multiplicities occurs in this region of the PESs. From this stabilized intermediate exothermic formation of the final product takes place, overcoming the barrier associated to the transition state for the contemporary breaking of the bond with proximal oxygen and bond forming with distal oxygen atom. The description reported here of the triplet PES parallels the recently reported theoretical investigation on the same system, carried out at the same level of theory. On the contrary, the mechanism proposed to occur along the singlet PES is completely new as well as is new the outline of the overall reaction mechanism. Moreover, the precise pathway for the rearrangement of the HOO moiety along the triplet PES has been individuated, even if, in light of the new results, the role it plays is of minor importance. This work demonstrates that the theoretical study of the interaction of Pd complexes with molecular oxygen has to be carried out fully optimizing stationary point structures lying on both triplet and singlet pathways. As can be inferred from the comparison with the outcomes of the previous works on the same subject, the strategy adopted in this Letter provides a new reaction profile in terms of intermediates structures, activation barriers and surface crossings. The reported results are of particular interest as they contribute to shed light on the elementary steps of the mechanism, not yet established, of this kind of palladium-catalyzed oxidation reactions.

Acknowledgment

Financial support from the Università della Calabria is gratefully acknowledged.

References

- [1] (a) K.M. Gligorich, M. Sigman, *Angew. Chem. Int. Ed.* 45 (2006) 6612;
(b) S.S. Stahl, *Science* 309 (2005) 1824;
(c) S.S. Stahl, *Angew. Chem. Int. Ed.* 43 (2004) 3400;
(d) M.M. Konnick, I.A. Guzei, S.S. Stahl, *J. Am. Chem. Soc.* 126 (2004) 10212.
- [2] (a) S.S. Stahl, J.L. Thorman, R.C. Nelson, M.A. Kozee, *J. Am. Chem. Soc.* 123 (2001) 7188;
(b) S.S. Stahl, J.L. Thorman, R.C. Nelson, M.A.J. Kozee, *Angew. Chem. Int. Ed.* 38 (1999) 3157.
- [3] (a) C.R. Landis, C.M. Morales, S.S. Stahl, *J. Am. Chem. Soc.* 126 (2004) 16302;
(b) B.V. Popp, J.E. Wendlandt, C.R. Landis, S.S. Stahl, *Angew. Chem. Int. Ed.* 46 (2007) 601.
- [4] M.C. Denney, N.A. Smythe, K.L. Cetto, R.A. Kemp, K.I. Goldberg, *J. Am. Chem. Soc.* 128 (2006) 2508.
- [5] M.M. Konnick, B.A. Gandhi, I.A. Guzei, S.S. Stahl, *Angew. Chem. Int. Ed.* 45 (2006) 2904.
- [6] J.M. Keith, R.P. Muller, R.A. Kemp, K.I. Goldberg, W.A. Goddard III, J. Oxgaard, *Inorg. Chem.* 45 (2006) 9631.
- [7] S. Chowdhury, I. Rivalta, N. Russo, E. Sicilia, *Chem. Phys. Lett.* 443 (2007) 183.
- [8] B.V. Popp, S.S.J. Stahl, *Am. Chem. Soc.* 129 (2007) 4410.
- [9] A.D. Becke, *J. Chem. Phys.* 98 (1993) 5648.
- [10] P.J. Stephens, F.J. Devlin, C.F. Chabalowski, M.J. Frisch, *J. Phys. Chem.* 98 (1994) 11623.
- [11] M.J. Frisch et al., *GAUSSIAN 03, Revision A.1*, Gaussian, Inc., Pittsburgh, PA, 2003.
- [12] D. Andrae, U. Häußermann, M. Dolg, H. Stoll, H. Preuß, *Theor. Chim. Acta* 77 (1990) 123.
- [13] K. Fukui, *J. Phys. Chem.* 74 (1970) 4161.
- [14] C. Gonzalez, H.B. Schlegel, *J. Chem. Phys.* 90 (1989) 2154.
- [15] A.A. Ovchinnikov, J.K. Labanowski, *Phys. Rev. A* 53 (1996) 3946.
- [16] (a) S. Miertus, E. Scrocco, J. Tomasi, *Chem. Phys.* 55 (1981) 117;
(b) S. Miertus, J. Tomasi, *Chem. Phys.* 65 (1982) 239.
- [17] P. Kollaman, *Chem. Rev.* 93 (1993) 2395.
- [18] J.N. Harvey, M. Aschi, H. Schwarz, W. Koch, *Theor. Chem. Acc.* 99 (1998) 95.
- [19] D. Schröder, S. Shaik, H. Schwarz, *Acc. Chem. Res.* 33 (2000) 139.

Article III
Theoretical Investigation of the Mechanism of
Acid-Catalyzed Oxygenation of a
Pd(II)-Hydride To Produce a
Pd(II)-Hydroperoxide.

Theoretical Investigation of the Mechanism of Acid-Catalyzed Oxygenation of a Pd(II)-Hydride To Produce a Pd(II)-Hydroperoxide

Sugata Chowdhury, Ivan Rivalta, Nino Russo,* and Emilia Sicilia

Dipartimento di Chimica and Centro di Calcolo ad Alte Prestazioni per Elaborazioni Parallele e Distribuite-Centro d'Eccellenza MURST, Università della Calabria, I-87030 Arcavacata di Rende, Italy

Received April 29, 2008; Revised Manuscript Received June 6, 2008; Accepted June 9, 2008

Abstract: Density Functional Theory (DFT) has been applied to a comprehensive mechanistic study of the conversion reaction of the Pd(II)-hydride complex, $(\text{IMe})_2(\text{RCO}_2)\text{PdH}$ ($\text{R}=\text{CH}_3$, Ph , and $p\text{-O}_2\text{NC}_6\text{H}_4$), to the corresponding Pd(II)-hydroperoxide in the presence of molecular oxygen. The calculations have evaluated the two mechanistic proposed alternatives, that are both considered viable on the basis of current data, of slow RCO_2H reductive elimination followed by oxygenation (*Path A*) and direct O_2 insertion (*Path B*). Results suggest that the mechanism of direct insertion of molecular oxygen into the Pd–H bond of the initial complex is energetically preferred. The activation energy relative to the rate-determining step of *Path A*, indeed, is calculated to be lower than the activation energy of the rate determining step of the alternative *Path B*, whatever ligand (CH_3CO_2 , Ph , CO_2 , $p\text{-O}_2\text{NC}_6\text{H}_4\text{CO}_2$) is coordinated to the Pd center. The calculated free activation energy of the rate-determining hydrogen abstraction step ($\Delta G^* = 24.8$ kcal/mol) in the case of the oxygenation reaction of the benzoate-ligated Pd(II)-hydride complex is in very good agreement with the experimentally determined value of 24.4 kcal/mol. In addition, according to the experimentally detected enhancement of the reaction rate due to the presence of a nitro group on the benzoate ligand, our calculations show that the transition state for the hydrogen atom abstraction by molecular oxygen along the pathway for the oxygenation reaction of $(\text{IMe})_2(p\text{-O}_2\text{NC}_6\text{H}_4\text{CO}_2)\text{PdH}$ lies lower in energy with respect to the analogous transition state calculated for $\text{R}=\text{Ph}$.

1. Introduction

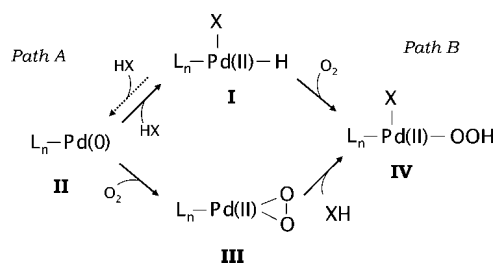
The use of molecular oxygen for the oxidative functionalization of organic molecules is a highly attractive option because O_2 is a readily available and nontoxic reagent. Additionally, a common byproduct of aerobic oxidations is the innocuous substance water. However, uncatalyzed chemical reactions between molecular oxygen and organic substrates generally result in complete combustion of the starting materials, and, consequently, the synthetic advantages these reactions possess cannot be exploited unless catalysts are

used. The homogeneously Pd-catalyzed oxidations have emerged as a particularly promising reaction type for selective and efficient aerobic oxidation^{1–7} even if the development of new and more efficient catalytic strategies has been hampered by an inadequate understanding of how O_2 interacts with the Pd center.⁷ Two are the pathways proposed to explain how the oxygen activation in palladium-catalyzed oxidations proceeds (Scheme 1).

One pathway (*Path A*) is the formation of a Pd(0) species **II** through the reductive elimination of a HX species from the Pd(II)-hydride complex followed by the oxygenation of the Pd(0) center to form a η^2 -peroxo Pd(II) species **III**. Upon protonation of the peroxopalladium(II) intermediate a pal-

* Corresponding author fax: +39-0984-492044; e-mail: nrusso@unical.it.

Scheme 1



ladium hydroperoxide species **IV** is formed.^{8–10} The second mechanistic possibility^{11–13} (*Path B*) involves the direct insertion of molecular oxygen into a palladium(II)-hydride intermediate **I** to form the same palladium hydroperoxide species **IV** (Scheme 1) and, therefore, avoiding to proceed through Pd(0). The former mechanism has substantial experimental support even if the reaction between Pd(0) and triplet oxygen is spin forbidden.^{8–10} Landis, Stahl, and co-workers have investigated this aspect performing a DFT theoretical study that showed the exothermic formation of the singlet Pd(II)-peroxido species requiring spin crossing between triplet and singlet surfaces mediated by spin–orbit coupling.¹⁴

The first observation of what can be assumed to be a direct insertion of molecular oxygen into a Pd(II)-hydride bond to form a hydroperoxopalladium complex has been reported by Goldberg, Kemp, and co-workers for a Pd complex that, due to the nature of the ligand, cannot undergo reductive elimination.¹⁵ The authors report that benzene solutions of (^tBuPCP)PdH (^tBuPCP=1,3-(CH₂P^tBu)₂C₆H₃[−]) exposed to O₂ cleanly react to yield (^tBuPCP)PdOOH, which is relatively stable at ambient temperature as a solid and structurally characterizable. A DFT theoretical investigation, carried out by Goddard and co-workers, of the involved mechanism has recently appeared in literature that demonstrates how an insertion mechanism is possible and plausible and supports the hypothesis that the hydrogen atom abstraction is the key step of the reaction.¹⁶ Namely, hydrogen atom is abstracted from the Pd center by molecular oxygen to form a HOO fragment that interacts only weakly with the Pd(I) center. Rotation of HO₂ moiety enables formation of a Pd–O bond to give the final Pd(II)-hydroperoxo product. A minimum energy crossing point (MECP) between triplet and singlet surfaces has been located at the exit channel of the reaction, whereas the mechanism for the rearrangement of the HOO fragment to give the hydroperoxide product has not been individuated. In the same work is discussed the difference with respect to a previous study of the same authors that underlined the subordination of the O₂ insertion process to the presence of a H-bond acceptor *cis* to the hydride.¹⁷

Stahl and co-workers have investigated the feasibility of the Pd(0) direct oxygenation pathway by subjecting [Pd(0)(IMes)₂] (IMes=Mesityl) to one equivalent of a carboxylic acid (acetic, benzoic, and *p*-nitrobenzoic) to produce the *trans*-[(IMes)₂(RCO₂)PdH] hydride, which subsequently exposed to O₂ yielded the corresponding hydroperoxide complex.¹⁸ Since the experimental findings could support both mechanisms, that is direct insertion of O₂ into the Pd(II)-H bond and oxygenation of Pd(0), both pathways

have been considered viable by the authors. Indeed, four possible alternative pathways have been computationally examined by Popp and Stahl to probe the reaction mechanism of the formal insertion of molecular oxygen into the Pd–H bond of *trans*-[PdH(OAc)(IMes)₂].¹⁹ The main conclusion of this investigation is that the energetically preferred pathways, exhibiting very similar kinetic barriers, are those corresponding to (a) hydrogen atom abstraction from the Pd–H bond by molecular oxygen and (b) reductive elimination AcOH followed by oxygenation of Pd(0) and protonolysis of the formed η²-peroxo-Pd(II) species. Also in this last case the proposed steps of the hydrogen abstraction mechanism are as follows: formation of a HOO moiety as a consequence of the hydrogen atom abstraction by molecular oxygen and formation of the final hydroperoxo product through rearrangement of the HO₂ fragment. In analogy with Goddard's analysis¹⁶ the MECP between singlet and triplet PESs has been located at the exit channel of the reaction, but not one of the surmised mechanisms for the rearrangement of the HO₂ fragment has been confirmed.

In the framework of a more extended project aiming to unravel the mechanistic details of the selective oxidation of organic molecules by molecular oxygen in the presence of metal catalysts we have theoretically investigated the direct O₂ insertion mechanism for both (^tBuPCP)PdH and [(IMes)₂(AcO)PdH] hydrides.^{20,21} With respect to the preceding computational analyses carried out on the same subject^{16,19} the new results are as follows: the recognition of a different pathway for the process and the determination of the rearrangement mechanism of the OOH fragment as the last step of the overall hydride oxygenation reaction. In the present work we have examined the possible alternative mechanisms of the oxygenation process of the Pd-hydride complex *trans*-[Pd(H)(O₂CR)(IMes)₂] with R=CH₃, Ph, *p*-O₂NC₆H₄ to yield the corresponding hydroperoxide, taking into account also the influence on the oxygenation pathways of the employed carboxylic acid. Kinetic measurements,¹⁸ indeed, have shown that the reaction rate exhibits a clear first-order dependence on the concentration of the Pd-hydride, and the presence of an electron-withdrawing nitro group on the benzoate ligand significantly enhances the reaction rate (when R=*p*-O₂NC₆H₄ the oxygenation is about eight times faster than when R=Ph). The ligand dependence could suggest that carboxylate dissociation is the rate determining step of the process and, as a consequence, supports the reaction mechanism involving reductive elimination of the carboxylic acid. Since many questions concerning the mechanistic details of the Pd-catalyzed oxidation reactions are still open,²² the results of our computations can contribute to the determination of the true pathway for the interaction between molecular oxygen and Pd(II)-H complexes.

2. Computational Details

Geometry optimizations as well as frequency calculations for all the reactants, intermediates, products, and transition states have been performed at the Density Functional level of theory, employing the Becke's three-parameter hybrid functional²³ combined with the Lee, Yang, and Parr (LYP)²⁴ correlation functional, denoted as B3LYP, as implemented

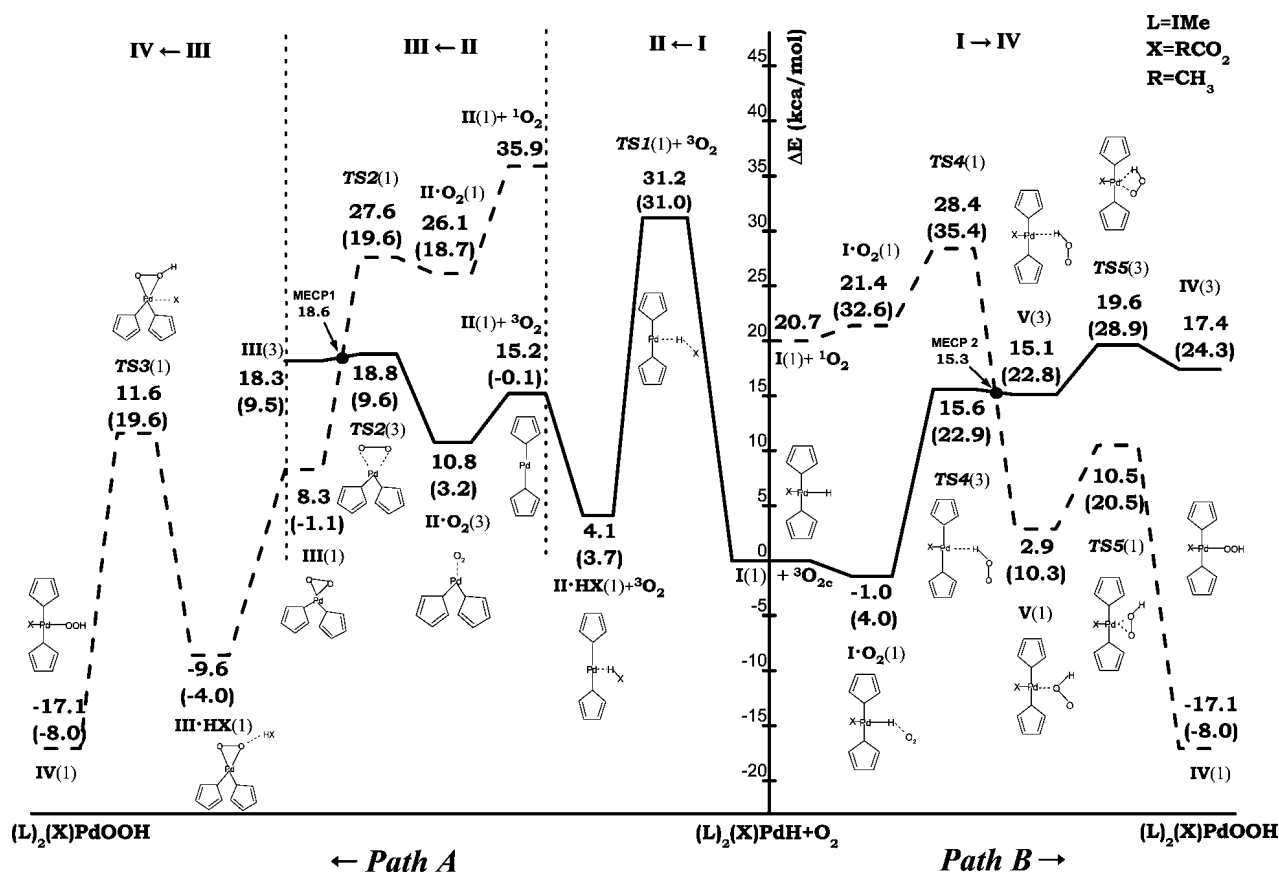


Figure 1. Calculated B3LYP PESs for the oxygenation reaction of (Ime)₂(CH₃CO₂)Pd(II)-H to give (Ime)₂(CH₃CO₂)Pd(II)-OOH. Gibbs free energies changes at 298.15 K in benzene are also reported in parentheses. Energies are in kcal/mol and relative to ground-state reactants. On the left the pathway that involves reductive elimination of CH₃COOH (*Path A*) and on the right the pathway for the direct O₂ insertion (*Path B*) are reported.

in Gaussian03 code.²⁵ For Pd the relativistic compact Stuttgart/Dresden effective core potential²⁶ has been used in conjunction with its split valence basis set. The 6-311G* basis sets of Pople and co-workers have been employed for the rest of the atoms. For each optimized stationary point vibrational analysis has been performed to determine its character (minimum or saddle point), and zero-point vibrational energy (ZPVE) corrections were included in all relative energies (ΔE). For transition states it was carefully checked that the vibrational mode associated with the imaginary frequency corresponded to the correct movement of involved atoms. Furthermore, the intrinsic reaction coordinate (IRC)^{27,28} method has been used to assess that the localized TSs correctly connect to the corresponding minima along the imaginary mode of vibration.

To speed up calculations the 2,4,6-trimethylphenyl groups of the IMes ligands have been substituted with methyl ones to obtain a palladium hydride complex that, although less sterically hindered, can give analogous results.¹⁹ For this reason, from now on we will indicate the 1,3-di(methyl)imidazoline-2-ylidene model of the ligand as IMe, and the starting points for our study are the *trans*[(RCO₂)(1,3-di(methyl)imidazoline-2-ylidene)₂PdH] species (R=CH₃, Ph, *p*-O₂NC₆H₄), also abbreviated as *trans*[(RCO₂)(Ime)₂PdH].

Both triplet and singlet reaction paths have been examined and for all the studied species $\langle S^2 \rangle$ values have been checked to assess whether spin contamination can influence the quality of the results. For triplet state structures no

significant contamination was found by unrestricted calculations. Unrestricted calculations, instead, revealed in some cases triplet spin contamination corresponding to $\langle S^2 \rangle$ values close to 1.0. For molecular oxygen, due to the contamination of the singlet wave function with the triplet state, a highly stable singlet ¹Δ_g state has been obtained corresponding to an excitation energy of 10.5 kcal/mol, compared with the experimental value of 22.5 kcal/mol.²⁹ Adopting the method proposed by Ovchinnikov and Labanowski³⁰ for correcting the mixed spin energies and removing the foreign spin components, a triplet-singlet energy gap of 20.7 kcal/mol was obtained, in very good agreement with the experimental value. The same scheme was adopted to correct the triplet contaminated energies of some structures along the singlet path, as will be underlined in the next paragraphs.

Solvent effects, both electrostatic and nonelectrostatic, have been treated implicitly making use of the Tomasi's integral equation formalism for the polarizable continuum model (IEF-PCM)^{31,32} as implemented in Gaussian03. All stationary points structures obtained from vacuum calculations were reoptimized in implicit benzene with the above IEF-PCM method.

The solvation Gibbs free energies have been evaluated using the well-known thermodynamic cycle,³³ where the reaction Gibbs free energy in solution, ΔG_{sol} , is calculated for each process as the sum of two contributions: a gas-

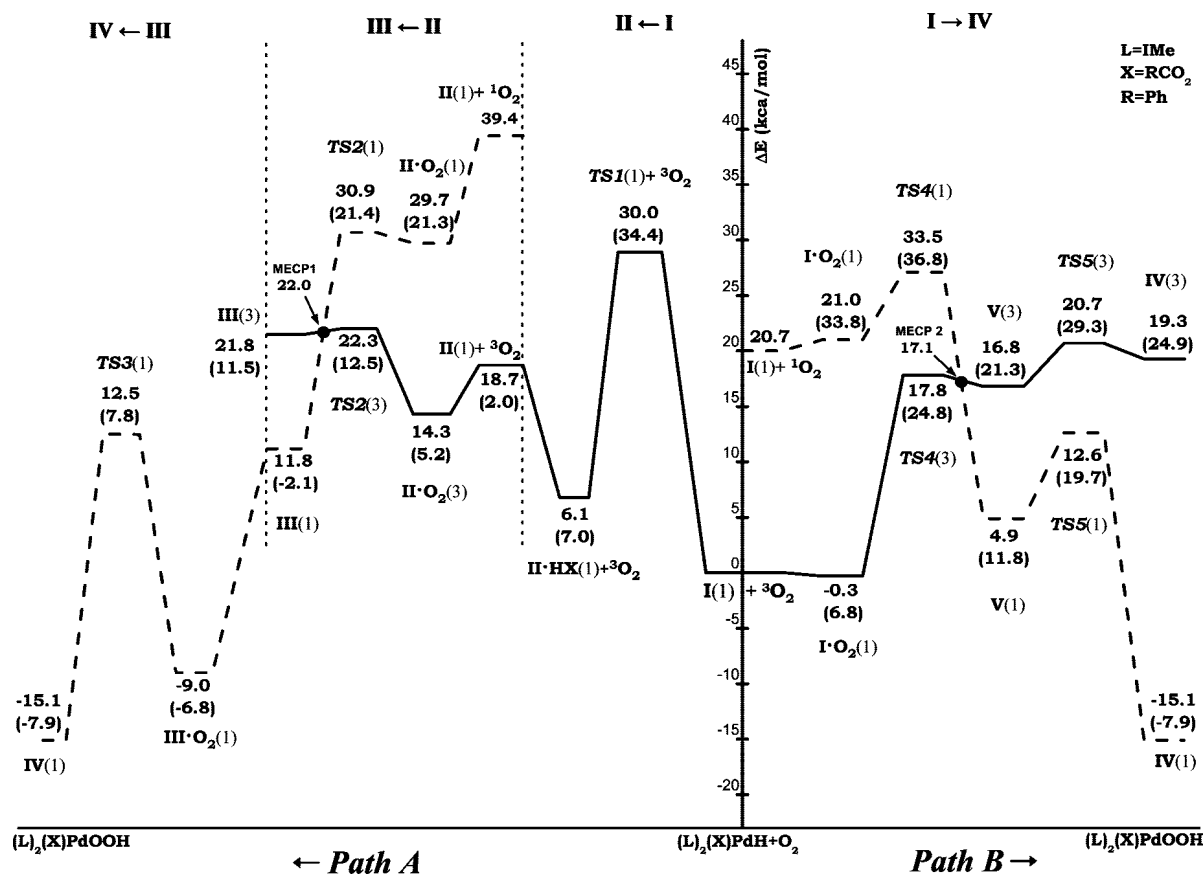


Figure 2. Calculated B3LYP PESs for the oxygenation reaction of (IME)₂(PhCO₂)Pd(II)-H to give (IME)₂(PhCO₂)Pd(II)-OOH. Gibbs free energies changes at 298.15 K in benzene are also reported in parentheses. Energies are in kcal/mol and relative to the ground-state reactants. On the left the pathway that involves reductive elimination of PhCOOH (*Path A*) and on the right the pathway for the direct O₂ insertion (*Path B*) are reported.

phase reaction free energy, ΔG_{gas} , and a solvation reaction free energy term calculated with the continuum approach, ΔG_{solv} :

$$\Delta G_{\text{sol}} = \Delta G_{\text{gas}} + \Delta G_{\text{solv}} \quad (1)$$

The gas-phase reaction free energy is the sum of two parts: electronic plus nuclear repulsion energy (ΔE_{ele}) and thermal contribution including zero-point energy ($\Delta G_{\text{gas}} = \Delta H + T\Delta S$). The last term, $T\Delta S$, that is the thermal correction, is evaluated using the calculated quantum mechanical vibrational frequencies.

To locate the minimum energy crossing points (MECP) between the triplet surfaces of reactants and the singlet ones of the products the methodology introduced by Harvey and co-workers has been used.³⁴

3. Results and Discussion

Calculated B3LYP PESs for the oxygenation process of (RCO₂)(IME)₂PdH hydrides are drawn in Figures 1–3 for R=CH₃, Ph, *p*-O₂NC₆H₄, respectively. Both singlet and triplet PESs have been computed. Relative energies are calculated with respect to the ground-state reactants asymptote (I(1)+³O₂). The energy profile for the steps of the pathway that, starting from the hydride species I, involves reductive elimination of RCOOH (R=CH₃, Ph, *p*-O₂NC₆H₄) to yield Pd(0) complex (II), oxygenation of II to yield the peroxo complex III, and subsequent protonation to form the

hydroperoxide complex IV are shown on the left side of each figure (*Path A*). The calculated PESs for the direct insertion of O₂ into the Pd–H bond of the hydride species to obtain the same hydroperoxides are drawn on the right side of each figure (*Path B*). Relative free energies calculated in benzene solvent are also reported in Figures 1–3.

The ground-state optimized structure of the reference hydride species chosen as the starting point for our study is shown in Figure 4 along with the optimized structure of the final hydroperoxide complex in the case of R=Ph. Ground-state geometrical structures of all stationary points intercepted along the pathway for the (PhCO₂)(IME)₂PdH hydride oxygenation through reductive elimination, Pd(0) oxygenation, and protonolysis of peroxo complex are reported in Figure 5, whereas ground-state optimized structures of the sequence of minima and transition states involved by the direct O₂ insertion pathway are shown in Figure 6. In Figures 5 and 6 are sketched also the structures of the calculated MECPs. Labels employed in Figures 4–6 to individuate geometrical parameters have to be used to read information reported in Table 1 for *Path A* and Table 2 for *Path B*, which collect selected bond lengths and angles along with dihedral angles of stationary points and MECPs for R=CH₃, Ph, and *p*-O₂NC₆H₄.

In the next two paragraphs we are going to illustrate the outcomes of our calculations for both *Path A* and *Path B* in the case of R=CH₃. Subsequently, the results of our DFT

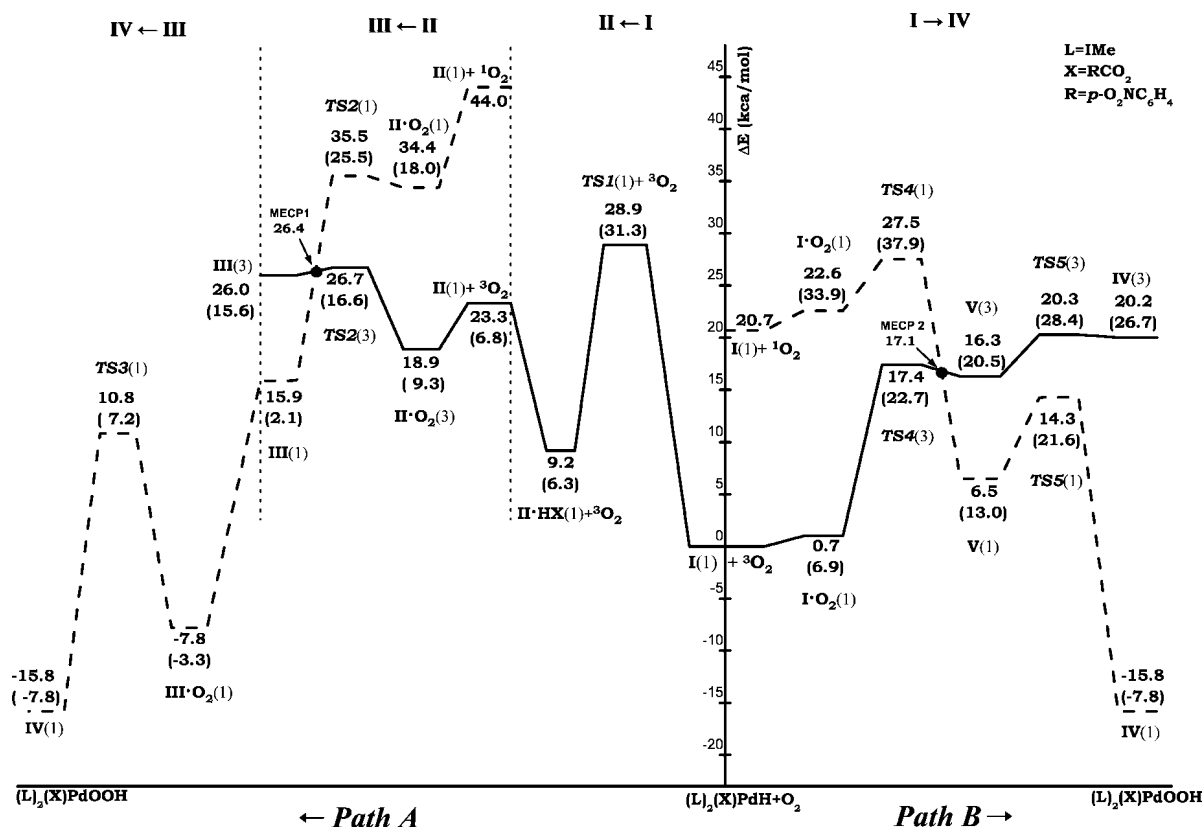


Figure 3. Calculated B3LYP PESs for the oxygenation reaction of $(\text{IMe})_2(p\text{-O}_2\text{NC}_6\text{H}_5\text{CO}_2)\text{Pd}(\text{II})\text{-H}$ to give $(\text{IMe})_2(p\text{-O}_2\text{NC}_6\text{H}_5\text{CO}_2)\text{Pd}(\text{II})\text{-OOH}$. Gibbs free energies changes at 298.15 K in benzene are also reported in parentheses. Energies are in kcal/mol and relative to the ground-state reactants. On the left the pathway that involves reductive elimination of $p\text{-O}_2\text{NC}_6\text{H}_5\text{COOH}$ (Path A) and on the right the pathway for the direct O_2 insertion (Path B) are reported.

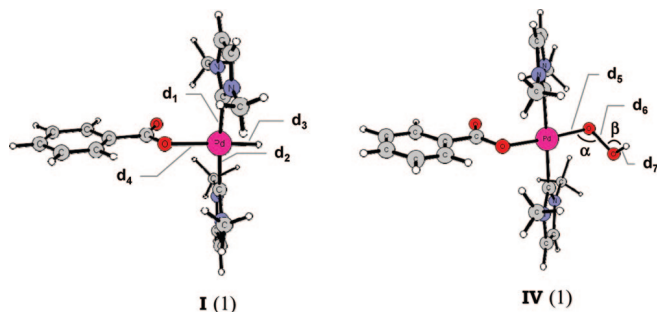


Figure 4. Ground-state optimized structures of the $\text{Pd}(\text{II})\text{-H}$ and $\text{Pd}(\text{II})\text{-OOH}$ complexes in the case of $R = \text{Ph}$. Labels employed to individuate geometrical parameters have to be used to read information reported in Tables 1 and 2.

analysis for $R = \text{Ph}$, $p\text{-O}_2\text{NC}_6\text{H}_4$ will be pointed out for comparison, and general conclusions on the viability of the alternative proposed mechanisms will be drawn.

3.1. Mechanism Proceeding via the Pd(0) Intermediate. The first step of the mechanism that involves formation of the $\text{Pd}(0)$ species proceeds by reductive elimination of CH_3COOH from the initial $\text{Pd}\text{-H}$ complex (Step $\text{I} \rightarrow \text{II}$). As shown in Figure 1 the transition state $\text{TS1}(1)$, which the reaction evolves through is very high in energy, with a calculated relative energy of about 31 kcal/mol both in gas phase and in solution. An inspection of Figure 1 clearly shows that this is the rate-determining step of the overall transformation. The calculated imaginary frequency is $485i \text{ cm}^{-1}$ and is mainly associated with the displacement of the

hydrogen atom from palladium to carbon atom. In the next minimum intercepted along the PES, $\text{II}\cdot\text{HX}(1)$, the carboxylic acid molecule still interacts with the $\text{Pd}(0)$ formed species, and the process results to be endothermic by 4.7 kcal/mol (4.1 kcal/mol in gas phase). Formation of final products, upon reductive elimination of CH_3COOH from the initial $\text{Pd}\text{-H}$ complex, is practically thermoneutral in solvent and endothermic by 15.2 kcal/mol in gas phase. The reaction between the formed $\text{Pd}(0)$ complex with triplet molecular oxygen (Step $\text{II} \rightarrow \text{III}$) requires that both singlet and triplet multiplicities are examined and leads initially to the formation of an $\eta^1\text{-O}_2$ adduct, $\text{II}\cdot\text{O}_2$, in which the IMe ligands retain their *trans* configuration. A stable closed-shell singlet complex, III , is formed by surpassing a low energy barrier (6.4 kcal/mol in solvent and 10 kcal/mol in gas phase) corresponding to the transition state, $\text{TS2}(3)$, for the IMe ligands *trans* to *cis* isomerization. The characteristics of this adduct III ($\text{O}\text{-O}$ distance of 1.4 Å and $\text{O}\text{-O}$ stretching frequency of 978 cm^{-1}) allow us to design it as a η^2 -peroxide.³⁵ Due to the multiplicity change, in this region of the PES the system must undergo a spin inversion that takes place after passage of the TS2 transition state. In the framework of the Two-State Reactivity paradigm³⁶ such a kind of spin crossover is not considered a rate-limiting factor as it involves species that are formed with excess energy, and even electronically excited states become accessible. Following the procedure outlined before, the MECP between the triplet and singlet surfaces has been individuated, and the structure at this point, MECP1 , exhibits a geometry very

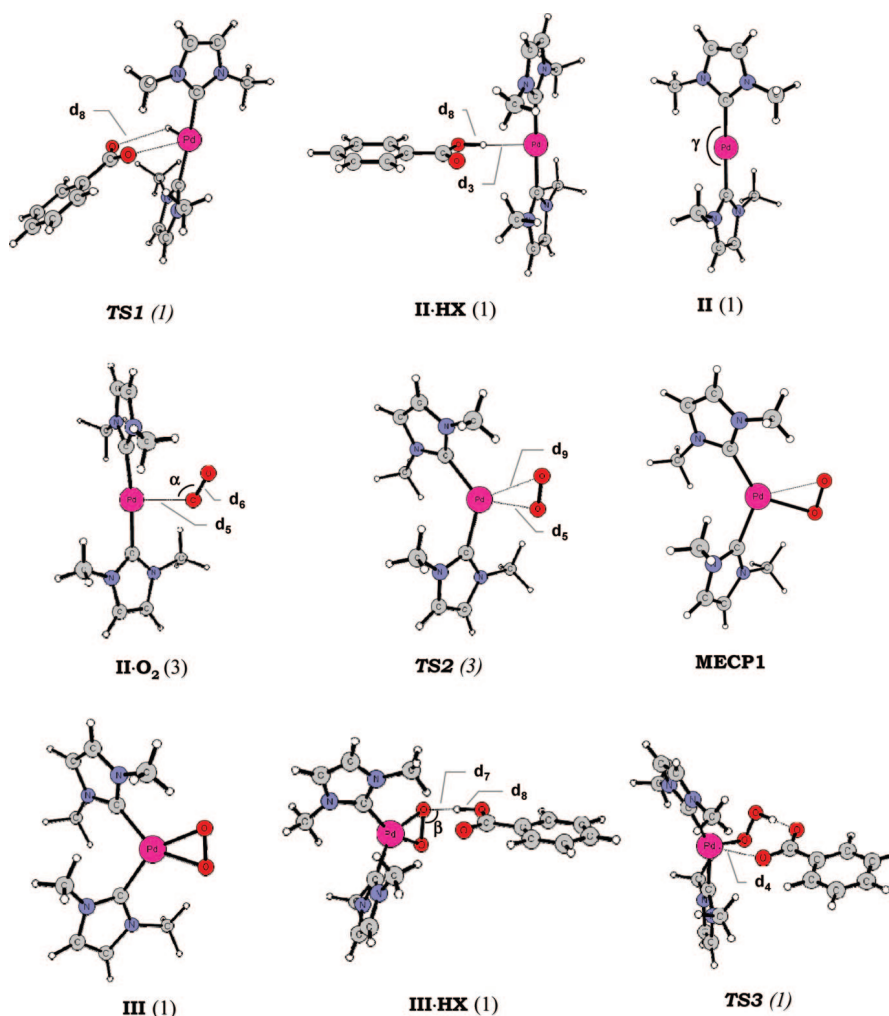


Figure 5. Ground-state optimized structures of stationary points and MECP intercepted along *Path A* in the case of $R=Ph$. Labels employed to individuate geometrical parameters have to be used to read information reported in Tables 1 and 2.

similar to **TS2(3)**. Crossing point relative energy calculated in gas phase is reported in Figure 1. The third and final step (Step **III**→**IV**) of the examined pathway involves protonolysis of the Pd–O bond of the η^2 -peroxo complex **III**. Computational analysis shows that initially CH_3COOH weakly interacts with **III** to give a hydrogen-bonded complex, **III**·HX, stabilized by 4 kcal/mol in solvent (9.6 kcal/mol in gas phase) with respect to ground-state reactants asymptote. Formation of the final hydroperoxide complex **IV** takes place overcoming an energy barrier of 23.6 and 21.2 kcal/mol in solvent and in gas phase, respectively, corresponding to the **TS3(1)** transition state. The normal mode associated with the imaginary frequency, calculated to be $161i\text{ cm}^{-1}$, corresponds to the concerted *cis* to *trans* isomerization of the IMe ligands, proton transfer from acetic acid to one of the oxygen atoms of the peroxide, and coordination of the formed acetate to the Pd center. As a result, the final singlet hydroperoxide product $(CH_3CO_2)-(Ime)_2Pd-OOH$ in its *trans* configuration is obtained, and the overall process is calculated to be exothermic by 8.0 kcal/mol in benzene solvent and 17.1 kcal/mol in gas phase.

3.2. Mechanism of Direct Dioxygen Insertion into the Pd–H Bond of *trans*–[(CH_3COO)(Ime) $_2$ Pd(H)]. Along the triplet pathway (see *Path B* Figure 1) the interaction of oxygen with the *trans*[(Ime) $_2$ (CH_3COO)Pd–H] complex

leads to the formation of a weakly bound van der Waals complex, **I**· O_2 (3), that is stabilized by about 1 kcal/mol in solution. The fully optimized structure of the corresponding complex in a singlet state is substantially different as O_2 coordinates directly to the Pd(II) center. The formed adduct, **I**· O_2 (1), is not stable and lies about 21 kcal/mol above the entrance channel of separated reactants in gas phase and 32.6 kcal/mol above, when solvation effects are included. The reported energy for this complex has been properly corrected, following the mentioned scheme,³⁰ since unrestricted calculations on this adduct showed a significant amount of triplet contamination.

The next step of the reaction, that results to be the rate-determining one, involves the abstraction of the hydrogen atom from the palladium center by O_2 . This step requires an activation energy of 15.6 kcal/mol in solution and 22.9 kcal/mol in gas phase for the formation of the **TS4(3)** transition state. In going from the first adduct to **TS4(3)** the Pd–H bond distance stretches from 1.565 to 1.763 Å, and at the same time the O–O bond length increases from 1.205 to 1.278 Å. The O–H distance is 1.237 Å indicating that the bond between oxygen and hydrogen is forming. The imaginary frequency for **TS4(3)** transition state is calculated to be $1516i\text{ cm}^{-1}$ and clearly corresponds to the movement of the hydrogen atom detaching from Pd and bonding to O

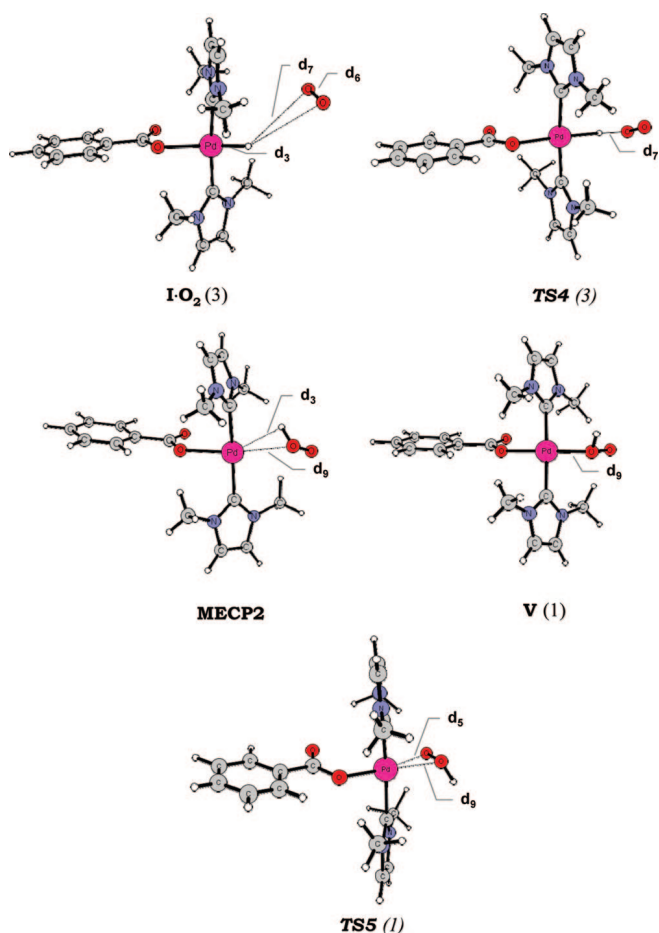


Figure 6. Ground-state optimized structures of stationary points and MECP intercepted along *Path B* in the case of $R=Ph$. Labels employed to individuate geometrical parameters have to be used to read information reported in Table 2.

atom. As a result, an intermediate is formed in which a peroxy radical HOO is coordinated to the T-shaped Pd(I) complex through a weak interaction between hydrogen and Pd atoms. Indeed, this intermediate is only slightly more stable than **TS4(3)** both in gas phase and solution. Along the singlet surface, instead, once molecular oxygen approaches the Pd center, at a distance of 1.472 Å between the closest oxygen and hydrogen, a transition state, **TS4(1)**, has been intercepted and characterized. Also for this singlet transition state, which is less stable than the separate reactants by 35.4 kcal/mol in solution (28.4 kcal/mol in gas phase), the energy has been corrected for spin contamination. From **TS4(1)** the reaction proceeds to yield a stable singlet intermediate, **V(1)**, whose formation is endothermic by 2.9 kcal/mol in gas phase and 10.3 kcal/mol in benzene. The main feature of this intermediate is that the hydrogen atom is bonded ($H-O=0.963$ Å) to the proximal oxygen. Until now the existence of this kind of intermediates has not been evidenced by previous theoretical investigations.^{16,19} IRC calculations confirmed that the **TS4(1)** transition state is connected to both reactant **I·O₂(3)** and product **IV(1)**. The analysis of the structures along the reaction coordinate from the transition state to the **IV(1)** intermediate shows that the

hydrogen atom approaches the proximal oxygen lengthening the O–O bond, whereas the distal oxygen atom rotates upward.

Since the singlet state of the **IV(1)** intermediate is more stable than the triplet one, in this region of the PES the system undergoes a spin inversion that takes place after passage of the **TS4(3)** transition state. Also in this case the spin crossover occurs after formation of the transition state and, as a consequence, cannot be considered a rate-limiting factor.³⁵ Relative energy calculated in gas phase of the minimum energy crossing point, **MECP2**, is reported in Figure 1. The crossing occurs in the vicinity of the triplet transition state, and the **MECP2** structure lies very close in energy to the preceding transition state. It is worthwhile to underline that all the attempts to individuate a singlet intermediate with a structure analogous to that of the triplet complex were unsuccessful in spite of the numerous strategies used to find it out.

Formation of the final hydroperoxy palladium(II) complex, along the singlet pathway involves breaking the bond between the proximal oxygen and the Pd center that makes a new bond with the distal oxygen. Triplet hydroperoxide product formation involves, instead, rearrangement of the HOO fragment in such a way that terminal oxygen and hydrogen atoms move in opposite directions toward and away from the Pd center, respectively. Both the corresponding transition states, **TS5(1)** and **TS5(3)**, have been intercepted and confirmed by IRC analysis. The singlet **TS5(1)** structure lies 10.5 kcal/mol, 20.5 kcal/mol when solvent effects are included, above the reactants dissociation limit and is characterized by an imaginary frequency of $339i$ cm⁻¹. Along the triplet PES the **TS5(3)** structure is destabilized respect to reactants by 19.6 kcal/mol in gas phase and by 28.9 kcal/mol in benzene, and the corresponding imaginary frequency is calculated to be $102i$ cm⁻¹.

Compared to the exothermic formation of the hydroperoxide product in its singlet multiplicity, **IV(1)**, the overall conversion process of the palladium hydride to the Pd-OOH species, **IV(3)**, along the spin conserving triplet surface is endothermic by 17.4 kcal/mol in gas phase and 24.3 kcal/mol in solvent.

3.3. Overall Mechanism for the RCO₂H Reductive Elimination Pathway with $R=Ph$, $p-O_2NC_6H_4$. As it appears, at a first glance, from the comparison between the left sides of Figures 1, 2, and 3 the presence of a different ligand does not introduce any significant qualitative change in the calculated energy profiles. We briefly comment the quantitative description of the envisaged multistep mechanism focusing our attention on those changes that could have an influence on the determination of the most likely pathway among the two proposed ones.

The first step of the process, that is reductive elimination of the carboxylic acids, involves again formation of the weak hydrogen-bonding adduct **II·HX(1)** that occurs surmounting a high free energy barrier (see Figures 2 and 3), corresponding to the **TS1(1)** transition state, of 34.4 kcal/mol for $R=Ph$ and of 31.3 kcal/mol for $R=p-O_2NC_6H_4$. These values are very similar to that computed for the examined acetic acid and confirm that this is the rate-determining step of the whole

Table 1. Selected Geometrical Parameters of Ground-State Reactants, Products, Intermediates, MECP, and Transition States Computed along *Path A*^a

	I(1)(exp)	TS1(1)	II·HX(1)	II(1)	II·O ₂ (3)	TS2(3)	MECP1	III(1)	III·HX(1)	TS3 (1)	IV(1)
d₁	2.052 <i>2.045(2.016)</i> 2.053	2.065 <i>2.059</i> 2.059	2.053 <i>2.052</i> 2.053	2.047	2.074	2.103	2.099	2.061	2.032 <i>2.027</i> 2.025	2.227 <i>2.218</i> 2.215	2.073 <i>2.071</i> 2.071
d₂	2.050 <i>2.051(2.022)</i> 2.053	2.058 <i>2.058</i> 2.057	2.053 <i>2.052</i> 2.053	2.047	2.072	2.105	2.099	2.061	2.061 <i>2.061</i> 2.059	2.001 <i>2.006</i> 2.005	2.058 <i>2.061</i> 2.064
d₃	1.565 <i>1.563(1.540)</i> 1.559	1.510 <i>1.510</i> 1.510	2.173 <i>2.154</i> 2.102	-	-	-	-	-	-	-	-
d₄	2.185 <i>2.187(2.134)</i> 2.195	2.932 <i>3.039</i> 3.116	3.840 <i>3.819</i> 3.816	-	-	-	-	-	3.383 <i>3.379</i> 3.399	2.903 <i>3.145</i> 3.238	2.097 <i>2.106</i> 2.113
d₅	-	-	-	-	2.392	2.256	2.279	2.036	2.009 <i>2.008</i> 2.007	1.982 <i>1.980</i> 1.979	2.030 <i>2.027</i> 2.016
d₆	-	-	-	-	1.259	1.284	1.305	1.400	1.418 <i>1.420</i> 1.422	1.373 <i>1.371</i> 1.374	1.454 <i>1.452</i> 0.967
d₇	-	-	-	-	-	-	-	-	1.551 <i>1.498</i> 1.424	1.067 <i>1.048</i> 1.035	0.966 <i>0.966</i> 1.452
d₈	-	2.414 <i>2.517</i> 2.578	1.000 <i>1.014</i> 1.024	-	-	-	-	-	1.031 <i>1.046</i> 1.074	1.435 <i>1.479</i> 1.514	-
d₉	-	-	-	-	3.218	2.572	2.312	2.036	2.084 <i>2.089</i> 2.097	2.539 <i>2.574</i> 2.579	-
α	-	-	-	-	120.5	88.8	74.8	69.9	72.6 <i>72.9</i> 76.2	96.7 <i>98.7</i> 99.0	113.4 <i>113.5</i> 101.3
β	-	-	-	-	-	-	-	-	104.0 <i>97.9</i> 102.6	96.7 <i>103.7</i> 103.5	101.2 <i>101.3</i> 113.7
γ	175.9 <i>175.3</i> 174.5	175.1 <i>175.1</i> 174.8	178.5 <i>179.2</i> 178.7	179.9	174.6	127.2	119.8	105.8	100.8 <i>100.2</i> 99.8	140.5 <i>150.8</i> 150.6	177.6 <i>177.2</i> 177.4
θ	48.6 <i>10.9</i> 0.3	-71.1 <i>-67.4</i> -69.7	0.0 <i>0.0</i> 0.0	-	-	-	-	-	-	-	-

^a Available experimental geometrical parameters for the benzoate analogue of the hydride complex are also reported in parentheses. Values are reported in **bold** for R=CH₃, in *italic* for R=Ph, and in regular for *p*-O₂NC₆H₄CO₂. Bond lengths are in Å and angles are in degrees. θ = N–C–C–N dihedral angle to individuate relative positions of IMe ligands.

oxygenation pathway. Formation of the Pd(0) complex is more endothermic for both R=Ph and R=*p*-O₂NC₆H₄ with respect to the elimination of acetic acid as well as, consequently, formation of the subsequent two minima and transition state since the (IMe)₂Pd(0) oxygenation step does not depend on the employed carboxylic acid. Identical is also the structure of the minimum energy crossing point, **MECP1**, between the triplet and singlet surfaces.

The interaction of the carboxylic acid RCOOH with the η^2 -peroxo complex **III**(1) is exothermic in solvent by -6.8 and -3.3 kcal/mol with respect to ground-state reactants asymptote for R=Ph and *p*-O₂NC₆H₄, respectively. The free energy barrier that is necessary to surmount to obtain the final hydroperoxide product **IV** is 14.6 kcal/mol for R=Ph and 10.5 kcal/mol for R=*p*-O₂NC₆H₄. Proton transfer from the carboxylic acid to one of the oxygen atoms of the peroxide, coordination of the formed anion to the Pd center, and *cis* to *trans* isomerization of the IMe ligands allow formation of the final singlet hydroperoxide complex (RCO₂)-(IMe)₂Pd-OOH in its *trans* configuration. The overall process is calculated to be exothermic by about 8 kcal/mol in benzene solvent for both R=Ph and *p*-O₂NC₆H₄, being that this value is very close to that calculated in the case of the reductive elimination of acetic acid.

3.4. Mechanism of Direct Dioxygen Insertion into the Pd–H Bond of *trans*-[RCOO](IMe)₂Pd(H) with R=Ph and *p*-O₂NC₆H₄. As it was pointed out yet in the previous paragraph, no significant qualitative differences emerge between the calculated energy profiles when the right sides of Figures 1, 2, and 3 are compared. However, it is worth highlighting some quantitative differences. The interaction of triplet oxygen with the *trans*-[(RCO₂)(IMe)₂PdH] complex leads to the formation of a weakly bound van der Waals complex, **II·HX**(1), that is endothermic in solvent by about 7 kcal/mol both for R=Ph and R=*p*-O₂NC₆H₄ and more endothermic than R=CH₃. Along the triplet surface the reaction evolves through the abstraction of the hydrogen atom from the palladium center by O₂. This step takes place overcoming a free energy barrier of 24.8 and 22.7 kcal/mol for R=Ph and R=*p*-O₂NC₆H₄, respectively, corresponding to the formation of the **TS4**(3) transition states. The imaginary frequencies that confirm the nature of these stationary points correspond to the shift of the hydrogen atom from Pd to one of the O atoms. The intermediate **V**(3) that is formed can be again classified as an adduct in which the peroxy radical HOO is coordinated to the T-shaped Pd(I) complex through a weak interaction between hydrogen and Pd atoms. Indeed, this reaction intermediate lies just a few

Table 2. Selected Geometrical Parameters of Ground-State Intermediates, MECP, and Transition States Computed along *Path B*^a

	I·O ₂ (3)	TS4(3)	MECP2	V(1)	TS5(1)
d ₁	2.051	2.063	2.093	2.075	2.074
	<i>2.052</i>	<i>2.064</i>	<i>2.091</i>	<i>2.073</i>	<i>2.073</i>
	2.052	2.066	2.092	2.074	2.072
d ₂	2.049	2.063	2.082	2.066	2.042
	<i>2.049</i>	<i>2.062</i>	<i>2.106</i>	<i>2.064</i>	<i>2.042</i>
	2.051	2.062	2.108	2.066	2.044
d ₃	1.565	1.762	2.452	-	-
	<i>1.562</i>	<i>1.764</i>	<i>2.455</i>	-	-
	1.559	1.764	2.457	-	-
d ₄	2.186	2.220	2.226	2.070	2.066
	<i>2.191</i>	<i>2.218</i>	<i>2.263</i>	<i>2.076</i>	<i>2.069</i>
	2.199	2.227	2.284	2.082	2.075
d ₅	4.662	3.679	3.449	2.999	2.478
	<i>4.573</i>	<i>3.649</i>	<i>3.444</i>	<i>3.000</i>	<i>2.476</i>
	4.548	3.646	3.441	2.990	2.468
d ₆	1.205	1.277	1.352	1.481	1.517
	<i>1.205</i>	<i>1.277</i>	<i>1.351</i>	<i>1.479</i>	<i>1.518</i>
	3.466	1.235	1.348	0.964	0.965
d ₇	3.386	1.237	0.984	0.963	0.965
	<i>3.488</i>	<i>1.239</i>	<i>0.983</i>	<i>0.963</i>	<i>0.965</i>
	1.205	1.276	0.983	1.478	1.519
d ₉	-	-	2.735	2.086	2.258
	-	-	<i>2.737</i>	<i>2.088</i>	<i>2.251</i>
	-	-	2.731	2.083	2.243
α	-	-	48.0	39.7	63.5
	-	-	47.7	39.7	63.4
	-	-	47.8	39.8	63.3
β	-	111.1	106.7	101.8	101.8
	-	<i>111.2</i>	<i>106.5</i>	<i>101.7</i>	<i>101.7</i>
	-	111.2	106.7	101.8	101.7
γ	176.1	174.4	177.7	177.2	176.9
	<i>175.8</i>	<i>175.2</i>	<i>178.3</i>	<i>177.6</i>	<i>177</i>
	175.3	174.7	178.2	178.0	177.5
θ	47.8	48.2	17.4	6.4	10.2
	<i>49.2</i>	<i>8.1</i>	<i>26.9</i>	<i>7.1</i>	<i>9.7</i>
	49.7	2.1	27.4	6.7	8.1

^a Values are reported in **bold** for R=CH₃, in *italic* for R=Ph, and in regular for *p*-O₂NC₆H₄CO₂. Bond lengths are in Å and angles are in degrees. θ = N-C-C-N dihedral angle to individuate relative positions of IMe ligands.

kcal/mol below the **TS4(3)** transition state for both PhCO₂ and *p*-O₂NC₆H₄CO₂ ligands.

Along the singlet surface, instead, overcoming the energy barrier for the intercepted transition state, **TS4(1)**, allows the formation of a singlet intermediate, **V(1)**, whose main feature is that the hydrogen atom is bonded to the proximal oxygen. Also in this case IRC calculations confirmed that the **TS4(1)** transition states are connected to both reactant **II·O₂(1)** and product **V(1)**. Formation of the singlet intermediate **V(1)** is more favorable with respect to formation of the corresponding triplet intermediate by about 10 kcal/mol in solvent, as for R=CH₃. This means that the system must undergo a spin inversion that takes place after passage of the **TS4(3)** transition state. Geometrical parameters of the computed structures of the minimum energy crossing points, **MECP2**, between the triplet and singlet surfaces, are reported in Table 2, and their relative energies calculated in gas phase are reported in Figures 2 and 3 for R=Ph and R=*p*-O₂NC₆H₄, respectively.

Formation of the final palladium(II) hydroperoxo product takes place, along the singlet pathway, through the **TS5(1)** transition state that lies 19.7 kcal/mol for R=Ph and 21.6

kcal/mol for R=*p*-O₂NC₆H₄ above the ground-state reactants asymptote. Rearrangement of the HOO fragment, instead, allows triplet hydroperoxide product formation through the corresponding less stable, for both benzoate and *p*-nitrobenzoate ligands, **TS5(3)** transition states. Energetics of the hydroperoxide product reaction formation along both singlet and spin conserving triplet surfaces have been reported in the preceding paragraph.

3.5. Preferred Mechanism and Ligand Influence. The detailed and systematic analysis of the two viable palladium-hydride oxygenation pathways carried out in this work reveals that the free activation energies for the rate determining-step of *Path A* and *Path B* are different enough, in spite of the intrinsic uncertainties of DFT computations, to determine which is the preferred mechanism. When the involved carboxylic acid is the acetic acid, the calculated barrier for the CH₃COOH reductive elimination initial step (*Path A*) is 31.2 kcal/mol in gas phase and 31.0 kcal/mol when solvation effects are included. The rate-determining step barrier that is necessary to overcome, instead, for the abstraction of the hydrogen atom by molecular oxygen (*Path B*) is 15.6 and 22.9 kcal/mol in gas phase and in benzene, respectively. The two examined mechanisms exhibit the same difference in the calculated activation barriers relative to the rate-determining step even when the ligands coordinated to the Pd center of the initial Pd-hydride complex are PhCO₂ and *p*-O₂NC₆H₄CO₂. Indeed, free activation energies calculated in solvent are 34.4 and 24.8 kcal/mol for the reductive elimination and hydrogen atom abstraction steps, respectively when R=Ph. Analogous barriers are 31.3 and 22.7 kcal/mol when R=*p*-O₂NC₆H₄. Therefore, on the basis of our results the oxygenation reaction is more likely to evolve through direct insertion of molecular oxygen into the Pd-H bond of the initial hydride complex. This conclusion is reinforced by the favorable comparison between the experimental activation energy, determined to be 24.4(5) kcal/mol for the benzoate ligand,¹⁸ and the corresponding calculated value of 24.8 kcal/mol. In addition, the experimentally detected enhancement of the oxygenation rate due to the presence of the nitro group on the benzoate ligand corresponds to the lower activation energy calculated by us for R=*p*-O₂NC₆H₄.

Conclusions

A detailed DFT study of the mechanism for the conversion of the Pd(II)-hydride complex, (Ime)₂(RCO₂)PdH (R=CH₃, Ph, and *p*-O₂NC₆H₄), to the corresponding Pd(II)-hydroperoxide in the presence of molecular oxygen has been carried out with the aim to probe the alternative reaction pathways, both considered viable on the basis of current data, of direct O₂ insertion, and slow reductive elimination followed by oxygenation. The outcome of our computational analysis supports the mechanism of direct insertion of molecular oxygen into the Pd-H bond of the initial complex. The activation energy relative to the rate-determining step of the direct insertion pathway is calculated to be lower than the activation energy of the rate determining step of the alternative pathway that

involves the carboxylic acid reductive elimination, whatever ligand (CH_3CO_2 , Ph, CO_2 , $p\text{-O}_2\text{NC}_6\text{H}_4\text{CO}_2$) is coordinated to the Pd center. The calculated free activation energy of the rate-determining hydrogen abstraction step ($\Delta G^* = 24.8$ kcal/mol) in the case of the oxygenation reaction of the benzoate-ligated Pd(II)-hydride complex is in very good agreement with the value experimentally determined ($\Delta G^* = 24.4$ kcal/mol). In addition, according to the experimentally detected enhancement of the reaction rate due to the presence of the nitro group on the benzoate ligand, our calculations show that the transition state for the hydrogen atom abstraction by molecular oxygen lies lower in energy along the pathway for the oxygenation reaction of $(\text{IME})_2(p\text{-O}_2\text{NC}_6\text{H}_4\text{CO}_2)\text{PdH}$.

Acknowledgment. We gratefully acknowledge financial help from the Università della Calabria.

References

- (1) Stahl, S. S. *Science* **2005**, *309*, 1824–1826.
- (2) Stahl, S. S. *Angew. Chem., Int. Ed.* **2004**, *43*, 3400–3420.
- (3) Sigman, M. S.; Schultz, M. J. *Org. Biomol. Chem.* **2004**, *2*, 2551–2554.
- (4) Stoltz, B. M. *Chem. Lett.* **2004**, *33*, 362–367.
- (5) Nishimura, T.; Uemura, S. *Synlett* **2004**, 201–216.
- (6) Sheldon, R. A.; Arends, I. W. C. E.; ten Brink, G.-J.; Dijkstra, A. *Acc. Chem. Res.* **2002**, *35*, 774–781.
- (7) Gligorich, K. M.; Sigman, M. S. *Angew. Chem., Int. Ed.* **2006**, *45*, 6612–6615.
- (8) Konnick, M. M.; Guzei, I. A.; Stahl, S. S. *J. Am. Chem. Soc.* **2004**, *126*, 10212–10213.
- (9) Stahl, S. S.; Thorman, J. L.; Nelson, R. C.; Kozee, M. A. *J. Am. Chem. Soc.* **2001**, *123*, 7188–7189.
- (10) Thiel, W. R. *Angew. Chem.* **1999**, *111*, 3349–3351. *Angew. Chem., Int. Ed.* **1999**, *38*, 3157–3158.
- (11) Nishimura, T.; Onoue, T.; Ohe, K.; Uemura, S. *J. Org. Chem.* **1999**, *64*, 6750–6755.
- (12) Hosokawa, T.; Murahashi, S.-I. *Acc. Chem. Res.* **1990**, *23*, 49–54.
- (13) Muzart, J.; Pete, J. P. *J. Mol. Catal.* **1982**, *15*, 373–376.
- (14) Landis, C. R.; Morales, C. M.; Stahl, S. S. *J. Am. Chem. Soc.* **2004**, *126*, 16302–16303.
- (15) Denney, M. C.; Smythe, N. A.; Cetto, K. L.; Kemp, R. A.; Goldberg, K. I. *J. Am. Chem. Soc.* **2006**, *128*, 2508–2509.
- (16) Keith, J. M.; Muller, R. P.; Kemp, R. A.; Goldberg, K. I.; Goddard, W. A., III; Oxgaard, J. *Inorg. Chem.* **2006**, *45*, 9631–9633.
- (17) Keith, J. M.; Nielsen, R. J.; Oxgaard, J.; Goddard, W. A., III. *J. Am. Chem. Soc.* **2005**, *127*, 13172–13179.
- (18) Konnick, M. M.; Gandhi, B. A.; Guzei, I. A.; Stahl, S. S. *Angew. Chem., Int. Ed.* **2006**, *45*, 2904–2907.
- (19) Popp, B. V.; Stahl, S. S. *J. Am. Chem. Soc.* **2007**, *129*, 4410–4422.
- (20) Chowdhury, S.; Rivalta, I.; Russo, N.; Sicilia, E. *Chem. Phys. Lett.* **2007**, *443*, 183–189.
- (21) Chowdhury, S.; Rivalta, I.; Russo, N.; Sicilia, E. *Chem. Phys. Lett.* **2008**, *456*, 41–46.
- (22) Gligorich, K. M.; Sigman, M. *Angew. Chem., Int. Ed.* **2006**, *45*, 6612–6615.
- (23) Becke, A. D. *J. Chem. Phys.* **1993**, *98*, 5648–5652.
- (24) Stephens, P. J.; Devlin, F. J.; Chabalowski, C. F.; Frisch, M. J. *J. Phys. Chem.* **1994**, *98*, 11623–11627.
- (25) Frisch, M. J.; Trucks, G. W.; Schlegel, H. B.; Scuseria, G. E.; Robb, M. A.; Cheeseman, J. R.; Montgomery, J. A., Jr.; Vreven, T.; Kudin, K. N.; Burant, J. C.; Millam, J. M.; Scalmani, G.; Rega, N.; Petersson, G. A.; Nakatsuji, H.; Hada, M.; Ehara, M.; Toyota, K.; Fukuda, R.; Hasegawa, J.; Ishida, M.; Nakajima, T.; Honda, Y.; Kitao, O.; Nakai, H.; Klene, M.; Li, X.; Knox, J. E.; Hratchian, H. P.; Cross, J. B.; Bakken, V.; Adamo, C.; Jaramillo, J.; Gomperts, R.; Stratmann, R. E.; Yazyev, O.; Austin, A. J.; Cammi, R.; Pomelli, C.; Ochtersky, J.; Ayala, P. Y.; Morokuma, K.; Voth, I.; Salvador, O.; Dannenberg, A. J.; Zakrzewski, M.; Dapprich, S.; Daniels, J.; Strain, M.; Farkas, M.; Malick, D. L.; Rabuck, A.; Raghavachari, K.; Foresman, J. B.; Ortiz, J. P.; Cui, Q.; Baboul, A. G.; Clifford, K.; Cioslowski, J.; Stefanov, B. B.; Liu, G.; Liashenko, G.; Piskorz, P.; Komaromi, I.; Martin, R. L.; Fox, D. J.; Keith, T.; Al-Laham, M. A.; Peng, D.; Nanayakkara, S.; Challacombe, M.; Gill, P. M. W.; Johnson, F.; Chen, Y.; Wong, M.; Gonzalez, C.; Pople, M. J. *Gaussian03, reVision B.05*; Gaussian, Inc.: Wallingford, CT, 2004.
- (26) Andrae, D.; Häussermann, U.; Dolg, M.; Stoll, H.; Preuss, H. *Theor. Chim. Acta* **1990**, *77*, 123–141.
- (27) Fukui, K. *J. Phys. Chem.* **1970**, *74*, 4161–4163.
- (28) Gonzalez, C.; Schlegel, H. B. *J. Chem. Phys.* **1989**, *90*, 2154–2161.
- (29) Weissbluth, M. *Atoms and Molecules*; Academic Press: New York, 1978; p 587.
- (30) Ovchinnicov, A. A.; Labanowski, J. K. *Phys. Rev. A* **1996**, *53*, 3946–3952.
- (31) Cancès, M.; Mennucci, B.; Tomasi, J. *J. Chem. Phys.* **1997**, *107*, 3032–3041.
- (32) Mennucci, B.; Cancès, E.; Tomasi, J. *J. Phys. Chem. B* **1997**, *101*, 10506–10507.
- (33) Kollaman, P. *Chem. Rev.* **1993**, *93*, 2395.
- (34) Harvey, J. N.; Aschi, M.; Schwarz, H.; Koch, W. *Theor. Chem. Acc.* **1998**, *99*, 95–99.
- (35) Cramer, C. J.; Tolman, W. B.; Theopold, K. H.; Rheingold, A. L. *PNAS* **2003**, *100*, 3635–3640.
- (36) Schröder, D.; Shaik, S.; Schwarz, H. *Acc. Chem. Res.* **2000**, *33*, 139–145.

CT8001442

Bibliography

- [1] S. S. Stahl, *Angew. Chem., Int. Ed.* **2004**, 43, 3400.
- [2] M. S. Sigman and M. J. Schultz, *Org. Biomol. Chem.* **2004**, 2, 2551.
- [3] T. Nishimura and S. Uemura, *Synlett* **2004**, 201.
- [4] B. M. Stoltz, *Chem. Lett.* **2004**, 362.
- [5] K. M. Gligorich, and M. S. Sigman, *Angew. Chem. Int. Ed.* **2006**, 45, 6612.
- [6] W. R. Theil, *Angew. Chem* **1999**, 111, 3349; W. R. Theil, *Angew. Chem. Int. Ed.* **1999**, 38, 3157.
- [7] M. M. Konnick, I. A. Guzei and S.S. Stahl, *J. Am. Chem. Soc.* **2004**, 126, 10212.
- [8] S. S. Stahl, J. L. Thorman, R. C. Nelson and M. A. Kozee, *J. Am. Chem. Soc.* **2001**, 123, 7188.
- [9] J. M. Keith, R. J. Nielsen, J. Oxgaard, and W. A. Goddard, III. *J. Am. Chem. Soc.* **2005**, 127, 13172.
- [10] J. M. Keith, R. J. Nielsen, J. Oxgaard and W. A. Goddard, III. *J. Am. Chem. Soc.* **2005**, 127, 13172.
- [11] M. C. Denney, N. A. Smythe, K. L. Cetto, R. A. Kemp, and K. I. Goldberg, *J. Am. Chem. Soc.* **2006**, 128, 2508.
- [12] J. M. Keith, R. P Muller, R. A. Kemp, K. I. Goldberg, W. A. Goddard, III. and J. Oxgaard, *Inorg. Chem.* **2006**, 45, 9631.
- [13] M. M. Konnick, B A. Gandhi, I. A. Guzei and S.S. Stahl, *Angew. Chem. Int. Ed.* **2006**, 45, 2904.

- [14] B. V. Popp and S.S. Stahl, *J. Am. Chem. Soc.* **2007**, 129, 4410.

Chapter 4

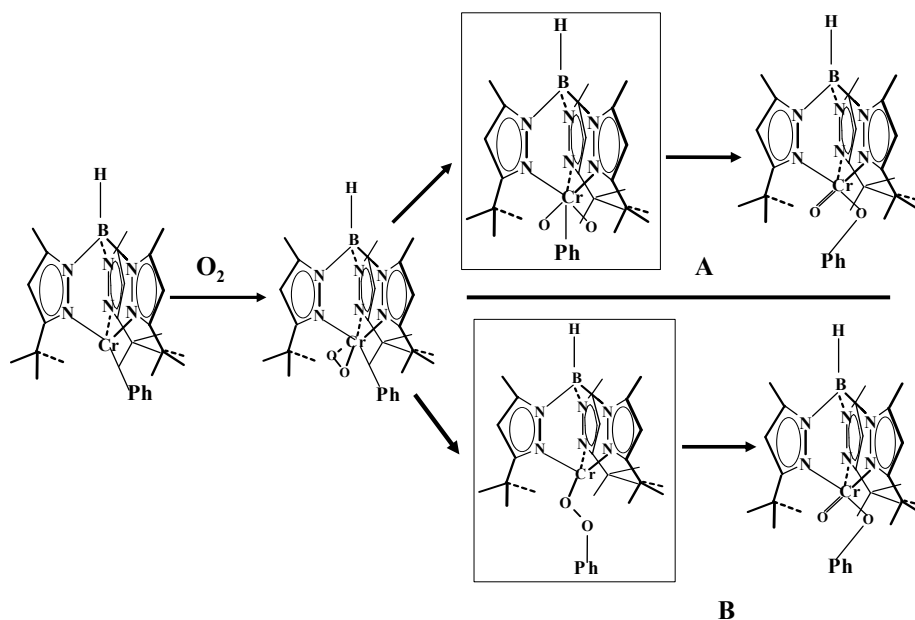
Oxygen Insertion into the Metal-Carbon Bond of the $\text{Tp}^{tBu,Me}\text{Cr}^{(IV)}\text{Ph}$ Complex: Exploring the Nature of Oxygen Migration Using DFT.

4.1 Introduction

The chemical process using dioxygen are a goal of “green” or “sustainable” chemistry since O_2 is a readily available, non-toxic reagent, and a common by-product of aerobic oxidations is the innocuous substance water. The reactions of O_2 with organic molecules are generally thermodynamically favored, but kinetically hampered by significant barriers. Catalysis is, obviously, the answer. As a consequence a great deal of work has already been devoted to the investigation of metal-catalyzed oxidations of organic substrates by air [1, 2]. Nevertheless the corresponding reaction mechanisms are very often obscure and only few of them are known in detail. In this context the insertion of dioxygen into metal-carbon bonds is of central interest since it represents an individual step of the metal-mediated oxidations by molecular. Theopold and co-workers have reported about the reaction of O_2 with a tris(pyrazolyl)borate chromium phenyl complex in a cold (-45°C) solution of penten (Scheme 4.1) [3]. Exposure of a solution of $[\text{Tp}^{tBu,Me}\text{CrPh}]$ ($\text{Tp}^{tBu,Me}$ =hydrotris(3-*tert*-butyl-5-methyl-pyrazolyl)borate)

to dioxygen yields as final product a phenoxide (Scheme 4.1), whose structure has been determined by X-ray diffraction [3].

Important questions pertaining to the formation of the phenoxide product concern the na-



Scheme 4.1: Proposed reaction mechanism for the insertion of O_2 into chromium-phenyl bond in order to form $Tp^{tBu,Me}Cr^{IV}(O)OPh$. Scheme 4.1: (A) O-O breaking mechanism, (B) Migratory insertion of coordinated molecular oxygen.

ture of the intermediate observed at low temperature and the details of the oxygen insertion mechanism. Indeed, the reaction of molecular oxygen with metal-alkyl complexes could proceed both by a radical chain mechanism. The authors have performed crossover experiment to check whether the reaction proceeds by a radical chain mechanism or an intramolecular insertion of O_2 into the Cr-C bond. They have concluded that the insertion of O, starting from the initial adduct, proceeds in an intramolecular fashion. This observation indicates that the process involves the activation of O_2 via coordination to the metal center and subsequent insertion. The coordination geometries of O_2 in 1:1 metal- O_2 complexes fall into two categories, η^1 -(end-on) and η^2 -(side-on) [4]. These latter adducts have been further defined as superoxo and peroxo complexes on the basis of the O-O bond length and stretching frequency (ν_{O-O}). Thus, compounds with an O-O distance of 1.4-1.5 Å and ν_{O-O} between 800 and 930 cm^{-1}

are classified as peroxides, whereas those with O-O bond length and stretching frequency of 1.2-1.3 Å and 1050-1200 cm⁻¹, respectively are designed as superoxides.

On the basis of detected IR spectra Theopold et al. have proposed that the first intermediate is a superoxo complex coordinated in a side-on η^2 fashion. Nevertheless, they have not excluded the alternative end-on η^1 coordination. Regarding the reaction mechanism they have proposed that, after the formation of the Cr(III) superoxo complex [Tp^{tBu,Me}Cr(O₂)Ph], the reaction proceeds by molecular oxygen insertion into the Cr-C bond to yield a phenyl peroxy intermediate [Tp^{tBu,Me}CrOOPh]. Through the breaking of the O-O bond and the formation of a new Cr-O bond the final phenoxide complex is obtained.

The aim of this work is the investigation by means of DFT of the overall mechanism of the oxygen insertion reaction into the Cr-Ph bond of the [Tp^{tBu,Me}CrPh] complex with the support of the pathway hypothesized on the basis of experimental observations. Here we have considered two potential insertion mechanisms of O₂ into the chromium-phenyl bond: (1) O-O bond cleavage (Scheme 4.1(A)) and (2) migratory insertion of coordinated molecular oxygen (Scheme 4.1(B)). As a result of the oxidative addition of O₂ to [Tp^{tBu,Me}CrPh] we have explored the formation of both a phenyl peroxide and a dioxo phenyl complex [Tp^{tBu,Me}Cr(O)₂Ph] as possible reaction intermediates. All the stationary points intercepted along the reaction pathways for the insertion reaction have been well characterized and the calculated Potential Energy Surfaces have been compared to establish which is the preferred pathway. Complete PESs have been characterized in a number of different electronic states to appreciate whether spin crossings between surfaces of different multiplicity can occur and influence the course of the reaction.

4.2 Computational Details

All calculations reported in this work were done using the Gaussian03 program [5]. All the molecular geometries and energies in this study are optimized using the Becke3LYP (B3LYP) density functional theory (DFT) method as implemented in Gaussian03 program package [6, 7, 8]. All optimizations, carried out without any constraints, were followed by vibrational analysis with the same theoretical approach to identify the stationary points located on the potential energy surfaces. Zero-point energy corrections were added to all the absolute energies. Intrinsic reaction coordinate (IRC) calculation was performed to verify the correction of

all transition states [9, 10]. For our work we have employed a strategy such as first we have optimized the different geometries with a small model system using the methyl group in place of the *tert*-butyl substituents of the $\text{Tp}^{tBu,Me}$ ligands in $\text{Tp}^{tBu,Me}\text{CrPh}$. With the help of the optimized small model geometries we have reoptimized the full geometries using the *tert*-butyl in place of the methyl group. For this work the standard 6-31G* basis sets by Pople and co-workers were employed for all atoms.

To, estimate the solvation effects we have done a single point calculations on the fully optimized geometry of each stationary point along the reaction path, using the polarized continuum solvation model, (PCM), initially devised by Tomasi and co-workers [11], as implemented in Gaussian03. The solute is placed inside the cavity according to the Gepol procedure [12] where the interlocking spheres centered on the solute atom and the Pauling atomic radii. Non-electrostatic dispersion and repulsion [13] and cavitation [29] contributions were also included into the solvation free energy calculation.

The solvation Gibbs free energies have been evaluated using the well-known thermodynamic cycle [15], where the reaction Gibbs free energy in solution, ΔG_{sol} , is calculated for each process as the sum of two contributions: a gas-phase reaction free energy, ΔG_{gas} , and a solvation reaction free energy term calculated with the continuum approach, ΔG_{solv} :

$$\Delta G_{sol} = \Delta G_{gas} + \Delta G_{solv} \quad (4.1)$$

The gas-phase reaction free energy is the sum of two parts: electronic plus nuclear repulsion energy (ΔE_{ele}) and thermal contribution including zero-point energy ($\Delta G_{gas} = \Delta H + T\Delta S$). The last term, $T\Delta S$, that is the thermal correction, is evaluated using the calculated quantum mechanical vibrational frequencies.

4.3 Results and Discussion

We have initiated our study by selecting a small model of tris(pyrazolyl)borate chromium phenyl complex which closely resembles the experimental complex. In the potential energy surface (PES) we have present only ground states intermediate, transition states.

4.3.1 Mechanism 1: O-O Breaking

We have presented the potential energy surface (PES) in Fig 4.1. In the PES we have mentioned the different electronic states to localized the spin crossing between two potential energy surfaces. The corresponding optimized ground state structures of reactant, intermediate and transition states have been depicted in the Fig 4.2. In Table 4.1 we have presented the geometrical parameters.

The reactant $\text{Tp}^{tBu,Me}\text{CrPh}$ is in quintet state. We have introduced the chromium phenyl complex to (triplet) molecular oxygen, which leads to immediate formation of a superoxo-complex, $\text{INT}_{trip} (\text{LPhCr}-\eta_2(\text{O}_2)_{trip})$, with $\Delta E = -31.1$ kcal/mol in gas phase. This is an exothermic process. From Fig. 5.2 it is clear that both atoms of O_2 are coordinating with the chromium center. The corresponding fully optimized singlet species is significantly higher in energy in the gas phase. The O-O bond distance is 1.321 \AA , which is little bit longer than the O-O bond distance in O_2 . Cramer *et. al.* [4] documented that in 1:1 metal- O_2 complexes the O-O bond distance is $1.2-1.3 \text{ \AA}$ for the superoxo complex, whereas it is $1.4-1.5 \text{ \AA}$ for the peroxo complex. Egan *et. al* [17] suggested that the superoxo ligand may well be coordinated in the side-on ($\eta^2\text{-O}_2$) fashion. From the above discussion and the calculated O-O bond distance we can conclude that this intermediate is a superoxo complex with a side-on ($\eta^2\text{-O}_2$) fashion. On the other hand, the bond lengths between Cr-O1 and Cr-O2 are 1.964 and 1.951 \AA respectively, and the chromium-phenyl bond length is 2.065 \AA , which means that the chromium-phenyl yet to be broken.

From this intermediate we find a transition state TS1_{trip} along the triplet surface with imaginary frequency 657 i cm^{-1} . The energy barrier is 28.9 kcal/mol in gas phase and it is 29 kcal/mol in solvent. In this transition state the chromium and oxygen bond lengths are decreased to 1.623 \AA for Cr-O1 and 1.881 \AA for Cr-O2, indicating a strong bond formation between the metal-oxygen. On the other hand, the O-O distances increased by 0.556 \AA , indicated that the O-O bond has completely broken. Also, the imaginary frequency is clearly corresponding to the breaking of the O-O bond. There is no significant change in the chromium-phenyl bond. Also, along the singlet surface, a transition state was located for breaking the bond of dioxygen, but it is energetically higher than the triplet surface. From this transition state the reaction proceeds to yield a very stable singlet intermediate, indicated as $\text{INT2}_{sing} (\text{LPhCr} - (\text{O})_2_{sing})$, which is -40.2 kcal/mol below with respect to the reactants in gas phase. In this intermediate state the oxygen atoms are far away ($\text{O-O} = 2.488 \text{ \AA}$) from each other. Another significant change is the reduction of the metal-oxygen bond (Cr-O1 = 1.560 \AA and Cr-O2 = 1.561 \AA). On

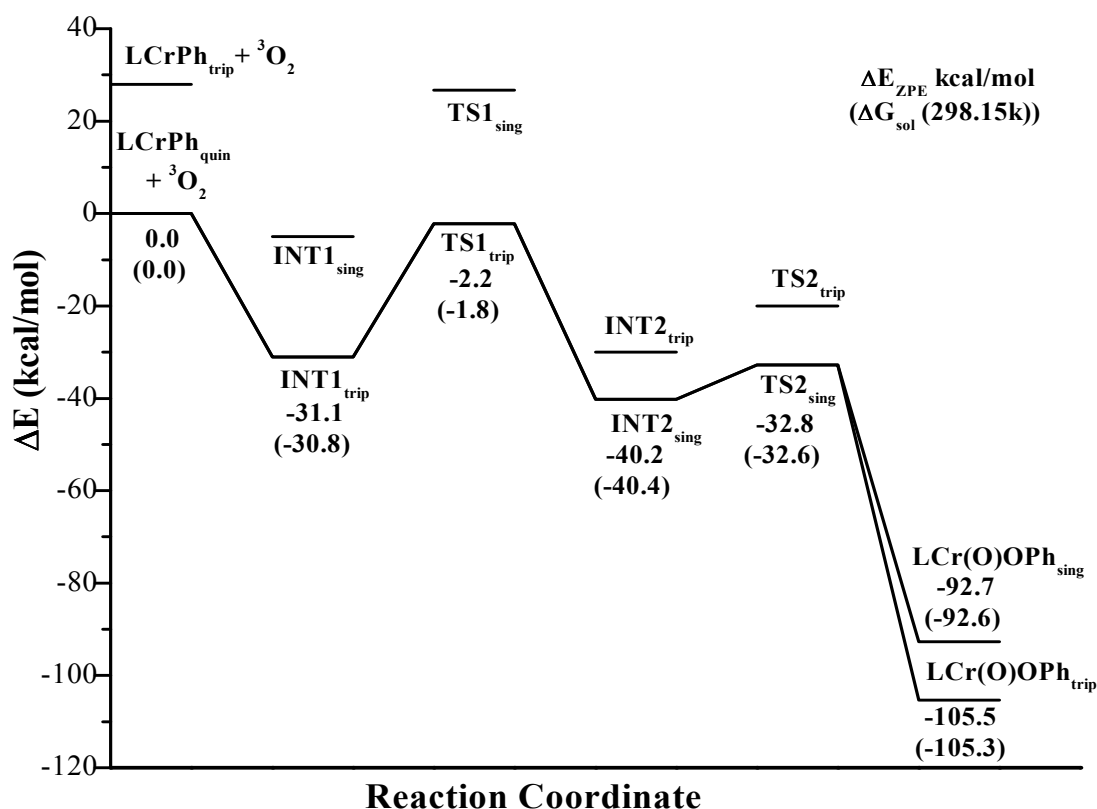


Figure 4.1: Potential energy surface for the O-O breaking mechanism. Gibbs free energies changes at 298.15 K in solvent are also reported in parentheses. Excited state structures are, also, mentioned to locate the spin crossing. Energies are relative to the ground state reactants.

the other hand the same kind of intermediate INT2_{trip} ($LPhCr - (O)_2_{trip}$) along the triplet surface is higher in energy.

Formation of stable INT2_{sing} ($LPhCr - (O)_2_{sing}$) requires intersystem crossing from the triplet to singlet reaction surfaces. This spin crossover is most probable at the minimum energy crossing point (MECP). This spin crossover is not considered as a rate-limiting factor. It is worthwhile to underline that for such kind of crossover the involved species, that are formed with excess energy, and even electronically excited states become accessible [16].

Along the reaction path at a Cr-phenyl distance of 2.159 Å, another transition state TS2_{sing} was located for the formation of O2-phenyle bond. The energy barrier is 7.4 kcal/mol in gas phase, whereas it is -7.8 kcal/mol in solvent. The imaginary frequency is $328i\text{cm}^{-1}$, which corresponds to the movement of O2 and phenyl fragment. The Cr-O2 bond distance is elongated to 1.606 Å from 1.561 Å. All these significant changes indicated the breaking of the

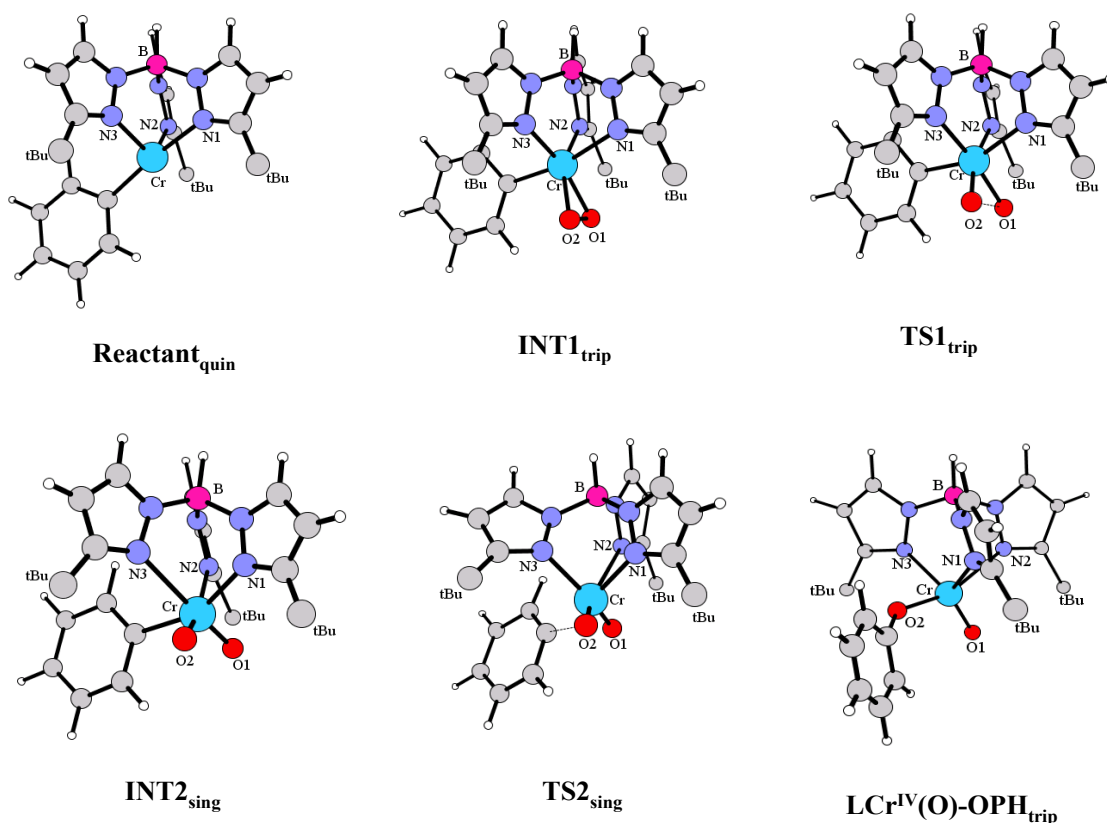


Figure 4.2: Ground-state structures of the reactant, intermediates and transition states along the O-O breaking pathway. Labels introduced to individuate geometrical parameters have to be used to read information reported in Table 4.1.

chromium-phenyl bond and the formation of the O2-phenyl bond. At the same point in the PES we found a transition state $TS2_{trip}$ along the triplet path, but this transition state is higher with respect to the $TS2_{sing}$. The triplet transition state is higher than the singlet one. In this area we have found another crossing between the triplet and singlet surfaces and this takes place after passage of the $TS2$ transition state. In the final step the reaction leads to a phenoxide complex, which takes place along the triplet surface. Also, we noticed that the several strategies to identify the final product state and we confirmed that the final product is in triplet state. This is a highly exothermic process by -105.5 kcal/mol with respect to the separate reactants in gas phase. A singlet version of phenoxide complex is possible, although higher in energy the final product is clearly a $Tp^{tBu,Me}Cr(O)OPh$ complex in triplet state, with a Cr-O2 bond distance of 1.827 \AA , which is comparable to that in the experimental structure (Cr-O2= 1.844 \AA (Exp)). The O2-Ph bond distance of 1.346 \AA is consistent with

those of similar species. This indicates that the bond between chromium and phenyl bond is completely broken and an oxygen-phenyl bond is formed. It should also be noted that the calculated bond lengths and angles are in close agreement with the bond lengths and angles

Parameter	Reactant _{quin}	INT1 _{trip}	TS1 _{trip}	INT2 _{sing}	TS2 _{sing}	LCr(O)OPh _{trip} (exp)
Cr-O1	-	1.964	1.623	1.560	1.553	1.576(1.576)
Cr-O2	-	1.951	1.881	1.561	1.606	1.827(1.844)
Cr-N1	2.161	2.113	2.197	2.548	2.124	2.096(2.097)
Cr-N2	2.161	2.133	2.142	2.072	2.031	2.340(2.191)
Cr-N3	2.142	2.317	2.188	2.349	3.436	2.100(2.099)
Cr-Ph	2.085	2.065	2.071	2.076	2.159	-
O1-O2	-	1.321	1.877	2.488	2.615	2.804
O2-Ph	-	2.910	2.936	2.724	2.019	1.346
O1-Cr-O2	-	39.4	64.2	105.7	111.7	110.8(103.8)
O1-Cr-N1	-	145.8	155.0	170.7	106.3	126.4(130.2)
O1-Cr-N2	-	111.5	103.4	102.7	103.9	88.9(87.9)
O1-Cr-N3	-	98.9	106.6	83.8	169.9	124.5(128.7)
O2-Cr-N1	-	106.4	90.9	83.0	134.5	92.2(89.7)
O2-Cr-N2	-	150.9	167.7	95.7	106.7	159.9(168.2)
O2-Cr-N3	-	98.9	101.5	170.4	64.2	85.3(90.7)
N1-Cr-N2	106.7	102.5	101.3	78.9	87.0	78.6(81.46)
N1-Cr-N3	83.9	82.5	79.8	87.4	81.7	104.3(98.1)
N2-Cr-N3	83.9	81.9	81.8	2.0	69.8	79.7(82.95)

Table 4.1: Selected geometrical parameter of Ground-State Reactants, Intermediates and transition States computed along the O-O breaking pathway. Available experimental geometrical parameters of $\text{Tp}^{tBu,Me}\text{Cr}^{IV}(\text{O})\text{OPh}$ are also reported in parantheses. Bond length are in Å and angles are in degree.

of the experimental structures [3].

4.3.2 Mechanism 2: O_2 Insertion

Theopold and coworkers have proposed a reaction mechanism regarding the insertion process of dioxygen [3]. According to the proposed catalytic cycle the reaction will go through the formation of peroxo complex and then migratory insertion of one of the oxygen atoms into the chromium-phenyl bond. In Fig. 4.3 we have presented the PES. In this case, also, we have mentioned the different electronic states to localized the spin crossing between two potential energy surfaces. In Fig. 4.4, we have depicted the optimized ground state structures of reactants, intermediate and transition states along the reactions paths. In Table 4.2 we have presented the geometrical parameters.

We have initiated our study of the possible mechanism for the formation of superoxo com-

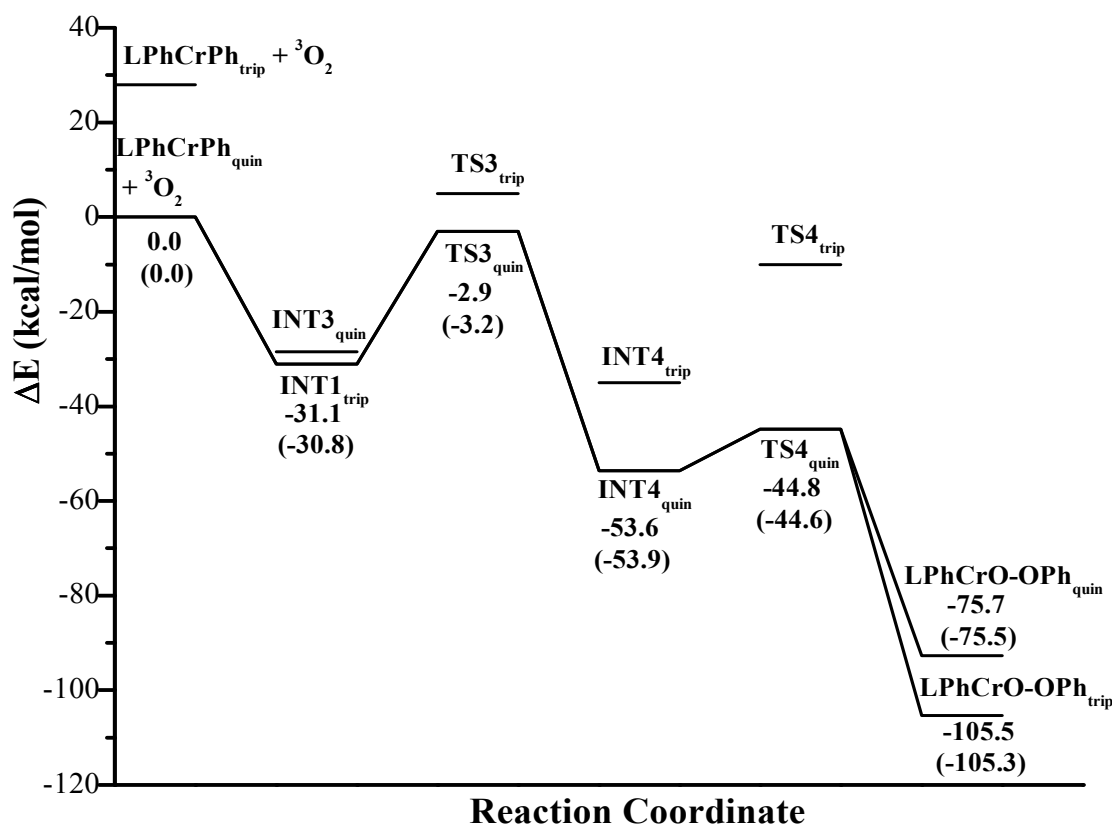


Figure 4.3: Potential energy surface for the migratory insertion of coordinated molecular oxygen pathway. Gibbs free energies changes at 298.15 K in solvent are also reported in parentheses. Excited states structures are, also, mentioned to locate the spin crossing. Energies are relative to the ground state reactants.

plex by probing the interaction of triplet oxygen with tris(pyrazolyl)borate chromium phenyl

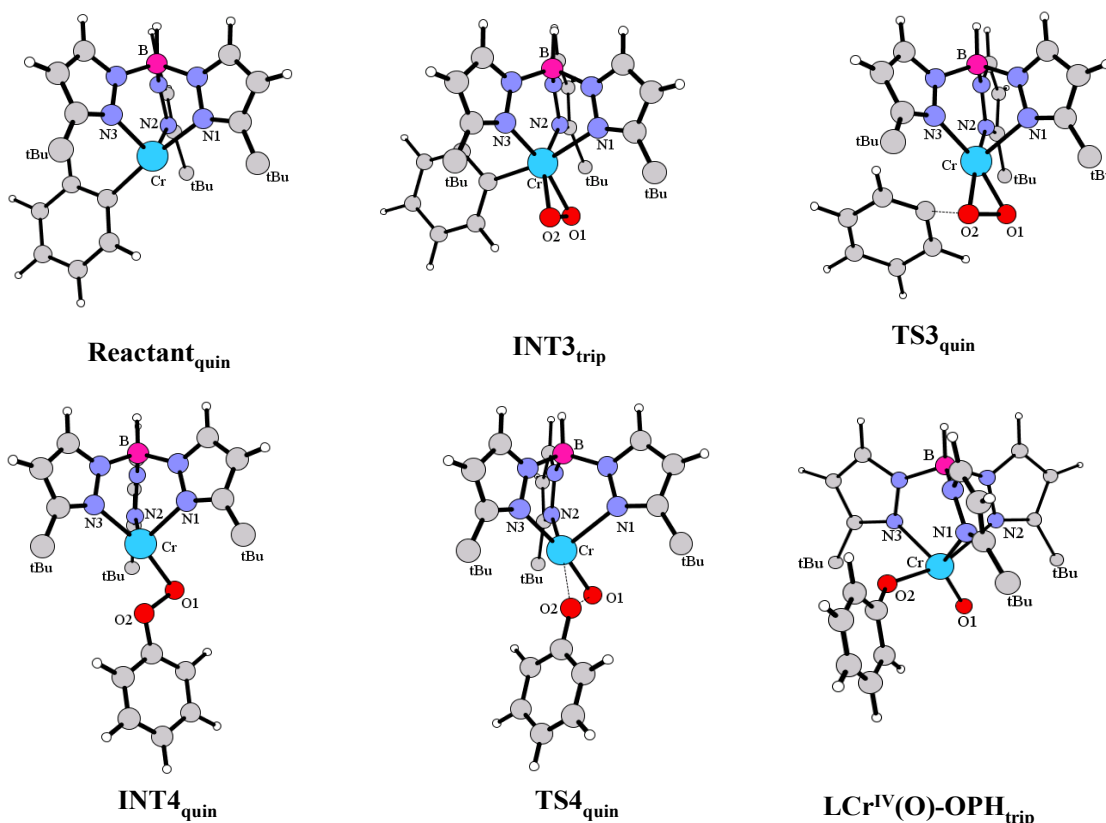


Figure 4.4: Ground-state structures of the reactant, intermediates and transition states along the migratory insertion of coordinated molecular oxygen pathway. Labels introduced to individuate geometrical parameters have to be used to read information reported in Table 4.2.

complex in the first step of the reaction. In this step our results show that INT1_{trip} ($\text{LPhCr-}\eta_2(\text{O}_2)_{trip}$) ($\Delta E = -31.1$ kcal/mol) is more stable than INT3_{quin} ($\text{LPhCr-}\eta_2(\text{O}_2)_{quin}$) in gas phase. The O1-O2 bond length is 1.321 Å for INT1_{trip} ($\text{LPhCr-}\eta_2(\text{O}_2)_{trip}$). The O1-O2 bond distance in this complex is more close to the O-O bond distance in the superoxo complex in side-on ($\eta^2\text{-O}_2$) fashion. On the other hand, the bond distances between Cr-O1 and Cr-O2 are Cr-O1 = 1.964 Å and Cr-O2 = 1.951 Å respectively for INT1_{trip} ($\text{LPhCr-}\eta_2(\text{O}_2)_{trip}$). This indicates that the coordination of dioxygen with chromium and confirms the formation of the superoxo complex. The geometrical parameters are also consistent with the geometrical parameters of the other same kind of species.

Along the reaction path after this intermediate state we have found a spin-crossover between the two surfaces and we have located a transition state TS3. Detlef *et. al.* have reported that the spin-inversion before the transition state could play a role for the rate-determining step of

the reaction [16]. So, we can consider that TS3 is the rate-determining step of the reaction. This transition state, TS3 is more stable than TS1 in O-O breaking mechanism.

The transition state, TS3_{quin} is more stable than the transition state TS3_{trip}. In this transition state instead of breaking the bond between O1 and O2, there is a breaking of bonds between Cr-phenyl and Cr-O2. The imaginary frequency is 412i cm⁻¹. The imaginary frequency corresponds to a mode in which the phenyl and O2 are coming closer to each other while keeping the O1-O2 bond intact. The O2-phenyl bond distance reduced to 1.850 Å, whereas the Cr-phenyl elongated to 2.239 Å. The O1-O2 bond distance is 1.429 Å, which is halfway between common single- and double-bond distances of 1.48 and 1.21 Å, respectively. All these significant changes indicated that the O2-phenyl bond has yet to be formed. We have performed an IRC calculation and the calculated result confirmed that TS3_{quin} is connecting both intermediates LPfCr-η₂(O₂)_{quin} and LCr-(OOPh)_{quin}.

From TS3_{quin} the energy falls by 50.7 kcal/mol in gas-phase when forming the species INT4_{quin} (LCr-(OOPH)_{quin}), which is very similar to the species in the proposed catalytic cycle. Indeed the significant changes are the stretching of the O1-O2 distance (to 1.475 Å), which is close to common the single-bond between the two oxygen atoms. Also, there are some other changes like, the stretching of the Cr-O2 distance (to 2.358 Å) and the reduction of the O2-Ph distance (to 1.371 Å). All these changes indicate the formation of the O2-Ph bond and the breaking of the Cr-O2 bond. All these changes indicated the formation of the Cr-phenyl peroxide. On the other hand, the INT4_{trip} (LCr-(OOPh)_{trip}) is energetically higher than the INT4_{quin} (LCr-(OOPh)_{quin}).

This intermediate state, INT4_{quin} reacts further through breaking of a bond and we have located a transition state TS4_{quin}. The imaginary frequency is 800i cm⁻¹, which is corresponds to a mode of breaking the bond between O1-O2. The O1-O2 distance is elongated to 1.784 Å. Another significant development is the reduction of the Cr-O2 bond length (to 2.184 Å), which indicates that the bond between Cr and O2-Ph moiety has yet to be formed. On the other hand the Cr-O1 bond length is reduced to 1.809 Å, which is a very strong metal-oxo bond. The transition state TS4_{trip} along the triplet path is energetically very high with respect to TS4_{quin}.

Parameter	Reactant _{quin}	INT1 _{trip}	TS3 _{quin}	INT4 _{quin}	TS4 _{quin}	LCr(O)OPh _{trip} (exp)
Cr-O1	-	1.964	1.913	1.936	1.809	1.576(1.576)
Cr-O2	-	1.951	1.918	2.358	2.184	1.827(1.844)
Cr-N1	2.161	2.113	2.229	2.099	2.149	2.096(2.097)
Cr-N2	2.161	2.133	2.187	2.188	2.353	2.340(2.191)
Cr-N3	2.142	2.317	2.224	2.182	2.108	2.100(2.099)
Cr-Ph	2.085	2.065	2.239	-	-	-
O1-O2	-	1.321	1.429	1.475	1.784	2.804
O2-Ph	-	2.910	1.850	1.371	1.347	1.346
O1-Cr-O2	-	39.4	43.8	38.6	52.0	110.8(103.8)
O1-Cr-N1	-	145.8	100.4	164.6	163.3	126.4(130.2)
O1-Cr-N2	-	111.5	80.8	102.0	100.3	88.9(87.9)
O1-Cr-N3	-	98.9	100.7	102.3	106.4	124.5(128.7)
O2-Cr-N1	-	106.4	116.9	126.0	111.4	92.2(89.7)
O2-Cr-N2	-	150.9	148.6	123.3	105.6	159.9(168.2)
O2-Cr-N3	-	98.9	104.8	125.6	153.7	85.3(90.7)
N1-Cr-N2	106.7	102.5	84.7	88.1	85.6	78.6(81.46)
N1-Cr-N3	83.9	82.5	80.8	88.2	88.7	104.3(98.1)
N2-Cr-N3	83.9	81.9	100.7	94.8	92.2	79.7(82.95)

Table 4.2: Selected geometrical parameter of Ground-State Reactants, Intermediates and transition States computed along the migratory insertion of coordinated molecular oxygen pathway. Available experimental geometrical parameters of $\text{Tp}^{t\text{Bu},\text{Me}}\text{Cr}^{\text{IV}}(\text{O})\text{OPh}$ are also reported in parantheses. Bond length are in Å and angles are in degree.

In this region of PES we have found a spin-crossover after the passage of TS4. In the framework of the Two-State Reactivity paradigm such a kind of spin crossover is not considered a rate-limiting factor as it involves species that are formed with excess energy and even electronically excited states become accessible [16].

From the transition state TS4, after the spin-inversion, the reaction proceeds to the triplet state (phenoxide)chromium(IV) product $[\text{LCr}(\text{O})\text{OPh}_{trip}]$ by formation of another strong metal-oxo bond between chromium and the O2-Ph fragment from TS4_{trip} . This is an exothermic process by 105.5 kcal/mol with respect to ground-state reactants. A quintet version of $\text{LCr}(\text{O})\text{OPh}_{quin}$ is also possible, although higher in energy. The Cr-O1 bond distance of $\text{LCr}(\text{O})\text{OPh}_{trip}$ is 1.576 Å, while the Cr-O2 bond distance is 1.827 Å. The geometrical parameters of $\text{LCr}(\text{O})\text{OPh}_{trip}$ are consistent with the experimental data. In Tables 4.1 and 4.2 we have presented the geometrical parameters of $\text{LCr}(\text{O})\text{OPh}_{trip}$ together with the experimental data.

4.4 Conclusion

In conclusion, here we have presented a detailed density functional calculations about the conversion of tris(pyrazolyl)borate chromium phenyl complex $[\text{Tp}^{tBu,Me}\text{CrPh}]$ to a phenoxide complex $[\text{Tp}^{tBu,Me}\text{Cr}(\text{O})\text{OPh}]$ in presence of molecular oxygen. The calculations were carried out with the aim to explore two possible alternative pathways. The above results show that the reaction started in a triplet state and there is a formation of a stable superoxo complex at the first step. For the first mechanism spin inversion is taking place two times, one is after the TS1 and second one in exit channel of the reaction. On the other hand for the second mechanism the first spin inversion occurred before the TS3 and another at the exit channel of the reaction. The results are in contrast to proposed catalytic cycle.

Bibliography

- [1] T. Punniyamurthy , S Velusamy and J. Iqbal *Chem. Rev.* **2005**, 105, 2329.
- [2] C.L. Hill, *Nature* **1999**, 40, 436.
- [3] A. Hess, M. R. Hrzs, L. M. Liabe-Sands, D. C. Lindner, A. L. Rheingold and K. H. Theopold, *Angew Chem Int Ed* **1999**, 38, 166.
- [4] C. J. Cramer, W. B. Tolman, K. H. Theopold and A. L. Rheingold, *Proc. Natl. Acad. Sci. USA* **2004**, 100, 3635.
- [5] M. J. Frisch, *et. al.*, *Gaussian03*, Revision B.04; Gaussian, Inc.: Pittsburgh PA, **2003**.
- [6] C. Lee, W. Yang and G. Parr, *Phys. Rev. B.* **1988**, 37, 785.
- [7] B. Miehlich, A. Savin, H. Stoll and H. Preuss, *Chem. Phys. Lett.* **1989**, 157, 200.
- [8] A. D. Becke, *J. Phys. Chem.* **1993**, 98, 5648.
- [9] K. Fukui, *J. Phys. Chem.* **1970**, 74, 4161.
- [10] K. Fukui, *Acc. Chem. Res.* **1981**, 14, 363.
- [11] S. Miertus, E. Scrocco and J. Tomasi, *Chem. Phys.* **1981**, 55, 117.
- [12] S. Miertus and J. Tomasi, *Chem. Phys.* **1982**, 65, 239.
- [13] J.L. Pascual-Ahuir, E. Silla, J. Tomasi and R. Bonaccorsi, *J. Comput. Chem.* **1987**, 8, 778.
- [14] R.A. Pierotti, *Chem. Rev.* **1976**, 76, 717.
- [15] P. Kollaman, *Chem. Rev.* **1993**, 93, 2395.
- [16] D. Schrder, S. Shaik and H. Schwarz, *Acc. Chem. Res.* **2000**, 33, 139.

-
- [17] J. W. Egan, Jr., B. S. Haggerty, A. L. Rheingold, S. C. Sendlinger and K. H. Theopold,
J. Am. Chem. SOC. **1990**, 112, 2445.

Chapter 5

Mechanistic Investigation of Homogeneous Catalytic Reduction of Dioxygen Using Transfer Hydrogenation Catalysts

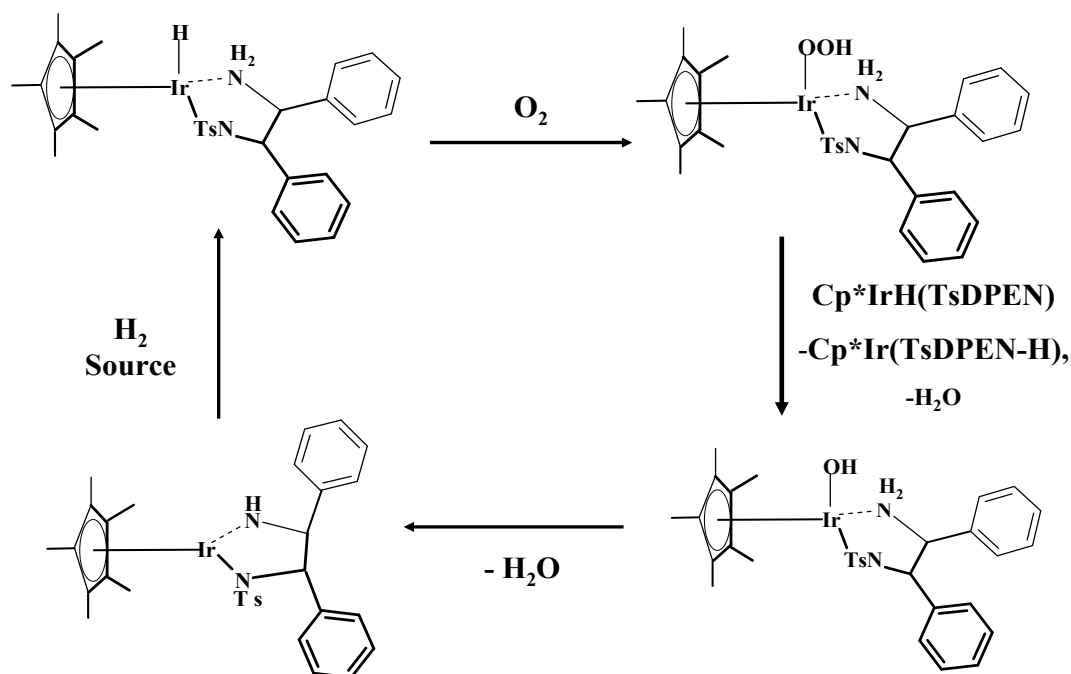
5.1 Introduction

The principle of “practical elegance” should always be pursued in developing chemical synthesis. In this regard, to development of efficient transfer hydrogenation catalysts is an important and substantial challenge in modern chemistry. Despite the efforts made to discover useful transfer hydrogen catalysts, there still remains much potential for the continued development of this area.

To produce two molecules of water (H_2O), two molecules of diatomic hydrogen (H_2) must be combined with one molecule of diatomic oxygen (O_2). This simple reaction is useful for fuel cells [1]. In recent years the research is going on in order to develop efficient fuel cell using better and less expensive catalysts. The “difficult side” of the fuel cell is the oxygen reduction reaction, not the hydrogen oxidation reaction [2]. Until now no one has make it work in a homogeneous solution. Most compounds react with either hydrogen or oxygen [3, 4]. It is very tough to get a catalyst, which is reactive to both. Rauchfuss and Heiden recently investigated a relatively new generation of transfer hydrogenation catalysts to use as metal hydrides for oxygen reduction [5]. The authors reported about the oxidative reactivity of iridium-based

transfer hydrogenation catalyst in a homogenous, non-aqueous solution. It reacts with hydrogen to form a hydride, and then reacts with oxygen to make water. The experimental observation supported that the iridium complex effects both the oxidation of alcohols, and the reduction of the oxygen. In order to understand the reaction mechanism in this chapter we will discuss our results regarding the hydrogenation process and the reduction of dioxygen using transfer hydrogenation catalyst previously synthesised [5].

There are two possible ways for the hydrogenation of an amide-complex: (1) the

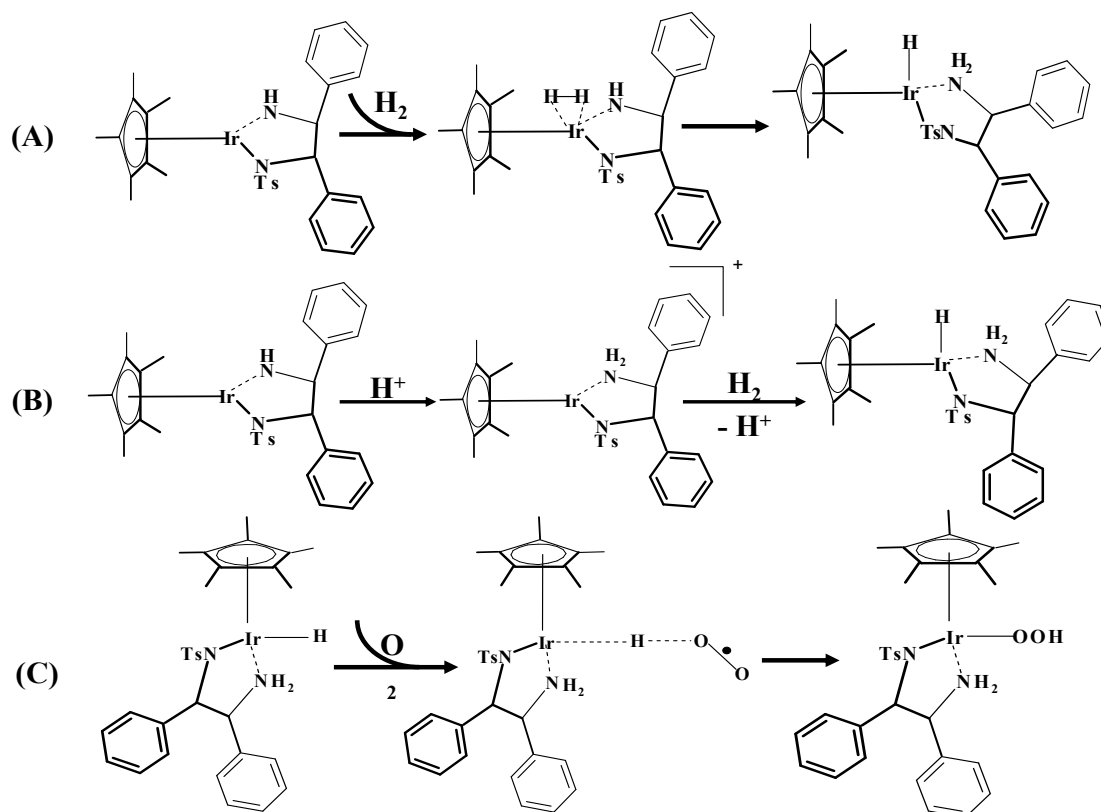


Scheme 5.1: Proposed Catalytic Cycle for Hydrogenation of O_2 by $\text{Cp}^*\text{IrH}(\text{TsDPEN})$.

direct addition of H_2 to the complex and (2) use of Bronsted acids for addition of H_2 to the catalyst (Scheme 5.1 and 5.2). Noyori and coworkers have recently examined the direct addition of H_2 to transfer hydrogenation catalysts, to make a metal-hydrided complex [6]. The Mashima-Ikariya system $\text{Cp}^*\text{Ir}(\text{TsDPEN-H})$ (**1**, $\text{TsDPEN} = \text{rac} - \text{H}_2\text{NCHPhCHPhN}(\text{SO}_2\text{C}_6\text{H}_4\text{CH}_3)^-$) slowly adds H_2 to give the amine hydride $\text{Cp}^*\text{IrH}(\text{TsDPEN})$ (**1H(H)**), which is reactive towards oxygen [7, 8]. Regarding hydrogenation process, Rauchfuss and Co-worker have reported that, the reaction could be faster

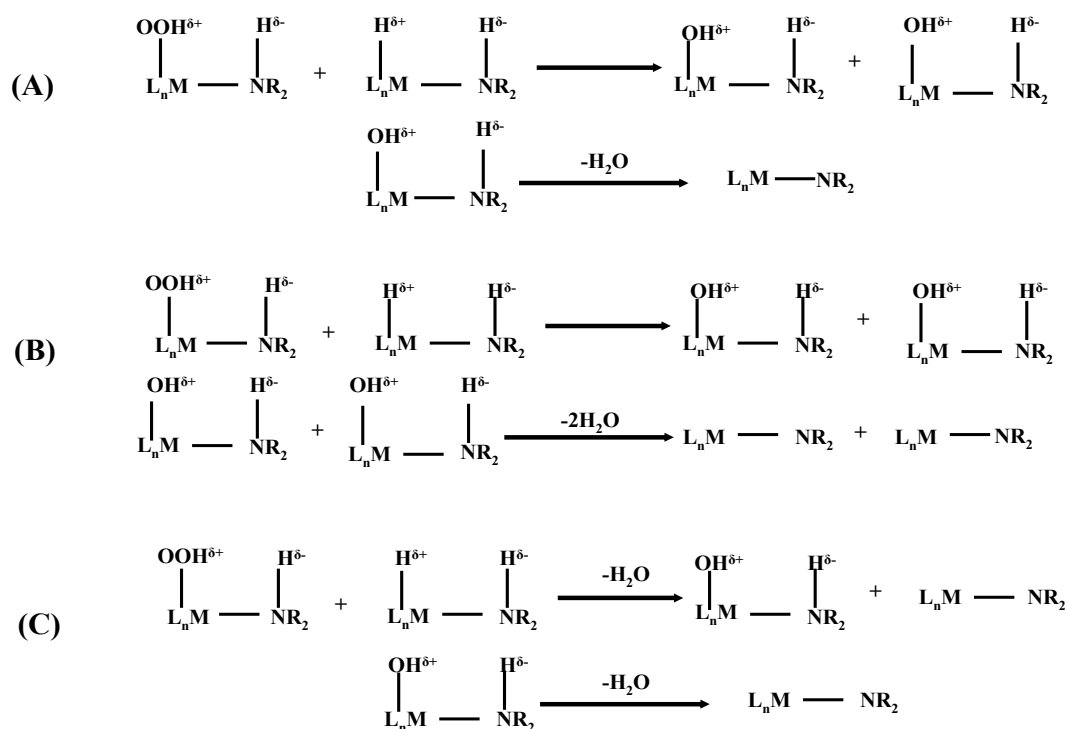
by the using Bronsted acids such as $\text{H}(\text{OEt}_2)_2\text{BAR}_4^F$ ($\text{BAR}_4^{F-} = \text{B}(\text{C}_6\text{H}_3 - 3,5 - (\text{CF}_3)_2)_4^-$), which converts complex **1** into the unsaturated iridium(III) amine cation $[\text{Cp}^*\text{Ir}(\text{TsDPEN})]^+$ ($[\text{1H}]^+$) [9].

To date, very few studies have been reported about the theoretical investigation of transition



Scheme 5.2: Proposed reaction mechanism for: (A) Addition of H₂ to Cp*IrH(TsDPEN); (B) Addition of H₂ to Cp*Ir(TsDPEN)⁺; (C) Insertion of O₂ into metal-hydride bond.

metal-catalyzed transfer hydrogenation reactions [10-14] and none of them concern the theoretical investigation of homogeneous catalytic reduction of dioxygen. In their study Rauchfuss and Heiden proposed a catalytic cycle depicted in Scheme 5.1. There they have proposed the reaction proceed through the formation of an iridium-hydroperoxide (**1H(OOH)**). Starting from the information coming from the experimental work we have undertaken a DFT analysis of dioxygen reduction by iridium based transfer hydrogenation catalyst. The first step of the work concerns the hydrogenation process. Here we have considered both neutral (Scheme 5.2 (A)) and protonated system (Scheme 5.2(B)). Regarding the dioxygen reduction we have consider the reaction proceed through the formation of a hydroperoxide complex and in next the



Scheme 5.3: Proposed reaction mechanisms for elimination of H_2O from $\text{Cp}^*\text{IrOOH}(\text{TsDPEN})$ to generate $\text{Cp}^*\text{Ir}(\text{TsDPEN} - \text{H})$.

elimination of H_2O from hydroperoxide complex. The formation of hydroperoxide complex proceeds by a hydrogen-atom abstraction mechanism (Scheme 5.2(C)) [15, 16, 17]. For the elimination of water we have consider three mechanism (Scheme 5.3): (A) formation of two hydroxy amine complexes followed by spontaneous elimination of 1 equivalent of water from each hydroxy amine; (B) elimination of two water molecules by concerted mechanism; (C) stepwise elimination of water molecules.

5.2 Computational Details

All calculations reported in this work were done using the Gaussian03 program [18]. Molecular geometries were optimized employing the density functional level of theory by using the B3LYP exchange correlation functional [21-23]. Frequency calculations at the same level of theory have also been performed to identify all stationary points as minima (zero imaginary

frequencies) or transition states (one imaginary frequency). The transition states involved were checked by IRC (intrinsic reaction coordinate) analysis [22, 23]. The effective core potentials (ECPS) of Hay and Wadt with double- ζ valence basis sets (LanL2DZ) [24] have been used for Ir. The standard 6-31G** basis sets of Pople and co-workers were employed for C, H, O and S. Final energies were calculated by performing single-point calculations on the optimized geometries at the B3LYP/6-311+G(2d,2p) level.

For the reduction of the hydroperoxides complexes by the amine complexes, we have reduced the real molecular system in order to speed up the calculations. Methyl group has substituted the phenyl one in TsDPEN and in the other ligands. For this reason in H_2O elimination process we will indicate the ligand TsDPEN as $\text{rac-H}_2\text{NCHCH}_3\text{CHCH}_3\text{N}(\text{SO}_2\text{CH}_3)^-$.

In the case of insertion of molecular oxygen into the metal-hydride bond both triplet and singlet reaction paths have been examined and for all the studied species. $\langle S^2 \rangle$ values have been checked to assess whether spin contamination can influence the quality of the results. For triplet state structures no significant contamination has been found by unrestricted calculations. On the other hand we have found, the two singlet state structures are contaminated by the triplet spin and $\langle S^2 \rangle$ values is close to 1.0. Here the method proposed by Ovchinnikov and Labanowski [25] was used for correcting the mixed spin energies and removing the foreign spin components. For example, after correction a triplet-singlet energy gap of O_2 is 20.7 kcal/mol, which is very good agreement with the experimental value.

To estimate the solvation effect we have used the polarised continuum solvation model, (PCM) [26] as implemented in Gaussian03, performing single point calculations on fully optimized geometry in gas phase of each stationary point along the reaction paths. The solute is placed inside the cavity defined in terms of interlocking spheres centered on solute atoms, using the Gepol procedure [27]. We have used the Pauling atomic radii. Non-electrostatic dispersion and repulsion [28] and cavitations [29] contributions were also included into the solvation free energy calculation.

To find out the minimum energy crossing point between singlet and triplet surfaces we have used the methodology introduced by Harvey and co-workers [30].

5.3 Results and Discussion

5.3.1 Addition of H_2 to Neutral System

In this section, we will discuss the reaction mechanisms for the insertion of H_2 into the complex **1**. We have considered both the systems: (1) neutral $Cp^*Ir(TsDPEN-H)$ (Scheme 5.2(A)) and (2) protonated $Cp^*Ir(TsDPEN)^+$ (Scheme 5.2(B)) catalysts [9].

Addition of H_2 to Neutral System

The potential energy profile for this reaction is shown in Fig. 5.1. The geometrical structures

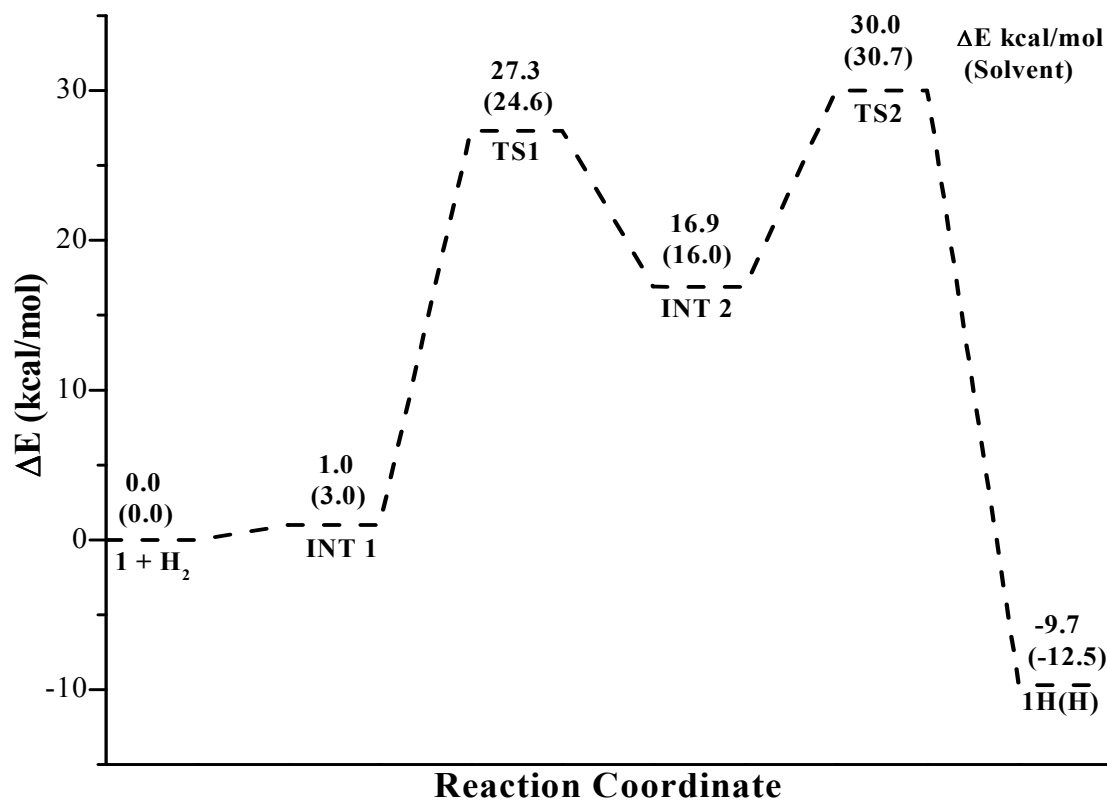


Figure 5.1: Potential Energy Surface (PES) for H_2 insertion into $Cp^*Ir(TsDPEN - H)$. The values in parentheses are reported to the solvent phase. Energies are in kilocalories and relative to the ground-state reactants.

involved in the reaction are illustrated in Fig 5.2 and the selected geometrical parameters reported in Table 5.1. The formation of the intermediate (**INT1**), is due to a weakly bound

van der Waals interaction and its energy result to be slightly endothermic (1 kcal/mol). As shown by the geometrical structure, both hydrogen atoms of H_2 are away from the Ir center. The H-H distance (0.743\AA), indicates that there is no bond between hydrogen atoms and metal center.

In the next step a transition state (**TS1**), in which the hydrogen molecule is coordinating

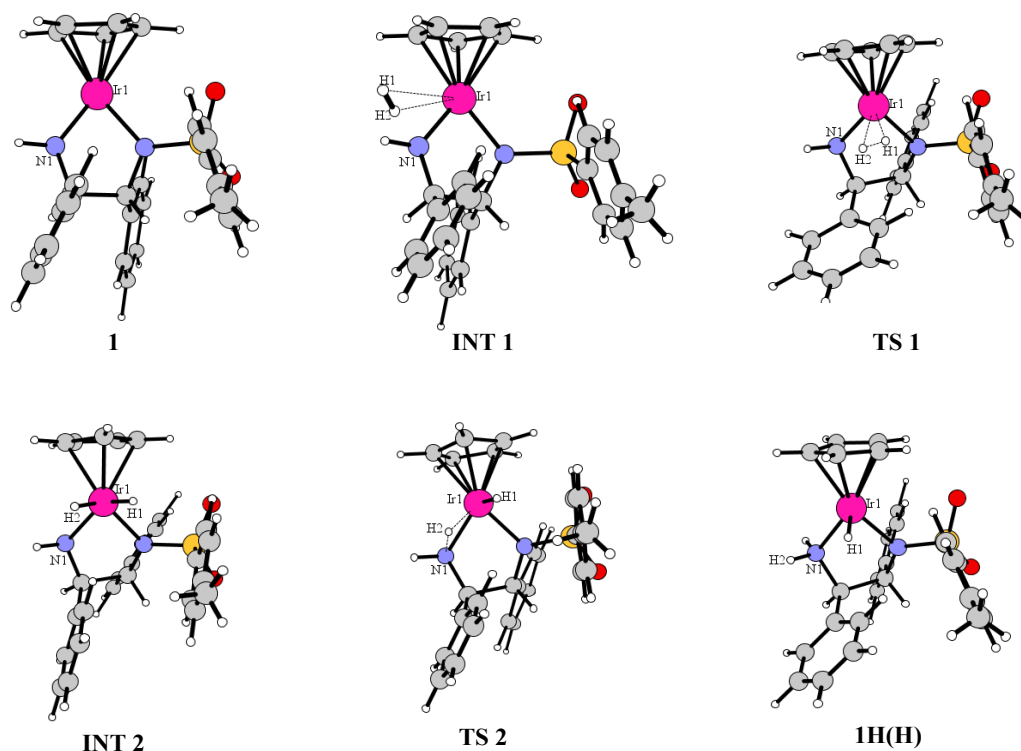


Figure 5.2: Ground-state structures of the reactant, intermediates and transition states for addition of H_2 into $Cp^*Ir(TsDPEN - H)$. Labels introduced to individuate geometrical parameters have to be used to read information reported in Table 5.1

with the Ir center is found. The activation energy barrier is 26.3 kcal/mol. The imaginary frequency for **TS1** is calculated to be $477i\text{ cm}^{-1}$. The Ir-H1 and Ir-H2 bond distances are 2.027\AA and 2.058\AA , respectively, whereas the distance between the two hydrogen atoms is 0.776\AA , which is slightly longer than in its free form (0.74\AA) both the hydrogen atoms are coordinating with the metal center. As a result, in the next step, an intermediate (**INT2**), which lies 16.9 kcal/mol high from the ground state reactants is formed. Now, the H1-H2 bond is broken and two metal-hydride bonds are formed (Fig. 5.2). The H1-H2 distance

Parameter	1	INT1	TS1	INT2	TS2	1H(H)
Ir1-N1	1.907	1.908	2.032	2.051	2.082	2.137
Ir1-NTs	2.038	2.039	2.073	2.080	2.073	2.095
H1-H2	-	0.743	0.776	1.881	1.986	-
Ir1-H1	-	4.935	2.027	1.585	1.569	1.578
Ir1-H2	-	5.012	2.058	1.579	1.650	-
N1-H2	-	-	-	2.364	1.527	1.019

Table 5.1: Selected geometrical parameters of Ground-State Reactants, Intermediates and transition States computed for addition of H_2 into $Cp^*Ir(TsDPEN - H)$.

in **INT2** is 1.881\AA and the Ir-H1 and Ir-H2 bonds become much shorter (1.585\AA , 1.579\AA , respectively). Along the reaction path we have located another transition state **TS2**, in which one of the two hydrogen atoms (H2) is migrated from the metal (Ir) to the nitrogen atom (N1 in Fig 5.2). The imaginary frequency is for this TS is $1089i\text{ cm}^{-1}$. In this structure the bond between Ir-H2 is elongated to 1.650\AA , the H2 becomes closer to N1 compared with that in **INT2** (from 2.364\AA to 1.527\AA), whereas the distance between Ir-H1 is 1.569\AA , which is smaller compared to **INT2**. The calculated barrier for this step is 14 kcal/mol.

Formation of the final product **1H(H)**, is an exothermic process. In gas phase it is 9.7 kcal/mol, whereas in acetonitrile it is 12.5 kcal/mol below the reactants. Now, the H2 is bonded to N1 (1.019\AA). Comparison between theoretical and experimental [9] geometries of the final product **1H(H)**, is very satisfactory.

Addition of H_2 to Protonated System

The calculated potential energy surface for hydrogenation of reactant $Cp^*Ir(TsDPEN)^+$

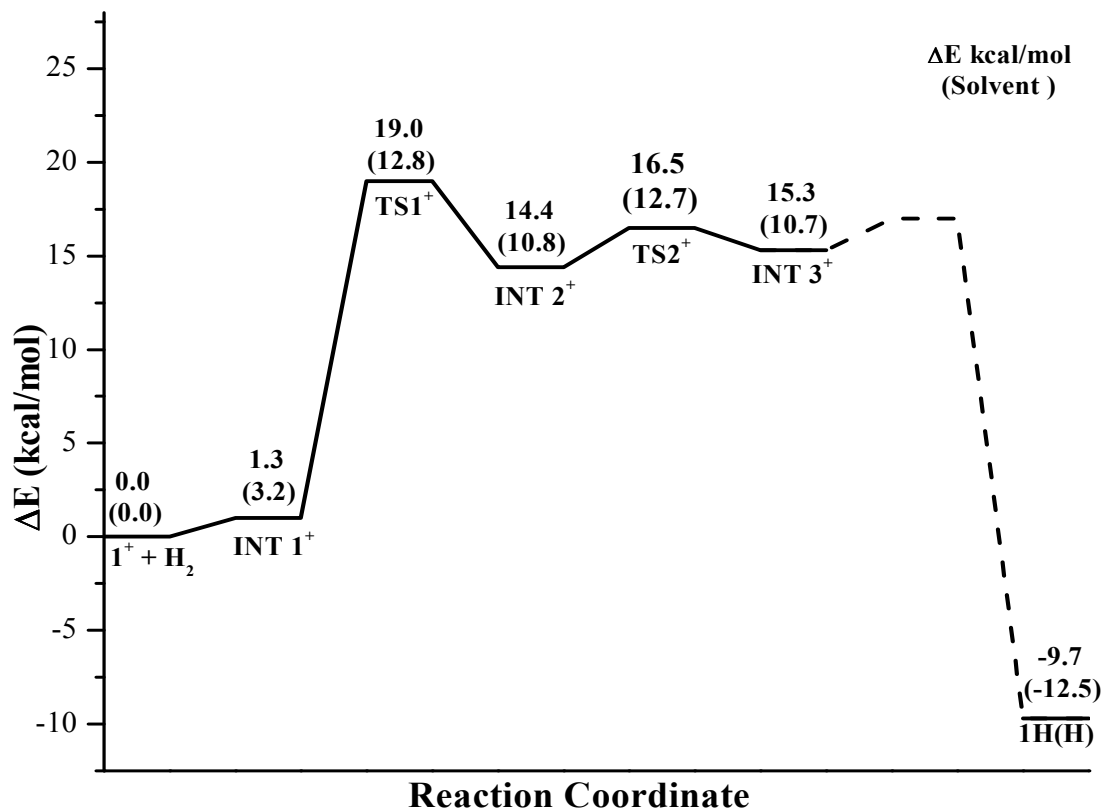


Figure 5.3: PES for H_2 addition into $Cp^*Ir(TsDPEN)^+$. The values in parentheses are reported to the solvent phase. Energies are in kilocalories and relative to the ground-state reactants.

($\overline{1H(H)}$) is depicted in Fig 5.3. The corresponding figures are illustrated in Fig 5.4 and the selected geometrical parameters reported in Table 5.2.

Also in this case, step 1, resulted in the formation of a weakly van der Waals complex $INT1^+$, that lies at 1.3 kcal/mol above the reactants. The distances between the metal center and the two hydrogen atoms of (H_2) are 4.527\AA (H1) and 4.882\AA (H2), respectively. From $INT1^+$, we found a transition state $[TS1]^+$, in which both hydrogen atoms are closer to the metal center. The ΔE for $TS1^+$, is 19.0 kcal/mol in gas phase. In this transition state the distance between the two hydrogen atoms has stretched from 0.743 to 0.773\AA , while the distances between the metal center and the two hydrogen atoms of H_2 are decreased to 2.084 and 2.109\AA respectively. The imaginary frequency is calculated to be $299i\text{ cm}^{-1}$.

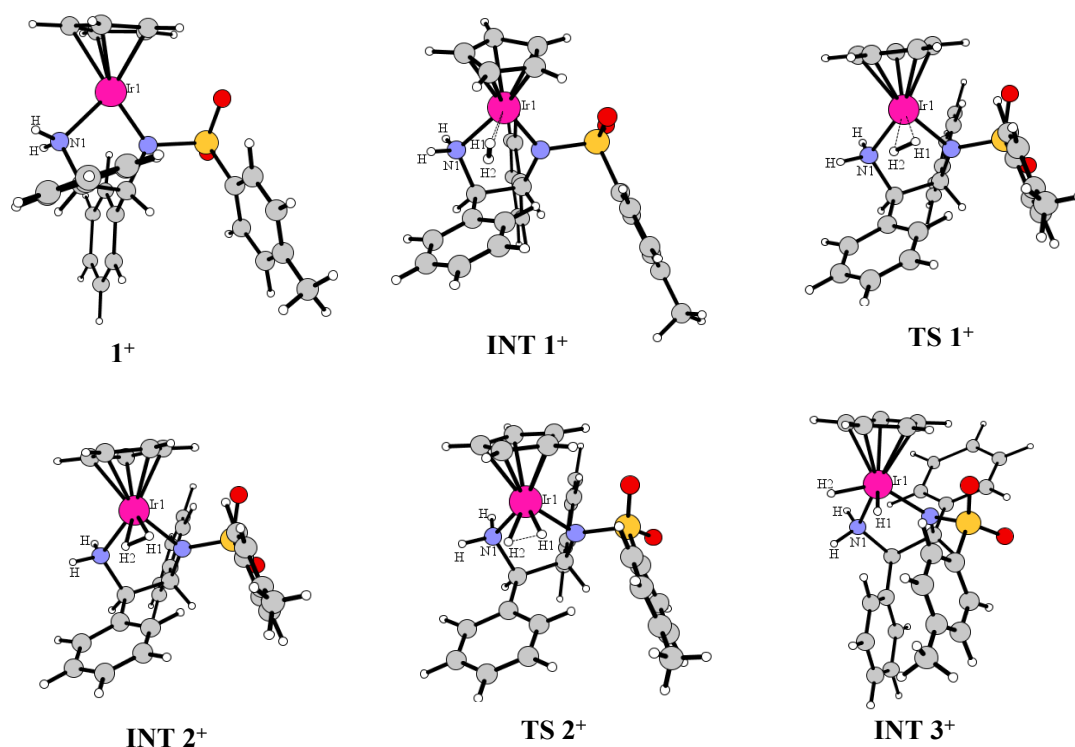


Figure 5.4: Ground-state structures of the reactant, intermediates and transition states for addition of H_2 into $Cp^*Ir(TsDPEN)^+$. Labels introduced to individuate geometrical parameters have to be used to read information reported in Table 5.2.

From $TS1^+$ a $INT2^+$ species is formed and its energy is 4.6 kcal/mol below the $TS1^+$. The main structural changes in this intermediate concern the H1-H2 bond (0.841 Å), the Ir-H1 (1.799 Å) and Ir-H2 (1.814 Å) distance. In the next step we have found a transition state $TS2^+$ is formed. The activation barrier is only 2.1 kcal/mol and the imaginary frequency is 798.9i cm^{-1} . The distance between the two hydrogen atoms became 1.088 Å, whereas the distances between the Ir-H1 and Ir-H2 are reduced to 1.649 and 1.656 Å, respectively. This indicates that the metal hydride bonds are formed. In the next step a new intermediate $INT3^+$, occurs and its lies in acetonitrile at 10.7 kcal/mol about the reactants. In this species the distance between the two hydrogen atoms confirm that the bond is broken (1.803 Å) and that the Ir-H1 (1.578 Å) and Ir-H2 (1.602 Å) bond are formed. The final product $1H(H)$, is exothermic process by 12.5 kcal/mol in solvent. In Fig 5.5 we have compared the two possibility.

Parameter	1 ⁺ (Exp)	INT1 ⁺	TS1 ⁺	INT2 ⁺	TS2 ⁺	INT3 ⁺
Ir1-N1	2.127(2.096)	2.126	2.129	2.128	2.129	2.156
Ir1-NTs	1.922(1.984)	1.922	2.043	2.080	2.087	2.032
H1-H2	-	0.743	0.773	0.841	1.088	1.803
Ir1-H1	-	4.527	2.084	1.799	1.649	1.578
Ir1-H2	-	4.882	2.109	1.814	1.656	1.602
N1-H2	-	-	-	-	-	2.417

Table 5.2: Selected geometrical parameters of Ground-State Reactants, Intermediates and transition States computed for addition of H_2 into $Cp^*Ir(TsDPEN)^+$.

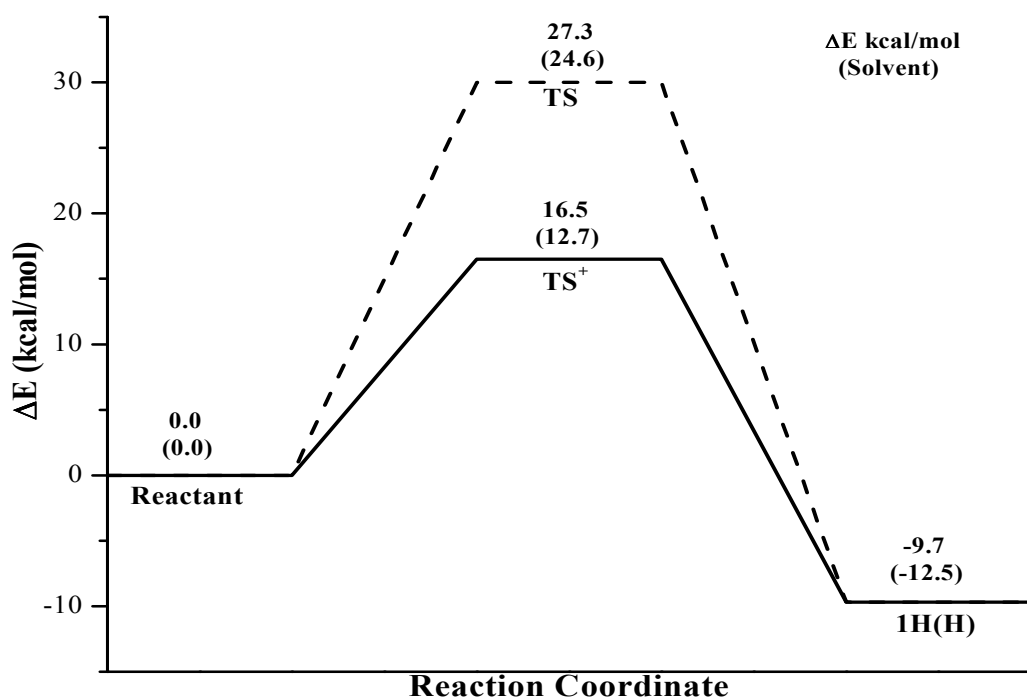


Figure 5.5: Comparison for addition of H_2 into $Cp^*Ir(TsDPEN - H)$ (dashed line) and $Cp^*Ir(TsDPEN)^+$ (solid line) systems. The values in parentheses are reported to the solvent phase. Energies are in kilocalories and relative to the ground-state reactants.

5.3.2 Insertion of O_2 into the metal-hydride bond

The calculated potential energy surface for insertion of molecular oxygen into the metal-hydride bond is represented in Fig 5.6. The singlet and triplet states optimized structures are depicted in Fig 5.7 and 5.8, respectively. The selected geometrical parameters are reported in Table 5. 3 and 5.4.

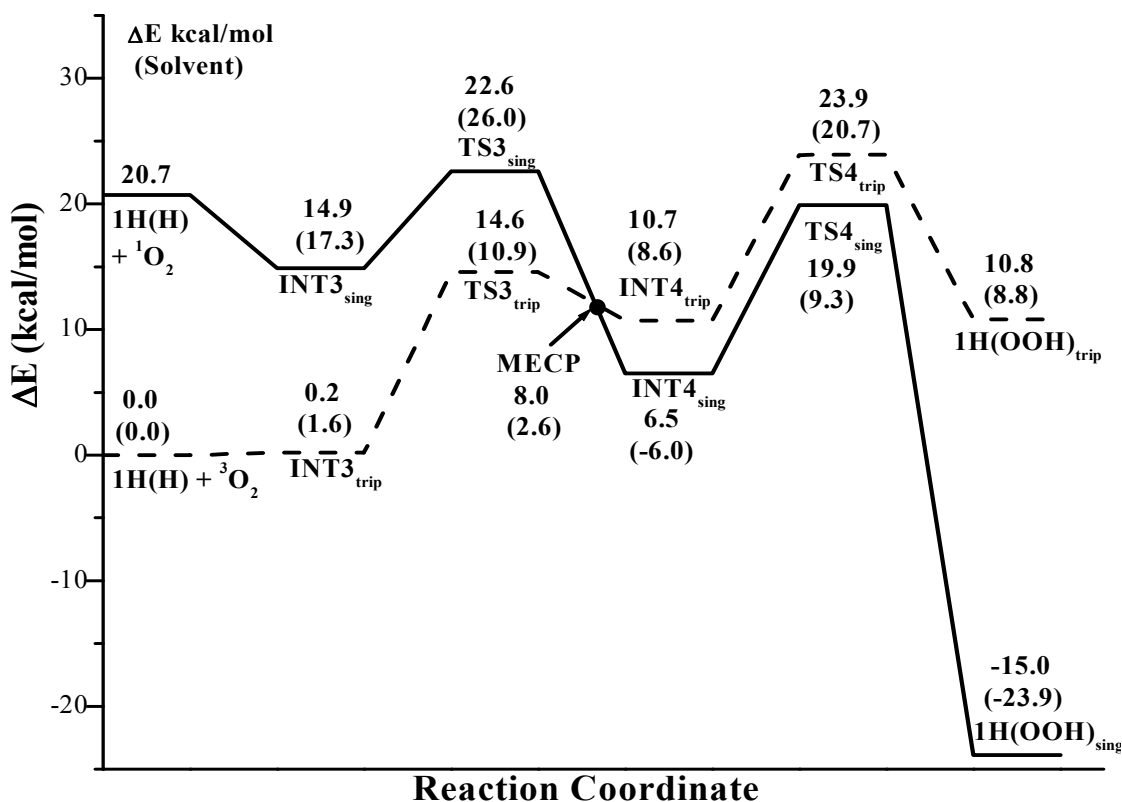


Figure 5.6: PES for O_2 insertion into $Cp^*IrH(TsDPEN)$ to form $Cp^*IrOOH(TsDPEN)$. The values in parentheses are reported to the solvent phase. Energies are in kilocalories and relative to the ground-state reactants.

The addition of (triplet) molecular oxygen leads to the formation of a weakly bound van der Waals complex $INT3_{trip}$ ($1(H)H.O_2$) which is slightly endothermic with $\Delta E = 0.2$ kcal/mol and 1.6 kcal/mol in gas-phase and solvent, respectively. The optimized structure of the corresponding complex in a singlet state ($INT3_{sing}$) is substantially different. In fact in this case O_2 is directly coordinating with the metal (Ir) center. It lies at 14.9 and 17.3 kcal/mol above the reactants in the gas phase and in solvent, respectively. The reported energy for the

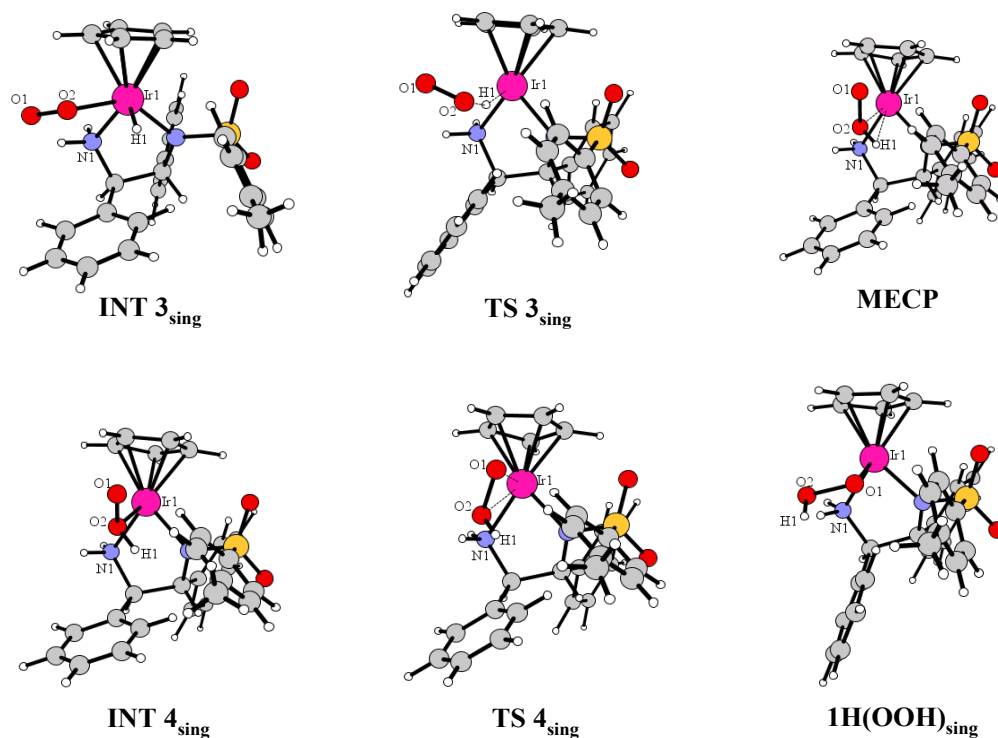


Figure 5.7: Ground-state structures of the reactant, intermediates and transition states for insertion of O_2 into $Cp^*IrH(TsDPEN)$ to form $Cp^*IrOOH(TsDPEN)$ along the singlet-path. Labels introduced to individuate geometrical parameters have to be used to read information reported in Table 5.3

complex $INT3_{sing}$ is corrected using the method mentioned in section 5.2 [25].

From this intermediate state, a transition state $TS3_{trip}$ is found. In this transition state, the triplet oxygen has a position for abstracting the hydrogen from the iridium center and the activation barrier is 14.6 kcal/mol in gas-phase. As a result the Ir-H1 bond was elongated from 1.574 to 1.685 Å and the O-O bond distance was stretched from 1.254 to 1.346 Å. The calculated O-H distance is 1.518 Å, indicating that the O2-H1 bond has yet to be formed. The imaginary frequency is $667i\text{ cm}^{-1}$, which corresponds to the breaking of the bond between metal and hydrogen atom. The reaction proceeds further to form an intermediate in which a peroxy **HOO** radical is coordinating with the metal center (Ir) of the complex and the interaction between Ir and hydrogen is very weak. The energy in gas-phase lies 3.9 kcal/mol below the TS_{trip} . In the $INT4_{trip}$, the O2-H1 bond length is 1.043 Å, which is similar to

Parameter	1H(H) _{sing}	INT3 _{sing}	TS3 _{sing}	MECP	INT4 _{sing}	TS4 _{sing}	1H(OOH) _{sing}
Ir1-N1	2.156	2.104	2.130	2.140	2.143	2.126	2.114
Ir1-NTs	2.032	2.072	2.062	2.091	2.087	2.064	2.074
Ir-H1	1.578	1.566	1.659	2.608	-	-	-
O1-O2	-	1.403	1.432	1.488	1.551	1.580	1.565
Ir1-O1	-	3.046	3.742	3.144	2.997	2.627	2.067
Ir2-O2	-	2.241	-	2.088	2.104	2.488	-
O2-H1	-	2.236	1.505	0.983	0.984	0.982	0.983
O1-O2-H1	-	-	113.3	96.8	103.8	102.3	98.8

Table 5.3: Selected geometrical parameters of Ground-State Reactants, Intermediates, MECP and Transition States computed for insertion of O_2 into $Cp^*IrH(TsDPEN)$ to form $Cp^*IrOOH(TsDPEN)$ along the Singlet-Path.

that of free HO_2 and the O-O bond length is 1.386 Å. The Ir1-H1 bond distance increased to 2.250 Å, which confirmed the complete breaking of this bond. On the other hand, along the singlet pathway the transition state **TS3**_{sing} has been intercepted when the closest oxygen and hydrogen distance is 1.505 Å. The activation energy in gas-phase is 22.6 kcal/mol. In the next step, along the singlet path, we found, the formation of **INT4**_{sing}, which lies at 6.5 kcal/mol above the reactant. The significant feature of this intermediate is that the hydrogen atom is bonded to the proximal oxygen and the bond distance between O-O has stretched to 1.551 Å. The distal oxygen atom is rotated upwards. Until now, only our group demonstrated the existence of this intermediate [15, 16, 17].

In this region after the **TS3**_{trip} it should be a crossing between the two surfaces at different electronic system. Using the method of Harvey *et. al.* [30], a crossing point structure (**MECP**) between the two surfaces, is located (see in Fig 5.4). The structure is very close to the triplet state intermediate, which supports that, the crossing happened in the vicinity of the **INT4**_{trip}.

After the crossing the reaction proceeds along the singlet path. The formation of the final hydroperoxo iridium complex **1H(OOH)**_{sing} is an exothermic process by 15.0 kcal/mol in gasphase and 23.9 kcal/mol in solvent (Fig 5.4). In this structure the bond between proximal oxygen and iridium center has been broken, whereas a new bond has been formed between

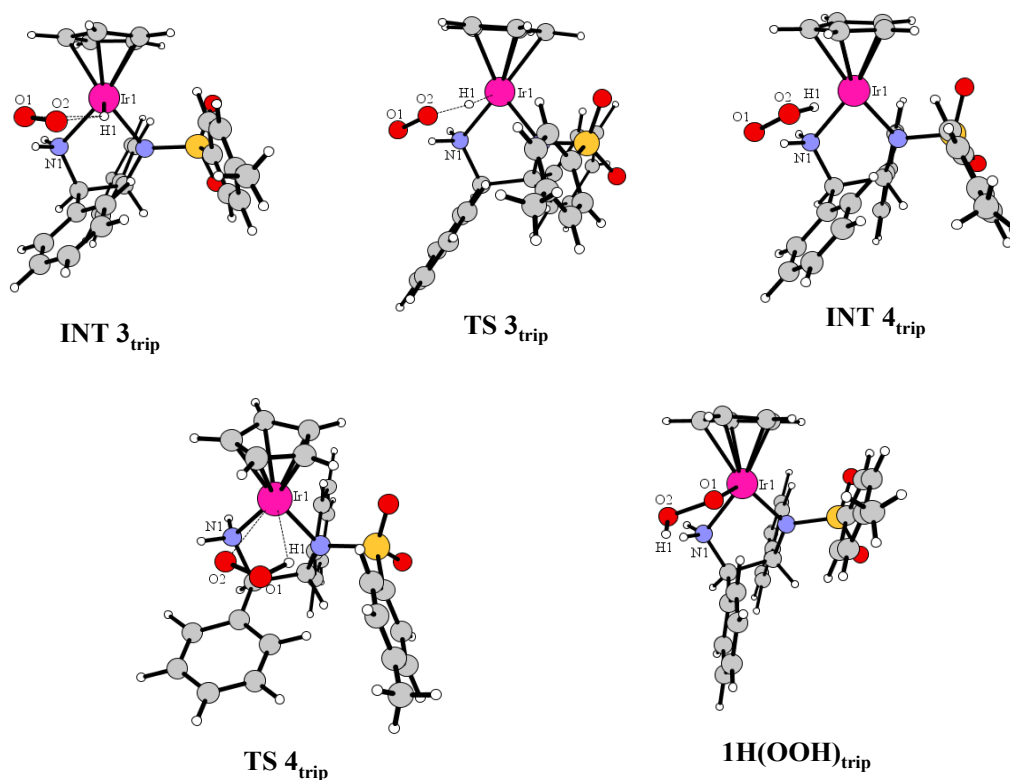


Figure 5.8: Ground-state structures of the reactant, intermediates and transition states for insertion of O_2 into $Cp^*IrH(TsDPEN)$ to form $Cp^*IrOOH(TsDPEN)$ along the triplet-path. Labels introduced to individuate geometrical parameters have to be used to read information reported in Table 5.4.

iridium center and distal oxygen. On the other hand, along the triplet path, the final hydroperoxide is formed due to the rotation of HO_2 fragment, which is an endothermic process and 10.8 kcal/mol in gas phase and 8.8 kcal/mol in solvent above the reactant. In this species the terminal oxygen moves towards the Ir center and the terminal hydrogen moves away. For both cases the corresponding transition states, $TS4_{sing}$ and $TS4_{trip}$, have been intercepted and confirmed by IRC calculation. The activation energies are 19.9 kcal/mol for $TS4_{sing}$ and 23.9 kcal/mol for $TS4_{trip}$. The imaginary frequencies are $340i\text{ cm}^{-1}$ for $TS4_{sing}$ and $255i\text{ cm}^{-1}$ for $TS4_{trip}$. From the above discussion, it is clear that, the reaction started in triplet surfaces and after the spin conversion the final product is in singlet state.

Parameter	1H(H) _{trip}	INT3 _{trip}	TS3 _{trip}	MECP	INT4 _{trip}	TS4 _{trip}	1H(OOH) _{trip}
Ir1-N1	2.156	2.135	2.109	2.140	2.128	2.144	2.146
Ir1-NTs	2.032	2.090	2.027	2.091	2.012	2.039	2.002
Ir-H1	1.578	1.574	1.685	2.608	2.250	2.695	-
O1-O2	-	1.254	1.346	1.488	1.386	1.436	1.559
Ir1-O1	-	-	-	3.144	3.708	2.709	2.208
Ir2-O2	-	-	-	2.088	-	-	-
O2-H1	-	2.957	1.518	0.983	1.043	0.993	0.982
O1-O2-H1	-	-	107.0	96.8	106.4	102.7	99.9

Table 5.4: Selected geometrical parameters of Ground-State Reactants, Intermediates and Transition States computed for insertion of O_2 into $Cp^*IrH(TsDPEN)$ to form $Cp^*IrOOH(TsDPEN)$ along Triplet-Path.

5.3.3 Mechanism for elimination for H_2O

In this section, the results concerning the reaction mechanism for iridium-hydroperoxide reduction reaction are represented. To reduce the computational time we have considered the smaller model previously described.

Formation of two hydroxy amine complexes

The calculated potential energy surface for insertion of molecular oxygen into the metal-hydride bond is explored in Fig 5.9. The illustrated optimized structures are depicted in Fig 5.10 and the selected geometrical parameters are reported in Table 5.5.

Starting from the reagent a transition state **TS5**_{1st} with an energy barrier of 8.6 kcal/mol in gas phase and 16.6 kcal/mol in solvent has been located. The calculated frequency is 679i cm^{-1} and corresponds to the breaking of the O1-O2 bond, and, simultaneously the transfer of hydride from **1H(H)**. The bond distance between Ir2-H3 is increased from 1.588 Å to 1.722 Å, which clearly indicates the breaking of the hydride bond.

After **TS5**_{1st} we found an intermediate state ITN5_{1st} when two hydroxy amine complexes are formed and its lies 62.4 kcal/mol and 61.6 kcal/mol below the reactants in the gas-phase and the solvent, respectively. The optimized structure of ITN5_{1st} is reported in Fig 5.10. In this

intermediate state the bond lengths between Ir1-O1 and O1-H1 are 2.091 Å and 0.992 Å, respectively and the Ir2-O2 and O2-H3 bond lengths are 2.093 Å and 0.979 Å respectively. The IRC analysis confirmed that the **TS5**_{1st} connect **1H(OOH)** and **INT5**_{1st} species.

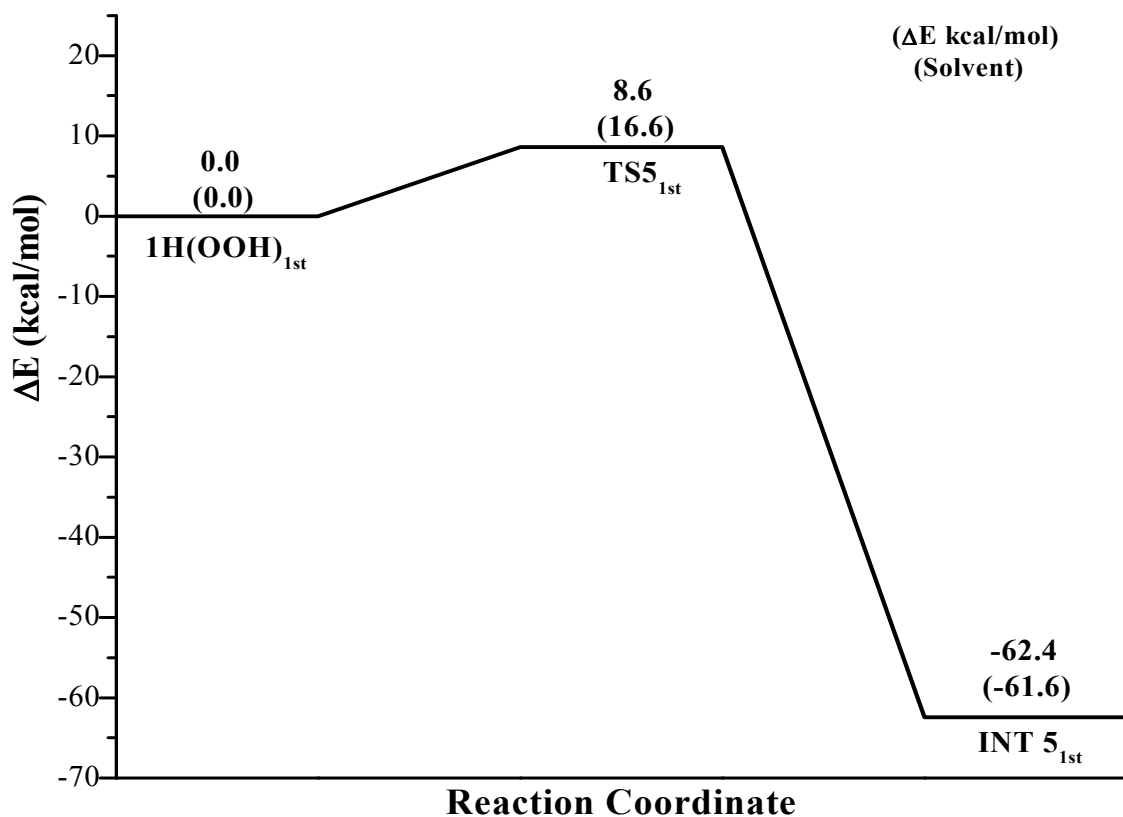


Figure 5.9: PES for formation of two $Cp^*IrOH(TsDPEN)$. The values in parentheses are reported to the solvent phase. Each $Cp^*IrOH(TsDPEN)$ will separately eliminate one H_2O molecule to form a $Cp^*Ir(TsDPEN - H)$. Energies are in kilocalories and relative to the ground-state reactants.

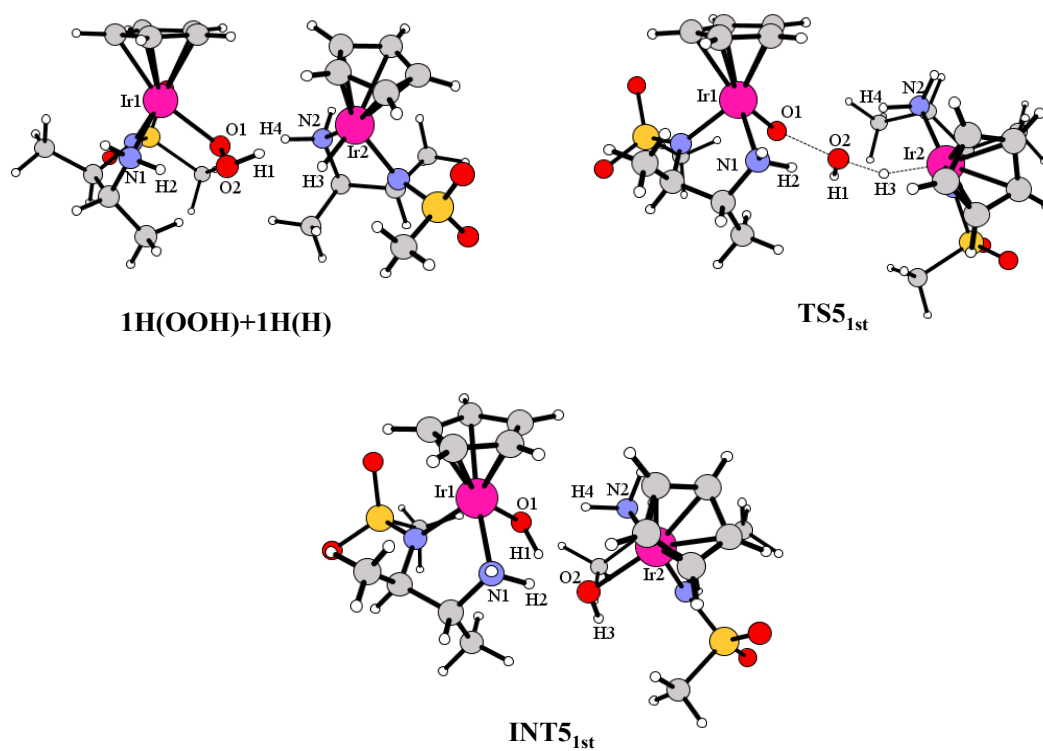


Figure 5.10: Ground-state structures of the reactant, intermediates and transition states in order to form two $Cp^*IrOH(TsDPEN)$. Labels introduced to individuate geometrical parameters have to be used to read information reported in Table 5.5.

Parameter	1H(OOH)+1H(H)	TS5 _{1st}	INT5 _{1st}
Ir1-O1	2.094	1.952	2.091
Ir1-N1	2.127	2.119	2.153
Ir2-O2	-	-	2.093
Ir2-H3	1.588	1.722	-
Ir2-N2	2.144	2.139	-
O1-O2	1.544	2.040	-
O1-H1	-	2.024	0.992
O1-H4	1.852	3.014	1.711
O2-H1	0.981	0.996	1.849
O2-H3	2.687	1.387	0.979
N1-H2	1.032	1.044	1.045
N2-H4	1.036	1.031	1.058

Table 5.5: Selected geometrical parameters of Ground-State Reactants, Intermediates and Transition States computed in order to form two $Cp^*IrOH(TsDPEN)$ according to Scheme 5.3(A).

Elimination of $2H_2O$

In this section we will discuss the elimination of two water molecules by concerted mechanism after the formation of two hydroxy amine complexes. The calculated potential energy surface for this reaction is depicted in Fig. 5.11. The related geometrical structures are depicted in Fig 5.12 and the selected geometrical parameters are reported in Table 5.6.

After the formation of two hydroxi amine we have found a transition state $TS6_{2nd}$. The

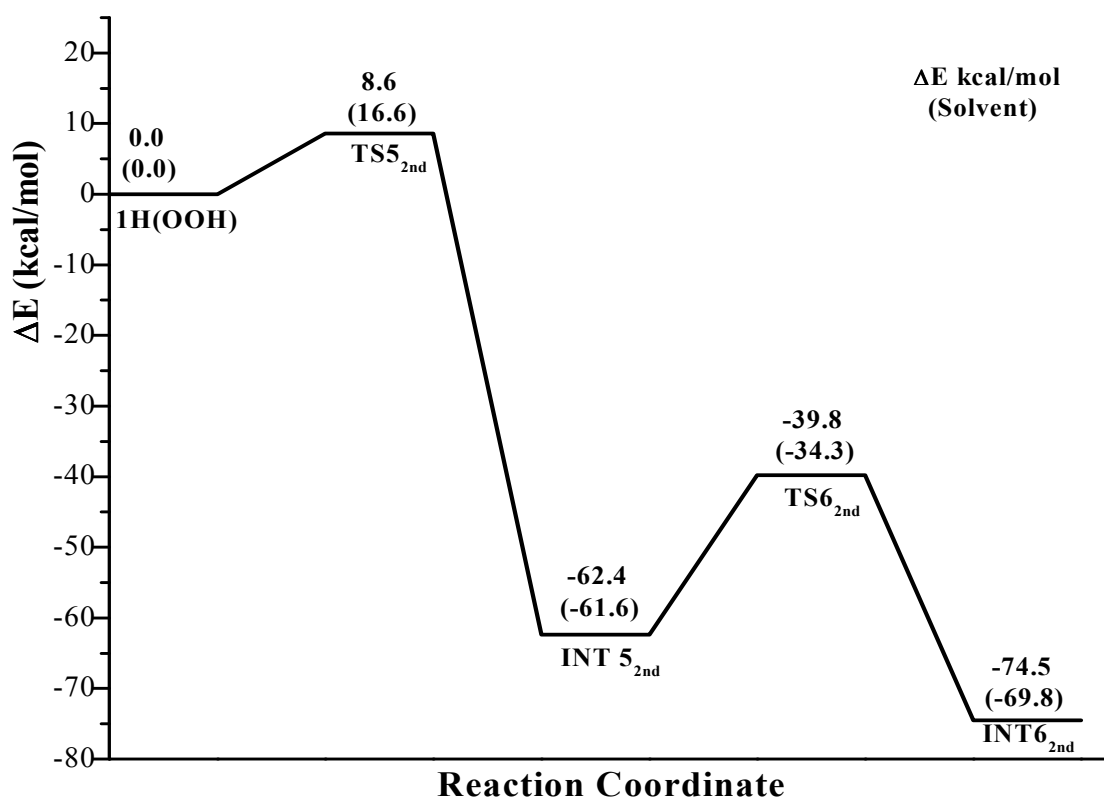


Figure 5.11: PES for formation of two $Cp^*IrOH(TsDPEN)$. The values in parentheses are reported to the solvent phase. Two $Cp^*IrOH(TsDPEN)$ molecules will react subsequently and eliminate two H_2O molecules to form two $Cp^*Ir(TsDPEN - H)$. Energies are in kilocalories and relative to the ground-state reactants.

energy barrier is 22.6 kcal/mol in the gas phase and 27.3 kcal/mol in the solvent. In this transition state the Ir1-O1 and Ir2-O2 distances have stretched from 2.091 to 2.145 Å and from 2.093 to 2.224 Å respectively. This indicates that the oxygen and metal centers (Ir1-O1 and Ir2-O2) bond are broken. In the transition states the calculated frequency is 92icm^{-1} , which corresponding the transfer of the hydrogen atoms from the nitrogen atoms center (Fig.

4.12). The bond between N1-H2 is broken and the bond distance between N2-H4 is elongated from 1.058 Å to 1.381 Å. The bond distance between O1-H4 reduced from 1.711 Å to 1.145 Å.

Continuing along the pathway, **TS6_{2nd}** now relaxes to **INT6_{2nd}**. The energy release in this process is 34.7 kcal/mol in the gas phase (35.5 kcal/mol in the solvent). This new intermediate clearly shows the formation of 2H₂O and two amido complexes. These two amido complexes are far away from each other.

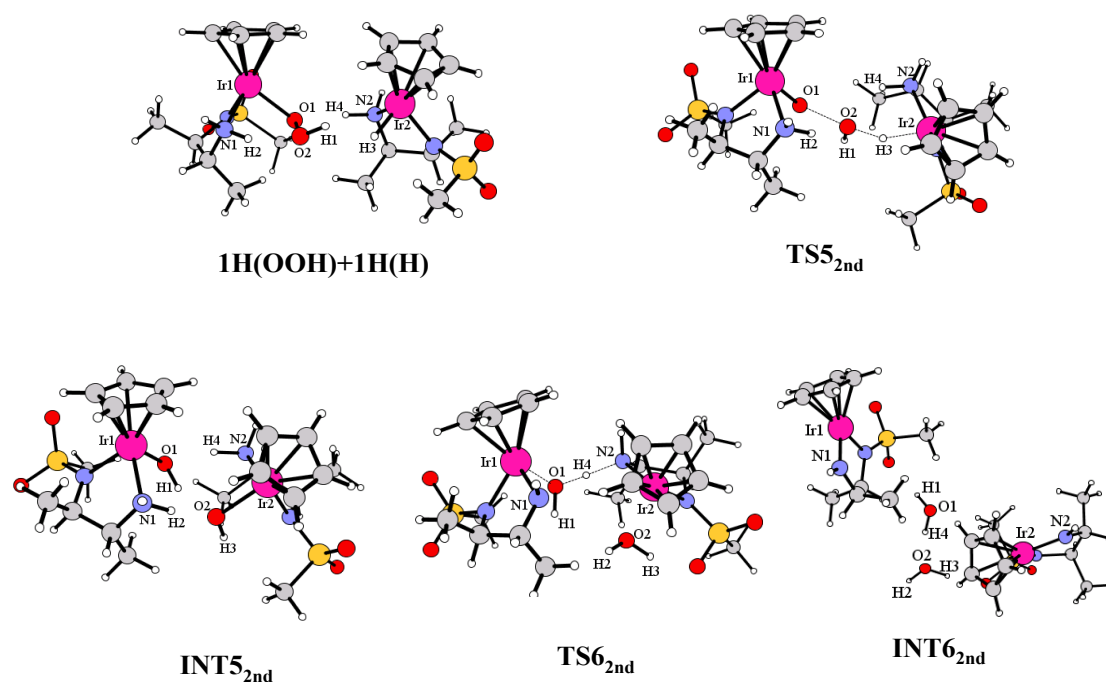


Figure 5.12: Ground-state structures of the reactant, intermediates and transition states for simultaneous elimination of 2H₂O from *Cp**IrOOH(*TsDPEN*) according to the Scheme 5.3(B). Labels introduced to individuate geometrical parameters have to be used to read information reported in Table 5.6.

Parameter	1H(OOH)+1H(H)	TS5 _{2nd}	INT5 _{2nd}	TS6 _{2nd}	INT6 _{2nd}
Ir1-O1	2.094	1.952	2.091	2.145	-
Ir1-N1	2.127	2.119	2.153	2.091	1.906
Ir2-O2	-	-	2.093	2.224	-
Ir2-H3	1.588	1.722	-	-	-
Ir2-N2	2.144	2.139	2.139	2.080	1.910
O1-O2	1.544	2.040	-	-	-
O1-H1	-	2.024	0.992	0.974	0.999
O1-H4	1.852	3.014	1.711	1.145	0.984
O2-H1	0.993	0.996	1.849	-	-
O2-H3	2.687	1.387	0.979	1.011	0.997
O2-H2	-	-	1.780	0.976	0.970
N1-H2	1.032	1.044	1.045	-	-
N2-H4	1.036	1.031	1.058	1.381	-

Table 5.6: Selected geometrical parameters of Ground-State Reactants, Intermediates and Transition States computed in order to elimination of two H₂O from *Cp*IrOOH(TsDPEN)* according to Scheme 5.3(B).

Stepwise elimination of H_2O

The calculated PES for this reaction is depicted in Fig. 5.13. The related structures are depicted in Fig. 5.14 and the selected geometrical parameters are reported in Table 5.7.

In the first step of the reaction we have found a transition state $TS5_{3rd}$ with an energy

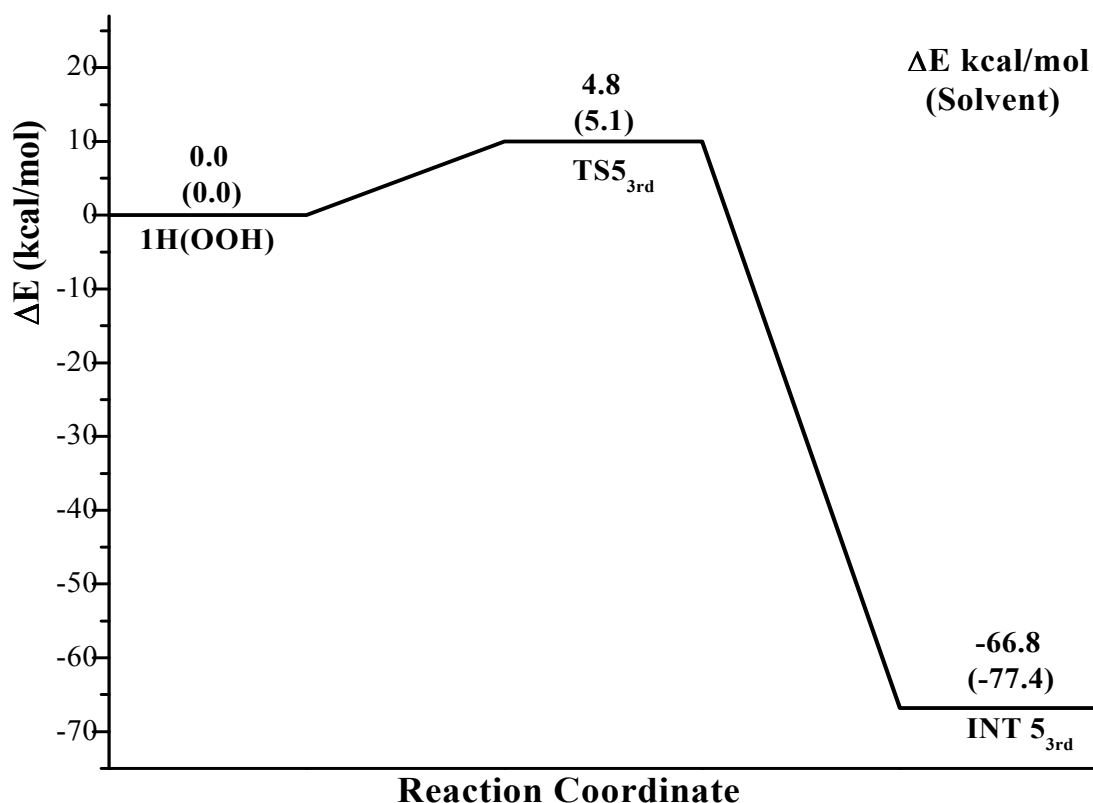


Figure 5.13: PES for the stepwise elimination of H_2O molecule to form $Cp^*Ir(TsDPEN-H)$. The values in parentheses are reported to the solvent phases. Energies are in kilocalories and relative to the ground-state reactants.

barrier of 4.8 kcal/mol in gas phase and 5.1 kcal/mol in solvent. The imaginary frequency is $683i\text{ cm}^{-1}$. This frequency corresponds to a mode in which simultaneously two hydrogen atoms transfer from $1H(H)$ to $1H(OOH)$ and to the breaking of the O1-O2 bond. The bond length between Ir2-H3 is stretched to 1.721 \AA from 1.588 \AA , indicating that the metal hydride bond is broken, while the O2-H3 distance (1.505 \AA) is reduced.

From **TS5_{3rd}** the reaction proceeds with the formation of **INT5_{3rd}** that was at 66.8 kcal/mol below the reactant in gas-phase. This intermediate state include one H_2O , one amine hydroxy complex and one iridium amido complex. Indeed, the only significant changes are the further stretching of the Ir1-O1 distance (to 2.125 Å) and the reduction of the O2-H3 distance (to 0.986 Å). In the next step the amine hydroxy complex will eliminate another H_2O molecule to produce another amido complex. In the next section we will discuss the elimination of H_2O from amine hydroxy complex.

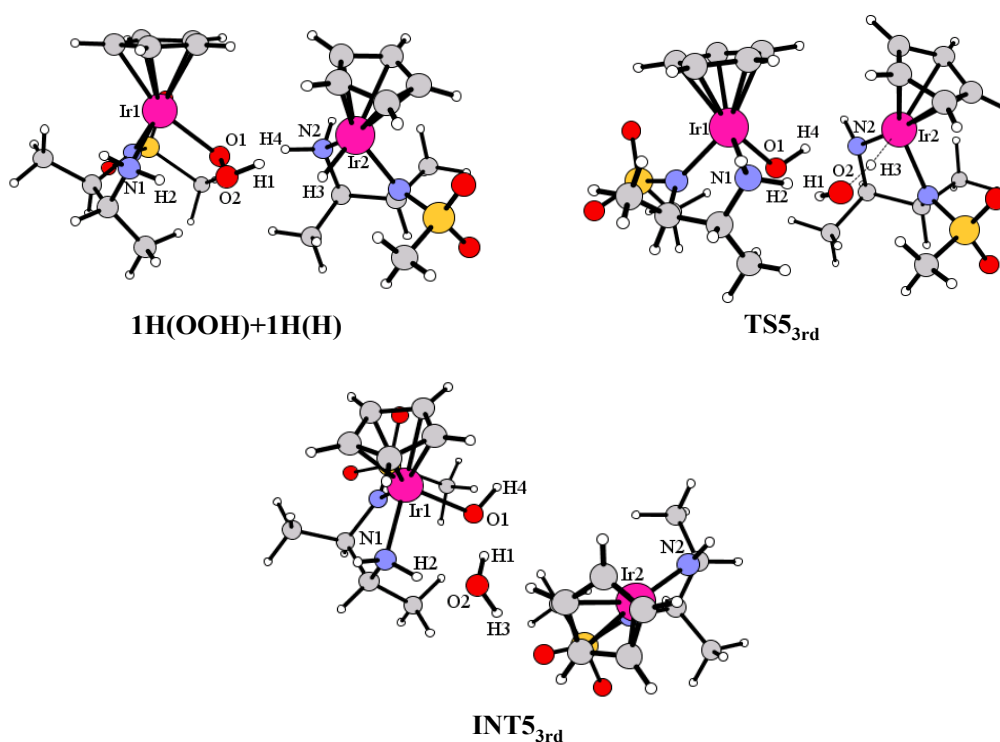


Figure 5.14: Ground-state structures of the reactant, intermediates and transition states for stepwise elimination of H_2O from $Cp^*IrOOH(TsDPEN)$. Labels introduced to individuate geometrical parameters have to be used to read information reported in Table 5.7.

Parameter	1H(OOH)+1H(H)	TS5 _{3rd}	INT5 _{3rd}
Ir1-O1	2.094	2.070	2.125
Ir1-N1	2.127	2.129	2.139
Ir2-H3	1.588	1.721	-
Ir2-N2	2.144	1.945	1.913
O1-O2	1.544	2.728	-
O1-H4	1.852	0.991	0.978
O2-H1	0.993	1.001	1.016
O2-H3	2.687	1.505	0.986
N1-H2	1.032	1.049	1.051
N2-H4	1.036	2.002	-

Table 5.7: Selected geometrical parameters of Ground-State Reactants, Intermediates and Transition States computed for elimination of H_2O from $Cp^*IrOOH(TsDPEN)$ according to Scheme 5.3(C).

Elimination of H_2O from 1(H)OH

The calculated potential energy surface for this reaction is depicted in Fig. 5.15. The optimized structures and the selected geometrical parameters are illustrated in Fig 5.16 and Table 5.8, respectively.

In the first step, we have found a transition state $TS6_{1st}$ with a energy barrier at 5.6 kcal/mol

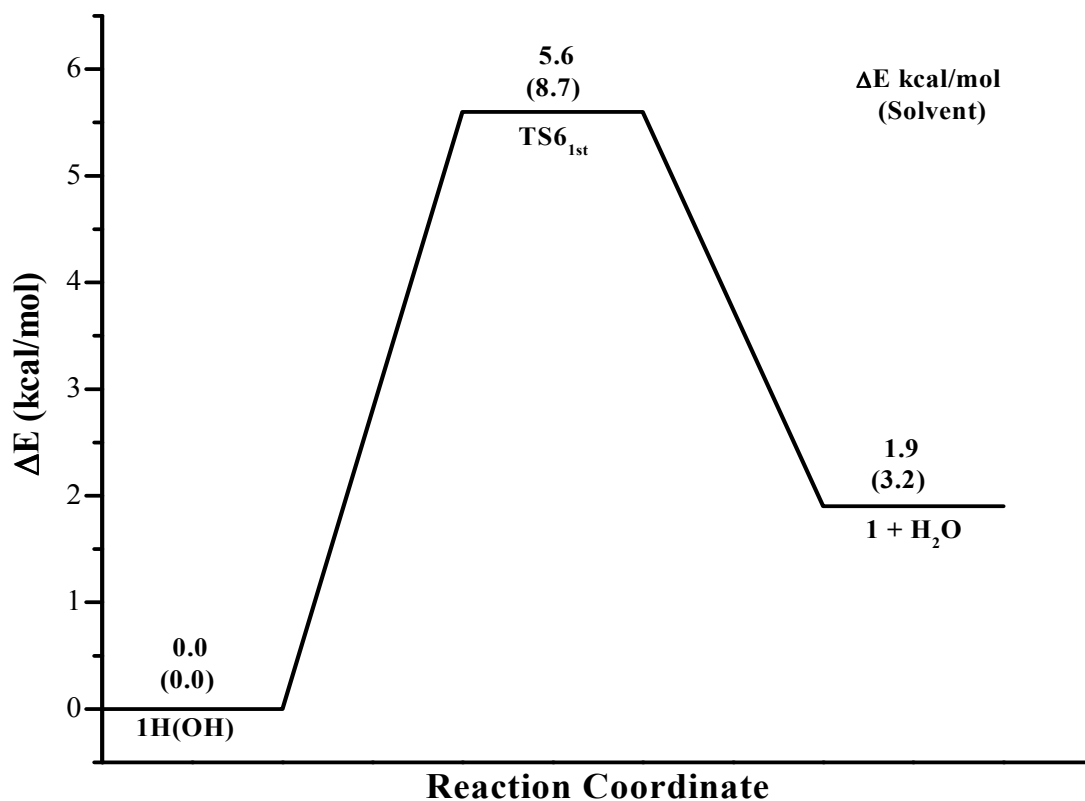


Figure 5.15: PES for the elimination of H_2O molecule from $Cp^*IrOH(TsDPEN)$ in order to form $Cp^*Ir(TsDPEN - H)$. The values in parentheses are reported to the solvent phase. Energies are in kilocalories and relative to the ground-state reactants.

in the gas phase and 8.7 kcal/mol in the solvent. The imaginary frequency is $754i\text{ cm}^{-1}$, corresponds to a movement of the hydrogen (H2 Fig. 5.16) atom from nitrogen (N1 Fig 5.16) to oxygen (O1 Fig 5.16). The significant features of this transition state are an elongation of N1-H2 bond from 1.038 \AA to 1.403 \AA , decreasing of the distance between O1-H2 from 1.898 \AA to 1.146 \AA . Also the bond distance between Ir-O1 is increased to 2.159 \AA from 2.090 \AA . It indicates the breaking of the bond between N1-H2 and yet to be formation of a bond between O1-H2.

The final products are iridium amide complex and H_2O , and the energy falls by $\Delta E = 3.7$ kcal/mol in the gas phase and 5.5 kcal/mol in the solvent. In this species the bond between oxygen and iridium center has been broken ($Ir-O1 = 2.187 \text{ \AA}$), whereas a strong bond occurs between hydrogen and oxygen ($O1-H2 = 1.030 \text{ \AA}$). The elimination of H_2O for the 3rd Mechanism is the same as for the 1st Mechanism.

In Fig. 5.17 we have compared all three mechanisms. From the comparison result that the

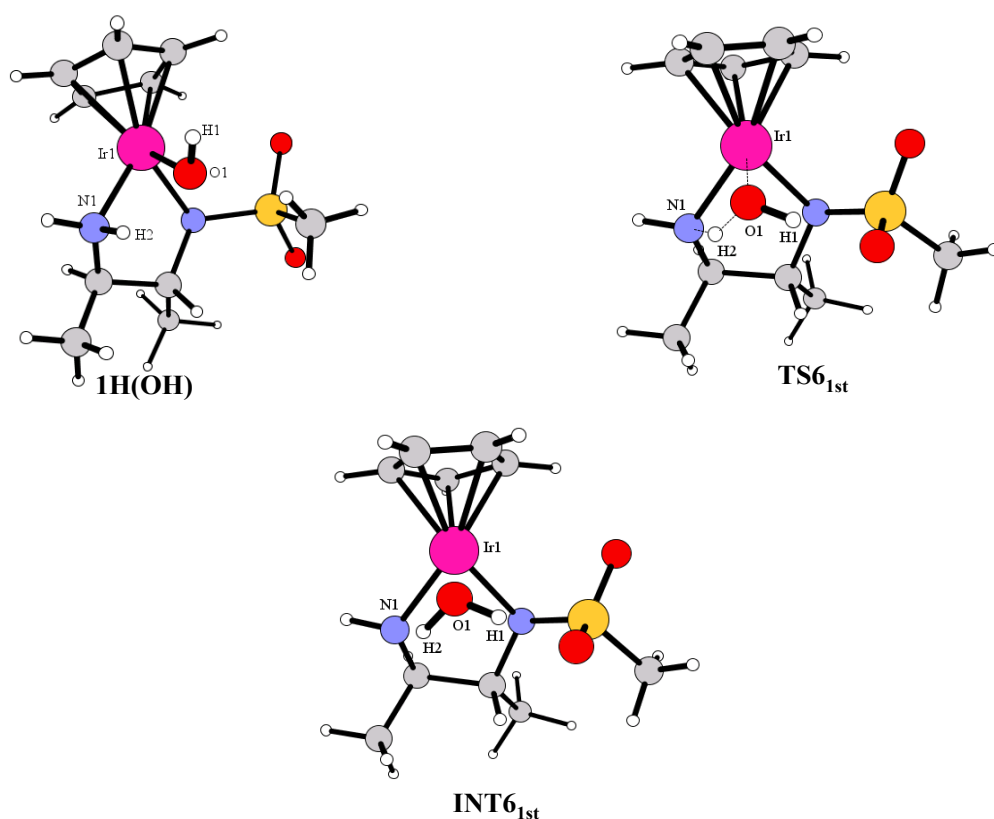


Figure 5.16: Ground-state structures of the reactant, intermediates and transition states for elimination of H_2O from $Cp^*IrOH(TsDPEN)$. Labels introduced to individuate geometrical parameters have to be used to read information reported in Table 5.8.

O-O bond breaking is the rate-limiting step and that the 3rd Mechanism is favorable over the other two mechanisms.

Parameter	1H(OH)	TS6 _{1st}	INT6 _{1st}
Ir1-O1	2.090	2.159	2.187
Ir-NTs	2.092	2.119	2.121
Ir1-N1	2.11	2.077	2.059
O1-H1	0.978	0.991	0.999
N1-H2	1.038	1.403	1.708
O1-H2	1.898	1.146	1.030

Table 5.8: Selected geometrical parameters of Ground-State Reactants, Intermediates and Transition States computed for elimination of H_2O from $Cp^*IrOH(TsDPEN)$.

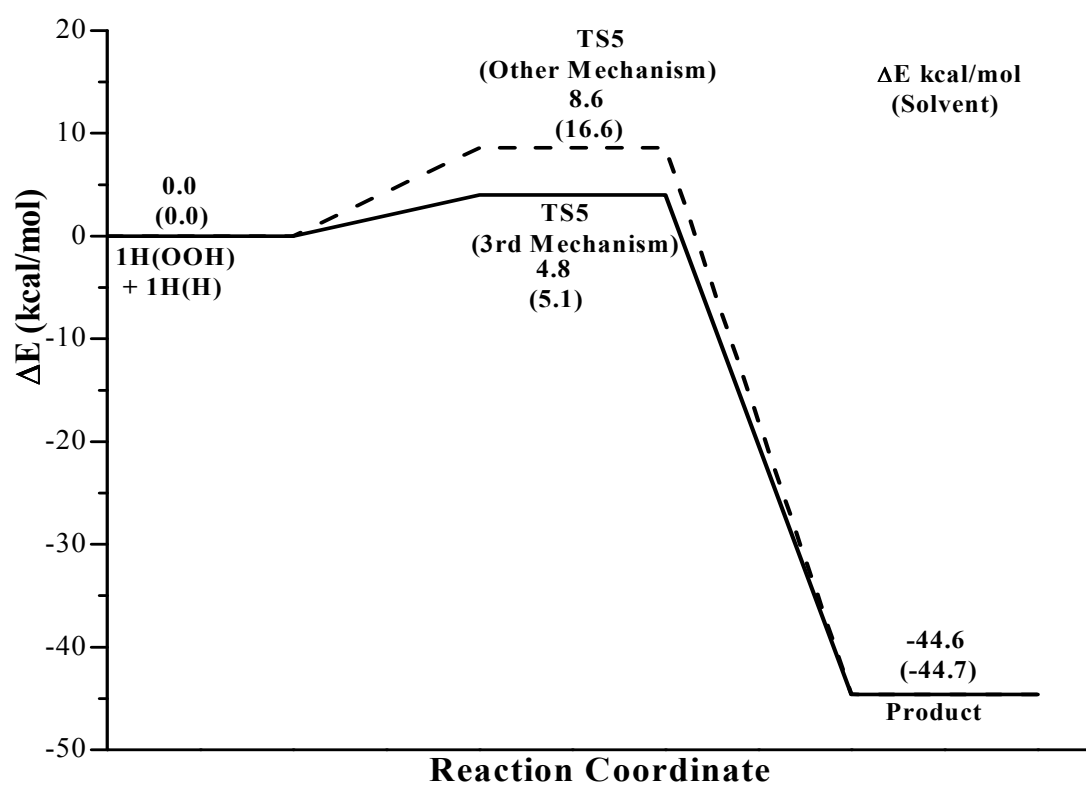


Figure 5.17: Energetics comparison for H_2O elimination. The values in parentheses are reported to the solvent phase. Energies are in kilocalories and relative to the ground-state reactants.

5.4 Conclusion

In this paper, we have investigated the mechanisms proposed by Rauchfus and coworker using by the density functional theory (DFT) for both H_2 oxidation and O_2 reduction reactions using iridium-based catalysts in homogeneous solution. For the hydrogenation reaction have been considered both neutral and non-protonated catalysts. The outcome of the study supports that the mechanism in which the protonated system is involved is favorable compared to the other.

Regarding the insertion of molecular oxygen into the metal-hydride bond, the reaction evolves through the abstraction of the hydrogen atom by O_2 . The reaction started along the triplet path and after the first transition state there is a crossing in the PES between singlet and triplet pathways. In the next step a very stable intermediate is formed, in which the hydrogen atom is bonded to the proximal oxygen. From this stabilized intermediate, the exothermic formation of the final product takes place, overcoming the barrier associated to the transition state for the contemporary breaking of the bond between the metal center and the proximal oxygen.

Finally, concerning the elimination of water molecules computations show that the O-O bond breaking is the rate-limiting step.

Bibliography

- [1] (a) R. Kanai, S. Miyachi and A. Takamiya, *Nature* **1960**, 188, 873; (b) T. Buhrke, O. Lenz, O. N. Krauss and B. Friedrich, *J. Biol. Chem.* **2005**, 280, 23791.
- [2] (a) R. Boulatov, *Pure Appl. Chem.* **2004**, 76, 303; (b) J. Fei, H. K. Song and G. T. R. Palmore, *emChem. Mater.* **2007**, 19, 1565.
- [3] G. Kubas, *Metal Dihydrogen and Bond Complexes*, Kluwer Academic/Plenum Publishers: New York, **2001**.
- [4] T. Katsuki, *In Comprehensive Coordination Chemistry II*, J. A. McCleverty and T. J. Meyer, Eds.; Elsevier Pergamon: Amsterdam, **2004**, 9, 207.
- [5] Z. M. Heiden, and T. B. Rauchfuss, *J. Am. Chem. Soc.* **2007**, 129, 14303.
- [6] K. J. Haack, S. Hashiguchi, A. Fujii, T. Ikariya and R. Noyori, *Angew. Chem., Int. Ed. Engl.* **1997**, 36, 285.
- [7] K. Murata, T. Ikariya and R. Noyori, *J. Org. Chem.* **1999**, 64, 2186.
- [8] K. Mashima, T. Abe and K. Tani, *Chem. Lett.* **1998**, 1201.
- [9] Z. M. Heiden, and T. B. Rauchfuss, *J. Am. Chem. Soc.* **2006**, 128, 13048.
- [10] D. A. Alonso, P. Brandt, S. J. M. Nordin and P. G. Andersson, *J. Am. Chem. Soc.* **1999**, 121, 9580.
- [11] D. G. I. Petra, J. N. H. Reek, J. W. Handgraaf, E. J. Meijer, P. Dierkes, P. C. J. Kamer, J. Brussee, H. E. Schoemaker and P. W. N. M. van Leeuwen, *Chem. Eur. J.* **2000**, 6, 2818.
- [12] M. Yamakawa, H. Ito and R. Noyori, *J. Am. Chem. Soc.* **2000**, 122, 1466.
- [13] R. Noyori, M. Yamakawa and S. Hashiguchi, *J. Org. Chem.* **2001**, 66, 7931.

- [14] J. W. Handgraaf, J. N. H. Reek and E. J. Meijer, *Organometallics* **2003**, 22, 3150.
- [15] S. Chowdhury, I.Rivalta, N. Russo and E. Sicilia, *Chem. Phys. Lett.* **2007**, 443, 183.
- [16] S. Chowdhury, I.Rivalta, N. Russo and E. Sicilia, *Chem. Phys. Lett.* **2008**, 456, 41.
- [17] S. Chowdhury, I.Rivalta, N. Russo and E. Sicilia, *J. Chem. Theory. Comput.* **2008**, 4, 1283.
- [18] M. J. Frisch, *et. al.*, *Gaussian03, Revision B.04*, Gaussian, Inc.: Pittsburgh PA, **2003**.
- [19] C. Lee, W. Yang and G. Parr, *Phys. Rev. B.* **1988**, 37, 785.
- [20] B. Miehlich, A. Savin, H. Stoll and H. Preuss, *Chem. Phys. Lett.* **1989**, 157, 200.
- [21] A.D. Becke, *J. Phys. Chem.* **1993**, 98, 5648.
- [22] K. Fukui, *J. Phys. Chem.* **1970**, 74, 4161.
- [23] K. Fukui, *Acc. Chem. Res.* **1981**, 14, 363.
- [24] P.J. Hay and W.R. Wadt, *Chem. Phys.* **1985**, 82, 299,.
- [25] A. A. Ovchinnicov and J. K. Labanowski, *Phys. Rev. A* **1996**, 53, 3946.
- [26] S. Miertus, E. Scrocco and J. Tomasi, *Chem. Phys.* **1981**, 55, 117.
- [27] S. Miertus and J. Tomasi, *Chem. Phys.* **1982**, 65, 239.
- [28] J.L. Pascual-Ahuir, E. Silla, J. Tomasi and R. Bonaccorsi, *J. Comput Chem.* **1987**, 8, 778.
- [29] R.A. Pierotti, *Chem. Rev.* **1976**, 76, 717.
- [30] J. N. Harvey, M.Aschi, H. Schwarz and W. Koch, *Theor. Chem. Acc.* **1998**, 99, 95.